Universiteit
Leiden
The Netherlands

Efficacy, safety and novel targets in cardiovascular disease : advanced applications in APOE*3-Leiden.CETP mice

Pouwer, M.G.

Citation
Pouwer, M. G. (2020, March 5). *Efficacy, safety and novel targets in cardiovascular disease : advanced applications in APOE*3-Leiden.CETP mice*. Retrieved from https://hdl.handle.net/1887/86022

Version:	Publisher's Version
License:	Licence agreement concerning inclusion of doctoral thesis in the Institutional Repository of the University of Leiden
Downloaded from:	https://hdl.handle.net/1887/86022

Note: To cite this publication please use the final published version (if applicable).

Cover Page

Universiteit Leiden

The handle http://hdl.handle.net/1887/86022 holds various files of this Leiden University dissertation.

Author: Pouwer, M.G.
Title: Efficacy, safety and novel targets in cardiovascular disease : advanced applications in APOE*3-Leiden.CETP mice
Issue Date: 2020-03-05

EFFICACY, SAFETY AND NOVEL TARGETS IN CARDIOVASCULAR DISEASE

Advanced applications in APOE*3-Leiden.CETP mice

Marianne G. Pouwer

EFFICACY, SAFETY AND NOVEL TARGETS IN CARDIOVASCULAR DISEASE

Advanced applications in APOE*3-Leiden.CETP mice

Marianne G. Pouwer

The printing of this thesis was kindly supported by
TNO, Metabolic Health Research
Daan Traas fonds
Pouvet BV
CardioGenx

Financial support by the Dutch Heart Foundation for the publication of this thesis is gratefully acknowledged.

ISBN
978-94-028-1639-6

Cover illustration
Louise te Poele
In collaboration with Utrecht University, Faculty of Veterinary Medicine, Department Pathobiology, Division Anatomy & Physiology.

Design/lay-out
Promotie In Zicht, Arnhem

Print
Ipskamp Printing, Enschede

© M. G. Pouwer, 2019

All rights reserved. No part of thesis may be reproduced, stored in a retrieval system or transmitted in any form or by any means without permission from the author or, when appropriate, permission from the publishers.

EFFICACY, SAFETY AND NOVEL TARGETS IN CARDIOVASCULAR DISEASE

Advanced applications in APOE*3-Leiden.CETP mice

Proefschrift

Ter verkrijging van de graad van Doctor
aan de Universiteit Leiden
op gezag van Rector Magnificus Prof.Mr. C.J.J.M. Stolker,
volgens besluit van het College voor Promoties
te verdedigen op donderdag 5 maart 2020
om 16:15

door

Marianne Godeline Pouwer
Geboren op 7 januari 1989
te Veghel, Nederland

Promotor
Prof. Dr. J.W. Jukema

Copromotor
Dr. J.M.G. Princen (TNO, Leiden)

Leden promotiecommissie
Prof. Dr. P.C.N. Rensen
Dr. I. Bot
Prof. Dr. A. van der Laarse
Prof. Dr. A.K. Groen (Amsterdam UMC locatie AMC)

The studies presented in this thesis were performed at the Gaubius Laboratory of TNO, Leiden, the Netherlands. The research was in part financially supported by 3M Company, AFFiRiS AG, AstraZeneca, Bristol-Myers Squibb, Regeneron Pharmaceuticals, The TNO research program "Preventive Health Technologies" and the European Union Seventh Framework Programme (FP7/2007-2013) grant no. 602936 (CarTarDis project).

Voor mijn ouders

All these weirdos,
and me getting a little better every day right in the midst of them.
I had never known, never even imagined for a heartbeat,
that there might be a place for people like us.

- Denis Johnson (Jesus' Son by Denis Johnson, 1992)

Contents

Chapter 1 11
General introduction
Toxicol Rep. 2016 Feb 11;3:306-309

Chapter 2 33
The AT04A vaccine against proprotein convertase subtilisin/kexin type 9 reduces total cholesterol, vascular inflammation, and atherosclerosis in APOE*3-Leiden.CETP mice
Eur Heart J. 2017 Aug 21;38(32):2499-2507

Chapter 3 55
Triple treatment with alirocumab and evinacumab on top of atorvastatin regresses lesion size and improves plaque phenotype in APOE*3-Leiden.CETP mice
Submitted

Chapter 4 77
The BCR-ABL1 inhibitors imatinib and ponatinib decrease plasma cholesterol and atherosclerosis, and nilotinib and ponatinib activate coagulation in a translational mouse model
Front Cardiovasc Med. 2018 Jun 12;5:55

Chapter 5 107
The BCR-ABL1 inhibitors imatinib and ponatinib decrease plasma cholesterol through different effects on lipoprotein metabolism
Submitted

Chapter 6 131
Dose effects of ammonium perfluorooctanoate on lipoprotein metabolism in APOE*3-Leiden.CETP mice
Toxicol Sci. 2019 Apr 1;168(2):519-534

Chapter 7 163
The APOE*3-Leiden.heterozygous glucokinase knockout mouse as novel translational disease model for type 2 diabetes, dyslipidemia and diabetic atherosclerosis
J Diabetes Res. 2019 Feb 21;2019:9727952

Chapter 8 187
Inflammatory cytokine oncostatin M induces endothelial activation in macro- and microvascular endothelial cells and in APOE*3-Leiden.CETP mice
PLoS One. 2018 Oct 1;13(10):e0204911

Chapter 9 211
Oncostatin M reduces atherosclerosis development in APOE*3-Leiden.CETP mice and is associated with increased survival probability in humans
PLoS One. 2019 Aug 28;14(8):e0221477

Chapter 10 239
General discussion and future perspectives

Summary 255

Samenvatting 259

Author affiliations 263

List of publications 267

Curriculum vitae 271

Dankwoord 273

1

General introduction

Hans M. G. Princen, Marianne G. Pouwer, Elsbet J. Pieterman

Toxicol Rep. 2016 Feb 11;3:306-309

Atherosclerosis

Prevalence

Cardiovascular disease (CVD) is the number 1 cause of death globally and the annual number of deaths from CVD is predicted to rise from 17.5 million in 2012 to 22.2 million by 2030 (1). Currently, 31% of all deaths worldwide is caused by CVD and low and middle-income countries are now most affected. Its major clinical manifestations include ischemic heart disease, ischemic stroke and peripheral arterial disease, all caused by the formation of atheromatous plaques in the vessels, and comprises 85% of all CVD deaths (1).

Development of atherosclerotic plaques

The build-up of an atherosclerotic plaque is a complex and slow process, which in humans begins in early childhood, and becomes clinical relevant after many decades. Atherogenesis begins with the recruitment of inflammatory cells into the intima. As response to irritative stimuli (e.g. dyslipidaemia, hypertension or pro-inflammatory mediators) endothelial permeability increases, the composition of the extracellular matrix beneath the endothelium changes, and the arterial endothelial cells express leukocyte adhesion molecules (2). As a result, blood monocytes are captured on the endothelial surface, and cholesterol-containing low-density lipoproteins (LDL) and remnant particles enter and accumulate in the arterial wall and are oxidized (2). Oxidized LDL (oxLDL) promotes monocyte adhesion and also binds to scavenger receptors on macrophages which triggers uptake of oxLDL leading to the formation of foam cells (type I and II lesions). These cells produce pro-inflammatory mediates, reactive oxygen species and tissue factor pro-coagulants, that amplify the inflammatory process and further increase endothelial permeability (2,3). Smooth muscle cells (SMCs) migrate from the media into the intima, proliferate, and produce extracellular matrix molecules, e.g. interstitial collagen, proteoglycans and elastin, to form a fibrous cap that overlies the lipid-laden foam cells (2,3). The subendothelial proteoglycans entrap LDL and subsequently extra-cellular lipids accumulate (type III lesions). Several plaque factors, including excessive inflammation, oxidized lipids and cholesterol, trigger macrophage cell death (4) leading to the formation of a pool with accumulated cellular debris and extracellular lipids, called the necrotic core of the plaque (type IV lesions). Also, as the result of necrosis, calcium deposits develop (type V lesions). In the advanced type IV and V lesions, thick layers of fibrous connective tissue cover the lipid-rich necrotic core. Activated macrophages and type 1 T-helper cells produce metalloproteinases and cytokines that weaken the tensile strength of the collagen cap (4). Consequently, lesions may rupture thereby releasing their fatty core into the lumen which triggers thrombus formation (type VI lesions) (5). Plaque rupture and subsequent thrombus formation can be clinically silent as they may heal, but can also induce CV ischaemic events through partial or total occlusion of the affected artery.

Risk factors

Several risk factors contribute to the initiation and progression of atherosclerosis development and can be divided in non-modifiable and modifiable risk factors. Non-modifiable risk factors include personal history of CVD, family history of CVD, age and gender. Modifiable risk factors include hypertension, obesity, diabetes mellitus, and elevated plasma glucose, LDL-cholesterol, and triglyceride (TG) levels, and lifestyle variables (poor dietary patterns, smoking, physical inactivity and harmful use of alcohol). Moreover, genetic disorders in the lipoprotein metabolism, e.g. familial dysbetalipoproteinema or type III hyperlipidemia, add to CVD risk. As lifestyle variables and metabolic perturbations are closely linked to each other, patients with CVD commonly present a cluster of risk factors. Estimated odds ratios of these risk factors demonstrate that abnormal plasma lipids are a major risk factor for atherosclerosis (**Table 1**) (6), and therefore, this thesis mainly focuses on the role of the lipoprotein metabolism in atherosclerosis development and CV safety. In addition, the contribution of diabetes and inflammation to CV risk will be discussed.

Table 1 Risk of acute myocardial infarction associated with risk factors in the overall population

Risk factor	Odds ratio (99% CI) adjusted for all risk factors
Current smoking	2.87
Current and former smoking	2.04
Diabetes	2.37
Hypertension	1.91
Abdominal obesity (2 vs 1)†	1.12
Abdominal obesity (3 vs 1)†	1.62
Vegetables and fruit daily	0.70
Exercise	0.86
ApoB/ApoA1 ratio (2 vs 1) §	1.42
ApoB/ApoA1 ratio (3 vs 1) §	1.84
ApoB/ApoA1 ratio (4 vs 1) §	2.41
ApoB/ApoA1 ratio (5 vs 1) §	3.25

The relation between the individual risk factors and first myocardial infarction is indicated. In total 15152 cases and 14820 controls from 52 countries representing every continent, were enrolled. †Top two tertiles vs lowest tertile. §Second, third, fourth, or fifth quintiles vs lowest quintile. Data are extracted from reference (6).

Lipoprotein metabolism

Lipids are transported within the plasma in the form of lipoprotein particles, and, depending on their density are classified as chylomicrons, very-low-density lipoprotein (VLDL), intermediate-density lipoprotein (IDL), LDL, and high-density lipoprotein (HDL). LDL and HDL predominantly transport cholesterol, whereas chylomicrons and VLDL are enriched in TGs. The metabolism of these lipoproteins is divided into two pathways, the exogenous pathway and the endogenous pathway (7) and lipids are removed from the peripheral tissues by reverse cholesterol transport (**Figure 1**).

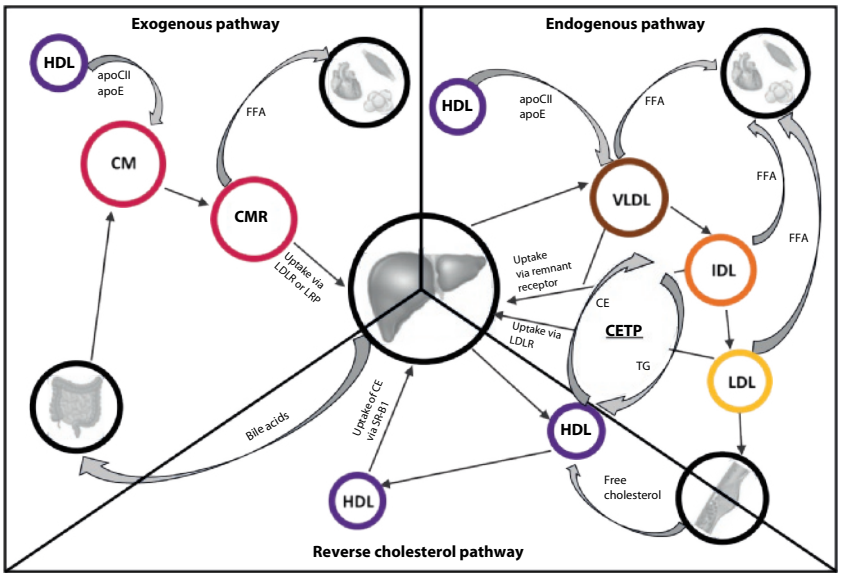

Figure 1 Pathways of lipoprotein metabolism. The liver plays a central role in the exogenous and endogenous pathway of lipid transport. HDL facilitates reverse cholesterol transport. CM, chylomicron; CMR, chylomicron remnant; VLDL, very-low-density lipoprotein; IDL, intermediate-density lipoprotein; LDL, low-density lipoprotein; HDL, high-density lipoprotein; FFA, free fatty acids; apoCII, apolipoprotein C-II; apoE, apolipoprotein E; CE, cholesterol ester; TG, triglycerides; CETP, cholesteryl ester transfer protein; LDLR, low-density lipoprotein receptor, SR-B1, scavenger receptor class B type 1.

The exogenous pathway

The exogenous pathway refers to the absorption of dietary lipids by the enterocytes in the intestine, where they are assembled with apolipoprotein(apo)B48 into chylomicrons and enter the blood stream via the lymphatic vessels. In the blood, the chylomicrons receive apoCII and apoE from HDL-particles. ApoCII binds and activates lipoprotein lipase (LPL),

an enzyme attached to the luminal surface of endothelial cells in capillaries of adipose, heart and skeletal muscle tissue. Upon binding, TGs from the chylomicron particles are hydrolysed into glycerol and fatty acids and the remnant particles are cleared by the liver through binding of apoE to the LDL receptor (7).

The endogenous pathway

The liver plays a central role in the endogenous pathway. Triacylglycerols and cholesterol esters (CE) are assembled with apoB100 into VLDL, and when they reach the blood stream they receive apoCII and apoE from HDL particles. Like chylomicrons, the TGs from the VLDL particles are hydrolysed by endothelial LPL and consequently transform into IDL. IDL particles are taken up by the liver through binding of the remnant and LDL receptor with apoE or apoB100, or are further hydrolysed into LDL. LDL particles contain a relatively high cholesterol content and transfer lipids to the peripheral cells or are cleared by the liver through LDLR-apoB100 interaction (7). However, more importantly with respect to atherosclerosis, LDL can enter the arterial wall, in contrast to the larger VLDL and chylomicrons, where they are oxidative and proteolytically modified and contribute to the formation of atherosclerotic lesions.

Reverse cholesterol transport

HDL is the main lipoprotein involved in the reverse cholesterol transport pathway, which starts with the formation of nascent HDL by the liver and intestine. HDL particles acquire free cholesterol and phospholipids that are effluxed from cells in the peripheral tissues, including the vessel wall, a process mediated by ABCA1 resulting in the formation of mature HDL. The HDL particles transport the cholesterol to the liver either directly by interacting with hepatic scavenger receptor B1 (SR-B1), or the CEs in HDL are exchanged for TGs from VLDL or LDL particles through cholesterol ester transfer protein (CETP) (7). When remnant particles and LDL are taken up by the liver, unesterified cholesterol can be secreted into the bile, or is converted into bile acids.

The contribution of LDL-C, HDL-C and TGs to CVD risk

1. LDL-C

LDL-C is recognized as a primary causal risk factor in CVD as evidenced from many experimental, epidemiological and genetic studies (8,9). In addition, intervention trials with statin therapy confirm a reduced incidence of coronary heart disease as a consequence of cholesterol-lowering in LDL (10,11), and recent trials indicate that intensive lipid-lowering with statins may be more beneficial in risk reduction than less intensive (or standard) therapy (12). According to results from the latter meta-analysis, every 1 mmol/L (39 mg/dL) reduction in LDL-C is associated with a 23% reduction in the risk of major vascular events (12) suggesting that a 2–3 mmol/L reduction in LDL-C would correspond with a 40–50% reduction in events.

2. HDL-C

Epidemiological studies consistently report an inverse association between coronary heart disease risk and HDL-C: results from 4 prospective epidemiologic studies indicate that an increase of 1 mg/dL (0.03 mmol/L) in HDL-C is associated with a 2–3% reduction in risk (13).

Besides its major role in reverse cholesterol transport, HDL has also been described to have anti-inflammatory, anti-oxidant, anti-platelet and vasodilatory properties and may therefore have a protective role in coronary heart disease (14). Several therapeutic approaches aimed at raising HDL-C levels have since been investigated. However, undisputed proof for causality of low HDL-C in CVD is lacking and clinical trials aimed at raising HDL-C to prevent disease (AIM-HIGH, HPS2-THRIVE, ILLUMINATE, dal-OUTCOMES, ACCELERATE, REVEAL) have failed to meet their primary goals (15–17). In addition, data from Mendelian randomization studies show that HDL-C and myocardial infarction risk are not causally related (14,18). A systematic review and meta-analysis of relevant preclinical studies and clinical trials on the contribution of non-HDL-C/LDL-C lowering versus HDL-C raising concluded that the protective role of lowering LDL-C and non-HDL-C is well-established (19). However, the contribution of raising HDL-C on inhibition of atherosclerosis and the prevention of CVD remains undefined and may be dependent on the mode of action of HDL-C-modification. Similar outcome data were found for the prevention of clinical events in randomized controlled trials and on inhibition of atherosclerosis in relevant, CETP-expressing, animals emphasizing the validity/translatability of these animal models to the human situation (19).

3. TGs and remnant cholesterol

Triglycerides are primarily carried by remnants, a combined term for IDL-, VLDL-, and chylomicron remnants (20). Because of the small size of remnants, they are able to penetrate the arterial wall, thereby promoting accumulation of cholesterol in the intimal space, foam cell formation, and atherosclerosis (21). It is most likely that the cholesterol content of remnants, and not TGs, causes atherosclerosis because most cells can degrade TGs but not cholesterol (20). However, the concentration of TGs is highly correlated with the cholesterol content of remnants (22) and Mendelian randomization analyses demonstrated that TG-lowering *LPL* variants and LDL-C lowering *LDLR* variants were similarly associated with lower risk of CVD per unit difference in apoB (23). As a result, targeting TGs has become an interesting approach to reduce CV events and several novel therapies that interfere with the LPL pathway are under development, including inhibition of apoCIII and angiopoietin-like protein 3 (ANGPTL3) (24–26). One of these agents, the ANGPTL3 antibody evinacumab, was evaluated in this thesis and is therefore discussed in the next section.

Lipid-lowering interventions

Primary prevention of CVD can be achieved by promoting healthy lifestyle behaviour to the general population and at the individual level, and by targeting CV risk factors, e.g.

increased blood pressure, plasma lipid and glucose levels (27). Lifestyle modifications to improve the plasma lipid profile include quit smoking, reduced intake of dietary unsaturated fat, saturated fat and cholesterol, increased intake of dietary fibre, vegetables and fruits, reduction of excessive body weight, and increased physical activity (6,27). Depending on the estimated total CV risk and plasma LDL-C levels, lifestyle modifications can be accompanied by lipid-lowering drugs. For patients that are at high risk, subjects with documented CVD, diabetes mellitus or markedly elevated plasma cholesterol, additional lipid lowering therapies should always be considered (27). **Table 2** summarizes the lipid lowering interventions currently available and their relative risk reduction for major vascular events. Two of these agents, statins and PCSK9 inhibitors, have been evaluated in this thesis and are therefore discussed below.

Table 2 Overview of lipid-lowering interventions currently available

Lipid-lowering intervention	Mechanism of LDL-C lowering	Relative risk reduction for major vascular events*1
PCSK9 inhibitors	Increased LDL-C clearance through upregulation of LDLR.	0.49
Ileal bypass	Reduced absorption of cholesterol by the intestine and restoration of the metabolic response to a meal.	0.65
Statins	Decreased cholesterol biosynthesis through inhibition of HMG-CoA reductase.	0.80
Bile acid sequestrants	Bind components of the bile in the intestine thereby preventing their reabsorption.	0.78
Dietary interventions	Reduced calorie/fat intake and binding of bile acids and cholesterol to fibers.	0.83
Fibrates	Activation of peroxisome proliferator-activated receptor α leading to decreased VLDL particle production and increased lipid clearance.	0.88
Ezetimibe	Reduced cholesterol absorption in the small intestine through blockage of the Niemann-Pick C1 like 1 transporter, essential for the sterol transport across the enterocytes.	0.94
Niacin	Increases clearance of VLDL particles.	0.94

*1 Data extracted from reference (12).

1. Statins

Statins are discovered in 1973 by Akira Endo who isolated the compound compactin from the fungus *Penicillium citrinum*, which was found to be a competitive inhibitor of HMG-CoA reductase, the rate-controlling enzyme in hepatic cholesterol synthesis (28). The first

commercially available statin based on this discovery was lovastatin, followed by 2 semi-synthetic statins (simvastatin and pravastatin) and 4 synthetic statins (fluvastatin, atorvastatin, rosuvastatin and pitavastatin) (28). Inhibition of HMG-CoA reductase lowers intracellular cholesterol concentration which results in a compensatory increased LDLR expression on the hepatocytes and consequently, increased LDL-C uptake and decreased plasma LDL-C levels. Statins reduce plasma LDL-C levels by 20 to 50%, depending on the type of statin and dose (27), and reduce CV risk by 23% per 1.0 mmol/L LDL-C reduction (12). Due to their proven efficacy, statins are among the most frequently prescribed drugs in the world, although there are some limitations. The response to statins is variable and despite maximally tolerated statin doses, a subgroup of patients does not reach their LDL-C goals and remain at significant residual risk. Also, meta-analyses demonstrate that further LDL-C lowering further reduces CVD risk (12), while an estimated 6% reduction of LDL-C is achieved per doubling of the statin dose, the so-called "6% rule" (29). Last, while statins are generally well-tolerated, "muscle complaints" have been reported (30,31) and are the primary reason for statin non-adherence and discontinuation (30). To overcome these limitations, additional therapeutic agents, including proprotein convertase subtilisin/kexin 9 (PCSK9) and ANGPTL3 inhibitors, have been introduced or are currently under development.

2. PCSK9 inhibitors

PCSK9 inhibitors are the most powerful cholesterol-lowering agents currently available. PCSK9 is an enzyme that binds to and shuttles the LDL receptor in the intracellular lysosomal degradation pathway in the liver and other cells thereby preventing the clearance of LDL-C from the plasma. Humans with loss-of-function mutations in the *PCSK9* gene exhibit extremely low levels of LDL-C and are protected from atherosclerosis, whereas gain-of-function mutations are associated with hypercholesterolemia (32). Consequently, antibodies (evolocumab and alirocumab) against PCSK9 have been developed. When administered on top of maximally tolerated doses of statins, these antibodies additionally reduce plasma LDL-C levels up to 60% and the risk of CV events by 15% (33,34). Evolocumab and alirocumab are FDA and EMA approved for subjects with heterozygous familial hypercholesterolemia or for those with clinical atherosclerotic CVD that do not reach their LDL-C goals despite maximally tolerated statin treatment.

3. ANGPTL3 inhibitors

ANGPTL3 is almost exclusively synthesized in the liver, and is an endogenous inhibitor of lipoprotein lipase (LPL), thereby reducing the hydrolysis of TGs in capillaries of adipose tissue and muscles (25). Genetic loss-of-function of *ANGPTL3* causes familial combined hypolipidemia, characterized by very low plasma TG, LDL-C and HDL-C concentrations, and decreased odds of atherosclerotic CVD (26). Pharmacologic antagonism of ANGPTL3 with the antibody evinacumab reduced atherosclerotic lesion area in dyslipidemic

APOE*3-Leiden.CETP mice, and dose-dependently reduced TG and LDL-C levels in healthy subjects evaluated in a phase I trial (26). This novel approach to reduce plasma lipids is particularly important for the treatment of patients with familial hypercholesterolemia with defects in the LDLR, as statins and PCSK9 inhibitors depend on functional LDLR, as well as for patients with the metabolic syndrome and type 2 diabetes, which are associated with elevated plasma TG levels (25). Evinacumab is currently being evaluated in a phase III trial for patients with homozygous familial hypercholesterolemia.

Diabetes and CVD risk

Type 2 diabetes is characterized by elevated blood glucose levels and insulin resistance, and is commonly associated with obesity and other components of the metabolic syndrome (**Table 3**) (35), including atherogenic dyslipidaemia, which consists of elevated plasma concentrations of both fasting and postprandial TG-rich lipoproteins, small dense LDL and low HDL-cholesterol (36). Consequently, CVD remains the leading cause of morbidity and mortality for patients with type 2 diabetes (36). Despite the close relation between hyperglycaemia and CVD, most studies that evaluated intensive glycaemic control in diabetic patients failed to show significant benefits in terms of CV morbidity and mortality (37), and some agents even increased adverse CV events, e.g. heart failure (38) and myocardial infarction (39,40). To establish the safety of new antidiabetic drugs, the FDA and EMA mandated all new diabetes drugs to demonstrate CV safety (41,42), of which the clinical trials with empagliflozin (EMPA-REG OUTCOME) (43), liraglutide (LEADER) (44) and piogliazone (45) were among the first that showed beneficial effects on CVD outcomes.

Table 3 Definition of the metabolic syndrome

Central obesity Plus any two:	
Raised TGs	>150 mg/dL (1.7 mmol/L) Specific treatment for this lipid abnormality
Reduced HDL-C	<40 mg/dL (1.03 mmol/L) in men <50 mg/dL (1.29 mmol/L) in women Specific treatment for this lipid abnormality
Raised blood pressure	Systolic >130 mmHg Diastolic >85 mmHg Treatment of previously diagnosed hypertension
Raised fasting plasma glucose	Fasting plasma glucose > 100 mg/dL (5.6 mmol/L) Previously diagnosed type 2 diabetes

Data extracted from reference (35).

Inflammation in atherosclerosis

The role of inflammation in atherosclerotic disease is well-established and it has been shown that inflammatory processes mediate all stages of atherosclerosis: from the initiation through progression and eventually, thrombotic complications (46). As a result, not only plasma lipid levels, but also plasma levels of the inflammatory biomarker C-reactive protein (CRP) are predictive for individual CVD risk (47). Important players in the inflammatory pathways are cytokines, that can be classified as pro- or anti-atherogenic. Examples of pro-atherogenic cytokines are tumour necrosis factor-α (TNF-α), interleukin (IL)-1, and IL-6, whereas transforming growth factor -β (TGF-β), IL-10, and IL-35 are among the anti-atherogenic cytokines (48). Cytokines are expressed by a variety of inflammatory cells but also by other tissues including white adipose tissue, liver, vascular SMCs and the endothelium. Plasma levels of the pro-inflammatory cytokines IL-6, IL-5 and interferon- γ (IFN-γ) have been found to be associated with CVD risk (49). From a clinical perspective, targeting cytokines would be an interesting approach to reduce inflammation-driven atherosclerosis progression. As a result, several therapeutic approaches that modulate cytokine production have been developed or are under investigation (48). Examples are the anti-IL-6 antibody tocilizumab which has been shown to attenuate the inflammatory response after coronary angiography in patients with non-ST-elevation myocardial infarction (50), and the CANTOS trial with the anti-IL-1β antibody canakinumab that demonstrated a lower rate of recurrent CV events in patients with previous myocardial infarction, which was related to the magnitude of CRP reduction (51). In this thesis, the pro-inflammatory cytokine Oncostatin M (OSM) has been evaluated as potential therapeutic target for CVD.

OSM

OSM is a member of the IL-6 family cytokines and plays an important role in various biologic actions. There are two types of functional OSM receptors, the leukaemia inhibitory factor receptor (LIFR) and the OSM receptor (OSMR) (53). OSM signals through both receptors in humans, whereas only the OSMR is used in mice (53). OSM is synthesized in hematopoietic cells and in various inflammatory cells such as activated T-cells, neutrophils, eosinophils, and macrophages (54). OSM has been found to be upregulated in multiple chronic inflammatory diseases (55–57) and it is expressed at sites of atherosclerotic lesions (58). Epidemiological studies have shown that an elevated serum OSM level is positively correlated with the degree of coronary stenosis in patients with coronary artery disease (59). Moreover, development of atherosclerosis is attenuated in OSMR-β deficient APOE$^{-/-}$ mice (60), indicating the pro-atherogenic properties of OSM. Currently, there are no therapies available that target OSM.

Experimental atherosclerosis

This thesis describes (I) novel strategies to reduce plasma lipids and atherosclerosis development, (II) the (cardio)vascular off-target effects of registered drugs and an environmental pollutant, (III) a novel mouse model for diabetic atherosclerosis combining modifiable elevated plasma lipid and glucose levels, and (IV) the potential of OSM as novel pro-inflammatory CV target. In all these studies we used the APOE*3-Leiden(.CETP) mouse model, a humanized model for lipoprotein metabolism and atherosclerosis.

Mouse versus man

Conventional mouse strains used in preclinical biomedical and toxicological research, for example C57BL/6 mice or BALB/c mice, are considered not to be the most appropriate animal models to study modulation of lipoprotein metabolism, since lipolysis of TG-rich particles as chylomicrons and VLDL and their remnants and clearance of the apoB-containing (non-HDL) lipoproteins via the apoE-LDL-receptor pathway are fast processes as compared to humans (61). Consequently, the mice have relatively low plasma TG and cholesterol levels with low levels of the atherogenic VLDL and LDL, and the majority of cholesterol is contained in HDL (**Figure 2A-B**). Severe dietary regimens with saturated fat and high amounts of cholesterol and cholic acid are required to increase the amount of non-HDL-C to some extent, but still lower than in humans (62). As a result, these strains only develop small lesions with features of the earliest state of atherosclerosis, but do not develop complex atherosclerotic lesions (63) as seen in CVD patients.

In humans, lipolysis is slower and removal of apoB-containing lipoproteins is delayed (61). In addition, humans unlike mice possess an important player in lipoprotein metabolism, CETP, which transfers cholesterol from HDL to (V)LDL in exchange for triglycerides, thereby increasing (V)LDL-C levels and decreasing HDL-C. Due to these differences, in man cholesterol is contained mainly in the pro-atherogenic LDL and to a lesser extent in HDL (**Figure 2C-D**).

The APOE*3-Leiden.CETP mouse model

To develop a mouse model with a more human-like lipoprotein metabolism for pharmacological, nutritional and toxicological research, the APOE*3-Leiden transgenic mouse was generated by the introduction of a genomic human DNA construct carrying the mutant *APOE*3-LEIDEN* gene, the *APOCI* gene, and all known regulatory elements, obtained from a patient with familial dysbetalipoproteinemia (FD) (64). FD or type III hyperlipoproteinemia is characterized by elevated levels of plasma cholesterol and an increased ratio of cholesterol to TG in the VLDL and IDL fractions, resulting in the appearance of β-VLDL particles (65). These mice were cross-bred with mice expressing human CETP under control of its natural flanking regulatory DNA-sequences (66) to obtain the APOE*3-Leiden.CETP mouse, as a humanized model for FD and mixed dyslipoproteinemia (67). While normal wild-type mice have a very rapid clearance of apoB-containing

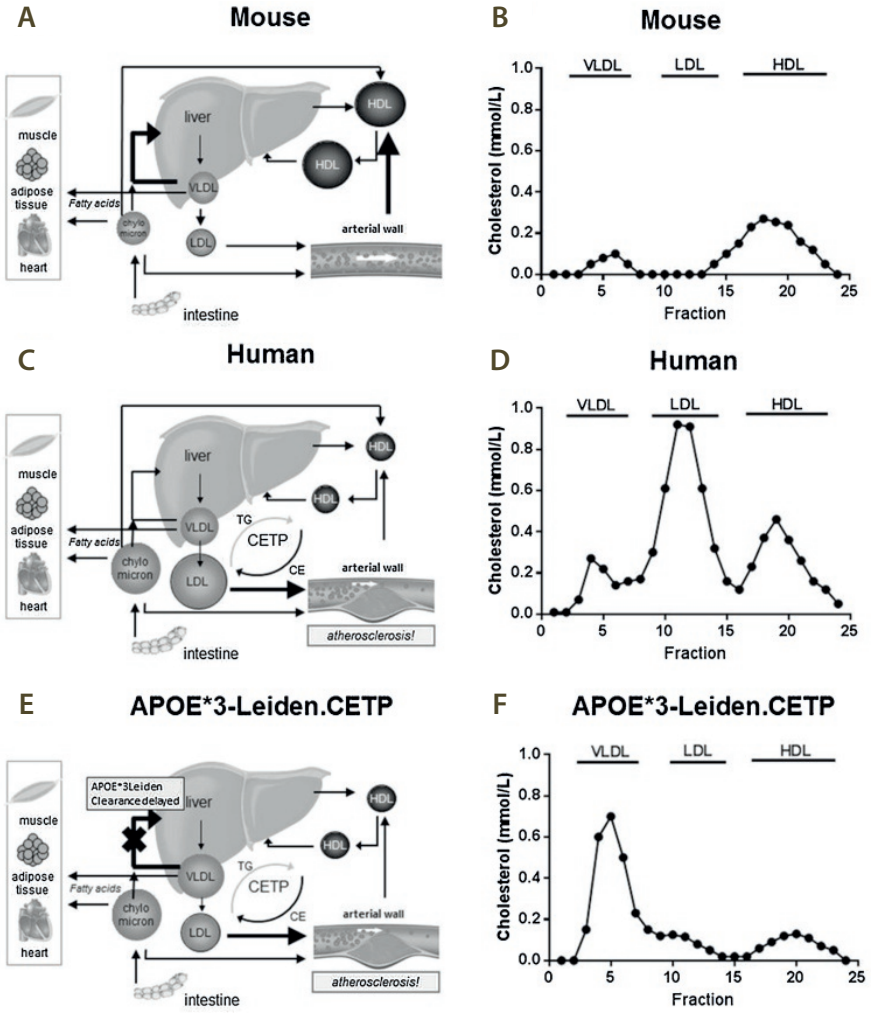

Figure 2 Mice have a fast clearance of apoB-containing lipoproteins and do not express CETP (A), as a result the majority of plasma cholesterol is confined to HDL (B), with TC and TG levels of 1.5–2.0 and 0.2–0.3 mmol/L in C57BL/6 mice. Humans have a slower clearance of apoB-containing lipoproteins and do express CETP (C) and normolipidemic man have TC and TG levels of <5.2 and 0.5–1.5 mmol/L, respectively, and cholesterol consists mainly of non-HDL-C (VLDL-C/LDL-C) (D). The APOE*3-Leiden. CETP mouse has a lipoprotein profile similar as in FD patients and a lipoprotein metabolism similar to that in man (E), and on a chow diet TC and TG levels are 3.0–4.0 and 2.5–3.0 mmol/L, mainly confined to the non-HDL-C fraction (F).

lipoproteins, APOE*3-Leiden(.CETP) mice have an impaired clearance and increased TG level, and are thereby mimicking the slow clearance observed in humans, particularly in patients with FD (61,65,68). Similarly as in FD patients, in APOE*3-Leiden and APOE*3-Leiden.CETP mice, the major part of plasma cholesterol is contained in the VLDL and VLDL-remnant particles, leading to formation of β-VLDL particles, which is further increased by cholesterol feeding (64,67) (**Figure 2E-F**). Consequently, APOE*3-Leiden.CETP mice develop advanced atherosclerotic lesions with characteristics of human pathology that can be histologically classified according to the American Heart Association (AHA) (5) (**Figure 3**).

Importantly, as compared to the widely used hyperlipidaemic and atherogenic apoE- and LDLR-deficient (apoE$^{-/-}$ and LDLR$^{-/-}$) mice, the APOE*3-Leiden(.CETP) mice possess an intact but delayed apoE-LDLR-mediated clearance, which is an essential characteristic of human lipoprotein metabolism and for the proper, human-like response on hypolipidemic drugs (69,70). APOE*3-Leiden.CETP mice respond well to dietary intervention using human-relevant (Westernized) diets with increases in plasma cholesterol and TG and these lipids can be titrated to levels mimicking those in humans. Therefore, APOE*3-Leiden.CETP mice are a translational and predictive animal model for the effect of drugs on lipoprotein metabolism and atherosclerosis. Also, the APOE*3-Leiden.CETP mouse model has proved to be a suitable model for investigation of the mechanism of action of off-target effects of drugs (71) and environmental pollutants (72). **Table 4** gives an overview of lipid-lowering interventions that have been evaluated in APOE*3-Leiden.CETP mice and compares the effects on plasma lipids and atherosclerosis with data in hyperlipidaemic and FD-patients. It should be noted that APOE*3-Leiden.CETP mice respond similarly as FD-patients to niacin and fibrates, whereas greater (V)LDL-C reductions are achieved in APOE*3-Leiden.CETP mice relative to hyperlipidaemic patients (73–75).

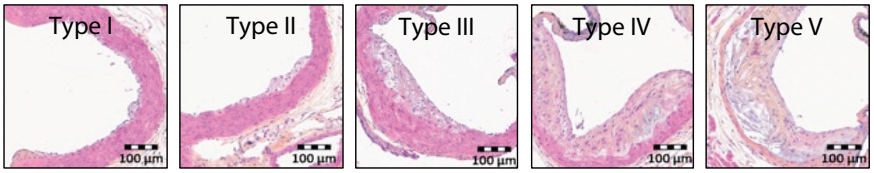

Figure 3 Atherosclerotic lesions in APOE*3-Leiden.CETP mice. Type I: early fatty streaks consist of ≤ 10 foam cells in the intima. Type II: regular fatty streaks consist of >10 foam cells in the intima. Type III: mild plaques consist of foam cells covered with a fibrotic cap. Type IV: moderate plaques consist of foam cells, often together with necrosis and cholesterol crystals, and severe disorganization of the intima. Inflammatory cells and foam cells infiltrate the media and intimal smooth muscle cells disarrange. Type V: severe plaques consist of foam cells, a fibrotic cap, necrosis, cholesterol crystals and calcium deposits. The media and adjacent adventitia may contain accumulations of lymphocytes, macrophages, and macrophage foam cells. Severe disarrangement of the media with disruption of the elastic fibers.

Table 4 Effects of lipid-lowering interventions in APOE*3-Leiden.CETP mice and humans

Lipid lowering intervention	APOE*3-Leiden.CETP mice		Humans		References
	Plasma cholesterol	Atherosclerosis	Plasma cholesterol	Cardiovascular risk	
HmgCoA reductase inhibitors/ statins					
Atorvastatin	↓	↓	↓	↓	(12,76–79)
Simvastatin	↓	↓	↓	↓	(12,73)
TG-lowering, HDL-raising drugs					
Niacin	↓/↑[*1]	↓	↓/↑[*1]	↔	(12,16,17,73,75,80)
Fibrates	↓/↑[*1]	↓[*2]	↓/↑[*1]	↓	(12,75,81–85)
HDL-modulating drugs					
Anacetrapib	↓/↑[*1]	↓	↓/↑[*1]	↓	(74,87,88)
Torcetrapib	↓/↑[*1]	↑	↓/↑[*1]	↑	(89,90)
PCSK9 inhibitors					
Alirocumab	↓	↓	↓	↓	(12,33,77)
Evolocumab	↓	↓	↓	↓	(69,91)
Miscellaneous					
Ezetimibe	↓	↓	↓	↓	(12,78)
Bile acid sequestrants	↓[*2]	nd	↓	↓	(12,86)
Evinacumab	↓	↓	↓	nd	(26)

[*1] HDL-C increased; [*2] In APOE*3-Leiden mice, unpublished data in APOE*3-Leiden.CETP mice; nd, not determined.

Outline of the thesis

This thesis describes a variety of studies on novel interventions and targets in lipid and lipoprotein metabolism and atherosclerosis, and on CV safety of anti-cancer drugs and a widely used industrial surfactant that persists in the environment. In all studies the APOE*3-Leiden(.CETP) mouse model was used as a well-established translational model for lipoprotein metabolism and atherosclerosis development.

In **Chapter 2** we evaluated whether a vaccine against PCSK9 could induce an effective immune response against PCSK9, thereby reducing plasma cholesterol levels and atherosclerosis progression. However, as most patients at CVD risk are treated after development of atherosclerosis, therapies that regress pre-existent lesions are warranted. It is known that the magnitude of regression is correlated with the percentage of LDL-C reduction, and therefore, **Chapter 3** evaluated if aggressive lipid-lowering interventions

using double and triple treatment with simple or combined inhibition of PCSK9 (alirocumab) and ANGPTL3 (evinacumab) on top of atorvastatin, could regress pre-existent lesions. **Chapter 4** describes the CV off-target effects of three generations tyrosine kinase inhibitors (TKIs), imatinib, nilotinib and ponatinib, respectively, that are being used for the treatment of patients with chronic myeloid leukaemia (CML). In contrast to the safe profile of imatinib, CV side effects have been reported in patients receiving nilotinib and ponatinib. Also, modulations in plasma lipids occur when CML patients are treated with these TKIs, therefore we investigated the mechanism of these lipid modulations in **Chapter 5**. The dose effects of perfluorooctanoic acid (PFOA) on lipoprotein metabolism are presented in **Chapter 6**. PFOA has been widely used as an emulsifier in the manufacture of fluoropolymers, is extremely stable and therefore persists in the environment. In addition to abnormalities in plasma lipids, diabetes can add to the CVD risk and the development of novel anti-diabetic drugs has shifted from solely glucose-lowering agents towards agents that additionally reduce CVD risk. This shift requires preclinical translational models that combine hyperlipidaemia and hyperglycaemia, and we therefore developed a mouse model with both features, the APOE*3-Leiden.glucokinase$^{+/-}$ mouse. The characteristics of this novel model are described in **Chapter 7.** The next two chapters describe the evaluation of the cytokine OSM as possible target to reduce endothelial inflammation, important in the initiation of atherosclerosis. In **Chapter 8** we evaluated the inflammatory response to OSM in different human vascular beds, and on markers of endothelial inflammation in plasma and the aortic root of APOE*3-Leiden.CETP mice. In **Chapter 9**, mice were prolonged exposed to OSM and atherosclerosis development was examined. In addition, we investigated possible associations between plasma OSM levels in CVD patients and survival from coronary heart disease.

The results obtained in these studies and future perspectives are discussed in **Chapter 10**.

References

1. WHO. Hearths: technical package for cardiovascular disease mangement in primary health care [Internet]. 2016. Available from: http://www.who.int/cardiovascular_diseases/publications/en/
2. Libby P, Ridker PM, Hansson GK. Progress and challenges in translating the biology of atherosclerosis. Nature. 2011 May;473(7347):317–25.
3. Sakakura K, Nakano M, Otsuka F, et al. Pathophysiology of atherosclerosis plaque progression. Heart Lung Circ. 2013 Jun;22(6):399–411.
4. Hansson GK, Libby P, Tabas I. Inflammation and plaque vulnerability. J Intern Med. 2015 Nov;278(5):483–93.
5. Stary HC, Chandler AB, Dinsmore RE, et al. A definition of advanced types of atherosclerotic lesions and a histological classification of atherosclerosis. A report from the Committee on Vascular Lesions of the Council on Arteriosclerosis, American Heart Association. Circulation. 1995 Sep;92(5):1355–74.
6. Yusuf S, Hawken S, Ounpuu S, et al. Effect of potentially modifiable risk factors associated with myocardial infarction in 52 countries (the INTERHEART study): case-control study. Lancet (London, England). 2004 Sep;364(9438):937–52.
7. Feingold KR, Grunfeld C. Introduction to Lipids and Lipoproteins. In: Feingold KR, Anawalt B, Boyce A, Chrousos G, Dungan K, Grossman A, et al., editors. South Dartmouth (MA); 2000.
8. Ridker PM. LDL cholesterol: controversies and future therapeutic directions. Lancet (London, England). 2014 Aug;384(9943):607–17.
9. Ference BA, Ginsberg HN, Graham I, et al. Low-density lipoproteins cause atherosclerotic cardiovascular disease. 1. Evidence from genetic, epidemiologic, and clinical studies. A consensus statement from the European Atherosclerosis Society Consensus Panel. Eur Heart J. 2017 Aug;38(32):2459–72.
10. Baigent C, Keech A, Kearney PM, et al. Efficacy and safety of cholesterol-lowering treatment: prospective meta-analysis of data from 90,056 participants in 14 randomised trials of statins. Lancet (London, England). 2005 Oct;366(9493):1267–78.
11. Lewington S, Whitlock G, Clarke R, et al. Blood cholesterol and vascular mortality by age, sex, and blood pressure: a meta-analysis of individual data from 61 prospective studies with 55,000 vascular deaths. Lancet (London, England). 2007 Dec;370(9602):1829–39.
12. Silverman MG, Ference BA, Im K, et al. Association Between Lowering LDL-C and Cardiovascular Risk Reduction Among Different Therapeutic Interventions: A Systematic Review and Meta-analysis. JAMA. 2016 Sep;316(12): 1289–97.
13. Gordon DJ, Probstfield JL, Garrison RJ, et al. High-density lipoprotein cholesterol and cardiovascular disease. Four prospective American studies. Circulation. 1989 Jan;79(1):8–15.
14. Kingwell BA, Chapman MJ, Kontush A, et al. HDL-targeted therapies: progress, failures and future. Nat Rev Drug Discov. 2014 Jun;13(6):445–64.
15. Armitage J, Holmes M V, Preiss D. Cholesteryl Ester Transfer Protein Inhibition for Preventing Cardiovascular Events: JACC Review Topic of the Week. J Am Coll Cardiol. 2019 Feb;73(4):477–87.
16. Boden WE, Probstfield JL, Anderson T, et al. Niacin in patients with low HDL cholesterol levels receiving intensive statin therapy. N Engl J Med. 2011 Dec;365(24):2255–67.
17. Landray MJ, Haynes R, Hopewell JC, et al. Effects of extended-release niacin with laropiprant in high-risk patients. N Engl J Med. 2014 Jul;371(3):203–12.
18. Barter P, Genest J. HDL cholesterol and ASCVD risk stratification: A debate. Atherosclerosis. 2019 Jan;283:7–12.
19. Kuhnast S, Fiocco M, van der Hoorn JWA, et al. Innovative pharmaceutical interventions in cardiovascular disease: Focusing on the contribution of non-HDL-C/LDL-C-lowering versus HDL-C-raising: A systematic review and meta-analysis of relevant preclinical studies and clinical trials. Eur J Pharmacol. 2015 Sep;763(Pt A):48–63.
20. Varbo A, Nordestgaard BG. Remnant Cholesterol and Triglyceride-Rich Lipoproteins in Atherosclerosis Progression and Cardiovascular Disease. Vol. 36, Arteriosclerosis, thrombosis, and vascular biology. United States; 2016. p. 2133–5.
21. Nordestgaard BG, Varbo A. Triglycerides and cardiovascular disease. Lancet (London, England). 2014 Aug;384(9943):626–35.

22. Varbo A, Benn M, Tybjaerg-Hansen A, et al. Remnant cholesterol as a causal risk factor for ischemic heart disease. J Am Coll Cardiol. 2013 Jan;61(4):427–36.
23. Ference BA, Kastelein JJP, Ray KK, et al. Association of Triglyceride-Lowering LPL Variants and LDL-C-Lowering LDLR Variants With Risk of Coronary Heart Disease. JAMA. 2019 Jan;321(4):364–73.
24. Gaudet D, Brisson D, Tremblay K, et al. Targeting APOC3 in the familial chylomicronemia syndrome. N Engl J Med. 2014 Dec;371(23):2200–6.
25. Olkkonen VM, Sinisalo J, Jauhiainen M. New medications targeting triglyceride-rich lipoproteins: Can inhibition of ANGPTL3 or apoC-III reduce the residual cardiovascular risk? Atherosclerosis. 2018 May;272:27–32.
26. Dewey FE, Gusarova V, Dunbar RL, et al. Genetic and Pharmacologic Inactivation of ANGPTL3 and Cardiovascular Disease. N Engl J Med. 2017 Jul;377(3):211–21.
27. Catapano AL, Graham I, De Backer G, et al. 2016 ESC/EAS Guidelines for the Management of Dyslipidaemias. Eur Heart J. 2016 Oct;37(39):2999–3058.
28. Endo A. A historical perspective on the discovery of statins. Proc Jpn Acad Ser B Phys Biol Sci. 2010;86(5):484–93.
29. Davidson MH, McGarry T, Bettis R, et al. Ezetimibe coadministered with simvastatin in patients with primary hypercholesterolemia. J Am Coll Cardiol. 2002 Dec;40(12):2125–34.
30. Stroes ES, Thompson PD, Corsini A, et al. Statin-associated muscle symptoms: impact on statin therapy-European Atherosclerosis Society Consensus Panel Statement on Assessment, Aetiology and Management. Eur Heart J. 2015 May;36(17):1012–22.
31. Hilton-Jones D. Statin-related myopathies. Pract Neurol. 2018 Apr;18(2):97–105.
32. Seidah NG, Prat A, Pirillo A, et al. Novel strategies to target proprotein convertase subtilisin kexin 9: beyond monoclonal antibodies. Cardiovasc Res. 2019 Mar;115(3):510–8.
33. Schwartz GG, Steg PG, Szarek M, et al. Alirocumab and Cardiovascular Outcomes after Acute Coronary Syndrome. N Engl J Med. 2018 Nov;379(22):2097–107.
34. Sabatine MS, Giugliano RP, Keech AC, et al. Evolocumab and Clinical Outcomes in Patients with Cardiovascular Disease. N Engl J Med. 2017 May;376(18):1713–22.
35. Alberti KGMM, Zimmet P, Shaw J. The metabolic syndrome--a new worldwide definition. Lancet (London, England). 2005 Sep;366(9491):1059–62.
36. Taskinen M-R, Boren J. New insights into the pathophysiology of dyslipidemia in type 2 diabetes. Atherosclerosis. 2015 Apr;239(2):483–95.
37. Paneni F, Luscher TF. Cardiovascular Protection in the Treatment of Type 2 Diabetes: A Review of Clinical Trial Results Across Drug Classes. Am J Cardiol. 2017 Jul;120(1S):S17–27.
38. Lago RM, Singh PP, Nesto RW. Congestive heart failure and cardiovascular death in patients with prediabetes and type 2 diabetes given thiazolidinediones: a meta-analysis of randomised clinical trials. Lancet (London, England). 2007 Sep;370(9593):1129–36.
39. Home PD, Pocock SJ, Beck-Nielsen H, et al. Rosiglitazone evaluated for cardiovascular outcomes--an interim analysis. N Engl J Med. 2007 Jul;357(1):28–38.
40. Nissen SE, Wolski K. Effect of rosiglitazone on the risk of myocardial infarction and death from cardiovascular causes. N Engl J Med. 2007 Jun;356(24):2457–71.
41. FDA. Guidance for industry: diabetes mellitus - evaluating cardiovascular risk in new antidiabetic therapies to treat type 2 diabetes Title [Internet]. 2008. Available from: http://www.fda.gov/downloads/drugs/guidancecomplianceregulatory-information/guidances/ucm071627.pdf
42. EMA. European Medicines Agency guideline on clinical investigation of medicinal products in the treatment or prevention of diabetes mellitus. London: Committee for Medicinal Products for Human Useitle [Internet]. 2012. Available from: https://www.ema.europa.eu/en/documents/scientific-guideline/guideline-clinical-investigation-medicinal-products-treatment-prevention-diabetes-mellitus-revision_en.pdf
43. Zinman B, Wanner C, Lachin JM, et al. Empagliflozin, Cardiovascular Outcomes, and Mortality in Type 2 Diabetes. N Engl J Med. 2015 Nov;373(22):2117–28.
44. Marso SP, Daniels GH, Brown-Frandsen K, et al. Liraglutide and Cardiovascular Outcomes in Type 2 Diabetes. N Engl J Med. 2016 Jul;375(4):311–22.
45. DeFronzo RA, Inzucchi S, Abdul-Ghani M, et al. Pioglitazone: The forgotten, cost-effective cardioprotective drug for type 2 diabetes. Diabetes Vasc Dis Res. 2019 Feb;1479164118825376.

46. Libby P. Inflammation in atherosclerosis. Nature. 2002 Dec;420(6917):868–74.
47. Ridker PM. Cardiology Patient Page. C-reactive protein: a simple test to help predict risk of heart attack and stroke. Circulation. 2003 Sep;108(12):e81-5.
48. Tousoulis D, Oikonomou E, Economou EK, et al. Inflammatory cytokines in atherosclerosis: current therapeutic approaches. Eur Heart J. 2016 Jun;37(22):1723–32.
49. Clarke R, Valdes-Marquez E, Hill M, et al. Plasma cytokines and risk of coronary heart disease in the PROCARDIS study. Open Hear. 2018;5(1):e000807.
50. Kleveland O, Kunszt G, Bratlie M, et al. Effect of a single dose of the interleukin-6 receptor antagonist tocilizumab on inflammation and troponin T release in patients with non-ST-elevation myocardial infarction: a double-blind, randomized, placebo-controlled phase 2 trial. Eur Heart J. 2016 Aug;37(30):2406–13.
51. Ridker PM, Everett BM, Thuren T, et al. Antiinflammatory Therapy with Canakinumab for Atherosclerotic Disease. N Engl J Med. 2017 Sep;377(12):1119–31.
52. Ridker PM, MacFadyen JG, Everett BM, et al. Relationship of C-reactive protein reduction to cardiovascular event reduction following treatment with canakinumab: a secondary analysis from the CANTOS randomised controlled trial. Lancet (London, England). 2018 Jan;391(10118):319–28.
53. Tanaka M, Hara T, Copeland NG, et al. Reconstitution of the functional mouse oncostatin M (OSM) receptor: molecular cloning of the mouse OSM receptor beta subunit. Blood. 1999 Feb;93(3):804–15.
54. Komori T, Morikawa Y. Oncostatin M in the development of metabolic syndrome and its potential as a novel therapeutic target. Anat Sci Int. 2018 Mar;93(2):169–76.
55. Bordon Y. Cytokines: Oncostatin M - a new target in IBD? Nat Rev Immunol. 2017 May;17(5):280.
56. Pradeep AR, S TM, Garima G, et al. Serum levels of oncostatin M (a gp 130 cytokine): an inflammatory biomarker in periodontal disease. Biomarkers Biochem Indic Expo response, susceptibility to Chem. 2010 May;15(3):277–82.
57. Richards CD. The enigmatic cytokine oncostatin m and roles in disease. ISRN Inflamm. 2013 Dec;2013:512103.
58. Albasanz-Puig A, Murray J, Preusch M, et al. Oncostatin M is expressed in atherosclerotic lesions: a role for Oncostatin M in the pathogenesis of atherosclerosis. Atherosclerosis. 2011 Jun;216(2):292–8.
59. Li X, Zhang X, Wei L, et al. Relationship between serum oncostatin M levels and degree of coronary stenosis in patients with coronary artery disease. Clin Lab. 2014;60(1):113–8.
60. Zhang X, Li J, Qin J-J, et al. Oncostatin M receptor beta deficiency attenuates atherogenesis by inhibiting JAK2/STAT3 signaling in macrophages. J Lipid Res. 2017 May;58(5):895–906.
61. Dietschy JM, Turley SD, Spady DK. Role of liver in the maintenance of cholesterol and low density lipoprotein homeostasis in different animal species, including humans. J Lipid Res. 1993 Oct;34(10):1637–59.
62. Nishina PM, Lowe S, Verstuyft J, et al. Effects of dietary fats from animal and plant sources on diet-induced fatty streak lesions in C57BL/6J mice. J Lipid Res. 1993 Aug;34(8):1413–22.
63. Whitman SC. A practical approach to using mice in atherosclerosis research. Clin Biochem Rev. 2004 Feb;25(1):81–93.
64. van den Maagdenberg AM, Hofker MH, Krimpenfort PJ, et al. Transgenic mice carrying the apolipoprotein E3-Leiden gene exhibit hyperlipoproteinemia. J Biol Chem. 1993 May;268(14):10540–5.
65. de Knijff P, van den Maagdenberg AM, Stalenhoef AF, et al. Familial dysbetalipoproteinemia associated with apolipoprotein E3-Leiden in an extended multigeneration pedigree. J Clin Invest. 1991 Aug;88(2):643–55.
66. Jiang XC, Agellon LB, Walsh A, et al. Dietary cholesterol increases transcription of the human cholesteryl ester transfer protein gene in transgenic mice. Dependence on natural flanking sequences. J Clin Invest. 1992 Oct;90(4):1290–5.
67. Westerterp M, van der Hoogt CC, de Haan W, et al. Cholesteryl ester transfer protein decreases high-density lipoprotein and severely aggravates atherosclerosis in APOE*3-Leiden mice. Arterioscler Thromb Vasc Biol. 2006 Nov;26(11):2552–9.
68. Wardell MR, Weisgraber KH, Havekes LM, et al. Apolipoprotein E3-Leiden contains a seven-amino acid insertion that is a tandem repeat of residues 121-127. J Biol Chem. 1989 Dec;264(35):21205–10.
69. Ason B, van der Hoorn JWA, Chan J, et al. PCSK9 inhibition fails to alter hepatic LDLR, circulating cholesterol, and atherosclerosis in the absence of ApoE. J Lipid Res. 2014 Nov;55(11):2370–9.
70. Zadelaar S, Kleemann R, Verschuren L, et al. Mouse models for atherosclerosis and pharmaceutical modifiers. Arterioscler Thromb Vasc Biol. 2007 Aug;27(8):1706–21.

71. de Vries-van der Weij J, de Haan W, Hu L, et al. Bexarotene induces dyslipidemia by increased very low-density lipoprotein production and cholesteryl ester transfer protein-mediated reduction of high-density lipoprotein. Endocrinology. 2009 May;150(5):2368–75.
72. Bijland S, Rensen PCN, Pieterman EJ, et al. Perfluoroalkyl sulfonates cause alkyl chain length-dependent hepatic steatosis and hypolipidemia mainly by impairing lipoprotein production in APOE*3-Leiden CETP mice. Toxicol Sci. 2011 Sep;123(1):290–303.
73. Kuhnast S, Louwe MC, Heemskerk MM, et al. Niacin Reduces Atherosclerosis Development in APOE*3Leiden. CETP Mice Mainly by Reducing NonHDL-Cholesterol. PLoS One. 2013;8(6):e66467.
74. Kuhnast S, van der Tuin SJL, van der Hoorn JWA, et al. Anacetrapib reduces progression of atherosclerosis, mainly by reducing non-HDL-cholesterol, improves lesion stability and adds to the beneficial effects of atorvastatin. Eur Heart J. 2015 Jan;36(1):39–48.
75. Hoogwerf BJ, Bantle JP, Kuba K, et al. Treatment of type III hyperlipoproteinemia with four different treatment regimens. Atherosclerosis. 1984;51(2–3):251–9.
76. Kuhnast S, van der Hoorn JWA, van den Hoek AM, et al. Aliskiren inhibits atherosclerosis development and improves plaque stability in APOE*3Leiden.CETP transgenic mice with or without treatment with atorvastatin. J Hypertens. 2012 Jan;30(1):107–16.
77. Kuhnast S, van der Hoorn JWA, Pieterman EJ, et al. Alirocumab inhibits atherosclerosis, improves the plaque morphology, and enhances the effects of a statin. J Lipid Res. 2014 Oct;55(10):2103–12.
78. Gierman LM, Kuhnast S, Koudijs A, et al. Osteoarthritis development is induced by increased dietary cholesterol and can be inhibited by atorvastatin in APOE*3Leiden.CETP mice--a translational model for atherosclerosis. Ann Rheum Dis. 2014 May;73(5):921–7.
79. van De Poll SW, Romer TJ, Volger OL, et al. Raman spectroscopic evaluation of the effects of diet and lipid-lowering therapy on atherosclerotic plaque development in mice. Arterioscler Thromb Vasc Biol. 2001 Oct;21(10):1630–5.
80. van der Hoorn JWA, de Haan W, Berbee JFP, et al. Niacin increases HDL by reducing hepatic expression and plasma levels of cholesteryl ester transfer protein in APOE*3Leiden.CETP mice. Arterioscler Thromb Vasc Biol. 2008 Nov;28(11):2016–22.
81. Kooistra T, Verschuren L, de Vries-van der Weij J, et al. Fenofibrate reduces atherogenesis in ApoE*3Leiden mice: evidence for multiple antiatherogenic effects besides lowering plasma cholesterol. Arterioscler Thromb Vasc Biol. 2006 Oct;26(10):2322–30.
82. van der Hoogt CC, de Haan W, Westerterp M, et al. Fenofibrate increases HDL-cholesterol by reducing cholesteryl ester transfer protein expression. J Lipid Res. 2007 Aug;48(8):1763–71.
83. Bijland S, Pieterman EJ, Maas ACE, et al. Fenofibrate increases very low density lipoprotein triglyceride production despite reducing plasma triglyceride levels in APOE*3-Leiden.CETP mice. J Biol Chem. 2010 Aug;285(33):25168–75.
84. Jun M, Foote C, Lv J, et al. Effects of fibrates on cardiovascular outcomes: a systematic review and meta-analysis. Lancet (London, England). 2010 May;375(9729):1875–84.
85. van den Hoek AM, van der Hoorn JWA, Maas AC, et al. APOE*3Leiden.CETP transgenic mice as model for pharmaceutical treatment of the metabolic syndrome. Diabetes Obes Metab. 2014 Jun;16(6):537–44.
86. Sugimoto-Kawabata K, Shimada H, Sakai K, et al. Colestilan decreases weight gain by enhanced NEFA incorporation in biliary lipids and fecal lipid excretion. J Lipid Res. 2013 May;54(5):1255–64.
87. Bowman L, Hopewell JC, Chen F, et al. Effects of Anacetrapib in Patients with Atherosclerotic Vascular Disease. N Engl J Med. 2017 Sep;377(13):1217–27.
88. van der Tuin SJL, Kuhnast S, Berbee JFP, et al. Anacetrapib reduces (V)LDL cholesterol by inhibition of CETP activity and reduction of plasma PCSK9. J Lipid Res. 2015 Nov;56(11):2085–93.
89. de Haan W, de Vries-van der Weij J, van der Hoorn JWA, et al. Torcetrapib does not reduce atherosclerosis beyond atorvastatin and induces more proinflammatory lesions than atorvastatin. Circulation. 2008 May;117(19):2515–22.
90. Barter PJ, Caulfield M, Eriksson M, et al. Effects of torcetrapib in patients at high risk for coronary events. N Engl J Med. 2007 Nov;357(21):2109–22.
91. Sabatine MS, Giugliano RP, Wiviott SD, et al. Efficacy and safety of evolocumab in reducing lipids and cardiovascular events. N Engl J Med. 2015 Apr;372(16):1500–9.

2

The AT04A vaccine against proprotein convertase subtilisin/kexin type 9 reduces total cholesterol, vascular inflammation, and atherosclerosis in APOE*3-Leiden.CETP mice

Christine Landlinger*, Marianne G. Pouwer*, Claudia Juno,
José W. A. van der Hoorn, Elsbet J. Pieterman, J. Wouter Jukema, Guenther Staffler,
Hans M. G. Princen*, Gergana Galabova*

*These authors contributed equally

Eur Heart J. 2017 Aug 21;38(32):2508–2510

Abstract

Objectives: Proprotein convertase subtilisin/kexin type 9 (PCSK9) has emerged as a promising therapeutic target for the treatment of hypercholesterolaemia and atherosclerosis. PCSK9 binds to the low density lipoprotein receptor and enhances its degradation, which leads to the reduced clearance of low-density lipoprotein-cholesterol (LDL-C) and a higher risk of atherosclerosis. In this study, the AT04A anti-PCSK9 vaccine was evaluated for its therapeutic potential in ameliorating or even preventing coronary heart disease in the atherogenic APOE*3-Leiden.CETP mouse model.

Methods and results: Control and AT04A vaccine-treated mice were fed a Western-type diet for 18 weeks. Antibody titres, plasma lipids, and inflammatory markers were monitored by ELISA, FPLC, and multiplexed immunoassay, respectively. The progression of atherosclerosis was evaluated by histological analysis of serial cross-sections from the aortic sinus. The AT04A vaccine induced high and persistent antibody levels against PCSK9, causing a significant reduction in plasma total cholesterol (-53%, $p<0.001$) and LDL-C compared with controls. Plasma inflammatory markers such as serum amyloid A (SAA), macrophage inflammatory protein-1β (MIP-1β/CCL4), macrophage-derived chemokine (MDC/CCL22), cytokine stem cell factor (SCF), and vascular endothelial growth factor A (VEGF-A) were significantly diminished in AT04A-treated mice. As a consequence, treatment with the AT04A vaccine resulted in a decrease in atherosclerotic lesion area (-64%, $p=0.004$) and aortic inflammation as well as in more lesion-free aortic segments (+119%, $p=0.026$), compared with control.

Conclusions: AT04A vaccine induces an effective immune response against PCSK9 in APOE*3-Leiden.CETP mice, leading to a significant reduction of plasma lipids, systemic and vascular inflammation, and atherosclerotic lesions in the aorta.

Introduction

Elevated circulating low density lipoprotein cholesterol (LDL-C) is one of the major risk factors positively correlated with premature development of cardiovascular disease (CVD) (1). The main pathway of LDL-C clearance from the blood circulation involves the low-density lipoprotein receptor (LDLR) on hepatocytes (2,3). The serine protease proprotein convertase subtilisin/kexin type 9 (PCSK9), mainly synthesized in the liver, binds to the LDLR and enhances its degradation, thereby modulating cholesterol levels of circulating apoB-containing lipoproteins (i.e., very-low density liporptein (VLDL) and LDL) (4,5). By inhibiting PCSK9, LDLR expression and its activity are increased, leading to plasma VLDL- and LDL-cholesterol lowering.

The current hypothesis relating to the role of cholesterol in cardiovascular disease (CVD) is that the effect of lowering LDL-C on CVD is independent of the means by which LDL-C is lowered (6). The most commonly-used drugs to treat hypercholesterolaemia are 3-hydroxy-3-methyl-glutaryl-CoA reductase inhibitors, known as statins. Statins in general have been shown to reduce LDL-C by 30–60%, providing an estimated 25–30% reduction in CVD (7). However, many patients are unable to achieve their optimal lipid levels despite intensive statin therapy (8,9), and high doses of statins may increase the incidence and severity of multiple adverse events such as myopathy and hepatotoxicity (10). Moreover, statins do not only induce a beneficial increase in LDLR, but also increase PCSK9, which leads to LDLR degradation, thus causing a negative feedback response that attenuates the statins' lipid effects (11).

The most advanced alternative approach for LDL-C lowering is the inhibition of PCSK9 action by monoclonal antibodies (mAbs). The novel anti-PCSK9 antibodies alirocumab and evolocumab, which were recently granted FDA approval, are safe and achieved a 50–70% reduction in LDL-C when used either as monotherapy or in combination with a statin (12,13). They are approved as second line treatment in patients at risk who are unable to reach the LDL-C goal despite maximally tolerated statin therapy or for patients who are statin-intolerant (14,15). Preclinical efficacy studies with the PCSK9 mAb alirocumab were performed in the APOE*3-Leiden.CETP mouse model. These double-transgenic mice represent a valuable model for the preclinical evaluation of interventions on atherosclerosis development, because of its humanized lipoprotein metabolism. The diet-induced development of atherosclerosis in these mice has a pro-inflammatory plaque phenotype, and shows responsiveness to all lipid-modulating interventions that are being used in the clinic (16–18). In this model, alirocumab was able to decrease plasma lipids and atherosclerosis development, and in combination with atorvastatin the beneficial effects of PCSK9 mAb treatment were enhanced (18,19). However, mAbs show relatively short *in vivo* half-lives, thus the long-term efficacy of mAb therapy is accompanied by frequent application and high costs. We developed an active immunization against the body's own PCSK9 for a widely-applicable and more cost-effective long-term LDL-C cholesterol

management (20). This so-called AT04A vaccine was tested for its efficacy in APOE*3-Leiden. CETP transgenic mice. AT04A was able to induce a high immune response against PCSK9 without any side-effects; leading to a significant reduction of plasma lipids over the whole intervention period. Consequently, a reduction of systemic and vascular inflammation and atherosclerotic lesions in the aorta at the end of the intervention period was observed.

Materials and methods

Animals

Female APOE*3-Leiden.CETP transgenic mice on a C57BL/6 background (7-9 weeks of age) received a Western-type diet (WTD) containing 15% cacao butter and 0.1% (w/w) cholesterol (AB Diets, Woerden, The Netherlands) for a time period of 3 weeks. Thereafter, the mice were matched by body weight, total plasma cholesterol (TC), and triglycerides (TG), and divided into control (n=15) and vaccine-treated (n=15) groups. The number of animals per group was calculated using a probability of 0.05. Based on our experience from previous studies, we expected to have a variance of 15% (sigma 40%) in plasma lipids and a minimal effect of treatment of 30%, resulting in 15 animals per group. Upon starting the immunization, the mice were fed a chow diet (ssniff Spezialdiäten GmbH, Soest, Germany) for 4 weeks, followed by WTD for 18 weeks, in order to induce atherosclerotic plaques. At the end of the experiment all animals were euthanized by CO_2 inhalation, and blood was collected via heart puncture. Hearts and livers were isolated to determine liver weight, atherosclerotic development, and lesion severity. Animal experiments were approved by the Animal Experiment Committee of The Netherlands Organization of Applied Scientific Research TNO under registration number 3655.

Vaccines

The proprietary AFFITOME® technology (21) was used to develop short immunogenic peptides, which mimic a N-terminal epitope of PCSK9 that is involved in the interaction with LDLR. The peptides were synthesized by Fmoc solid phase peptide synthesis and HPLC-purified (EMC microcollections GmbH, Germany). These peptides contain an additional C-terminal cysteine residue and were activated with the crosslinker N-γ-maleimidobutyryl-oxysuccinimide ester (GMBS, Pierce, ThermoFisher Scientific) according to the manufacturer's protocol, and covalently linked to the carrier protein Keyhole Limpet Haemocyanin (KLH, Biosyn GmbH). The KLH-conjugated peptides were adsorbed to 0.2% Alhydrogel® (Brenntag Biosector, Denmark). Scrambled peptide conjugated to KLH was used as a negative control vaccine. Vaccines were stored at 4°C. Prior to injection, the vaccines were brought to room temperature (RT) and carefully mixed.

Treatment and immunization scheme

Mice were immunized 5 times (subcutaneous, 500 µl in both the right and left flanks) either with AT04A or a control vaccine, in bi-weekly intervals. During the first two immunizations the mice were fed a chow diet (t=-4 to 0 weeks). The time point at which the food was switched to WTD 0.1% (w/w) cholesterol in order to induce atherosclerosis development refers to week 0. Three more immunizations were then performed at t=0, 2 and 4 weeks (**Figure 1**). Blood was withdrawn every four weeks after a 4 hour fasting period at the time points t=-4, 0, 4, 8, 12, and 16 weeks, and the final bleeding was performed at week 18 (**Figure 1**). Plasma samples were prepared and used for titre analysis, total cholesterol (t=-4, 0, 4, 8, 12 and 18 weeks) and lipoprotein profile analyses (t=-4, 0, 4, 8 and 18 weeks), which were determined from group pooled plasma samples.

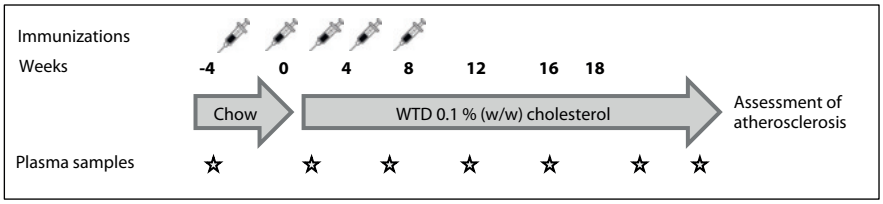

Figure 1 Study design. Mice were immunised 5 times either with AT04A or a control vaccine. Four weeks after prime immunization (t=0 weeks) normal chow was switched to WTD 0.1% (w/w) cholesterol. After 18 weeks mice were sacrificed to assess atherosclerosis development. Abbreviations: WTD, Western type diet.

ELISA analyses

To determine the titre of AT04A vaccine-induced antibodies, plasma samples were collected and analysed by ELISA. Briefly, 1 µM of the antigenic peptides coupled to BSA were coated in 0.1 M $NaHCO_3$ (pH 9.2–9.4) to a 96-well Nunc-MaxiSorp plate. In order to test the reactivity against the target protein, a recombinant expressed human PCSK9 ("huPCSK9-V5-His", AFFiRiS AG) was coated in 1× PBS. Free binding sites were blocked by the incubation with blocking buffer (1× PBS, 1% BSA) for 1 h at 37°C. Diluted plasma (1:400 and 1:100 in 1× PBS/0.1% BSA/0.1% Tween-20 for peptide and protein ELISA, respectively) were added, serially diluted 1:2, and incubated for 1 hour at 37°C. Each ELISA plate contained a standard antibody as internal control. For the detection, biotinylated anti-mu IgG (H + L) (Southern Biotech.; 1:2000) in 1× PBS/0.1% BSA/0.1% Tween-20 was applied and incubated for 1 h at 37°C. As a next step, horseradish peroxidase coupled to streptavidin (Roche) was added (30 min, 37°C) followed by the addition of the substrate 2,2'-Azinobis [3-ethylbenzothiazoline-6-sulfonic acid]-diammonium salt (ABTS) (Bio-Chemica, AppliChem) (30 min, RT). The optical density (OD) at 405 nm was measured with a microwell plate

reader (Sunrise, Tecan, Switzerland) and the titres were defined as the dilution factor referring to 50% of the maximal optical density ($OD_{max}/2$). The mean titres ± SEM of all animals per group are presented.

PCSK9 protein level in circulation

The plasma muPCSK9 concentration was determined by CircuLex muPCSK9 ELISA (CircuLex, Cy-8078, MBL), according to the manufacturer's protocol.

Plasma lipids and lipoprotein analysis

Plasma TC and TG were determined by the "Cholesterol CHOD-PAP" and "Triglycerides GPO-PAP" kit, respectively (Roche/Hitachi). Lipoprotein profiles for TC were measured after lipoprotein separation by fast protein liquid chromatography (FPLC) (16).

SAA measurements

Plasma SAA levels were measured at t=4, 8, 12, and 16 weeks after the onset of WTD, 0.1% cholesterol and 7 weeks before, as a reference value on normal chow diet. The ELISA kit of Tridelta Development Limited was used and analyses were performed according to manufacturer's protocol.

Immunological analyses

Myriad RBM's mouse inflammation multi analyte profile (Mouse Inflammation MAP® v.1.0) was used for quantitative analysis of multiple inflammatory analytes and pathways including cytokines, chemokines, and growth factors.

Histological assessment of atherosclerosis

Atherosclerotic lesion area and severity were assessed in the aortic root area, as reported previously (22). Briefly, the aortic root was identified by the appearance of aortic valve leaflets, and serial cross-sections of the entire aortic root area (5 µm thick with intervals of 50 µm) were mounted on 3-aminopropyl triethoxysilane-coated slides and stained with haematoxylin-phloxine-saffron (HPS). For each mouse, the lesion area was measured in 4 subsequent sections. Each section consisted of 3 segments (separated by the valves). For determination of atherosclerotic lesion size and severity, the lesions were classified into five categories according to the American Heart Association (AHA) criteria (23): type I (early fatty streak), type II (regular fatty streak), type III (mild plaque), type IV (moderate plaque), and type V (severe plaque). Images were taken with an Olympus BX 51 microscope, and areas were measured with Olympus analySIS image processing software cell^D. The total lesion area and number of lesions were calculated per cross-section. Lesion severity was calculated as relative amount of type I-V lesions in which the lesion-free segments are included. From this, the relative amounts of lesion-free segments and diseased segments were calculated, and the relative amount of diseased segments was further subdivided

into type I–V lesions, where types I-III refer to mild, and types IV-V to severe lesions. Lesion composition of type IV and V lesions was assessed after double immunostaining with anti-α smooth muscle actin (1:400; PROGEN Biotechnik GmbH, Germany) for α smooth muscle cells (αSMC), and anti-mouse MAC-3 (1:200; BD Pharmingen, the Netherlands) for macrophages. Sirius red staining was performed to assess collagen content. The necrotic area and cholesterol clefts were measured in the HPS-stained slides. Lesion stability index, as the ratio of collagen and αSMC area (i.e. stabilization factors) to macrophage and necrotic area (i.e. destabilisation factors) was calculated as described previously (18,22). In each segment used for lesion quantification, intracellular adhesion molecule 1 (ICAM-1) expression, NLR family pyrin domain containing 3 (NLRP3) expression, and the number of monocytes adhering to the endothelium were counted after immunostaining with mouse monoclonal antibody to ICAM-1 (1:400; Santa Cruz Biotechnology, Dallas, USA), rabbit polyclonal antibody to NLRP3 (1:400; Abcam, Cambridge, UK), and AIA 31240 antibody (1:500; Accurate Chemical and Scientific, New York, USA) respectively (24).

Statistical and correlation analysis

All values were evaluated for homoscedasticity and normality assumption using both Kolmogorov–Smirnov and Shapiro–Wilk normality tests. For the comparison of two groups, the unpaired two-tailed Student's t-test was used, followed by the Mann–Whitney correction for non-parametric data as indicated in the respective figure legend. A Spearman's rank-order correlation was used to determine the relation between two parameters. The software used for statistical analyses were IBM SPSS Statistics version 18. All data are presented as mean ± SD unless stated otherwise. The p-values ≤ 0.05 was considered statistically significant.

Results

AT04A induces a strong and persistent immune response and decreases plasma PCSK9 levels

APOE*3-Leiden.CETP mice were used as a model for atherosclerosis with a pro-inflammatory plaque phenotype that can be induced upon a high fat and cholesterol-containing diet. A peptide (AFFITOPE®) which was previously designed to mimic the N-terminal epitope of the mature human and homolog mouse PCSK9 protein (153aa-692aa) was formulated into the AT04A vaccine (20). The mice were immunized with AT04A and control vaccine five times in bi-weekly intervals, and an 18-week WTD was started 4 weeks after prime immunization, which refers to time point t=0 weeks (**Figure 1 and 2).** Titre analyses over time revealed that AT04A was able to induce a specific and long-lasting immune response against PCSK9, which reached a maximum mean titre of 1/12 243 ($OD_{max}/2$) 12 weeks after prime immunization, which corresponds to t=8 weeks of WTD. The immune response to

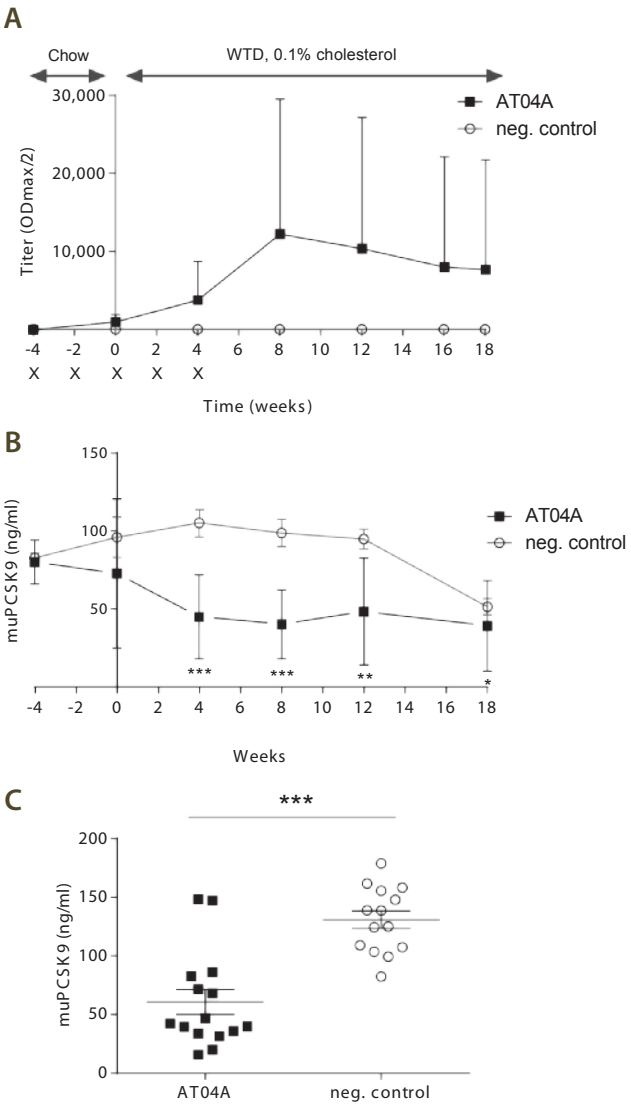

Figure 2 AT04A immunization induces a high and long-lasting immune response, and decreases plasma muPCSK9 levels. Antibody titres were assessed at different time points throughout the study. Crosses indicate the time points of the bi-weekly immunizations of control and AT04A vaccine (A). The muPCSK9 plasma concentration was determined at different time points throughout the study and compared to control (B–C). To compare AT04A and control treated group, the unpaired two-tailed Student's t-test was used, followed by the Mann–Whitney correction for non-parametric data. Data are presented as group means ± SD (n=15).*p<0.05, ***p<0.001.

PCSK9 highly varies between individual mice and no statistically significant differences in titres of t=4 to 18 weeks were found (**Figure 2A**). As expected, control immunized mice did not show any immune response against PCSK9 (**Figure 2A**). As evidence for a direct interaction between the induced anti-PCSK9 antibodies and the target protein, the plasma concentration of muPCSK9 in AT04A-treated vs. control immunized mice was determined over time (**Figure 2B and C**). At the immunization start (t=−4 weeks) the PCSK9 level in AT04A and control treated group was comparable. However, in t=4, 8, 12 and 18 AT04A vaccine treated mice showed a highly significant decrease in PCSK9 concentration of 57, 59, 49, and 24%, respectively ($p<0.001$, $p<0.001$, $p=0.001$, and $p=0.029$, respectively) (**Figure 2B**) demonstrating a consistent and long-lasting effectiveness of the AT04A vaccine (**Figure 2C**). Due to unknown reasons, the plasma PCSK9 level of control treated mice dropped in t=18 weeks, however, the difference between AT04A and control treated mice remained significant (**Figure 2B**).

AT04A decreases plasma TC and non-HDL-C levels in APOE*3-Leiden.CETP mice

Four weeks after the cholesterol-containing WTD was initiated, control immunized APOE*3-Leiden.CETP mice showed a strong increase of plasma TC level from 3.4 mmol/L (t=0 weeks) to 15.5 mmol/L (t=4 weeks), which remained elevated until t=18 weeks (12.1 mmol/L) (**Figure 3A**). In contrast, in the AT04A immunized mice a sustained reduction of plasma TC from t=0 weeks (2.8 mmol/L, $p=0.002$) to t=18 weeks (7.8 mmol/L, $p=0.002$) was observed (**Figure 3A**). Thus, cholesterol exposure over the whole time period of atherosclerosis inducing WTD (t=0 to 18 weeks) was decreased by 53% ($p<0.001$) in AT04A vs. control-treated mice (**Figure 3B**). The TC lipoprotein profile of pooled plasmas per group was determined by FPLC (**Figure 3C–F**). Plasma levels of HDL-C remained unaffected by AT04A vaccination, however the levels of non-HDL-C (VLDL and LDL) were clearly reduced (**Figure 3F–H**), indicating that the anti-PCSK9 vaccine may be a powerful therapeutic approach for long-term non-HDL-C/LDL-C management. A strong positive correlation between TC and plasma PCSK9 concentration was found ($R^2=0.75$; $p<0.001$) suggesting a specific and effective targeting of PCSK9 by AT04A vaccine.

AT04A reduces number, size, and severity of atherosclerotic lesions in the aorta

In order to assess the effect of AT04A on atherosclerotic development upon 18 weeks of WTD, the aortic root was isolated and the lesions as well as the lesion severity were determined. AT04A vaccine-treated mice showed a significantly reduced lesion area (−64%, $p=0.004$) (**Figure 4A**) and number of lesions per cross-section (−35%, $p=0.037$) (**Figure 4B**), compared with controls. Moreover, in AT04A-vaccinated mice a significant higher percentage of lesion-free area per section (+119%, $p=0.026$) was detected (**Figure 4C**). The lesion severity was categorized according to the American Heart Association guidelines

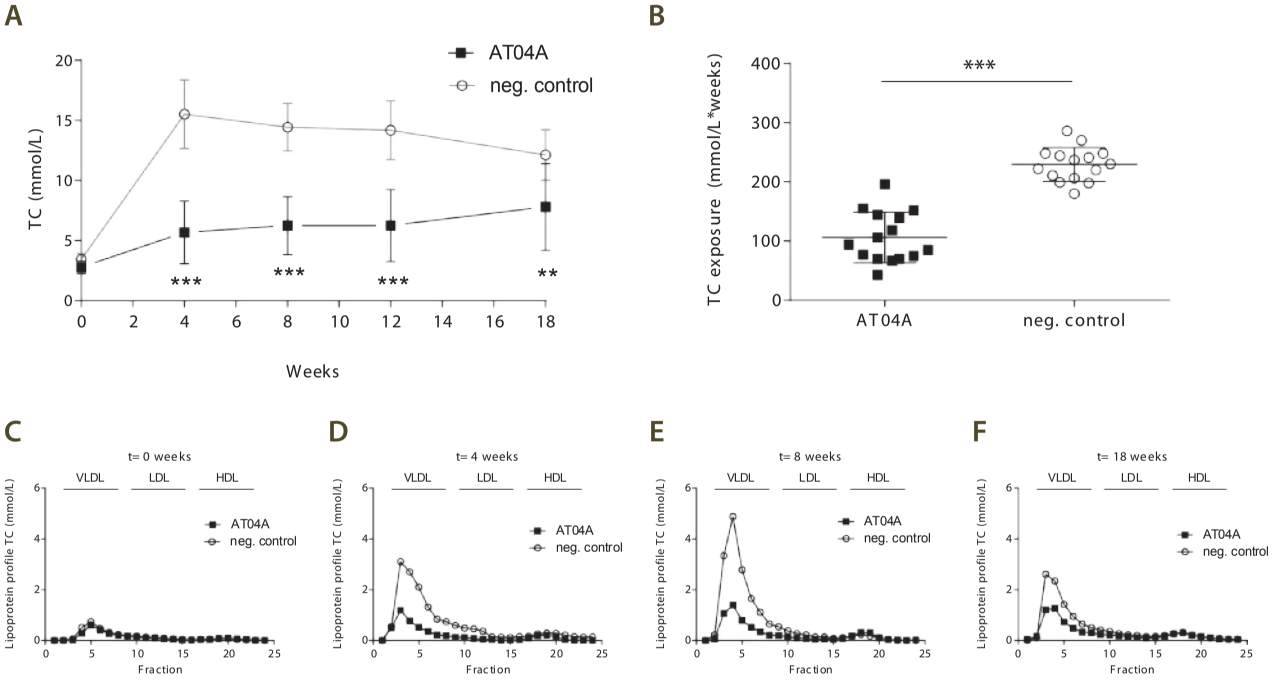

Figure 3 AT04A immunization decreases plasma TC and non-HDL-C. Plasma cholesterol levels were measured at various time points throughout the study (A) and TC exposure (mmol/L*weeks) was calculated (B). Plasma was pooled per group and the distribution of cholesterol over the individual lipoproteins was determined after separation by FPLC (C–F). To compare AT04A and control treated group, the unpaired two-tailed Student's t-test was used, followed by the Mann–Whitney correction for non-parametric data. Data are presented as group means ± SD (n=15). **p<0.01, ***p<0.001. Abbreviations: TC, total cholesterol, FPLC, fast protein liquid chromatography.

(23). Although the relative amount of mild lesions (type I–III) was similarly distributed between AT04A and control immunized mice, the more severe lesions (type IV–V) were decreased in AT04A treated mice (−64%, p=0.051) (**Figure 4C**). Representative images of the differently categorized atherosclerotic lesions in the aortic root of AT04A and control immunized mice are depicted in **Figure 4D**. A strong positive correlation between the atherosclerotic lesion area and plasma TC as well as plasma PCSK9 levels was observed (R^2=0.75, p<0.001 and R^2=0.6, p=0.001, respectively).

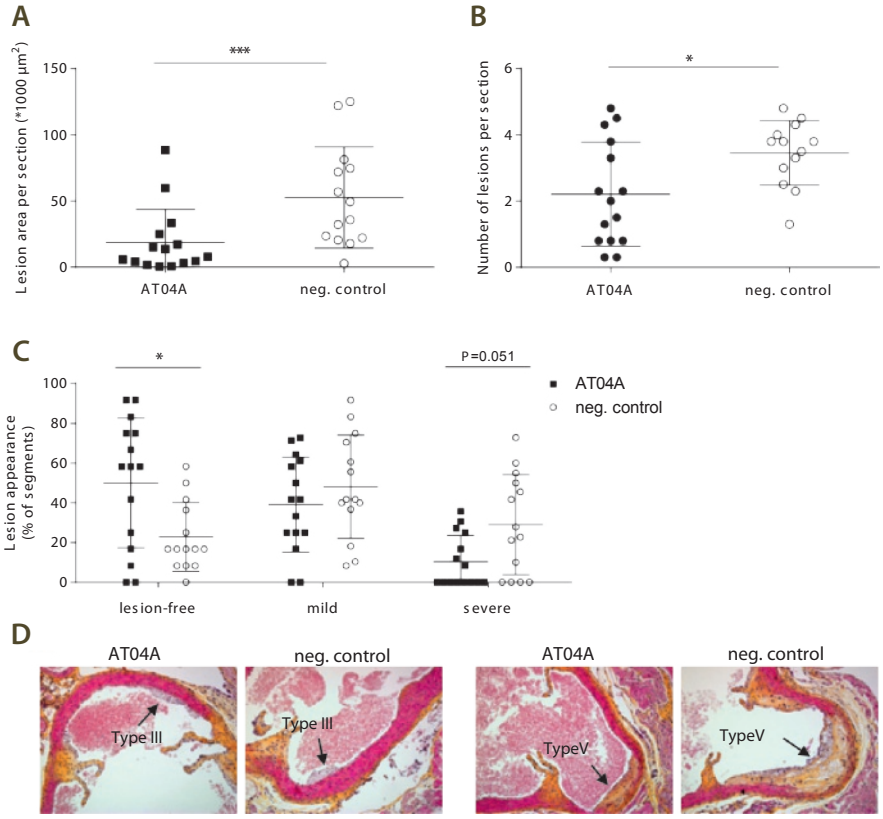

Figure 4 AT04A immunization decreases lesion size and severity. After 18 weeks of treatment, lesion area (A), number of lesions (B), and lesion severity (C) were determined per cross-section in the aortic sinus. Due to a technical error one mouse of the control group was excluded from analysis. Lesion severity was classified as mild (type I–III) or severe (type IV–V). Representative images of HPS-stained type III and V lesions in a cross-section (D). A Mann–Whitney U test was used for statistical analysis. Data are presented as group means ± SD (n=14–15). *p<0.05, **p<0.01. Abbreviations: HPS, haematoxylin-phloxine-saffron.

AT04A immunization reduces necrotic core content

The effects of AT04A vaccination on the plaque composition of severe lesions (type IV–V) were assessed by immunohistochemistry. The necrotic core areas including cholesterol clefts and lesion macrophages were quantified as pro-inflammatory factors, and αSMCs in the fibrotic cap and collagen area as fortifying factors (**Figure 5A**). Representative images are shown in **Figure 5B**. All data are expressed as percentages of total plaque areas. In AT04A-treated mice the necrotic core area was 1.9 vs. 8.1% in the control-treated group, representing a reduction of 77% (**Figure 5A**) (p=0.001). Macrophage, αSMCs, and collagen content were not significantly altered by AT04A treatment. Despite the decrease in necrotic core content, the plaque stability index was not changed, and was 2.3 in control and 3.0 in AT04A treated mice.

AT04A reduces vascular inflammation

Since atherosclerosis is not only a lipid-driven disease, but also a chronic low-grade inflammatory disease of the vessel wall, the number of monocytes adhering to the activated endothelium, the expression of the adhesion molecule ICAM-1 in the endothelium as well as the expression of the caspase-1-activating inflammasome protein NLRP3 in macrophages was determined in the diseased aortic root area. In the control group 2.3 monocytes per cross-section were counted, compared with 1.4 in the AT04A-treated group (–38%, p=0.014) (**Figure 6A**). The reduction in monocyte adherence was reinforced by a similar significant decrease in ICAM-1 expression in endothelial cells upon AT04A vaccination (–37%, p=0.018) (**Figure 6B and C**). Since NLRP3 is predominantly expressed by myeloid cells, we determined the amount of NLRP3 expression in the macrophage area and a decrease by 68% in AT04A compared with control treated mice was observed (0.3 ± 0.2 vs. 0.9 ± 0.8, p=0.06) (**Figure 6D and E**). Together, these findings suggest that AT04A immunization results in a reduction of activated endothelial cells and pro-inflammatory macrophages.

AT04A decreases inflammatory biomarkers

In order to assess system inflammation upon high-fat diet-induced atherosclerosis in APOE*3-Leiden.CETP mice, a panel of plasma inflammatory markers was analysed. The liver-derived inflammation marker SAA, reported to be elevated in diet-induced atherosclerosis in mice (25), showed a significant reduction in anti-PCSK9 AT04A treated mice at t=4 weeks (–21%; p=0.007) and t=8 weeks (–28%; p<0.001) relative to the negative control, but was not significantly affected later in the study (**Figure 7**). Myriad RBM's mouse inflammation multi-analyte profile represents a comprehensive and quantitative analysis of multiple inflammatory biomarkers and pathways including cytokines, chemokines, and growth factors. In plasma obtained 18 weeks after the start of WTD, 4 markers, namely macrophage inflammatory protein-1β (MIP-1β/CCL4), macrophage-derived chemokine (MDC/CCL22), the cytokine stem cell factor (SCF), and vascular endothelial growth factor

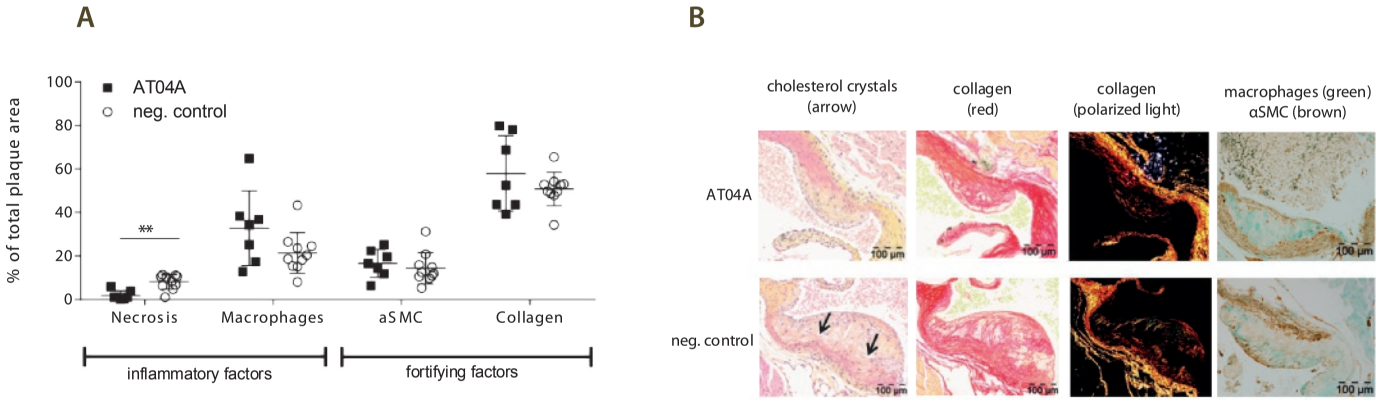

Figure 5 AT04A immunization reduces necrotic content and cholesterol crystals in plaques. Necrotic and macrophage content as unstable factors, and αSMCs and collagen as stable factors, were determined in the severe (type IV–V) lesions, and expressed as percentage of total plaque area. 10 mice in the control and 7 in vaccine group had severe lesions and were included in this analysis (A). Representative images of HPS staining, Sirius red staining for collagen, collagen expression under polarized light and double immunostaining with α-actin for αSMCs (brown) and MAC-3 for macrophages (green) (B). The arrows depict necrotic areas, including cholesterol clefts. A Mann–Whitney U test was used for statistical analysis. Data are presented as group means ± SD (n=7–10). **p<0.01. Abbreviations: αSMCs, α-smooth-muscle-cells; MAC-3, purified anti-mouse CD107b.

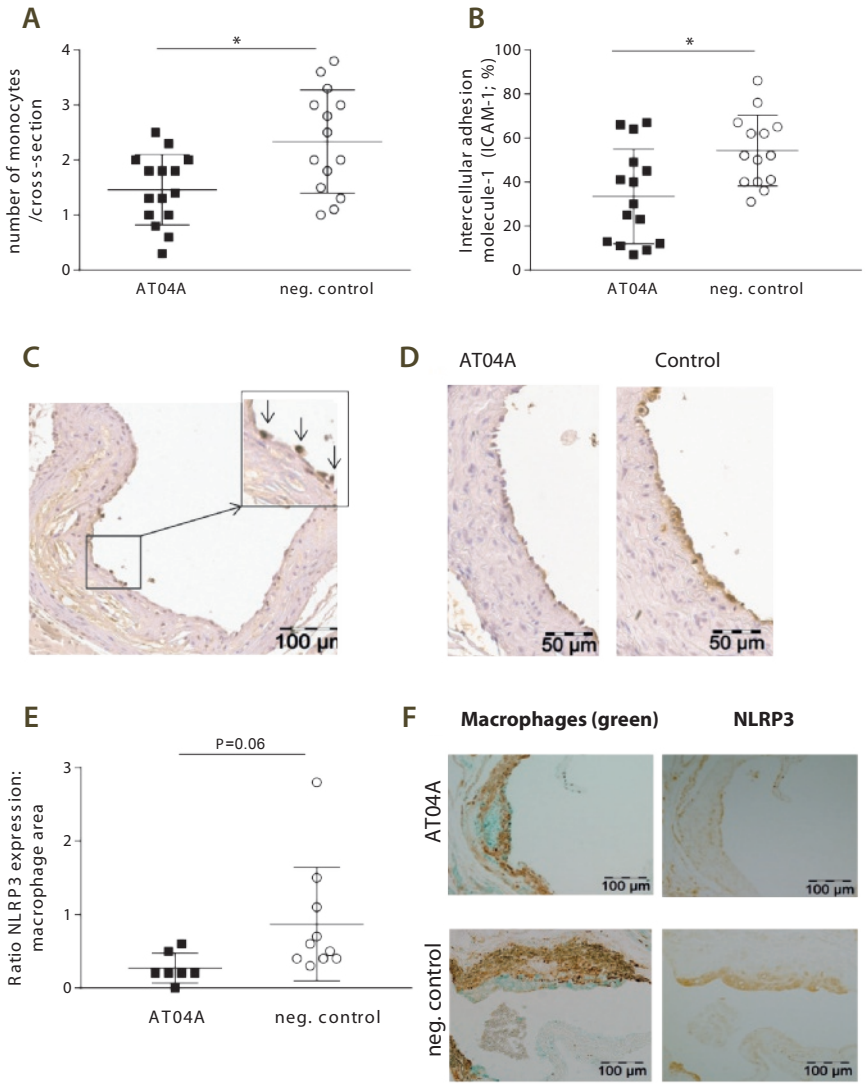

Figure 6 AT04A immunization reduces the number of monocytes adhering to the endothelium, ICAM-1 expression and NLRP3 expression in macrophages. (A) The number of monocytes was counted per cross-section after staining with AIA 31240 and (B) endothelial ICAM-1 was determined as percentage of the endothelial surface in the cross-sections and (C-D) a representative image is shown. (E) NLRP3 expression was determined in the severe (type IV–V) lesions after immune staining with anti-NLRP3 antibodies and the amount of NLRP3 expression in the macrophage area was calculated. (F) Photographs of atherosclerotic plaques stained with αSMC (brown), macrophages (green) and NLRP3 (brown). Data are presented as means ± SD (n=14–15 in A–B, n=7–10 in D). *p<0.05.

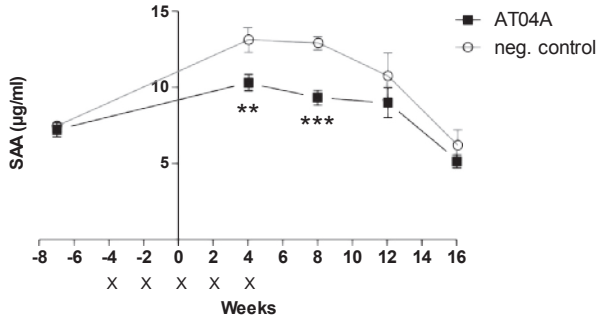

Figure 7 The liver-derived inflammation marker SAA was measured over time. SAA concentrations were assessed at t=-7, 4, 8, 12 and 16 weeks after the initiation of WTD, 0.1% cholesterol. A Mann-Whitney U-test was used for statistical analysis. Data are presented as group means ± SD (n=15). **p<0.01, ***p<0.001. Abbreviations: SAA serum A amyloid; WTD, Western type diet.

A (VEGF-A), showed a significant reduction in AT04A compared with control-immunized mice whereas the decreases in SCF was most pronounced (**Table 1**). Furthermore, the macrophage colony stimulating factor 1 (M-CSF-1) and monocyte chemotactic protein 5 (MCP-5/CCL12) tended to be decreased (**Table 1**). A Spearman's test showed a strong, positive correlation between TC and SCF (R^2=0.65; p<0.001) and VEGF-A (R^2=0.58; p=0.001), but not for TC and MIP-1β/CCL4 (R^2=0.02; p=0.93) and MDC/CCL22 (R^2=0.26; p=0.18).

Safety aspects

No effects on viability, body weight, or food intake were found in the AT04A-compared with control-immunized mice (**Table 2**) Liver weight, which is considered as a sensitive indicator for toxicity, was not affected by AT04A vaccine-treated mice (**Table 2**). Moreover, plasma pooled per group showed no apparent differences in AST and ALT values as markers of hepatocellular damage (**Table 2**) Other safety aspects such as absence of target-specific T-cell response and absence of cross-reactivity of induced antibodies with other endogenous proteins have been previously reported by Galabova et al (20).

Table 1 Quantitative analyses of multiple inflammatory biomarkers using the Myriad RBM mouse inflammation multi-analyte profile

Marker*1	Neg. control		AT04A		AT04A vs control
	Mean (n=15)	SD	Mean (n=15)	SD	p-value
SCF (pg/mL)	1097.0	235.1	760.6	196.9	0.0002
VEGF-A (pg/mL)	549.1	66.5	246.8	75.5	0,0304
MIP-1 beta (pg/mL)	229.6	60.6	174.0	70.9	0.0319
MDC (pg/mL)	395.5	132.9	308.5	56.5	0.0397
M-CSF-1 (ng/mL)	9.3	1.6	8.2	1.0	0.0533
MCP-5 (pg/mL)	19.9	5.3	16.4	5.1	0.0552
IP-10 (ng/mL)	105.9	22.7	92.0	26.7	0.0848
MIP-3 beta (pg/mL)	3.6	1.3	3.0	0.8	0.1190
TIMP-1 Mouse (ng/mL)	1.7	0.8	1.4	0.3	0.2101
IL-18 (ng/mL)	34.5	12.4	35.1	7.9	0.2576
EGF Mouse (pg/mL)	189.7	30.1	179.7	17.2	0.3605
MCP-1 (pg/mL)	117.7	40.3	112.4	32.3	0.4427
MIP-1 alpha (pg/mL)	7.5	0.9	7.7	2.7	0.5066
MCP-3 (pg/mL)	215.7	83.7	207.2	37.1	0.6186
Thrombopoietin (ng/mL)	48.2	6.8	43.4	12.2	0,7400
IL-1 beta (ng/mL)	12.7	2.4	12.0	2.1	0.7996
Eotaxin (pg/mL)	434.0	90.8	450.7	138.0	0.8034

*1 the inflammatory markers FGF-9, FGF-basic, GM-CSF, KC/GRO, INF-gamma, IL-1 alpha, IL-2, IL-3, IL-4, IL-5, IL-6, IL-7, IL-10, IL-11, IL-12, IL-17A, LIF, MIP-2, OSM, TNF-alpha were measured, but were either below the limit of detection or the limit of quantification.

Table 2 Safety aspects of PCSK9 immunisation

	Body weight	Food intake	Liver weight	ALT	AST
	gram	*gram/mouse/day*	*gram*	*U/L*	*U/L*
Baseline	22.5 ± 1.2	3.4 ± 0.1	NA	80	141
Control	25.2 ± 2.7	2.7 ± 0.2	1.5 ± 0.4	69	251
AT04A	25.6 ± 2.8	2.5 ± 0.1	1.4 ± 0.3	74	289

No differences in body weight, food intake (per cage), liver weight, plasma ALT (pooled per group), and plasma AST (pooled per group) between the control and AT04A group at sacrifice (t=18 weeks). Data are presented as group means ± SD (n=14-15). Abbreviations: alanine transaminase (ALT), aspartate transaminase (AST).

Discussion

The present study shows that active immunization against PCSK9 with the so-called AT04A peptide-based vaccine elicits antibodies that effectively bind and remove PCSK9 from the circulation and reduce circulating TC, (V)LDL-C, TG, and biomarkers of inflammation, which is accompanied by reduction of vascular inflammation and atherosclerotic lesions and plaques in the aortas of a mouse model of atherosclerosis.

PCSK9 plays a fundamental role in LDL metabolism through the binding and degradation of LDLR. With respect to LDL-C as one of the major risk factors positively correlated with premature development of CVD (1), PCSK9 inhibition is supposed to reduce atherosclerotic events. Recently, the human PCSK9 mAbs evolocumab and alirocumab reached FDA approval and were recommended in the 2016 ESC/EAS Guidelines (14) as second line treatment for high LDL-C for adults whose cholesterol is not adequately controlled by diet or statin treatment. However, whereas both mAbs reduced the incidence of cardiovascular events in a post-hoc exploratory analysis, trial results whether anti-PCSK9 mAb therapy actually reduces atherosclerotic burden and CVD events is still under investigation (13).

The main limitation for mAb therapies with broader applications certainly is that their use for chronic disorders is cost-prohibitive. Moreover, it has been reported that a substantial proportion of patients undergoing a sustained treatment with mAbs lose responsiveness over time due to the induction of anti-drug antibodies (26). Thus, an appealing new alternative to mAb-based therapies is the active immunization against self-antigens involved in chronical disorders (27,28).

Previously, we showed that our AFFITOPE®-based anti-PCSK9 active immunization approach is able to induce a strong humoral immune response against PCSK9, which persisted for up to one year in vaccinated mice (20). Furthermore, TC concentration was reduced by up to 30% and LDL-C up to 50% in anti-PCSK9 immunized compared with control mice. Immunization against PCSK9 has also been tested by others using different approaches (29). In the first approach, human recombinant PCSK9, along with a DNA oligonucleotide as an adjuvant, was tested and found to induce an approximately 40% reduction of LDL-C in mice (30). Crossey et al.(29) designed a human PCSK9 vaccine where PCSK9 peptides are displayed at high valency on the surface of a bacteriophage virus-like particle, resulting in a ~55% reduction of TC relative to controls.

However, the present study is the first to show that active immunization against PCSK9 does not only reduce TC and (V)LDL-C, but also has an impact on systemic and vascular inflammation and atherosclerotic development in a mouse model of diet-induced atherosclerosis. Vaccination with AT04A, which led to a reduction of TC exposure by 53%, had a strong impact on atherosclerotic development. The AT04A vaccine was able to induce a specific immune response against PCSK9. In contrast to previously reported studies where an anti-PCSK9 peptide vaccine (20) as well as monoclonal anti-PCSK9 antibodies (19) rather stabilized the target protein and increased the murine plasma PCSK9

level, AT04A-treated APOE*3-Leiden.CETP mice showed a reduction of the target protein exposure during the study by 48%. Already after the second immunization with AT04A vaccine the induced anti-PCSK9 antibody concentration was sufficient to significantly decrease TC in APOE*3-Leiden.CETP mice on normal chow (t=0 weeks). Four weeks after the onset of WTD the anti-PCSK9 titre in AT04A-vaccinated mice rose to approximately 1/4000, corresponding to an antibody concentration of ~200 µg/mL, and resulted in a TC decrease of 63% compared with control ($p<0.001$). Although the mean anti-PCSK9 titre reached its maximum in week 8, no additional TC lowering was found at this timepoint, indicating a plateau effect after 4 weeks with maximally retained efficacy during the study. Due to this sustained TC reduction, anti-PCSK9 vaccine-treated mice showed significantly less lesion areas (–64%, $p=0.004$) and severity (–64%, $p=0.051$) in the aortic root compared with control. Consistent with our data, Kühnast et al. (18) reported a dose-dependent decrease in atherosclerosis development in APOE*3-Leiden.CETP mice treated with the human PCSK9 monoclonal antibody alirocumab. Notably, the AT04A vaccination was applied as a stand-alone therapy and thus, future evaluations are required to test whether these effects are still ensured on a statin background treatment.

For many years, atherosclerosis was considered to be mainly a lipid-driven disease caused by the continuous accumulation of cholesterol in the arterial intima. However, it is increasingly recognized that atherosclerosis is predominately a chronic low-grade inflammatory disease of the vessel wall with an interplay of humoral, cellular, and locally produced pro-inflammatory factors (31,32). One of the initial stages of atherosclerotic disease is endothelial cell activation and the recruitment of inflammatory cells to the vessel wall (31,32). Multi-analyte profiling of inflammatory markers showed a reduction of several cytokines with chemotactic activity for monocytes by AT04A vaccine (**Table 1**) which is in line with the reduced expression of endothelial ICAM-1 and adherence of monocytes to the vessel wall. The decreased levels of M-CSF-1 and VEGF-A, which activate endothelial cells and stimulate monocyte/macrophage migration, may have additionally contributed to the reduction in lesion number and size.

Interestingly, despite the reduced monocyte adherence, the macrophage content was not affected by AT04A immunization. A potential explanation is that the amount of macrophages is similar but that the macrophages in the control group are more activated and overloaded with cholesterol which may result in damage and necrosis. The necrotic core is a major characteristic of advanced atherosclerotic lesions and plays an important role in both their progression to a hazardous state and their vulnerability (33). To test this hypothesis, we measured the necrotic core and NLRP3 as marker of macrophage activation. Morphological analysis indicated that vaccination with AT04A strongly decreased the necrotic core content, including cholesterol clefts, by 77%. Overload of lipid material in the vessel wall leads to apoptosis and necrosis of foam cells (34), and to deposition of cholesterol crystals (35,36), which stimulate caspase-1-activating NLRP3 inflammasomes and aggravate the inflammatory response (35,37). Indeed NLRP3

expression in the macrophage area was three-fold increased in the control mice as compared to the AT04-treated mice, which substantiates this hypothesis. Collectively, these data indicate that immunization with AT04A diminishes the formation of a necrotic core and macrophage inflammation, which may have contributed to the reduced inflammatory response in the vessel wall and attenuation of atherosclerotic development.

Little is known about the pro-inflammatory role of PCSK9. Inflammatory cytokines were measured in the plasma from septic shock patients carrying either a PCSK9 LOF allele or a PCSK9 GOF allele. Significantly lower plasma cytokine concentrations in patients carrying a LOF allele were found (38). These results mirrored the data obtained from PCSK9 knockout mice, which displayed decreases in inflammatory cytokine production in response to LPS (38). It was also reported that PCSK9 of macrophage origin directly promotes lesion inflammation in mice, independently of systemic lipid changes. PCSK9 accumulated in the artery wall induced infiltration of pro-inflammatory $Ly6C^{High}$ monocytes into the atherosclerotic lesion, indicating a local effect of human PCSK9 on atherosclerotic lesion composition (39). Thus, lowering of plasma PCSK9 levels per se may also have direct local effects on vascular inflammation and atherosclerotic plaque formation. Unfortunately, we were not able to examine the local effects of PCSK9 in aortic plaques due to known technical limitations (40).

The current challenge for the prevention of atherosclerotic events is certainly the side-effect free lowering of lifetime LDL-C exposure, thus preventing chronic low-grade inflammatory disease of the vessel walls. The association between the change in relative risk for CHD and the absolute change in LDL-C levels over lifetime due to genetic variation has recently been emphasized (41).

The AT04A anti-PCSK9 vaccine would be an ideal therapeutic agent to fulfill these requirements for long-term LDL-C management, because of its sustained efficacy and cost-effective application, accompanied by anti-inflammatory effects. AT04A is currently being tested in a phase I clinical trial.

Acknowledgments

We thank O. Otava for statistical analyses and J. Hutchins for correcting the scientific English.

Disclosures

AT04A is a product invented and developed by AFFiRiS which is currently under trial. C.L., C.J., G.S. and G.G. are employees of AFFiRiS. J.W.A.v.d.H., E.J.P. and H.M.G.P. are employees of TNO during the conduct of this work. TNO performed this study partially as fee-for-service work funded by AFFiRiS. J.W.J. received research grants from and was speaker on (CME-accredited) meetings sponsored by Amgen, Astellas, Astra-Zeneca, Biotronik, Boston Scientific, Daiichi Sankyo, Lilly, Genzyme, Medtronic, Merck-Schering-Plough, Pfizer, Orbus Neich, Novartis, Roche, Servier, Sanofi-Aventis, the Netherlands Heart Foundation, the Interuniversity Cardiology Institute of the Netherlands, and the European Community Framework KP7 Program.

References

1. Yusuf S, Hawken S, Ounpuu S, et al. Effect of potentially modifiable risk factors associated with myocardial infarction in 52 countries (the INTERHEART study): case-control study. Lancet (London, England). 2004 Sep;364(9438):937–52.
2. Brown MS, Goldstein JL. A receptor-mediated pathway for cholesterol homeostasis. Science. 1986 Apr;232(4746):34–47.
3. Ishibashi S, Brown MS, Goldstein JL, et al. Hypercholesterolemia in low density lipoprotein receptor knockout mice and its reversal by adenovirus-mediated gene delivery. J Clin Invest. 1993 Aug;92(2):883–93.
4. Poirier S, Mayer G, Benjannet S, et al. The proprotein convertase PCSK9 induces the degradation of low density lipoprotein receptor (LDLR) and its closest family members VLDLR and ApoER2. J Biol Chem. 2008 Jan;283(4):2363–72.
5. Zhang D-W, Lagace TA, Garuti R, et al. Binding of proprotein convertase subtilisin/kexin type 9 to epidermal growth factor-like repeat A of low density lipoprotein receptor decreases receptor recycling and increases degradation. J Biol Chem. 2007 Jun;282(25):18602–12.
6. Ference BA, Majeed F, Penumetcha R, et al. Effect of naturally random allocation to lower low-density lipoprotein cholesterol on the risk of coronary heart disease mediated by polymorphisms in NPC1L1, HMGCR, or both: a 2 x 2 factorial Mendelian randomization study. J Am Coll Cardiol. 2015 Apr;65(15):1552–61.
7. Law MR, Wald NJ, Rudnicka AR. Quantifying effect of statins on low density lipoprotein cholesterol, ischaemic heart disease, and stroke: systematic review and meta-analysis. BMJ. 2003 Jun;326(7404):1423.
8. Chong PH, Bachenheimer BS. Current, new and future treatments in dyslipidaemia and atherosclerosis. Drugs. 2000 Jul;60(1):55–93.
9. Waters DD, Brotons C, Chiang C-W, et al. Lipid treatment assessment project 2: a multinational survey to evaluate the proportion of patients achieving low-density lipoprotein cholesterol goals. Circulation. 2009 Jul;120(1):28–34.
10. Beltowski J, Wojcicka G, Jamroz-Wisniewska A. Adverse effects of statins - mechanisms and consequences. Curr Drug Saf. 2009 Sep;4(3):209–28.
11. Taylor BA, Thompson PD. Statins and Their Effect on PCSK9-Impact and Clinical Relevance. Curr Atheroscler Rep. 2016 Aug;18(8):46.
12. Robinson JG, Farnier M, Krempf M, et al. Efficacy and safety of alirocumab in reducing lipids and cardiovascular events. N Engl J Med. 2015 Apr;372(16):1489–99.
13. Sabatine MS, Giugliano RP, Wiviott SD, et al. Efficacy and safety of evolocumab in reducing lipids and cardiovascular events. N Engl J Med. 2015 Apr;372(16):1500–9.
14. Catapano AL, Graham I, De Backer G, et al. 2016 ESC/EAS Guidelines for the Management of Dyslipidaemias. Eur Heart J. 2016 Oct;37(39):2999–3058.
15. Lloyd-Jones DM, Morris PB, Ballantyne CM, et al. 2016 ACC Expert Consensus Decision Pathway on the Role of Non-Statin Therapies for LDL-Cholesterol Lowering in the Management of Atherosclerotic Cardiovascular Disease Risk: A Report of the American College of Cardiology Task Force on Clinical Expert Cons. J Am Coll Cardiol. 2016 Jul;68(1):92–125.
16. Westerterp M, van der Hoogt CC, de Haan W, et al. Cholesteryl ester transfer protein decreases high-density lipoprotein and severely aggravates atherosclerosis in APOE*3-Leiden mice. Arterioscler Thromb Vasc Biol. 2006 Nov;26(11):2552–9.
17. de Haan W, van der Hoogt CC, Westerterp M, et al. Atorvastatin increases HDL cholesterol by reducing CETP expression in cholesterol-fed APOE*3-Leiden.CETP mice. Atherosclerosis. 2008 Mar;197(1):57–63.
18. Kuhnast S, van der Hoorn JWA, Pieterman EJ, et al. Alirocumab inhibits atherosclerosis, improves the plaque morphology, and enhances the effects of a statin. J Lipid Res. 2014 Oct;55(10):2103–12.
19. Ason B, van der Hoorn JWA, Chan J, et al. PCSK9 inhibition fails to alter hepatic LDLR, circulating cholesterol, and atherosclerosis in the absence of ApoE. J Lipid Res. 2014 Nov;55(11):2370–9.
20. Galabova G, Brunner S, Winsauer G, et al. Peptide-based anti-PCSK9 vaccines - an approach for long-term LDLc management. PLoS One. 2014;9(12):e114469.
21. Schneeberger A, Mandler M, Mattner F, et al. AFFITOME(R) technology in neurodegenerative diseases: the doubling advantage. Hum Vaccin. 2010 Nov;6(11):948–52.

22. Kuhnast S, van der Hoorn JWA, van den Hoek AM, et al. Aliskiren inhibits atherosclerosis development and improves plaque stability in APOE*3Leiden.CETP transgenic mice with or without treatment with atorvastatin. J Hypertens. 2012 Jan;30(1):107–16.
23. Stary HC, Chandler AB, Dinsmore RE, et al. A definition of advanced types of atherosclerotic lesions and a histological classification of atherosclerosis. A report from the Committee on Vascular Lesions of the Council on Arteriosclerosis, American Heart Association. Circulation. 1995 Sep;92(5):1355–74.
24. Kooistra T, Verschuren L, de Vries-van der Weij J, et al. Fenofibrate reduces atherogenesis in ApoE*3Leiden mice: evidence for multiple antiatherogenic effects besides lowering plasma cholesterol. Arterioscler Thromb Vasc Biol. 2006 Oct;26(10):2322–30.
25. Lewis KE, Kirk EA, McDonald TO, et al. Increase in serum amyloid a evoked by dietary cholesterol is associated with increased atherosclerosis in mice. Circulation. 2004 Aug;110(5):540–5.
26. Bartelds GM, Krieckaert CLM, Nurmohamed MT, et al. Development of antidrug antibodies against adalimumab and association with disease activity and treatment failure during long-term follow-up. JAMA. 2011 Apr;305(14):1460–8.
27. Bachmann MF, Dyer MR. Therapeutic vaccination for chronic diseases: a new class of drugs in sight. Nat Rev Drug Discov. 2004 Jan;3(1):81–8.
28. Bachmann MF, Whitehead P. Active immunotherapy for chronic diseases. Vaccine. 2013 Apr;31(14):1777–84.
29. Crossey E, Amar MJA, Sampson M, et al. A cholesterol-lowering VLP vaccine that targets PCSK9. Vaccine. 2015 Oct;33(43):5747–55.
30. Fattori E, Cappelletti M, Lo Surdo P, et al. Immunization against proprotein convertase subtilisin-like/kexin type 9 lowers plasma LDL-cholesterol levels in mice. J Lipid Res. 2012 Aug;53(8):1654–61.
31. Libby P. Inflammation in atherosclerosis. Nature. 2002 Dec;420(6917):868–74.
32. Ross R. Atherosclerosis--an inflammatory disease. N Engl J Med. 1999 Jan;340(2):115–26.
33. Libby P. Mechanisms of acute coronary syndromes and their implications for therapy. N Engl J Med. 2013 May;368(21):2004–13.
34. Tabas I. Free cholesterol-induced cytotoxicity a possible contributing factor to macrophage foam cell necrosis in advanced atherosclerotic lesions. Trends Cardiovasc Med. 1997 Oct;7(7):256–63.
35. Abela GS. Cholesterol crystals piercing the arterial plaque and intima trigger local and systemic inflammation. J Clin Lipidol. 2010;4(3):156–64.
36. van De Poll SW, Romer TJ, Volger OL, et al. Raman spectroscopic evaluation of the effects of diet and lipid-lowering therapy on atherosclerotic plaque development in mice. Arterioscler Thromb Vasc Biol. 2001 Oct;21(10):1630–5.
37. Duewell P, Kono H, Rayner KJ, et al. NLRP3 inflammasomes are required for atherogenesis and activated by cholesterol crystals. Nature. 2010 Apr;464(7293):1357–61.
38. Walley KR, Thain KR, Russell JA, et al. PCSK9 is a critical regulator of the innate immune response and septic shock outcome. Sci Transl Med. 2014 Oct;6(258):258ra143.
39. Giunzioni I, Tavori H, Covarrubias R, et al. Local effects of human PCSK9 on the atherosclerotic lesion. J Pathol. 2016 Jan;238(1):52–62.
40. Liu M, Wu G, Baysarowich J, et al. PCSK9 is not involved in the degradation of LDL receptors and BACE1 in the adult mouse brain. J Lipid Res. 2010 Sep;51(9):2611–8.
41. Wadhera RK, Steen DL, Khan I, et al. A review of low-density lipoprotein cholesterol, treatment strategies, and its impact on cardiovascular disease morbidity and mortality. J Clin Lipidol. 2016;10(3):472–89.

3

Triple treatment with alirocumab and evinacumab on top of atorvastatin regresses lesion size and improves plaque phenotype in APOE*3-Leiden.CETP mice

Marianne G. Pouwer, Elsbet J. Pieterman, Nicole Worms, Nanda Keijzer,
J. Wouter Jukema, Jesper Gromada, Viktoria Gusarova, Hans M. G. Princen

Submitted

Abstract

Objectives: Regression of atherosclerotic plaque is modest with the current standard therapy, therefore it is beneficial to evaluate new therapeutic options. We investigated the effect of aggressive lipid-lowering interventions using double and triple treatment with simple or combined inhibition of PCSK9 and ANGPTL3 using the monoclonal antibodies alirocumab and evinacumab, respectively, on top of atorvastatin on regression of pre-existent atherosclerosis in APOE*3-Leiden.CETP mice.

Methods and results: Mice were fed a Western-type diet (WTD) for 13 weeks and thereafter matched into a baseline group (sacrificed at t=13), and 5 groups that continued to receive WTD alone or with treatment for 25 weeks: regression control, atorvastatin, atorvastatin and alirocumab, atorvastatin and evinacumab or atorvastatin, alirocumab and evinacumab. All interventions decreased plasma total cholesterol (-37% with atorvastatin to -80% with triple treatment, all $p<0.001$) by reduction of non-high-density lipoprotein cholesterol (non-HDL-C). Triple treatment decreased non-HDL-C levels at end-point from 10.7 mmol/L in control to 1.0 mmol/L (-91%, $p<0.001$). Mono-treatment with atorvastatin reduced the progression of atherosclerosis (-28%, $p<0.001$ vs control), double treatments completely blocked further progression and improved plaque stability, whereas triple treatment regressed lesion size in the thoracic aorta (-50%, $p<0.05$ vs baseline) and in the aortic root (-36%, $p<0.05$ vs baseline), diminished macrophage accumulation through reduced proliferation and further improved plaque stability.

Conclusions: This preclinical study using APOE*3-Leiden.CETP mice demonstrates that high-intensive cholesterol-lowering triple treatment with atorvastatin, alirocumab and evinacumab targeting all apoB-containing lipoproteins is a promising approach for regression of pre-existent atherosclerosis along with improvement in plaque phenotype.

Introduction

Atherosclerosis is the main cause of cardiovascular disease (CVD), and the annual number of deaths from CVD is predicted to rise from 17.5 million in 2012 to 22.2 million by 2030 (1). In addition to lifestyle changes (2), lipid-lowering has proven to be highly effective in reducing CVD, as every 1 mmol/L reduction in low-density-lipoprotein-cholesterol (LDL-C) is associated with a 23% CVD risk reduction (3). Since most patients at CVD risk are treated after development of atherosclerosis, therapies that regress pre-existent lesions are warranted.

Currently, statins are the 'golden standard' to lower LDL-C and to reduce CVD risk, but monotherapy with statins remains suboptimal as the achieved regression is modest, reflected by the small reductions in plaque volume (0.3-1.2% per year) (4,5). Furthermore, plaque regression is only seen in those patients with LDL-C reductions of >40% (6,7), or at plasma LDL-C levels below 78 mg/dL (2.0 mmol/L) (5,7), while a subgroup of patients still does not reach their LDL-C goals. Notably, the magnitude of regression is correlated with the percentage of LDL-C reduction (5,6), indicating the potential for further lipid-lowering. In this context, dual lipid-lowering therapies using ezetimibe or inhibition of proprotein convertase subtilisin/kexin type 9 (PCSK9) on top of a statin further reduce plaque volume relative to monotherapy with statins (5). While currently available therapies aim mostly to decrease plasma LDL-C, remnant cholesterol and triglyceride (TG) levels are considered to be an important residual risk factor for CVD as well (8,9). Actually, the clinical benefit of lowering TG and LDL-C may be proportional to the absolute change in apoB, implicating that all apoB-containing lipoproteins have approximately the same effect on the risk of CVD per particle (10). Therefore, novel high-intensive lipid-lowering or combination therapies targeting all apoB-containing lipoproteins may provide additional benefit to regress atherosclerosis and further reduce clinical events.

Since the severity and progression of coronary atherosclerosis are associated with adverse cardiovascular outcomes (4,11), the modest reduction in plaque volume achieved by statins cannot fully explain the reduced CVD risk, suggesting an important role for improved lesion stability (5,12,13). Animal models represent an opportunity to study plaque composition during regression. However, many mouse models have limited translational capability due to lack of responsiveness to lipid-lowering treatment (13). In this study we utilized APOE*3-Leiden.CETP mice, a well-established model with a human-like lipoprotein metabolism and atherosclerosis development (14) that responds well to hypolipidemic drugs (15–17).

We tested alirocumab and/or evinacumab on top of atorvastatin as high-intensive lipid-lowering strategy to evaluate their effect on regression of pre-existent atherosclerosis in APOE*3-Leiden.CETP mice. In addition, we assessed the effects on plaque composition and stability, and further looked into the process of macrophage reduction during regression. Alirocumab is a fully human monoclonal antibody to PCSK9 that reduces the

risk of recurrent ischemic cardiovascular events in patients with acute coronary syndrome when administered on top of atorvastatin (18). Evinacumab (REGN1500) is a monoclonal antibody against angiopoietin-like protein 3 (ANGPTL3) (19), a circulating protein that inhibits the hydrolysis of TG by lipoprotein lipase (LPL) in TG-rich lipoproteins. Loss-of-function mutations in the ANGPTL3 gene correlate with protection against CVD and treatment with evinacumab decreased plasma TG and LDL-C levels in human subjects (17,20).

Methods

Animals

Female APOE*3-Leiden.CETP transgenic mice on a C57BL/6 background (8-12 weeks of age) were obtained from the breeding facility of the Organization of Applied Scientific Research (TNO). The number of animals per group was calculated using a power of 0.80. Based on our experience from previous studies, we expected to have a variance of 23% in atherosclerosis, a minimal difference of 40% and a two-sided test with 95% confidence interval, which resulted in 16 animals per group. The mice entered the study in a staggered way of 5 weeks apart with two equal batches of each 8 mice per group to limit the difference in animal age. Groups that received the fully human monoclonal antibody evinacumab consisted of 32 (atorvastatin and evinacumab) or 48 (atorvastatin, alirocumab and evinacumab) mice as some mice develop mouse-anti-human auto-antibodies to evinacumab, leading to loss of efficacy. During the 38-week study with in total 144 mice, 4 mice were found dead in their cage and 4 mice were sacrificed based on human end-point criteria (atorvastatin: 3; atorvastatin and alirocumab: 2; atorvastatin and evinacumab: 1; atorvastatin, alirocumab and evinacumab: 2). In total, 48 mice developed auto-antibodies to evinacumab, as determined by Elisa (atorvastatin and evinacumab: 18; atorvastatin, alirocumab and evinacumab: 30) and were excluded from all analyses. The study was performed at the research facility of TNO-Metabolic Health Research, the Netherlands, and animal experiments were approved by the Animal Experiment Committee of The Netherlands Organization of Applied Scientific Research TNO under registration number 3682.

Diet and treatments

Mice were fed a Western-type diet (WTD) with 0.30% cholesterol and 15% saturated fat for 13 weeks to induce development of atherosclerosis. After 13 weeks mice were matched into 6 groups based on age, body weight, plasma total cholesterol (TC) and triglycerides (TG), and cholesterol exposure (mmol/L*weeks) measured at 12 weeks, and thereafter 16 mice were sacrificed as the baseline control group (see **Figure 1** for study design). The other 5 groups continued to receive WTD alone or with treatment for 25 weeks: regression

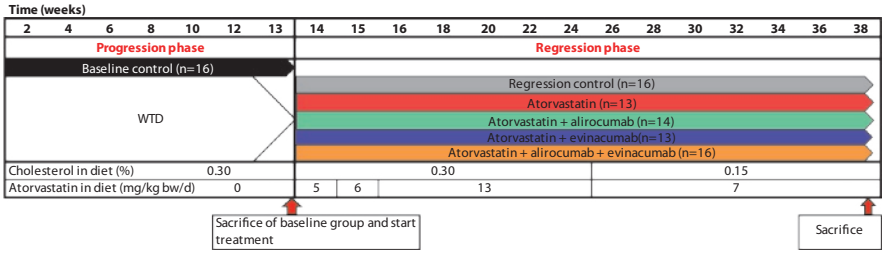

Figure 1 Study design. Female APOE*3-Leiden.CETP mice were fed a WTD diet for 13 weeks. Next, mice were matched in 6 groups based on age, body weight, plasma total cholesterol, triglycerides and cholesterol exposure (mmol/L*weeks). The baseline control group was sacrificed at t=13 weeks and the other 5 groups continued to receive a WTD alone or with treatment as indicated for 25 weeks until week 38. The number of mice used for the analyses are depicted, this number exclude the mice that died during the study (see Methods section) and mice that were excluded because of development of auto-antibodies to the human monoclonal antibody evinacumab. Abbreviations: WTD, Western type diet.

control, atorvastatin (5-13 mg/kg/d), atorvastatin and alirocumab (10 mg/kg/week), atorvastatin and evinacumab (25 mg/kg/week) or atorvastatin, alirocumab and evinacumab. Atorvastatin was mixed with the diet in a dose of 5 mg/kg/d (week 13-14), 6 mg/kg/d (week 15), 13 mg/kg/d (week 16-24) and 7 mg/kg/d (week 25-38). Alirocumab and evinacumab were administered by weekly subcutaneous injections. The cholesterol content in the diet was decreased from 0.30% to 0.15% in week 24 to reach plasma TC levels of an average 11-13 mmol/L to obtain more human-like levels, similarly as observed in untreated hyperlipidemic (FH) patients. Body weights, food intake per cage, and plasma parameters were measured throughout and the development of atherosclerosis was analyzed at t=13 weeks (baseline control group) and at t=38 weeks (control and treatment groups) in the aortic arch and aortic root. Lesion severity was determined in the aortic root. Plaque composition, monocyte adherence and macrophage proliferation were determined in the complex lesions of the aortic root.

Plasma lipids and lipoprotein analysis

Plasma TC and TG were determined at week 0, 4, 8, 12, 14, 15, 16, 20, 24, 28, 32, 36 and 38 using enzymatic colorimetric methods (Roche Diagnostics GmbH, Germany) according to the manufacturer's protocols and total cholesterol exposure was calculated as mmol/L*weeks. HDL-C was measured at week 12, 18, 28 and 36 after precipitation of apoB-containing particles (21) and non-HDL-C was calculated by subtracting HDL-C from total cholesterol.

En face determination of atherosclerosis in the thoracic aorta

To determine the total plaque load in the aortic arch, perfusion-fixed aortas (from the aortic origin to the diaphragm) were cleaned of extravascular fat, opened longitudinally, pinned en face, and stained for lipids with oil-red O (Sigma-Aldrich Chemie BV) as described previously (22). Photographs of the aorta's were taken by an Olympus SZX10 microscope with an Olympus DP74 camera. Data were normalized for the analyzed surface area and expressed as percentage of the stained area.

Determination of lipid content in the thoracic aorta

The thoracic aortas were cleaned of extravascular fat, homogenized in phosphate-buffered saline, and the protein content was measured using a Lowry protein assay. Lipids were extracted as described previously (23), separated by high-performance thin-layer chromatography on silica gel plates, stained and analyzed with ChemiDoc Touch Imaging System (Bio-Rad). TG, cholesterol ester (CE) and free cholesterol (FC) content were quantified using Image-lab version 5.2.1 software (Bio-Rad) and expressed per mg protein.

Histological assessment of atherosclerosis in the aortic root

Atherosclerotic lesion area and severity were assessed in the aortic root area, as reported previously (24). Briefly, the aortic root was identified by the appearance of aortic valve leaflets, and serial cross-sections of the entire aortic root area (5 µm thick with intervals of 50 µm) were mounted on slides and stained with haematoxylin-phloxine-saffron (HPS). For each mouse, the lesion area was measured in 4 subsequent sections. Each section consisted of 3 segments (separated by the valves). The total lesion area and number of lesions were calculated per cross-section. Lesion severity was calculated as relative amount of early and complex lesions in which the lesion-free segments are included. The lesions were classified as early lesions (type I-III according to the American Heart Association (AHA)) and complex lesions, which include type IV-V lesions (according to the AHA (16,25)) and the so-called 'regression lesions'. Although the 'regression lesions' were generally smaller than type IV and V lesions, they could not be defined as early lesions/fatty streak since they did not consist of macrophages, but mainly of collagen and α-smooth muscle cells (SMCs). Slides were scanned by an Aperio AT2 slide scanner (Leica Biosystems) and atherosclerotic area was measured in Image Scope (version 12-12-2015).

Histological assessment of plaque composition

Lesion composition in complex lesions was assessed after double immunostaining with anti-α smooth muscle actin (1:400; PROGEN Biotechnik GmbH, Germany) for SMCs, and anti-mouse LAMP2 (M3/84) (1:500; BD Pharmingen, the Netherlands) for macrophages. Anti-α smooth muscle actin was labeled with Vina green (Biocare Medical, Pacheco, USA), and LAMP2 with DAB (Vector laboratories, Burlingame, USA). After slides were scanned and analyzed, cover slips were detached overnight in xylene and Sirius Red staining for

collagen was performed. Color intensity of Sirius Red staining was determined in ImageJ and the used threshold was confirmed by evaluation of the sections under polarized light. The necrotic area and cholesterol clefts were measured in the Sirius Red-stained slides. Lesion stability index, as the ratio of collagen and αSMC area (i.e. stabilization factors) to macrophage and necrotic area (i.e. destabilization factors) was calculated as described previously (24). In each segment used for lesion quantification, intracellular adhesion molecule (ICAM-1) expression and the number of monocytes adhering to the endothelium were counted after immunostaining with mouse monoclonal ICAM-1 antibody (1:400; Santa Cruz Biotechnology, Dallas, USA) and AIA 31240 antibody (1:500; Accurate Chemical and Scientific, New York, USA), respectively (25). The number of proliferating macrophages in the plaques was counted after triple staining with Ki67 (1:1600, Abcam, Cambridge, UK) for cellular proliferation labeled with DAB (black) (Vector laboratories, Burlingame, USA), anti-mouse LAMP2 (M3/84) (1:500; BD Pharmingen, the Netherlands) for macrophages labeled with DAB (brown) (Vector Laboratories, Burlingame, USA) and anti-α smooth muscle actin (1:400; PROGEN Biotechnik GmbH, Germany) labeled with vina green (Biocare Medical, Pacheco, USA). Slides were scanned by an Aperio AT2 slide scanner (Leica Biosystems). Monocyte adherence, ICAM-1 expression and the number of Ki67 positive macrophages were assessed in Image Scope (version 12-12-2015), and plaque composition was measured in Fiji (version 30-5-2017).

Statistical analysis

Significance of differences between the groups was calculated using a one-way ANOVA, followed by Dunnett's 2-sided post-hoc test for comparisons against the control and baseline control group. The Bonferroni post-hoc test was used to correct for multiple comparisons between the different treatment groups. For the atherosclerosis measurements the non-parametric Kruskall-Wallis test was used to test for differences between groups, followed by a Mann-Whitney U test for comparisons against the baseline and control group and between the different treatment groups. Linear regression analyses were used to assess correlations between variables. IBM SPSS v24.0 was used for all analyses. p-values ≤ 0.05 were considered statistically significant.

Results

Double and triple treatment with alirocumab and evinacumab on top of atorvastatin gradually decrease total and non-HDL-cholesterol

Mice were fed WTD for 13 weeks which led to increased plasma TC levels of about 25 mmol/L. At that point, the mice were matched into groups and treatment started. All treatments decreased plasma cholesterol (**Figure 2A**) and cholesterol exposure (mmol/L*weeks) in comparison to control (**Figure 2B**) with a gradual decline in the

atorvastatin, double (alirocumab and atorvastatin, evinacumab and atorvastatin) and triple (alirocumab, evinacumab and atorvastatin) treatment groups. Triple treatment lowered plasma TC levels to 1.8 mmol/L at the end-point and reduced cholesterol exposure by 80% (p<0.001) relative to control, and by 68% (p<0.001), 45% (p<0.001) and 38% (p=0.035) when compared to atorvastatin or double treatment with alirocumab or evinacumab, respectively. All treatments, except monotreatment with atorvastatin, consistently decreased plasma TG levels (**Figure 2C**). Non-HDL-C levels were decreased by all treatments, with the largest reduction, down to 1.0 mmol/L, achieved by triple treatment at the end of the study (-91%, p<0.001), which was significantly lower when compared to double treatment with alirocumab (-74%, p=0.010) and evinacumab (-72%,

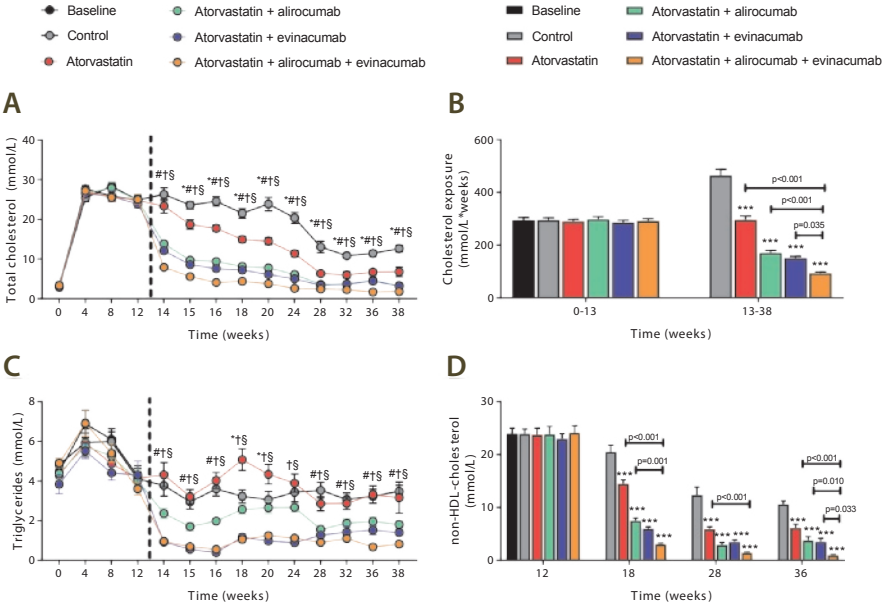

Figure 2 Double and triple treatment with alirocumab and evinacumab on top of atorvastatin gradually decrease triglycerides and total and non-HDL-cholesterol. APOE*3-Leiden.CETP mice were fed a WTD for 13 weeks to induce atherosclerosis and remained on the diet without or with treatment until end-point. Plasma TC (A), total cholesterol exposure (mmol/L*weeks) (B), plasma TG (C). Non-HDL (D) was calculated by subtracting HDL-C from TC. The dotted line represents start of treatment and sacrifice of the baseline group. Data are presented as means ± SEM (n=13-16 per group). Figure A and C: *p<0.05 atorvastatin vs control, #p<0.05 atorvastatin + alirocumab vs control, †p<0.05 atorvastatin + evinacumab vs control, §p<0.05 atorvastatin + alirocumab + evinacumab vs control. Figure B and D: ***p<0.001 compared to control. Abbreviations: WTD, western type diet; TC, total cholesterol; TG, triglycerides; HDL-C, high-density-lipoprotein-cholesterol.

p=0.033) (**Figure 2D**). The reduction in TC was confined to the apoB-containing lipoproteins (VLDL-LDL) (**Figure 3**). Altogether, these data demonstrate that evinacumab on top of atorvastatin and alirocumab has an additional cholesterol-lowering effect resulting in non-HDL-C levels of 1.0 mmol/L.

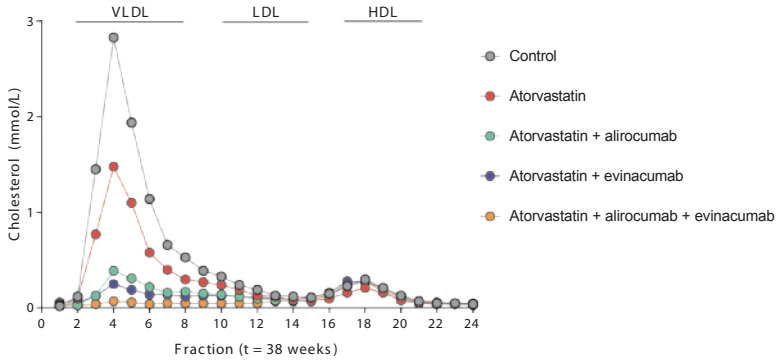

Figure 3 Lipoprotein profiles at end-point. APOE*3-Leiden.CETP mice were fed a WTD for 13 weeks to induce atherosclerosis and remained on the diet without or with treatment until end-point (t=38 weeks). Lipoprotein profiles were assessed by FPLC lipoprotein separation in group-wise pooled plasma (n=13-16 per group). Abbreviations: VLDL, very-low density lipoprotein; LDL, low-density lipoprotein; HDL, high-density lipoprotein; WTD, Western type diet; FPLC, fast protein liquid chromatography.

Triple treatment with alirocumab and evinacumab on top of atorvastatin regresses pre-existent lesions and reduces lipid content in the thoracic aorta

We assessed the effect of intensive lipid-lowering on the progression and regression of pre-existing atherosclerosis at different sites along the aorta, in the thoracic aorta and the aortic root. After 13 weeks of WTD (at treatment baseline), 1.6% of the thoracic aorta was covered with oil-red-O positive lesions. WTD feeding for 25 more weeks led to further progression of atherosclerosis to 5.7% coverage in the control group. Treatment with alirocumab or evinacumab on top of atorvastatin fully blocked progression of atherosclerosis (**Figure 4A and C**). Double treatment with alirocumab and evinacumab decreased the amount of CE and double treatment with evinacumab the TG content beyond baseline (**Figure 4B**). Triple treatment did not only block the progression (-86%, p<0.001 vs control) but also resulted in regression of the pre-existent lesions by 50% (p=0.045) compared to baseline. Furthermore, triple treatment reduced CE and TG content beyond the baseline level in the thoracic aorta (-45%, p=0.033 and -83%, p=0.001, respectively).

The effect of triple and double treatments was stronger than atorvastatin monotreatment on all parameters.

In the aortic root, 208*1 000 um^2 lesion area per cross-section was present at baseline, which further increased to 438*1 000 um^2 in the control group. Atorvastatin modestly decreased lesion size (-28%, p=0.001 vs control), whereas double treatment with alirocumab or evinacumab on top of atorvastatin completely blocked the progression (-55%, p<0.001; -51%, p<0.001, respectively vs control). Triple treatment further decreased lesion size (-70%, p<0.001 vs control) and regressed the atherosclerotic lesion size (-36%, p<0.001 vs baseline) (**Figure 5A**). All treatments led to smaller lesions compared to control and triple treatment lesions were smaller than initial lesions size at baseline (**Figure 5B**). The area that consisted of complex lesions was decreased by triple treatment compared to control

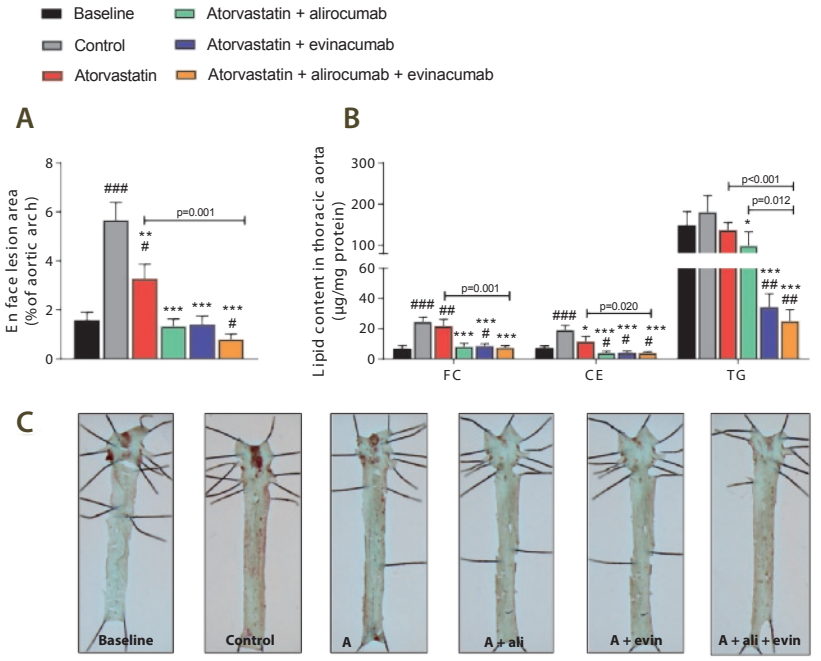

Figure 4 Triple treatment with alirocumab and evinacumab on top of atorvastatin regresses pre-existent lesions and reduces aortic lipid content in the thoracic aorta. En face analysis of atherosclerosis (A) and lipid content (B) in the thoracic aorta with representative images (C). Data are presented as means + SEM (n=12 per group). #P<0.05, ##P<0.01, ###P<0.001 when compared to baseline. *p<0.05, **p<0.01, ***p<0.001 when compared to control. Abbreviations: A, atorvastatin; ali, alirocumab; evin, evinacumab; FC, free cholesterol; CE, cholesterol ester; TG, triglycerides.

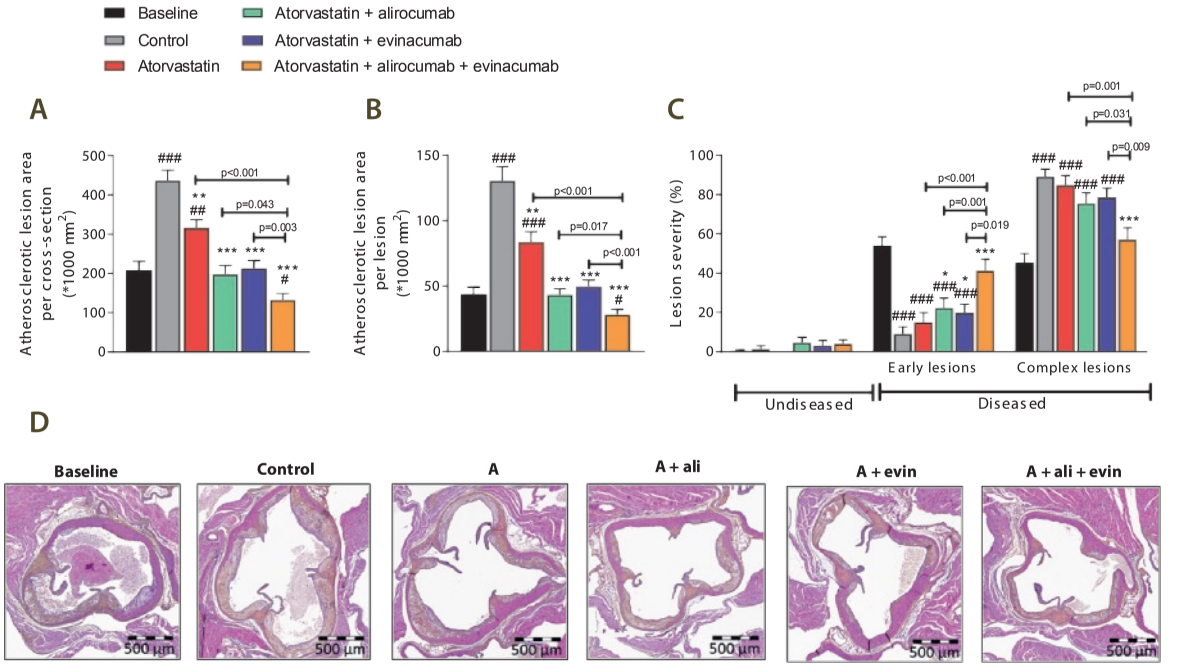

Figure 5 Double treatment with alirocumab or evinacumab on top of atorvastatin blocks the progression of atherosclerosis and triple treatment regresses pre-existent lesions in the aortic root. Lesion size (A) in aortic root after 13 weeks of WTD (baseline) and in control and treatment groups at end-point (week 38). Number of lesions per cross-section was assessed and the average size per lesion was calculated (B). Lesion severity as relative amount of early and complex lesions together with lesion-free segments (C). Representative images (D). Data are presented as means ± SEM (n=13-16 per group). #P<0.05, ##P<0.01, ###P<0.001 when compared to baseline. *p<0.05, **p<0.01, ***p<0.001 when compared to control. Abbreviations: A, atorvastatin; ali, alirocumab; evin, evinacumab.

(-36%, p<0.001), with more early lesions present (**Figure 5C**). Additionally, triple treatment decreased lesion area and improved plaque phenotype as compared to mono- and double treatment. Representative images of the aortic root area are shown in **Figure 5D**. These data demonstrate that alirocumab and evinacumab on top of atorvastatin equally block the progression of atherosclerosis, but that regression of pre-existent, advanced atherosclerotic plaques is only achieved by aggressive lipid lowering using triple combination treatment.

The reduction in lesion size is correlated with the decrease in plasma cholesterol

We evaluated whether the reduction in lesion size could be explained by the reduction in plasma TC during treatment. The mean TC level at baseline was subtracted from the TC levels of each individual mouse at each time point and the cumulative decrease in cholesterol exposure was calculated as mmol/L*weeks. These data were plotted against the lesion size at end-point minus the mean lesion size at baseline (**Figure 6**). A strong correlation between the difference in lesion area and the cumulative TC decrease during treatment was observed (R=0.85, p<0.001), indicating an important role of therapeutic cholesterol lowering in lesion regression.

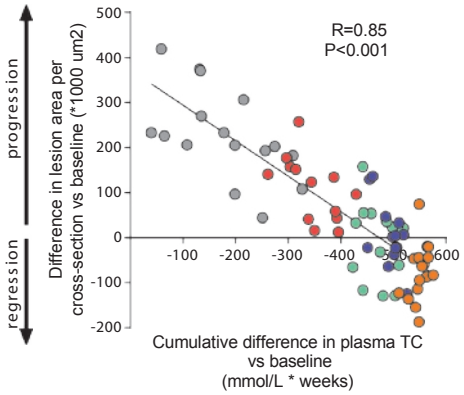

Figure 6 Correlation between the cumulative decrease in plasma cholesterol exposure and atherosclerotic lesion area. Mean TC at baseline was subtracted from TC levels of each individual mouse at each time point and the cumulative decrease in TC exposure during treatment was calculated as mmol/L*weeks. Data were plotted against the difference in lesion size at end-point and mean lesion size at baseline. Linear regression analysis was performed (n=13-16 per group). Abbreviations: TC, total cholesterol.

Double and triple treatment improve plaque composition

To evaluate whether plaque composition was affected by the treatments, the necrotic core, amount of macrophages, collagen and αSMC in the cap were quantified. Only triple treatment further decreased the macrophage content (-56%, p=0.012) compared to control, in parallel with increased αSMC (+38%, p=0.015) and collagen (+23%, p<0.001) content (**Figure 7A**). The plaque stability index improved by double (+66%, alirocumab and +64%, evinacumab, both p<0.001) and triple (+74%, p<0.001) treatment compared to control (**Figure 7B**). Representative images are shown (**Figure 7C**).

Triple treatment reduces monocyte adherence and macrophage proliferation

Vascular inflammation is recognized to play an important role in both the initiation and progression of atherosclerosis, whereas proliferation of macrophages further increases the plaque burden. Therefore, we measured endothelial ICAM-1 expression and adherence of monocytes to the activated endothelium as markers of vascular inflammation, and counted the number of currently proliferating macrophages after immunostaining for Ki67. All regimens except monotreatment with atorvastatin decreased ICAM-1 expression when compared to control, but only triple treatment decreased ICAM-1 expression when compared to baseline (-37%, p=0.010) (**Figure 8A and C**). In addition, triple treatment decreased the number of monocytes adhering to the endothelium when compared to baseline (-78%, p<0.001) and control (-69%, p=0.003), whereas mono- and double treatment only decreased monocyte adherence when compared to control (**Figure 8B**). The number of proliferating macrophages per plaque (**Figure 8D**) decreased over time by 91% (p<0.001; control vs baseline), which was further reduced by monotreatment with atorvastatin (-60%, p=0.019), double treatment with alirocumab or evinacumab on top of atorvastatin (-87%, p=0.001 and -58%, p=0.012 vs control) and triple treatment (-88%, p<0.001 vs control). Representative images are shown (**Figure 8E**).

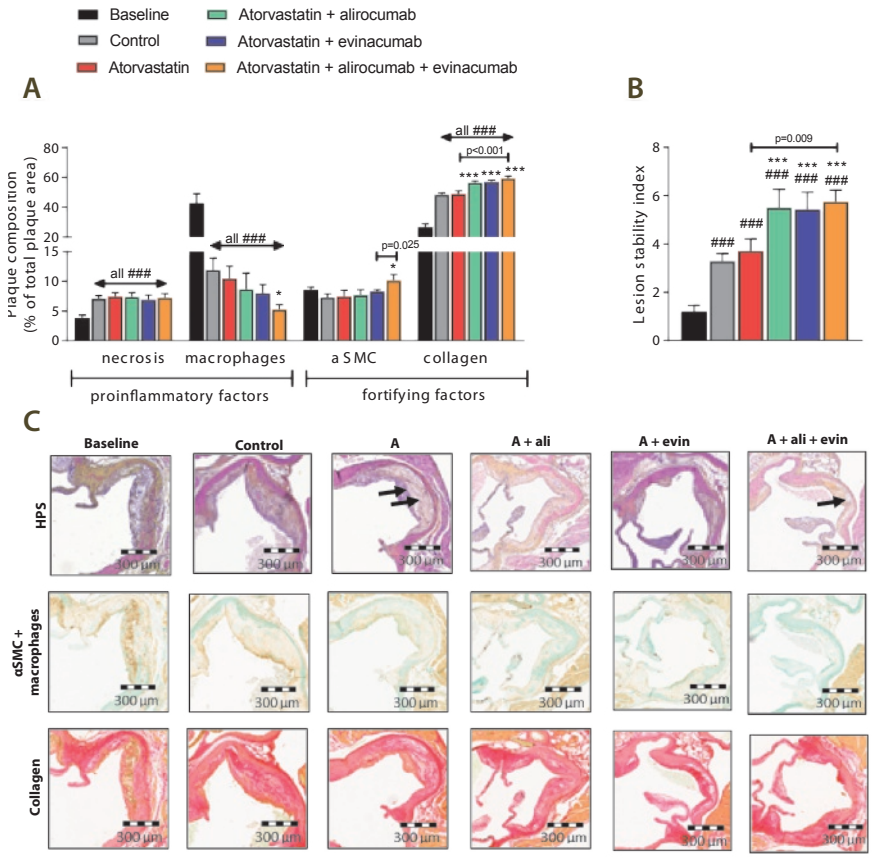

Figure 7 Double and triple treatment improve plaque phenotype. Necrotic and macrophage content as pro-inflammatory factors and αSMCs and collagen as fortifying factors were determined in the complex lesions in the aortic root and expressed as percentage of total plaque area (A). Lesion stability index, as the ratio of collagen and αSMC area (i.e. stabilization factors) to macrophage and necrotic area (i.e. destabilization factors) was calculated (B). Representative images of HPS staining, double-immunostaining with α-actin for SMCs (Vina green) and LAMP2 (M3/84) for macrophages (DAB, brown), and Sirius Red staining for collagen. The arrows depict necrotic areas, including cholesterol clefts (C). Data are presented as means ± SEM (n=13-16 per group). ###P<0.001 when compared to baseline. *p<0.05 , ***p<0.001 when compared to control. Abbreviations: HPS, hematoxylin-phloxine-saffron; SMCs, smooth muscle cells; DAB, 3,3'-Diaminobenzidine; Abbreviations: A, atorvastatin; ali, alirocumab; evin, evinacumab.

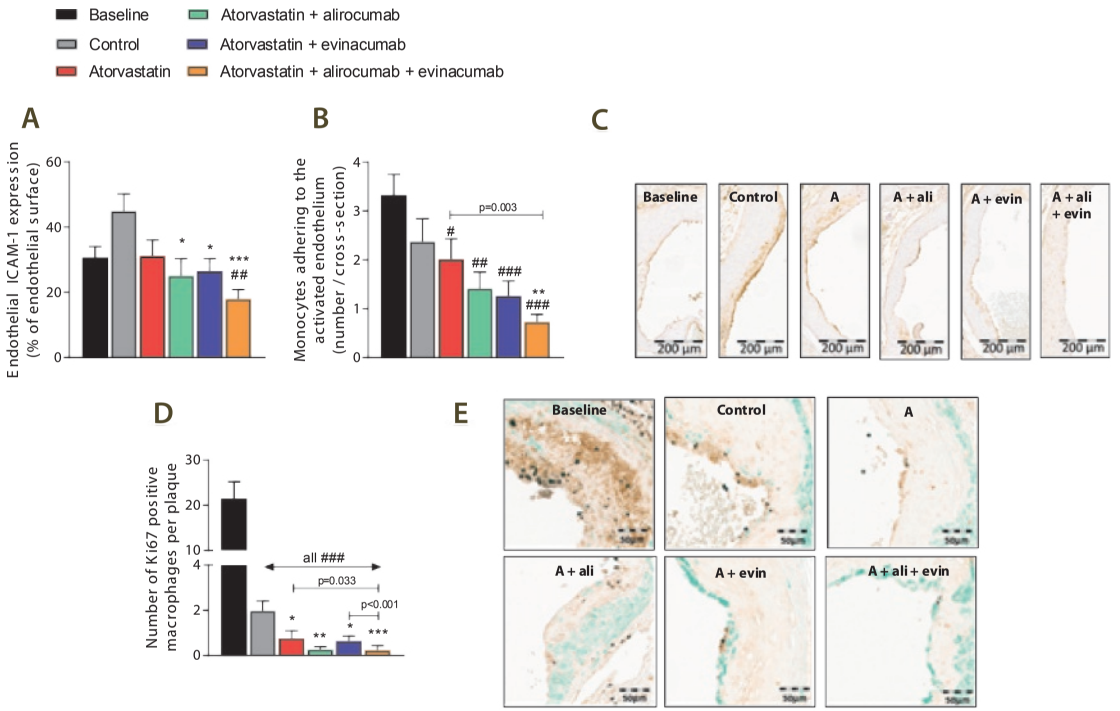

Figure 8 Monocyte adherence and the number of proliferative macrophages decrease in regression plaques. In each segment used for lesion quantification in the aortic root, endothelial ICAM-1 expression was determined as percentage of the luminal surface (A). Number of monocytes adhering to the activated endothelium per cross-section after staining with AIA 31240 (B). Representative images of ICAM-1 expression (C). Number of Ki67 positive macrophages as marker for proliferation in type IV and V plaques after triple-immunostaining with Ki67 (DAB, black), LAMP2 (M3/84) for macrophages (DAB, brown) and α-actin for αSMC (green). Number of proliferative macrophages was counted per plaque (D). Representative images (E). Four mice were excluded from figure D (2 mice in control, 2 mice in alirocumab + atorvastatin) due to extensive infiltration of the plaques by Ki67 positive inflammatory cells. Data are presented as means ± SEM (n=11-16 per group). #p<0.05, ##p<0.01, ###p<0.001 when compared to baseline. *p<0.05, **p<0.01, ***p<0.001 when compared to control. Abbreviations: ICAM-1, intercellular adhesion molecule 1; SMCs, smooth muscle cells; DAB, 3,3'-Diaminobenzidine; A, atorvastatin; ali, alirocumab; evin, evinacumab.

Discussion

PCSK9 inhibition with alirocumab has been shown to strongly lower LDL-C and non-HDL-C alone and on top of a statin, and reduce the risk of recurrent ischemic cardiovascular events in patients with acute coronary syndrome (18). ANGPTL3 monoclonal antibody evinacumab was reported to reduce plasma TG and LDL-C levels in healthy subjects and homozygous hypercholesterolemia patients (17,20). Recent data suggest not only LDL-C but also remnant cholesterol, thus all apoB-containing lipoproteins are important predictors of cardiovascular outcome (9,10). The present study was designed to investigate the effect of gradual and aggressive reduction of cholesterol in both LDL and remnant lipoproteins by alirocumab and/or evinacumab on top of atorvastatin on regression of pre-existent atherosclerosis in hyperlipidemic mice. Our data revealed that alirocumab and evinacumab in combination with atorvastatin fully block further progression of atherosclerosis and triple treatment reduces lesion size beyond the treatment baseline level. In addition, double and triple treatments improve lesion morphology and composition in APOE*3-Leiden.CETP mice with pre-existent atherosclerosis. This is the first study in mice that shows real regression of lesion size using the combination of clinical hypolipidemic drugs.

Therapeutic interventions in mice have been hampered due to the lack of responsiveness to current lipid-lowering therapies in murine models of regression. Commonly used models are the aortic transplant model, the Reversa mouse ($Ldlr^{-/-}$Apob100/100Mx1-$Cre^{+/+}$), and $ApoE^{-/-}$ and $LDLR^{-/-}$ mice (reviewed in (13,26)). In these models, progression of atherosclerosis is induced by a WTD and regression is accomplished by a switch to chow, eventually together with genetic alterations or treatment strategies. Regression of atherosclerosis was generally defined by a decrease of macrophages or lipid content (13,26), though some studies reported a reduced total lesion size using experimental interventions, which was independent of plasma TC levels (reviewed in (13,26)). While these models are of great value to elucidate the molecular characteristics of the regressive plaque, they are less suitable for the evaluation of lipid-lowering interventions and their effect on atherosclerosis regression, as they poorly respond to registered lipid-lowering drugs (27,28). In the present study, we used the APOE*3-Leiden.CETP mouse, which possesses a delayed but intact apoE-LDLR-mediated clearance pathway and expresses CETP (14,28). These mice respond to all lipid-lowering drugs used in the clinic, including statins, alirocumab and evinacumab (15–17). Thus, treatments of APOE*3-Leiden.CETP mice on WTD with atorvastatin or alirocumab on top of the statin in our study decreased TC levels (-31% to -51% vs control and -32% to -52% vs atorvastatin, respectively) by a reduction of non-HDL-C, similarly as in humans (18,29). Evinacumab has an additive effect on treatment with atorvastatin and alirocumab by further reducing TC (-62% to -75% vs atorvastatin; -34% to -63% vs atorvastatin + alirocumab) and, in addition, TG levels (-62% to 80% vs atorvastatin; -42% to -65% vs atorvastatin + alirocumab).

We have previously shown that the lipid-modifying effects of PCSK9 and ANGPTL3 inhibition have an atheroprotective effect in a preventive design (16,17). However, to date,

the effect of pharmacological inhibition on regression of atherosclerosis, more closely mimicking the human situation, has not been investigated. Here, we show for the first time that double treatment with alirocumab or evinacumab on top of atorvastatin completely blocks progression of pre-existent atherosclerosis and that triple treatment regresses atherosclerosis in the aortic arch and the aortic root. The treatment effects on lesion area were mainly predicted by the gradual and aggressive reduction in plasma TC levels as illustrated by the strong association between the decreased cholesterol exposure and lesion size during treatment (R=0.85). All triple treated mice except one showed a lesion size below that at baseline, indicating regression. Reduction of non-HDL-C levels to about 1 mmol/L (38.7 mg/dL) was required to observe the regression. This finding is in accordance with studies in CVD patients that show exclusively reduction of plaque volume at LDL-C lowering of more than 40% or at a target level below 2.0 mmol/L (78 mg/dL) (5–7). Similar levels of 1 mmol/L were achieved in the recent outcome trials with PCSK9 inhibition which further reduced the risk of cardiovascular events as compared to statins and other hypolipidemic therapy (18,30).

Vulnerable plaques with high macrophage content, a large necrotic core and a thin, collagen-poor, fibrous cap are more prone to rupture (31). Thus, lesion composition, not only lesion size, is another important characteristic of the plaque. In the present study, the decline in plasma cholesterol reduced the lipid content of the aorta and resulted in smaller and less inflamed lesions. Double and triple treatment decreased endothelial expression of ICAM-1 and consequently reduced monocyte adhesion to the activated vascular endothelium, well-recognized processes in the initiation of atherosclerosis. In hypercholesterolemia, modified lipoproteins induce endothelium activation, thereby mediating the arrest and transmigration of circulating monocytes into the subendothelial space where they differentiate into macrophages (32). All treatments in the present study reduced the macrophage content, and double and triple treatment increased the amount of collagen in the lesions, resulting in a strongly improved plaque morphology. The large reduction in macrophage content in the present and other studies is a key feature of regression, and depends on the balance between recruitment of monocytes and their differentiation into macrophages, proliferation of macrophages, and on apoptosis and migratory egress from the plaques. However, whereas impaired monocyte transmigration during the initiation of atherosclerosis diminishes plaque volume (33), monocyte depletion per se does not affect further progression of plaque burden (34). Local proliferation of aortic macrophages has been reported to be a key event in the progression of atherosclerosis and to substantially contribute to lesional macrophage accumulation (34). Here we provide evidence that cholesterol lowering-induced regression decreases the number of Ki67-positive macrophages, a marker of currently proliferating macrophages. This finding suggests that diminished proliferation of macrophages is an important process in the reduction in macrophage content during regression of atherosclerosis.

In conclusion, we show that high-intensive lipid-lowering triple treatment with atorvastatin, alirocumab and evinacumab regresses atherosclerosis, improves plaque phenotype, and

reduces the proliferation of macrophages in the plaques. These data show that further reduction of plasma cholesterol together with TG-lowering to target all apoB-containing lipoproteins may be an effective approach to further reduce existing atherosclerosis in dyslipidemic patients at CV risk resulting in further decline of clinical events and increase of symptom-free years.

Acknowledgements

We thank Erik Offerman for his excellent technical assistance.

Disclosures

Alirocumab (Praluent®) and evinacumab (REGN1500) are developed by Regeneron Pharmaceuticals and evinacumab is currently under trial. JG and VG are employees of Regeneron Pharmaceuticals and MGP, EJP, NW, NK, HMGP are employees of TNO during the conduct of this work.

Funding

This work was supported in part by Regeneron Pharmaceuticals, by an allowance for TKI-LSH from the Ministry of Economic Affairs in the Netherlands (reference number 060.23203), and the TNO research program "Preventive Health Technologies". JWJ received research grants from and was speaker on (CME-accredited) meetings sponsored by Amgen, Astellas, Astra-Zeneca, Daiichi Sankyo, Lilly, Merck-Schering-Plough, Pfizer, Roche, Sanofi-Aventis, the Netherlands Heart Foundation, the Interuniversity Cardiology Institute of the Netherlands, and the European Community Framework KP7 Program.

References

1. WHO. Hearths: technical package for cardiovascular disease mangement in primary health care [Internet]. 2016. Available from: http://www.who.int/cardiovascular_diseases/publications/en/
2. Catapano AL, Graham I, De Backer G, et al. 2016 ESC/EAS Guidelines for the Management of Dyslipidaemias. Eur Heart J. 2016 Oct;37(39):2999–3058.
3. Silverman MG, Ference BA, Im K, et al. Association Between Lowering LDL-C and Cardiovascular Risk Reduction Among Different Therapeutic Interventions: A Systematic Review and Meta-analysis. JAMA. 2016 Sep;316(12): 1289–97.
4. Puri R, Nissen SE, Shao M, et al. Coronary atheroma volume and cardiovascular events during maximally intensive statin therapy. Eur Heart J. 2013 Nov;34(41):3182–90.
5. Gragnano F, Calabro P. Role of dual lipid-lowering therapy in coronary atherosclerosis regression: Evidence from recent studies. Atherosclerosis. 2018 Feb;269:219–28.
6. Noyes AM, Thompson PD. A systematic review of the time course of atherosclerotic plaque regression. Atherosclerosis. 2014 May;234(1):75–84.
7. Gao W-Q, Feng Q-Z, Li Y-F, et al. Systematic study of the effects of lowering low-density lipoprotein-cholesterol on regression of coronary atherosclerotic plaques using intravascular ultrasound. BMC Cardiovasc Disord. 2014 May;14:60.
8. Nordestgaard BG, Varbo A. Triglycerides and cardiovascular disease. Lancet (London, England). 2014 Aug;384(9943): 626–35.
9. Sandesara PB, Virani SS, Fazio S, et al. The Forgotten Lipids: Triglycerides, Remnant Cholesterol, and Atherosclerotic Cardiovascular Disease Risk. Endocr Rev. 2019 Apr;40(2):537–57.
10. Ference BA, Kastelein JJP, Ray KK, et al. Association of Triglyceride-Lowering LPL Variants and LDL-C-Lowering LDLR Variants With Risk of Coronary Heart Disease. JAMA. 2019 Jan;321(4):364–73.
11. Nicholls SJ, Hsu A, Wolski K, et al. Intravascular ultrasound-derived measures of coronary atherosclerotic plaque burden and clinical outcome. J Am Coll Cardiol. 2010 May;55(21):2399–407.
12. Banach M, Serban C, Sahebkar A, et al. Impact of statin therapy on coronary plaque composition: a systematic review and meta-analysis of virtual histology intravascular ultrasound studies. BMC Med. 2015 Sep;13:229.
13. Burke AC, Huff MW. Regression of atherosclerosis: lessons learned from genetically modified mouse models. Curr Opin Lipidol. 2018 Apr;29(2):87–94.
14. Princen HMG, Pouwer MG, Pieterman EJ. Comment on "Hypercholesterolemia with consumption of PFOA-laced Western diets is dependent on strain and sex of mice" by Rebholz S.L. et al. Toxicol. Rep. 2016 (3) 46-54. Toxicol reports. 2016;3:306–9.
15. van De Poll SW, Romer TJ, Volger OL, et al. Raman spectroscopic evaluation of the effects of diet and lipid-lowering therapy on atherosclerotic plaque development in mice. Arterioscler Thromb Vasc Biol. 2001 Oct; 21(10):1630–5.
16. Kuhnast S, van der Hoorn JWA, Pieterman EJ, et al. Alirocumab inhibits atherosclerosis, improves the plaque morphology, and enhances the effects of a statin. J Lipid Res. 2014 Oct;55(10):2103–12.
17. Dewey FE, Gusarova V, Dunbar RL, et al. Genetic and Pharmacologic Inactivation of ANGPTL3 and Cardiovascular Disease. N Engl J Med. 2017 Jul;377(3):211–21.
18. Schwartz GG, Steg PG, Szarek M, et al. Alirocumab and Cardiovascular Outcomes after Acute Coronary Syndrome. N Engl J Med. 2018 Nov;379(22):2097–107.
19. Gusarova V, Alexa CA, Wang Y, et al. ANGPTL3 blockade with a human monoclonal antibody reduces plasma lipids in dyslipidemic mice and monkeys. J Lipid Res. 2015 Jul;56(7):1308–17.
20. Gaudet D, Gipe DA, Pordy R, et al. ANGPTL3 Inhibition in Homozygous Familial Hypercholesterolemia. Vol. 377, The New England journal of medicine. United States; 2017 Jul;377(3):296–7.
21. Kuhnast S, van der Tuin SJL, van der Hoorn JWA, et al. Anacetrapib reduces progression of atherosclerosis, mainly by reducing non-HDL-cholesterol, improves lesion stability and adds to the beneficial effects of atorvastatin. Eur Heart J. 2015 Jan;36(1):39–48.
22. Groot PH, van Vlijmen BJ, Benson GM, et al. Quantitative assessment of aortic atherosclerosis in APOE*3 Leiden transgenic mice and its relationship to serum cholesterol exposure. Arterioscler Thromb Vasc Biol. 1996 Aug;16(8):926–33.

23. Post SM, Zoeteweij JP, Bos MH, et al. Acyl-coenzyme A:cholesterol acyltransferase inhibitor, avasimibe, stimulates bile acid synthesis and cholesterol 7alpha-hydroxylase in cultured rat hepatocytes and in vivo in the rat. Hepatology. 1999 Aug;30(2):491–500.
24. Kuhnast S, van der Hoorn JWA, van den Hoek AM, et al. Aliskiren inhibits atherosclerosis development and improves plaque stability in APOE*3Leiden.CETP transgenic mice with or without treatment with atorvastatin. J Hypertens. 2012 Jan;30(1):107–16.
25. Landlinger C, Pouwer MG, Juno C, et al. The AT04A vaccine against proprotein convertase subtilisin/kexin type 9 reduces total cholesterol, vascular inflammation, and atherosclerosis in APOE*3Leiden.CETP mice. Eur Heart J. 2017 Aug;38(32):2499–507.
26. Rahman K, Fisher EA. Insights From Pre-Clinical and Clinical Studies on the Role of Innate Inflammation in Atherosclerosis Regression. Front Cardiovasc Med. 2018;5:32.
27. Zadelaar S, Kleemann R, Verschuren L, et al. Mouse models for atherosclerosis and pharmaceutical modifiers. Arterioscler Thromb Vasc Biol. 2007 Aug;27(8):1706–21.
28. Ason B, van der Hoorn JWA, Chan J, et al. PCSK9 inhibition fails to alter hepatic LDLR, circulating cholesterol, and atherosclerosis in the absence of ApoE. J Lipid Res. 2014 Nov;55(11):2370–9.
29. LaRosa JC, Grundy SM, Waters DD, et al. Intensive lipid lowering with atorvastatin in patients with stable coronary disease. N Engl J Med. 2005 Apr;352(14):1425–35.
30. Sabatine MS, Giugliano RP, Keech AC, et al. Evolocumab and Clinical Outcomes in Patients with Cardiovascular Disease. N Engl J Med. 2017 May;376(18):1713–22.
31. Libby P. Mechanisms of acute coronary syndromes and their implications for therapy. N Engl J Med. 2013 May;368(21):2004–13.
32. Moore KJ, Sheedy FJ, Fisher EA. Macrophages in atherosclerosis: a dynamic balance. Nat Rev Immunol. 2013 Oct;13(10):709–21.
33. Combadiere C, Potteaux S, Rodero M, et al. Combined inhibition of CCL2, CX3CR1, and CCR5 abrogates Ly6C(hi) and Ly6C(lo) monocytosis and almost abolishes atherosclerosis in hypercholesterolemic mice. Circulation. 2008 Apr;117(13):1649–57.
34. Robbins CS, Hilgendorf I, Weber GF, et al. Local proliferation dominates lesional macrophage accumulation in atherosclerosis. Nat Med. 2013 Sep;19(9):1166–72.

4

The BCR-ABL1 inhibitors imatinib and ponatinib decrease plasma cholesterol and atherosclerosis, and nilotinib and ponatinib activate coagulation in a translational mouse model

Marianne G. Pouwer, Elsbet J. Pieterman, Lars Verschuren,
Martien P. M. Caspers, Cornelis Kluft, Ricardo A. Garcia, Jurjan Aman,
J. Wouter Jukema, Hans M. G. Princen

Front Cardiovasc Med. 2018 Jun 12;5:55

Abstract

Objectives: Treatment with the second and third generation BCR-ABL1 tyrosine kinase inhibitors (TKIs) increases cardiovascular risk in chronic myeloid leukemia (CML) patients.

Methods and results: We investigated the vascular adverse effects of three generations of TKIs in a translational model for atherosclerosis, the APOE*3-Leiden.CETP mouse. Mice were treated for sixteen weeks with imatinib (150 mg/kg BID), nilotinib (10 and 30 mg/kg QD) or ponatinib (3 and 10 mg/kg QD), giving similar drug exposures as in CML-patients. Cardiovascular risk factors were analyzed longitudinally, and histopathological analysis of atherosclerosis and transcriptome analysis of the liver was performed. Imatinib and ponatinib decreased plasma cholesterol (imatinib, −69%, $p<0.001$; ponatinib 3 mg/kg, −37%, $p<0.001$; ponatinib 10 mg/kg, −44%, $p<0.001$) and atherosclerotic lesion area (imatinib, −78%, $p<0.001$; ponatinib 3 mg/kg, −52%, $p=0.002$; ponatinib 10 mg/kg, −48%, $p=0.006$), which were not affected by nilotinib. In addition, imatinib increased plaque stability. Gene expression and pathway analysis demonstrated that ponatinib enhanced the mRNA expression of coagulation factors of both the contact activation (intrinsic) and tissue factor (extrinsic) pathways. In line with this, ponatinib enhanced plasma levels of FVII, whereas nilotinib increased plasma FVIIa activity.

Conclusions: While imatinib showed a beneficial cardiovascular risk profile, nilotinib and ponatinib increased the cardiovascular risk through induction of a pro-thrombotic state.

Introduction

Chronic myeloid leukemia (CML) is a myeloproliferative neoplasm caused by a translocation of the chromosomes 9 and 22 that results in formation of the Bcr-Abl1 oncogene (1) and a constitutively active c-Abl kinase domain, which drives uncontrolled cell growth and tumorigenesis.

Patients with CML are treated with specific tyrosine kinase inhibitors (TKIs). The first-line TKI imatinib is widely used and has proven to be successful in the treatment of CML. However, relapses are seen in up to 17% of patients treated with imatinib (2) due to amplification and mutations in the Bcr-Abl1 gene (3) that lead to imatinib resistance. The second and third generation TKIs, nilotinib and ponatinib among others, are effective against these mutations (3), and promising results have been found in relapsed patients (4). Unfortunately, side effects have been reported in patients receiving these TKIs including myocardial infarction and progressive arterial occlusive disease (PAOD) (5–7). As a result, ponatinib was temporarily removed from the US market, and was later reintroduced for the treatment of patients with T315I-positive CML or those in whom no other TKI was indicated.

Since the first reports of vascular adverse effects (VAEs), many authors related the adverse effects of TKI treatment to atherosclerosis and abnormal platelet function (4,7–9). However, it is still unclear whether the side effects are caused by enhanced vascular inflammation and endothelial dysfunction, atherosclerosis development, increased thrombotic activity per se, or a combination of these processes. Furthermore, the underlying disease has been reported to affect metabolic parameters (10) and coagulation (11), which may interfere with the onset of the side-effects upon treatment. Therefore, to elucidate the role of TKI treatment on VAE's independently of a background of leukemia, we performed a detailed experimental study in healthy pro-atherogenic mice. The aim of this study was to assess the (cardio)vascular side effects of the second and third generation of TKIs, nilotinib and ponatinib, and to compare their effects to the first generation TKI imatinib.

In this study, we used the APOE*3-Leiden.CETP mouse as a well-established model for dyslipidemia and atherosclerosis, with a human-like lipoprotein metabolism and atherosclerosis development. These mice show a human-like response to all lipid-modulating interventions that are being used in the clinic (12–18) and have been used previously to investigate the underlying mechanism of cardiovascular safety issues (19).

We found that imatinib and ponatinib decreased plasma cholesterol, which was associated with decreased atherosclerosis development. Gene expression and pathway analysis demonstrated adverse alterations in genes involved in coagulation which were in line with increased plasma levels of FVII and FVIIa by ponatinib and nilotinib respectively, pointing towards thrombosis instead of atherosclerosis as inducer of the VAEs.

Materials and methods

Animals

Female APOE*3-Leiden.CETP transgenic mice (9 to 14 weeks of age) from the SPF breeding stock at TNO-Metabolic Health Research (TNO-Leiden) were used in this study. Females were used because they are more responsive to dietary cholesterol and fat than males. APOE*3-Leiden females have a higher VLDL production (20) than males resulting in higher plasma total cholesterol (TC) and triglyceride (TG) levels and more pronounced development of atherosclerosis (21,22). During the study, mice were housed under standard conditions with a 12 h light-dark cycle and had free access to food and water. Body weight, food intake and clinical signs of behavior were monitored regularly during the study. Animal experiments were approved by the Institutional Animal Care and Use Committee of The Netherlands Organization for Applied Research under registration number 3557.

Experimental design and analyses

Mice were fed a semi-synthetic diet, containing saturated fat from 15% (w/w) cacao butter and 0.15% cholesterol (Western-type diet [WTD]; Hope Farms, Woerden, The Netherlands). All studies started after a run-in period of 3 weeks on WTD, which is designated as t=0 weeks/baseline, after which mice were matched into groups based on body weight, total cholesterol (TC), plasma triglycerides (TG) and age. For the pharmacokinetic (PK) study, mice were randomized in 3 groups (n=9 per group) and received a single oral gavage with imatinib (100 mg/kg), nilotinib (50 mg/kg) or ponatinib (5 mg/kg). At 0.5, 1 and 2 h after oral gavage, blood was sampled from 3 mice per group per time point, and at 4, 7 and 24 h blood was collected by heart puncture after sacrifice. For the (cardio)vascular risk factor and atherosclerosis study, mice were randomized in 6 groups (n=15 per group, n=20 in control group) and received, based on the results of the PK study, a once-daily oral gavage with nilotinib (10 or 30 mg/kg), ponatinib (3 or 10 mg/kg), or a twice-daily gavage with imatinib (150 mg/kg). The TKIs were suspended in 5% carboxymethyl cellulose and all mice except the imatinib group received a second oral gavage with the vehicle alone (5% carboxymethyl cellulose). The TKIs were purchased at LC laboratories, Woburn (MA), USA. After 12 weeks 5 mice of the control group were sacrificed to asses atherosclerosis development and to determine the end-point of the study. After sixteen weeks of treatment all animals were sacrificed by CO_2 inhalation. Plasma cholesterol, TG, high-density lipoprotein cholesterol (HDL-C), lipoprotein profiles, serum amyloid A (SAA), E-selectin and monocyte chemoattractant protein 1 (MCP-1), aspartate transaminase (AST) and alanine transaminase (ALT) were measured throughout the study. Blood pressure was measured at 2 and 15 weeks of treatment. Measurement of hepatic lipid and protein content; protein and albumin content in broncho-alveolar lavage (BAL) fluid; urinary albumin/creatinine levels; and histology of lung and hearts was performed at 16 weeks. Total FVII coagulant

activity was measured at 4 and 12 weeks and FVIIa activity at 4 weeks. Gene expression analysis using Next Generation Sequencing with the Illumina Nextseq 500 and subsequent pathway analysis of liver of 8 mice per group was performed following established protocols (23,24).

PK analysis and plasma drug concentrations

EDTA plasma samples collected during the 24-hour PK study and at week 16 of the (cardio) vascular risk factor-atherosclerosis study were subsequently stored at -80°C until analysis. Thawed plasma samples (50 µL) were de-proteinized with two volumes of acetonitrile containing an appropriate src-inhibitor chemotype as internal standard for each analyte. Following deproteinization, a 5 µL portion of clear supernatant was then subjected to solvent gradient separation in an Agilent 1100 series HPLC system interfaced to a Micromass triple-quadrupole mass spectrometer, which was operated in the positive ion electrospray MRM mode to obtain daughter ions for quantitation: Ion transitions used for quantitation were as follows: imatinib [494.3 -> 394.2], nilotinib [530.2 -> 289.2], ponatinib [533.3 -> 260.3]. Standard curves ranging from 1 nM to 6 µM were fitted with a quadratic regression weighted by reciprocal concentration (1/x). LLOQ for the purposes of this assay was between 1 and 2 nM for all compounds analyzed. QC samples at three levels in the range of the standard curve were used to accept individual analytical sets, and all results were calculated as the mean of triplicate determinations ± standard error. T_{max}, C_{max} and AUCs were calculated using the software Berkeley Madonna (version 8.3.18).

Biochemical analyses and blood pressure

EDTA plasma samples were collected throughout the study. Plasma cholesterol and triglycerides were determined every 4 weeks using enzymatic kits (Roche/Hitachi) according to the manufacturer's protocols and average plasma levels over week 4 to 16 were calculated. HDL-C was measured after precipitation as described previously (17). The distribution of cholesterol over plasma lipoproteins was determined in group wise-pooled plasma by fast protein liquid chromatography (FPLC) (25). The inflammatory markers SAA, E-selectin and MCP-1 were measured using the ELISA kits from Tridelta (SAA) and R&D (MCP-1, E-selectin) according to the manufacturer's instruction. Plasma ALT and AST were determined using a spectrophotometric assay (Boehringer Reflotron system) in group wise-pooled samples. Systolic blood pressure (SBP), diastolic blood pressure (DBP) and heart rate were measured using the tail cuff method in 8 mice per group at 2 and 15 weeks (26).

Hepatic lipid analysis

Livers were isolated and partly homogenized (30 s at 5000 rpm) in saline (~10% wet wt/vol) using a mini-bead beater (Biospec Products, Inc., Bartlesville, OK). Lipids were extracted as described (27) previously and separated by high-performance thin-layer chromatography (HPTLC). Lipid spots were stained with color reagent (5 g $MnCl_{2\cdot4}H_2O$, 32 mL 95–97%

H_2SO_4 added to 960 mL of CH_3OH:H_2O 1:1 vol/vol) and quantified using TINA version 2.09 software (Raytest, Straubenhardt, Germany) (27).

BAL and urinary albumin/creatinine

The lungs were flushed two times with 750 µL PBS into the trachea using a BD 20G angio-catheter to collect broncho-alveolar lavage (BAL) fluid. Protein and albumin content in BAL fluid were determined in the supernatant using the protein determination kit from Pierce and the mouse albumin ELISA kit (ALPCO, Salem, USA). Urinary albumin and creatinine levels were determined using the mouse albumin ELISA kit (ALPCO, Salem, USA) and the creatinine kit (Exocell, Philadelphia, USA) according to manufacturer's instruction.

Flow cytometric analysis

White cell profiling was performed via fluorescence activated cell sorting (FACS) using the BD FACS Canto II apparatus (Becton Dickinson, Franklin Lakes, New Jersey, USA). After 12 weeks of treatment, peripheral blood mononuclear cells (PBMCs) were isolated from fresh blood samples of 8 mice per group, and were sorted into CD11b+/CD11c- (monocytes), and further divided into CD11b+/Ly6C^{Low} and CD11b+/Ly6C^{High} monocytes. The following conjugated monoclonal antibodies, all from eBiosciences, were used: CD11b-FITC, CD11c-PE/Cy7, Ly6C-APC.

Coagulation factor VII and VIIa

Total clotting FVII and FVIIa activity were measured on a STA compact apparatus (Diagnostica Stago Inc. Parsippany, NJ). For the determination of total clotting FVII a one stage Prothrombin assay with Dade Innovin PT reagent (Siemens) and Hemoclot FVII reagent (Hyphen Biomed) as deficient agent were used and calibration was performed with pooled normal mouse plasma. Staclot VIIa rTF (Diagnostica Stago Inc.) and Hemoclot FVII reagent (Hyphen Biomed) were used to determine FVIIa activity, calibrated with Novoseven® (Novonordisk).

Histological assessment of lung morphology and atherosclerosis

Tissues were isolated, fixed in formalin, and embedded in paraffin. The caudal lung was cross sectioned (3 µm thick) and stained with hematoxylin-eosin (HE), Sirius Red for collagen, and with isolectin B4 (1:50; Sigma-Aldrich, Missouri, USA) for endothelial cells. Hearts were sectioned perpendicular to the axis of the aorta, starting within the heart and working in the direction of the aortic arch. Once the aortic root was identified by the appearance of aortic valve leaflets and smooth muscle cells instead of collagen-rich tissue, serial cross sections (5 µm thick with intervals of 50 µm) were taken and mounted on AAS-coated slides. These sections were stained with hematoxylin-phloxine-saffron (HPS) for histological analysis. For each mouse, atherosclerosis was measured in 4 subsequent cross-sections. Each section consisted of 3 segments. The average total lesion area per

cross-section was then calculated (17,28). For determination of lesion severity the lesions were classified into five categories according to the American Heart Association classification (29): 0) no lesion I) early fatty streak, II) regular fatty streak, III) mild plaque, IV) moderate plaque, and V) severe plaque. The percentage of each lesion type was calculated, where type I-III lesions were classified as mild lesions and type IV-V lesions were classified as severe lesions (17,28). In the aortic root, lesion composition was determined for the severe lesions (type IV-V) as a percentage of lesion area after immunostaining with anti-human alpha-actin (1:400; PROGEN Biotechnik GmbH, Germany) for smooth muscle cells (SMC), and anti-mouse Mac-3 (1:50; BD Pharmingen, the Netherlands) for macrophages followed by Sirius Red staining. After Sirius Red staining for collagen, color intensity was determined in ImageJ and the used threshold was confirmed by evaluation of the sections under polarized light (30). Necrotic area and cholesterol clefts were measured after HPS staining (17,28,31). Lesion stability index was calculated as described previously (17,31). In each segment used for lesion quantification, the number of monocytes adhering to the endothelium were counted after immunostaining with AIA 31240 antibody (1:1000; Accurate Chemical and Scientific, New York, New York, USA) (16,17).

Gene expression analysis

Messenger RNA was isolated from liver of 8 mice per group, using the NEBNext Ultra RNA sample Prep Kit. After fragmentation of the mRNA, cDNA synthesis was performed. The quality and yield after sample preparation was measured with the Fragment Analyzer. Clustering and DNA sequencing was performed using the Illumina Nextseq 500. The genome reference and annotation file Mus_Musculus.GRCm38 was used for analysis in FastA and GTF format. The reads were aligned to the reference sequence using Tophat 2.0.14 combined with Bowtie 2.1.0, and based on the mapped read locations and the gene annotation HTSeq-count version 0.6.1p1 was used to count how often a read was mapped on the transcript region. Calculated p-values <0.01 were used as threshold for significance. Selected differentially expressed genes (DEGs) were used as an input for pathway analysis through Ingenuity Pathway Analysis (IPA) suite (www.ingenuity.com, accessed 2015). Gene set enrichment analysis was used to highlight the most important processes and pathways. Relevance of these pathways and processes is indicated as p-value and visualized in a graph by calculating the –log(p-value).

Statistical analysis

Significance of differences between the groups was calculated in SPSS 22.0 for Windows. Normally distributed data was tested parametrically using a one-way ANOVA for multiple comparisons with a Dunnett's post-hoc test. Non-parametric data were compared separately with a Mann-Whitney U test with adjusted rejection criteria using a Bonferroni-Holm correction. Correlations between lesion size (after square root transformation) and cholesterol exposure were calculated with a Pearson's correlation test. All groups

were compared with the control group. Values are presented as means ± SD and p-values <0.05 were considered statistically significant.

Results

PK analysis and plasma drug concentrations

Pharmacokinetic analysis was performed after a single dose of imatinib (100 mg/kg), nilotinib (50 mg/kg) or ponatinib (5 mg/kg) (**Table 1**) and based on these results the doses for the atherosclerosis study were adjusted to twice daily 150 mg/kg for imatinib, once daily 10 or 30 mg/kg for nilotinib and once daily 3 or 10 mg/kg for ponatinib. The relatively high dose of imatinib needed to achieve plasma concentrations comparable to those in CML-patients was due to the short half-life of the drug in mice and is in line with previous reports (32). Drug exposure after repeated dosing was measured in sacrifice plasma and calculated AUCs were similar to those in CML-patients for imatinib and the low doses of nilotinib and ponatinib (**Table 1**).

Safety aspects of treatments with TKIs

No clinical signs of deviant behavior and no effects on body weight and food intake were noted in any treatment group as compared with control. Plasma ALT and AST, measured at the start and after 16 weeks of treatment, showed no aberrant results (**Table 2**). The number of circulating peripheral blood mononuclear cells (PBMC's) in the blood as measured by FACS analysis at 12 weeks (**Table 2**) was reduced by imatinib (–42%, p=0.006) and by the high-dose ponatinib (–44%, p=0.003). In addition, imatinib and the high doses of nilotinib and ponatinib decreased pro-inflammatory Ly6C^{High} monocytes, all consistent with the mode of action of TKIs. Two mice (ponatinib 3 mg/kg) died during blood pressure measurements at t=15 weeks, and one mouse (nilotinib 30 mg/kg) was excluded from atherosclerosis measurement due to deviating heart anatomy.

(Cardio) vascular risk factors

Imatinib and ponatinib reduce plasma cholesterol levels

As dyslipidemia is a major risk factor for cardiovascular disease, we measured plasma cholesterol and triglyceride levels throughout the study, and HDL-C at the end point. The WTD resulted in an average plasma cholesterol of 17.3 ± 3.5 mmol/L, TGs of 3.3 ± 1.0 mmol/L, and an HDL-C level of 1.4 ± 0.2 mmol/L in the control group. When compared to the control group, imatinib reduced average cholesterol and TG levels by 69% (p<0.001) and 36% (p=0.019), respectively. Ponatinib decreased cholesterol levels by 37% (3 mg/kg, p<0.001) and 44% (10 mg/kg, p<0.001), whereas nilotinib had no significant effect on plasma lipid levels (**Figure 1A–D**). At 16 weeks of treatment, HDL-C was decreased by ponatinib in both the low (–30%, p=0.003) and high (–25%, p=0.016) dose. The reduction

Table 1 Pharmacokinetics of imatinib, nilotinib and ponatinib in APOE*3-Leiden.CETP mice and CML-patients

TKI	APOE*3-Leiden.CETP mice					CML patients				
	Dose (mg/kg)		T_{max} (h)	C_{max} (µg/mL)	AUC_{0-24} (µg/mL*h)	Dose (mg/kg)		subject	AUC_{0-24} (µg/mL*h)	reference
Imatinib	Single	100	2.28	5.29	32.79	Day 1, BID	400	CML-patients	36.2 ± 7.4	(33)
	Repeated dose, BID	150	2.47	11.07	78.13	Steady state, BID	400	CML-patients	68.4 ± 29.8	(33)
Nilotinib	Single	50	3.26	10.97	117.49	Single, QD	400	Healthy subjects	14.7 ± 5.0	(34)
	Repeated dose, QD	10	3.17	2.30	24.60	Repeated dose, QD	400-1200	CML-patients	36.0 ± 11.8	(34)
	Repeated dose, QD	30	3.17	6.89	73.81					
Ponatnib	Single	5	8.00	0.19	3.24	Single, QD	60	CML-patients	0.7 ± 0.4	(35)
	Repeated dose, QD	3	6.72	0.14	2.43	Repeated dose, QD	15-60	CML-patients	1.3	(36)

T_{max}, C_{max} and AUC_{0-24} were calculated after a single dose or after 16 weeks of treatment (repeated dose) for imatinib, nilotinib and ponatinib and compared with plasma concentrations in CML patients. Data are presented as means (APOE*3-Leiden.CETP mice) and means ± SD (CML-patients), unless SD was not given in the reports. Abbreviations: AUC, area under the curve; BID, twice a day; CML, chronic myeloid leukemia; QD, once a day.

Table 2 Safety aspects of TKI treatment, the number of PBMCs and the fraction CD11b+Ly6C$^{High/Low}$ monocytes. Body weight, food intake (per cage) plasma ALT (pooled), and plasma AST (pooled) at baseline and after 16 weeks of treatment with imatinib (150 mg/kg, BID), nilotinib (10 and 30 mg/kg) or ponatinib (3 and 10 mg/kg). After 12 weeks, FACS analysis was performed.

	Dose	Body weight	Food intake	ALT	AST	Number of live/single PBMCs per mL blood	% of monocyte population	
	mg/kg	*gram*	*gram/mouse/day*	*U/L*	*U/L*	*(*10^6/mL)*	**CD11b+Ly6C^{High}**	**CD11b+Ly6C^{Low}**
Baseline	-	21.6 ± 1.7	3.0	57	163	-	-	-
Control	-	23.3 ± 2.4	2.5	54	224	6.8 ± 1.3	19.0 ± 4.4	71.7 ± 3.9
Imatinib	150	22.1 ± 0.8	2.6	31	147	3.9 ± 1.3**	11.0 ± 3.6**	69.1 ± 5.9
Nilotinib	10	22.5 ± 1.5	2.3	64	210	6.5 ± 2.4	27.5 ± 4.3	61.4 ± 4.8
	30	22.2 ± 1.3	2.4	81	221	6.4 ± 1.4	11.4 ± 3.8*	73.2 ± 4.9
Ponatinib	3	22.5 ± 2.3	2.4	44	196	7.1 ± 1.7	26.1 ± 2.9	58.4 ± 2.5
	10	22.3 ± 2.8	2.3	31	207	3.8 ± 0.8**	12.6 ± 3.1*	69.1 ± 6.4

Data are presented as means ± SD (n=13-15 per group; n=7-8 per group for FACS analysis) or as means (cage or group level) (n=2-4 mice per cage).
*p<0.05, **p<0.01 as compared to control. Abbreviations: ALT, Alanine transaminase; AST, aspartate transaminase; PBMCs, peripheral blood mononuclear cells.

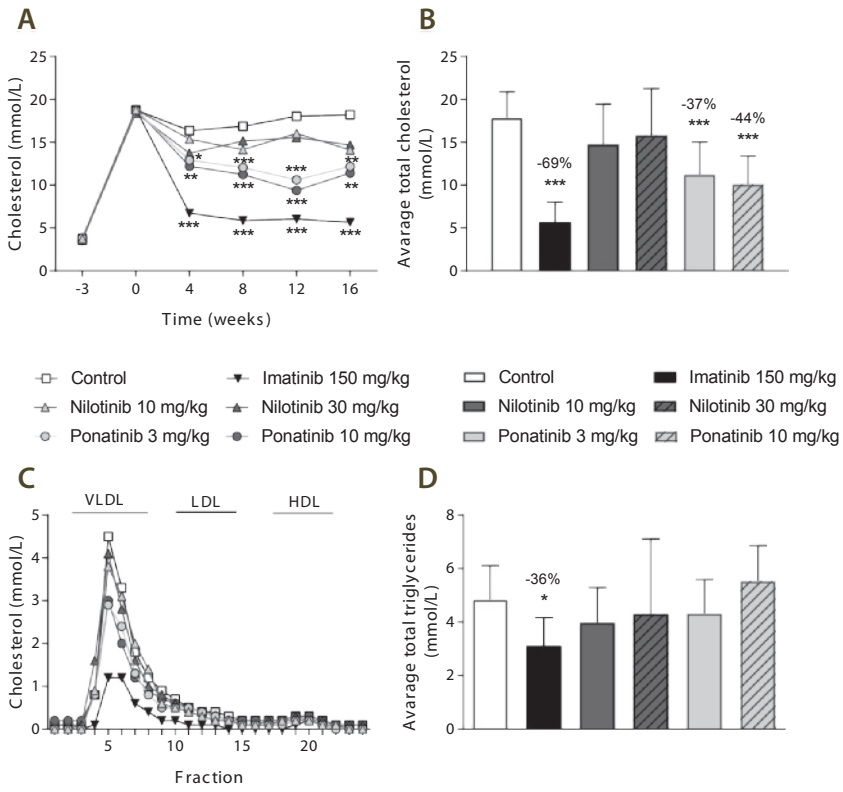

Figure 1 Imatinib and ponatinib reduce plasma cholesterol levels and imatinib decreases average TGs. Plasma cholesterol was measured throughout the 16 week study (A) and average plasma cholesterol (B) and TGs (D) were calculated. Lipoprotein profiles were assessed by FPLC lipoprotein separation after 16 weeks of treatment (C). Data are presented as means ± SD (n = 13–15 per group). *p < 0.05, **p < 0.01 ***p < 0.001. Abbreviations: FPLC, Fast protein liquid chromatography; VLDL, very-low-density-lipoprotein; LDL, low-densitylipoprotein; HDL, high-density-lipoprotein; TGs, triglycerides.

of plasma cholesterol by imatinib and ponatinib was mainly confined to VLDL-LDL (i.e., non-HDL) (**Figure 1C**). These findings show that imatinib decreases plasma cholesterol and TG levels in APOE*3-Leiden.CETP mice, which is consistent with the cholesterol-lowering effect observed in patients (37–40).

Ponatinib and imatinib decrease hepatic lipid content

Liver lipid storage may give insight into how lipid metabolism is affected by imatinib and ponatinib. Therefore, hepatic lipid content was measured by HPTLC. Free cholesterol

content was decreased by 10 mg/kg ponatinib (–21%, p=0.007) (**Figure 2A**), cholesterol ester content was decreased by imatinib (–30%, p=0.001) and by both the low (–49%, p<0.001) and high (–61%, p<0.001) dose of ponatinib (**Figure 2B**). TG content was decreased by the low (–32%, p=0.048) and high (–43%, p=0.005) dose of ponatinib (**Figure 2C**). These data point to a shortage of cholesterol in the liver and suggest that not cholesterol clearance, but VLDL production and/or intestinal absorption of cholesterol are affected by ponatinib and imatinib.

Blood pressure and vascular dysfunction

Increased blood pressure and endothelial activation may lead to vascular dysfunction and atherosclerosis. SBP, measured after 2 and 15 weeks of treatment, was 91 ± 7 and 86 ± 5 mmHg, respectively, in the control group, and heart rate was 726 ± 46 and 716 ± 29 beats per minute. SBP and heart rate were not affected by imatinib, nilotinib or ponatinib treatment. As markers of vascular integrity and leakage or edema formation, we evaluated lung histology, determined the wet/dry weight ratio of the lungs and measured the amount of protein in the BAL fluid. None of the anti-CML drugs showed significant effects on histology and wet/dry weight ratio (data not shown), and ponatinib decreased the amount of protein in BAL fluid by 51% (3 mg/kg, p=0.029) and by 47% (10 mg/kg, p=0.041) (**Table 3**). In contrast, ponatinib increased the urinary albumin/creatinine ratio (approximately 13-fold, N.S.), mainly due to 3 mice with very high levels of urinary albumin (**Table 3**). These data indicate that the anti-CML drugs did not cause damage to the microvasculature in the lungs but that ponatinib may lead to microvascular dysfunction in the kidney.

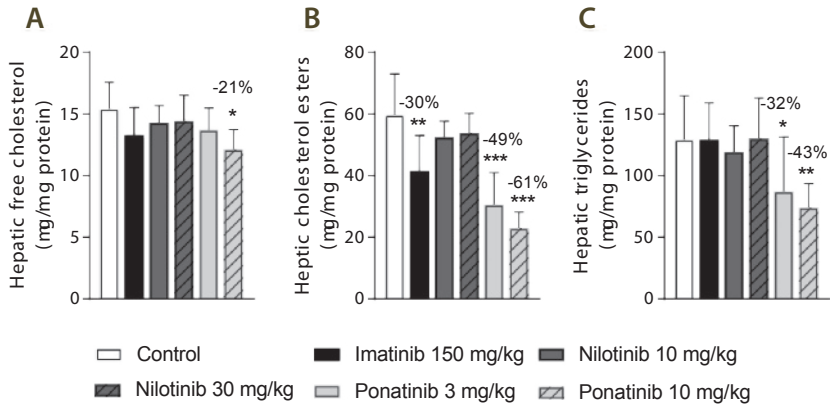

Figure 2 Imatinib and ponatinib decrease hepatic lipid content. Hepatic free cholesterol (A), cholesterol ester (B) and triglyceride (C) content were measured by HPTLC after 16 weeks of treatment. Data are presented as means ± SD (n=8 per group).*p < 0.05, **p < 0.01 ***p < 0.001. Abbreviations: HPTLC, high-performance thin-layer chromatography.

Table 3 Ponatinib increases markers of inflammation

Treatment	Dose	BAL fluid		Urinary ureum/ creatinine ratio	MCP-1	SAA	E-selectin
	mg/kg	*Protein (µg/mL)*	*Albumin (µg/mL)*		*pg/mL*	*µg/mL*	*ng/mL*
Baseline	-	-	-	-	45 ± 23	6.8 ± 4.4	87 ± 9
Control	-	405 ± 291	243 ± 168	12.4 ± 4.6	102 ± 44†	10.1 ± 1.2	96 ± 18
Imatinib	150	330 ± 176	192 ± 94	20.5 ± 9.6	54 ± 44	9.6 ± 0.5	71 ± 18
Nilotinib	10	400 ± 207	235 ± 126	10.5 ± 8.8	144 ± 82‡	10.6 ± 1.0	79 ± 23
	30	265 ± 103	168 ± 66	10.1 ± 2.6	117 ± 60‡	10.6 ± 1.1	99 ± 17
Ponatinib	3	198 ±75*	129 ± 54	12.3 ± 6.0	78 ± 29	10.4 ± 1.9	77 ± 22
	10	215 ± 61*	144 ± 38	158.2 ± 371.9	92 ± 68	15.2 ± 21.1†	250 ± 307**/‡

Effect of imatinib, nilotinib and ponatinib on BAL fluid, urinary ureum/creatinine ratio and inflammatory markers as measured at baseline (t=0 weeks) and after 16 weeks of treatment. Data are presented as means ± SD (n = 8–15 per group).*p<0.05, **p<0.001 as compared to control, †p<0.05, ‡p<0.001 as compared to baseline. Abbreviations: BAL, broncho-alveolar lavage; MCP-1, monocyte chemoattractant protein-1; SAA, serum amyloid A.

Ponatinib increases plasma E-selectin

Inflammation is widely considered as an important contributing factor to cardiovascular events (41). Therefore, we measured plasma levels of macrophage-derived chemokine MCP-1, the adhesion molecule E-selectin as marker of endothelial activation, and SAA, an acute phase protein mainly produced by the liver (**Table 3**). None of the inflammatory markers were significantly altered by imatinib. The WTD increased MCP-1 relative to baseline (t=0 weeks) (+126%, p=0.015), as did nilotinib (10 mg/kg, +220%, p<0.001; 30 mg/kg, +160%, p<0.001). Ponatinib increased SAA relative to baseline (+123%, p=0.013), but not relative to control. In four of the fifteen ponatinib-treated mice, E-selectin levels were 3 to 10 times increased, leading to an overall increase of 161% (p<0.001) when compared to control, which may point to endothelial activation by ponatinib. Collectively, these data confirm the safety profile of imatinib and suggest endothelial activation and potential endothelial dysfunction in some animals by ponatinib.

Atherosclerosis

Imatinib and ponatinib reduce lesion size and severity

Next we analyzed the effects of long-term exposure of the anti-CML TKIs on the progression of atherosclerosis as a cardiovascular endpoint, as shown by representative images (**Figure 3**). Sixteen weeks of WTD resulted in the development of 4.0 ± 0.8 atherosclerotic lesions and 156 ± 61*1 000 µm^2 lesion area per cross-section in the control group (**Figure 4A**). Approximately 55% of these lesions were severe (type IV–V) lesions and only 10% of the segments were unaffected (**Figure 4B**). The total number of lesions was not

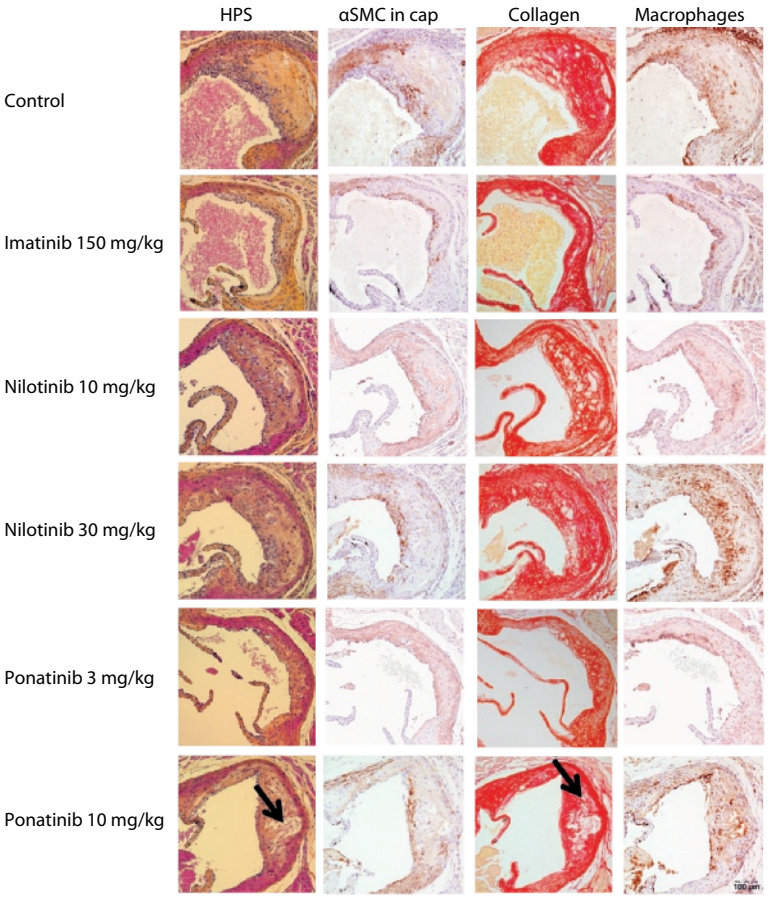

Figure 3 Effect of imatinib, nilotinib and ponatinib on plaque composition. Representative images of HPS staining, immunostaining with α-actin for SMCs, Sirius red staining for collagen and immunostaining with Mac-3 for macrophages. The arrows depict necrotic areas, including cholesterol clefts. Abbreviations: HPS, hematoxylin-phloxine-saffron; SMCs, smooth muscle cells; MAC-3, Purified anti-mouse CD107b Mac-3 Antibody.

affected by any treatment (data not shown), but imatinib and ponatinib diminished the lesion area by 78% ($p<0.001$), 52% (3 mg/kg, $p=0.002$), and 48% (10 mg/kg, $p=0.006$), respectively (**Figure 4A**). In addition, the total lesion area that consisted of severe lesions was reduced by imatinib (–56%, $p<0.001$) (**Figure 4B**). Next, we evaluated whether this anti-atherogenic effect of imatinib and ponatinib could be explained by the reduction in plasma cholesterol levels. The square root of the lesion size was positively correlated with

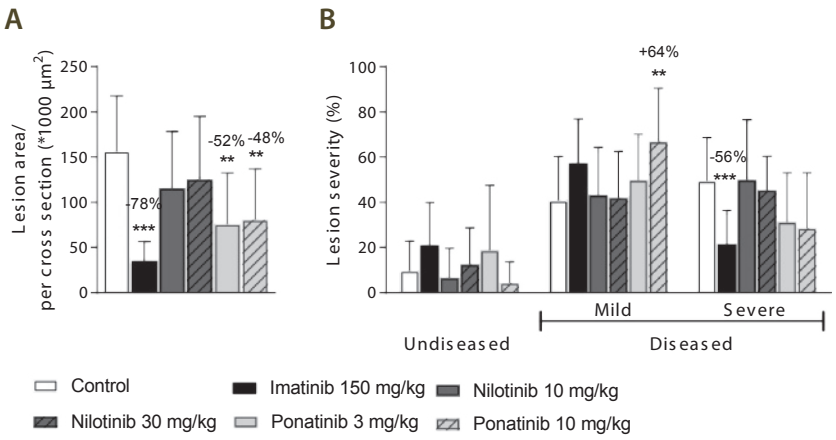

Figure 4 Imatinib and ponatinib reduce atherosclerotic progression. After 16 weeks of treatment, the total lesion area per cross-section was assessed (A). Lesion severity was assessed, categorized as no lesions/undiseased, mild lesions (type I-III) and severe lesions (type IV-V) and expressed as percentage of total lesion area. (B). Data are presented as means ± SD (n=13–15 per group).**p<0.01 ***p<0.001.

plasma cholesterol exposure (mmol/L*weeks) in control, imatinib and high dose nilotinib and ponatinib treated mice (control R^2=0.79, p=0.001; imatinib R^2=0.71, p=0.003; ponatinib 10 mg/kg R^2=0.79, p<0.001; nilotinib 30 mg/kg R^2=0.63, p=0.016) (**Figure 5**). Lesion size per cross-section was not correlated with inflammation markers or blood pressure, indicating a dominant role of plasma cholesterol and cholesterol-lowering by the drugs in the development of atherosclerosis.

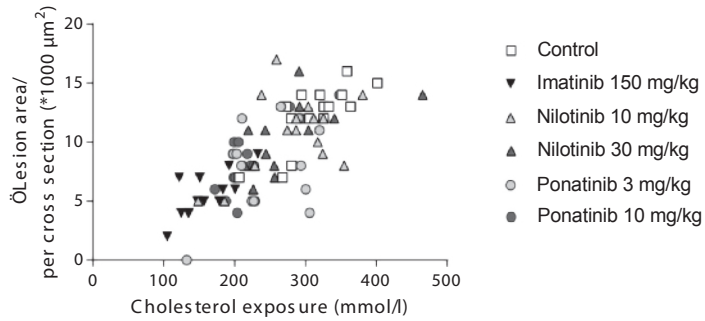

Figure 5 Atherosclerotic lesion area is correlated with cholesterol exposure. Correlation between cholesterol exposure (mmol/L*weeks) and the square root of the lesion area was calculated with a Pearsons's correlation test (n=13–15 per group).

Imatinib improves plaque morphology

To assess the plaque phenotype as a marker for vulnerability to rupture, lesion morphology was analyzed in the type IV and V lesions from mice treated with imatinib and the high dosages of nilotinib and ponatinib, as shown by representative images (**Figure 3**). The macrophage and necrosis content were quantified as factors that decrease plaque stability, and smooth muscle cell area in the cap of the lesions and collagen as factors that improve plaque stability (17,26,31) (**Figure 6A**). Average macrophage, necrotic core, collagen and αSMC content in the control group were 24 ± 8%, 4 ± 2%, 42 ± 10% and 4 ± 3%, respectively (**Figure 6A**). Imatinib increased the collagen content by 47% (62 ± 17%, p=0.004) and tended to increase αSMC content (+38%, p=0.050), resulting in an enhanced lesion stability index (+216%, p=0.004) (**Figure 6B**). Nilotinib (10 mg/kg) decreased collagen content (–32%, p=0.003), resulting in a decreased lesion stability index (–43%, p=0.003). Ponatinib (3 mg/kg) decreased necrotic core content (–58%, p=0.001) without affecting plaque stability. Collectively, these data indicate that imatinib induces a more stable plaque phenotype with collagen-rich lesions.

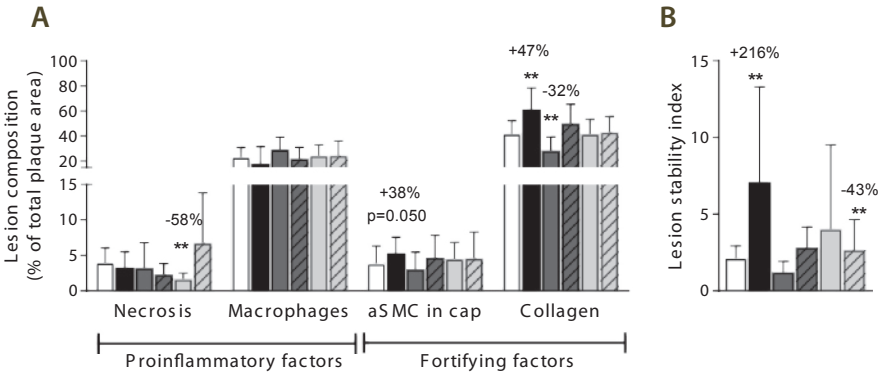

Figure 6 Imatinib increases plaque stability. Necrotic and macrophage content as pro-inflammatory factors, and αSMCs and collagen as fortifying factors, were determined in the severe (type IV-V) lesions and expressed as percentage of total plaque area (A). Plaque stability index was calculated (B). Data are presented as means ± SD (n=13–15 per group). **p<0.01. Abbreviations: aSMC; α smooth muscle cells.

Transcriptome analysis

Ponatinib adversely alters gene expression of coagulation factors

To find early molecular signatures of other clinically relevant processes induced by the anti-CML drugs, gene expression and pathway analysis was performed in the liver as the central organ in lipid metabolism and synthesis of coagulation factors. To identify drug-specific molecular responses and overlap between the various treatments, the total

number of differentially expressed genes (DEGs) was assessed and a Venn-diagram was constructed comprising all DEGs compared to control group. Both ponatinib and nilotinib displayed a dose-dependent increase in the total number of DEGs as compared to control and the molecular response of the high-dose ponatinib had more overlapping genes with imatinib than nilotinib (**Figure 7**).

General categorization of biological functions showed that all anti-CML drugs affect canonical pathways associated with mitochondrial dysfunction and oxidative phosphorylation, most likely induced by oxidative stress and leading to reduced energy production, and processes involved in protein synthesis and cell growth (EIF2 signaling), confirming the target-related molecular responses of anti-CML drugs. (**Figure 8**).

The processes relevant to (cardio)vascular (side) effects of the anti-CML drugs are highlighted in **Figure 9** and **Figure 10**. Although gene expression data from the liver cannot be directly extrapolated to atherosclerosis signaling in the vascular wall, gene expression profiles of different organs have affiliation with each other and may be predictive for these biological processes. Therefore, the transcriptome data of the liver as predicting organ are given. As compared to the other TKI's, imatinib showed the most pronounced effects on atherosclerosis signaling, with favorable regulation of genes involved in cell adhesion (*Integrin β2* and *α4, Icam1, Vcam1, Psgl-1*), macrophage activation (*Cd40, Tnfrsf14, Scara1, Nfκb*), lipid regulation (*Lpl, Apoa1, Apoa2, Apoc2, Apoc4, Pla2g7*), inflammatory processes (*Cd40, Nfκb, Il1a, Tnfrsf14, Icam1, Vcam1*) and genes related to extracellular matrix modulation (*Col1a2, Col3a1, Col1a1, Mmp13, Tgf-β*) (**Figure 9**). Ponatinib showed similar effects, but to a lesser extent, whereas these effects were not observed after nilotinib treatment (**Figure 9**).

As the site of synthesis of a large number of coagulation factors, the liver plays an important role in the regulation of hemostatic and thrombotic processes. Although all three TKIs to some extent affected the coagulation pathways, ponatinib had the most adverse profile (**Figure 10**). Ponatinib increased the gene expression of members of the intrinsic or contact activation pathway, *Kng1a* and *Klkb1*, mainly involved in growth of a thrombus, and of the extrinsic or tissue factor pathway *F7*, involved in initiation of thrombus formation, and decreased gene expression of *Upa* and *Tpa*, both involved in fibrinolysis. Nilotinib showed down-regulation of the expression of *F5*, *F9*, and *Protein S*, while *Serpina1* (PAI-1) was up-regulated. Imatinib down-regulated the expression of *Upa*, *Tpa* and *Protein S* and up-regulated *Serpina1* and *Protein C*. This analysis demonstrates that among the three anti-CML drugs investigated ponatinib most prominently induces adverse alterations in the gene expression of coagulation factors in both the intrinsic and extrinsic pathway, which may lead to a state of hypercoagulability.

A

	Number of differentially expressed genes versus control group				
	Imatinib 150 mg/kg BID	Nilotinib 10 mg/kg QD	Nilotinib 30 mg/kg QD	Ponatinib 3 mg/kg QD	Ponatinib 10 mg/kg QD
Imatinib 150 mg/kg BID	1575	224	417	213	670
Nilotinib 10 mg/kg QD		474	313	41	248
Nilotinib 30 mg/kg QD			1066	78	484
Ponatinib 3 mg/kg QD				504	235
Ponatinib 10 mg/kg QD					1344

B

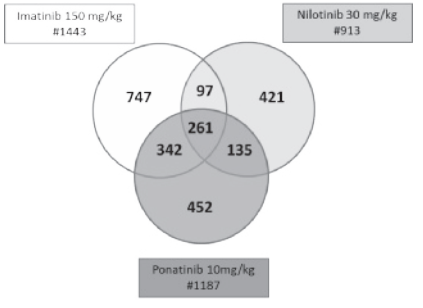

C

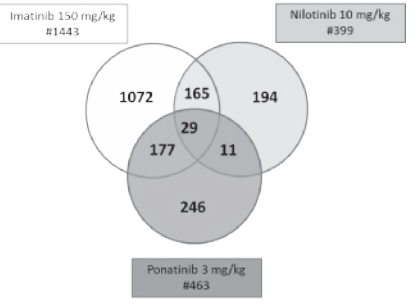

Figure 7 Overview of differentially expressed genes (DEGs). The numbers in the diagonal display DEG compared to control. The numbers above the diagonal indicate the number of DEGs shared between the treatment groups. Bayes pvalues of <0.01 were used as cut-off (A). To evaluate which biological processes are affected with the various treatments, all genes (p<0.01) were uploaded in the Ingenuity Pathway Analysis (IPA) tool to perform gene set enrichments. The number of differentially expressed genes that are annotated in IPA are indicated in Venn-diagrams (B-C). This number is slightly different between A and B-C since the RNA-seq method also detects genes that are not yet annotated in the IPA database (n=8 per group).

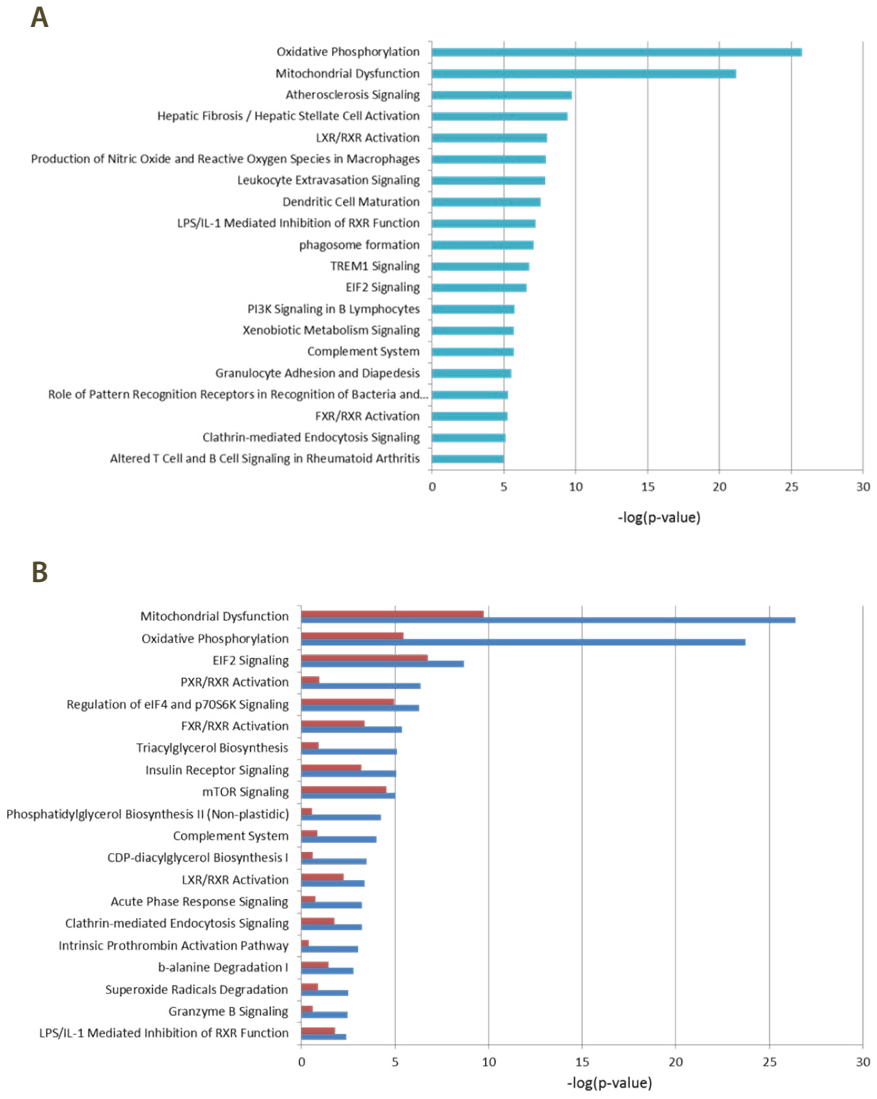

Figure 8 To identify the most relevant processes affected by TKI treatment, we calculated the canonical biological processes/ pathways affected by imatinib 150 mg/kg (A), nilotinib 10 mg/kg (red bars) and 30 mg/kg (blue bars) (B) and by ponatinib 3 mg/kg (red bars) and 10 mg/kg (blue bars) (C). The relevance of each process is indicated by a pvalue of overlap. The p-value of overlap is calculated based on Fisher's exact test which is set standard for overlap analysis in IPA-software. For visualization purposes the –log of the p-value of the top 20 processes are plotted on the x-axes (n=8 per group).

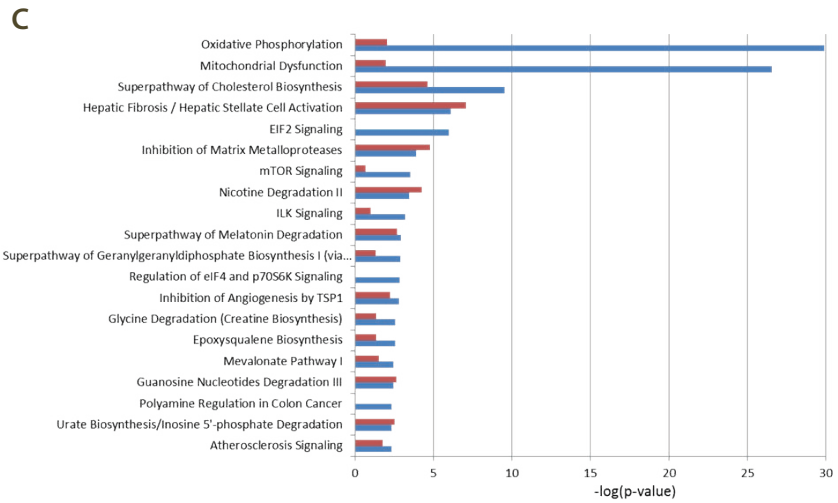

Figure 8 Continued.

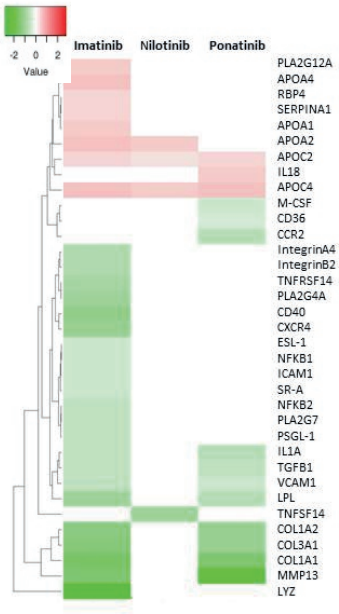

Figure 9 TKI treatment regulates many genes related to atherosclerosis signaling, with the most pronounced effect by imatinib. The heat map shows all significantly upregulated (red) and down-regulated (green) genes involved in atherosclerosis signaling of mice treated with imatinib (150 mg/kg), nilotinib (30 mg/kg) or ponatinib (10 mg/kg) as compared to control mice. P-values of <0.01 were used as cut-off (n=8 per group).

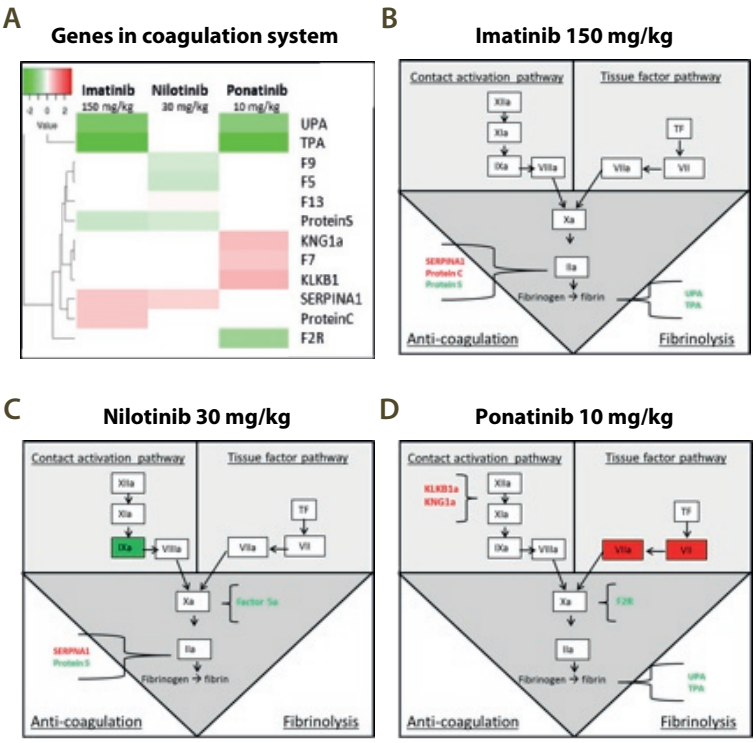

Figure 10 Genes in the coagulation system regulated by imatinib, nilotinib and ponatinib. The heat map shows all significantly ($p<0.01$) upregulated (red) and downregulated (green) genes involved in coagulation of mice treated with imatinib (150 mg/kg), nilotinib (30 mg/kg) or ponatinib (10 mg/kg) as compared to control mice (A). Imatinib regulates genes involved in anti-coagulation and fibrinolysis (B). Factor 9a and 5a were down-regulated and SERPINA1 up-regulated by nilotinib (C). Ponatinib showed the most adverse profile with upregulation of genes in both the contact activation and tissue factor pathway, together with downregulation of genes involved in fibrinolysis (D). pvalues of <0.01 were used as cut-off (n=8 per group).

Coagulation

Ponatinib increases plasma factor VII and nilotinib increases factor VIIa activity

Next, we measured total factor VII coagulant activity (FVII) and VIIa activity (FVIIa) in plasma. Ponatinib increased FVII after 4 weeks (10 mg/kg, +265%, $p<0.001$) and 12 weeks of treatment (3 mg/kg, +28%, $p=0.07$; 10 mg/kg + 82%, $p<0.001$) (**Figure 11A**). In addition, nilotinib increased the activity of FVIIa at 4 weeks by 82% (30 mg/kg, $p<0.001$) (**Figure 11B**). Together, these data confirm our findings on gene expression analysis and reveal the pro-thrombotic characteristics of nilotinib and ponatinib.

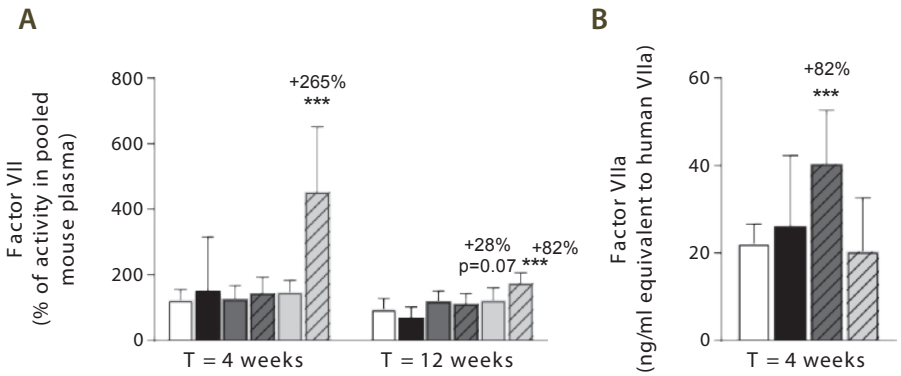

Figure 11 Ponatinib increases factor VII and nilotinib increases factor VIIa activity. Factor VII was measured after 4 and 12 weeks of treatment as the percentage of activity in reference pooled mouse plasma (A). Factor VIIa activity was measured after 4 weeks of treatment (B). Data are presented as means ± SD (n=6–20 per group).***p<0.001.

Discussion

This is the first study that compared the effect of a first, second and third generation BCR-ABL1 tyrosine kinase inhibitor on (cardio)vascular risk factors and atherosclerosis. Imatinib and ponatinib decreased plasma cholesterol and atherosclerosis, while nilotinib and ponatinib activated coagulation. The pharmacokinetic data we provide enabled us to use drug exposures translatable to CML-patients and can be used to optimize future TKI research. In addition, we provide a robust data set obtained by gene expression and pathway analysis of the liver, which predicted that ponatinib may lead to a pro-coagulant state by adversely affecting coagulation factors of both the contact activation (intrinsic) and tissue factor (extrinsic) pathways, which was confirmed by increased levels of the coagulation factor VII. In addition, nilotinib increased activity of FVIIa. These findings can be used by clinicians to carefully monitor coagulation parameters in CML-patients to predict risk of cardiovascular events.

The choice to perform this study in a non-leukemic mouse model has several reasons. First, there is, inherent to the diagnosis and progression of the disease, a shortage of suitable high quality plasma samples of CML patients collected at both baseline and follow-up under similar conditions. Second, CML affects both metabolic (10) and coagulation (11) parameters which makes it difficult to elucidate the role of TKI treatment on the reported VAEs independently of the underlying disease. Last, we were able to investigate a broad range of parameters, including atherosclerosis and gene expression and pathway analysis of the liver, which is not possible in CML-patients.

Imatinib and ponatinib, but not nilotinib, decreased plasma cholesterol contained in the pro-atherogenic apoB-containing lipoproteins. Cholesterol reduction and even normalization in hypercholesterolemic CML-patients is repeatedly described in retrospective studies with CML-patients for imatinib (37–39,42) and is consistent with our findings. Data on ponatinib are scarce (42) and it is unclear whether nilotinib affects plasma cholesterol in CML-patients. Some studies reported increased plasma cholesterol (5,8,40,42), whereas others question this (43). These opposing findings may be explained by the response to the underlying disease. It should be noted that nilotinib is often prescribed as a second-line treatment after resistance to imatinib. Reduced caloric intake induced by the leukemia and increased energy requirements imposed by tumor growth may result in lower cholesterol levels at baseline, while a positive response to treatment is often accompanied by increased cholesterol levels in oncologic patients (44). This response-related cholesterol elevation may be abolished by the cholesterol-lowering effects of imatinib and ponatinib per se as found in our study, resulting in decreased (imatinib) or normalized (ponatinib) plasma cholesterol levels in CML patients.

Several mechanisms are involved in cholesterol homeostasis, including intestinal uptake, hepatic uptake and secretion as lipoproteins, synthesis and storage, and fecal excretion. The decreased hepatic lipid content in imatinib and ponatinib treated mice (**Figure 2**) points to a shortage of cholesterol in the liver and suggests that not lipoprotein clearance, but VLDL production and/or intestinal absorption of cholesterol are affected by imatinib and ponatinib. Indeed, when myeloid tumor cells are treated with imatinib, de novo fatty acid synthesis is reduced, pointing towards decreased VLDL particle production (45). However, besides the shared activity of TKIs used for CML-treatment against the BCR-ABL1 tyrosine kinase, the potency and activity to affect off-target kinases differs markedly, and thus different processes may be involved. To our knowledge, no *in vivo* studies are available that investigated the effects of TKI treatment on cholesterol and lipoprotein metabolism, and functional studies are required.

Important observations from our study are the reduced development of atherosclerosis by imatinib and ponatinib which was correlated to decreased plasma cholesterol levels, and the increased plaque stability induced by imatinib, which has not been reported previously by others. There are no reports that describe the effect of ponatinib on atherosclerosis development in an animal model, and there are inconsistent reports on imatinib and nilotinib. In line with our findings, imatinib reduced atherosclerosis in STZ-induced diabetic ApoE$^{-/-}$ mice (46) and high fat fed ApoE$^{-/-}$ mice (47), though lesion reduction was independent of plasma cholesterol lowering and attributed to vascular wall remodeling and reduced inflammation. Interestingly, and in contrast with previous (46–48) and the present findings, Hadzijusufovic et al (49). did not find an effect of imatinib on atherosclerosis in ApoE$^{-/-}$ mice, but reported increased atherosclerosis by nilotinib. In addition, a direct pro-atherogenic effect on human endothelial cells was found, as shown by upregulation of adhesion factors ICAM-1, E-selectin and VCAM-1 (49), which is in line with the increase of

markers of endothelial activation found in CML patients treated with nilotinib (50). Unfortunately, no data on plasma cholesterol and markers of endothelial activation in the mice were provided. We do not have a clear explanation for the discrepancy with our findings, but the use of different animal models and dosages, as well as the underlying disease may play a role.

Ponatinib increased plasma E-selectin and urinary albumin/creatinine in some animals, suggesting endothelial activation and potential endothelial dysfunction, wherein aberrant angiogenesis might be involved. Indeed, an *in vitro* study using human umbilical vein endothelial cells (HUVECs) demonstrated the potential of ponatinib to reduce endothelium viability, and to induce apoptosis, reduce migration, inhibit tube formation, and to negatively affect endothelial progenitor cell function, all important for angiogenesis (51). In addition, ponatinib reduced von Willebrand factor (vWF) expression on lung endothelial cells in rats (52), which is an interesting finding, because vWF is not only a specific marker for endothelial cells, but also functions in coagulation.

Although there were no clinical signs of thrombosis or bleeding in our long-term study, an unbiased and exploratory transcriptome analysis revealed that ponatinib treatment lead to a pro-thrombotic state by affecting important players in the activation of the coagulation pathway. Ponatinib increased gene expression of *Klkb1*, *Kng1a* (part of the intrinsic or contact activation pathway) and *F7* (part of the extrinsic or tissue factor pathway) and decreased expression of *Upa* and *Tpa*, which function in resolution of thrombi by fibrinolysis. Consistent with the increased gene expression, plasma levels of factor VII were increased by 265%. Nilotinib had less pronounced effects on gene expression of coagulation factors but increased activity of FVIIa by 82%. Using a different experimental design, Alhawiti et al. (50) recently reported that a single dose of nilotinib but not imatinib increased platelet aggregation and thrombus growth *ex vivo* and *in vivo* in mice, and increased *ex vivo* platelet adhesion and thrombin generation in CML-patients receiving nilotinib (50). On the other hand, Loren et al. (53) demonstrated that ponatinib, but not imatinib and nilotinib, inhibited *ex vivo* human platelet activation, spreading and aggregation, and hypothesized that the cardiovascular events observed in patients treated with ponatinib may be the result of effects on other organs and cell types. Indeed, we show that FVII is involved, which is produced by the liver, and is an important factor in the coagulation pathway. Mice lacking FVII have delayed thrombus formation (54) and pharmacological doses of rFVIIa induce hemostasis in severe hemophilia and in non-hemophilia patients with profuse, heavy bleeding (55). Collectively, these data indicate that nilotinib and ponatinib can both potentiate a pro-thrombotic state via different mechanisms of action.

The presence of one or more risk factors for (cardio)-metabolic disease together with the increased platelet aggregation and increased plasma activity of factor VII/VIIa may contribute to the onset of thrombosis, especially when combined with increased levels of tissue factor (TF), which activates the TF pathway (**Figure 10**). Hypercoagulability has been described in a variety of malignancies, including hematological malignancies (55,56), and many tumor cells express high levels of TF, the primary initiator of the extrinsic

coagulation pathway (57). Therefore, we propose that nilotinib and ponatinib induce (athero) thrombosis in a subgroup of CML-patients through a combination of (cardio)-metabolic risk factors, enhanced levels of TF and increased plasma levels of coagulation factors. Our findings can be used to develop a multivariate risk model for CVD in CML patients, which include (cardio) vascular risk factors and coagulation parameters at baseline and during treatment, facilitating an early detection strategy for patients prone to cardiovascular events, which will improve therapy decision and patient care.

In conclusion, using a comprehensive approach to measure the cardiovascular effects of various BCR-ABL1 inhibitors, we demonstrate that first, second and third generation BCR-ABL1 inhibitors have very distinct effects on lipid metabolism, blood coagulability and atherosclerosis. The first-generation inhibitor imatinib was proven safe, with evident benefit for plasma lipid concentrations, atherosclerotic plaque size and stability. The third-generation inhibitor ponatinib showed similar, albeit less pronounced effects on lipid concentrations and atherosclerosis, but also showed a hypercoagulable phenotype. These data perfectly match retrospective clinical observations on cardiovascular effects of BCR-ABL1 inhibitors, and besides providing a biological basis for these observations, may well contribute to safer application of these drugs in the future.

Acknowledgments

The authors thank Anne Kozijn (TNO) for her help with the FACS analysis, Joost Westerhout (TNO) for the analysis of the pharmacokinetics and Kees van Leuven (GBS) for performing the measurements of coagulation factors.

Disclosures

C.K. has ownership interests in 'Good Biomarker Sciences'. R.G. is an employee at Bristol-Meyers Squibb, New York, USA. J.W.J. received research grants from and has spoken at (CME-accredited) meetings sponsored by Amgen, Astellas, Astra-Zeneca, Daiichi Sankyo, Lilly, Merck-Schering-Plough, Pfizer, Roche, Sanofi-Aventis, the Netherlands Heart Foundation, the Interuniversity Cardiology Institute of the Netherlands, and the European Community Framework KP7 Program.

The remaining authors declare that the research was conducted in the absence of any commercial or financial relationships that could be constructed as a potential conflict of interest.

Funding

This work was supported in part by Bristol-Meyers Squibb, New York, USA, by an allowance for TKI-LSH from the Ministry of Economic Affairs in the Netherlands (TKI1413P01), the TNO research program "Preventive Health Technologies" and the European Union Seventh Framework Programme (FP7/2007-2013) grant nr. 602936 (CarTarDis project). JA is funded by the Dutch Heart Foundation (Grant number 2014T064).

References

1. de Klein A, van Kessel AG, Grosveld G, et al. A cellular oncogene is translocated to the Philadelphia chromosome in chronic myelocytic leukaemia. Nature. 1982 Dec;300(5894):765–7.
2. Druker BJ, Guilhot F, O'Brien SG, et al. Five-year follow-up of patients receiving imatinib for chronic myeloid leukemia. N Engl J Med. 2006 Dec;355(23):2408–17.
3. O'Hare T, Walters DK, Stoffregen EP, et al. In vitro activity of Bcr-Abl inhibitors AMN107 and BMS-354825 against clinically relevant imatinib-resistant Abl kinase domain mutants. Cancer Res. 2005 Jun;65(11):4500–5.
4. Cortes JE, Kim D-W, Pinilla-Ibarz J, et al. A phase 2 trial of ponatinib in Philadelphia chromosome-positive leukemias. N Engl J Med. 2013 Nov;369(19):1783–96.
5. Castagnetti F, Breccia M, Gugliotta G, et al. Nilotinib 300 mg twice daily: an academic single-arm study of newly diagnosed chronic phase chronic myeloid leukemia patients. Haematologica. 2016 Oct;101(10):1200–7.
6. Moslehi JJ, Deininger M. Tyrosine Kinase Inhibitor-Associated Cardiovascular Toxicity in Chronic Myeloid Leukemia. J Clin Oncol. 2015 Dec;33(35):4210–8.
7. Valent P, Hadzijusufovic E, Schernthaner G-H, et al. Vascular safety issues in CML patients treated with BCR/ABL1 kinase inhibitors. Blood. 2015 Feb;125(6):901–6.
8. Kim TD, Rea D, Schwarz M, et al. Peripheral artery occlusive disease in chronic phase chronic myeloid leukemia patients treated with nilotinib or imatinib. Leukemia. 2013 Jun;27(6):1316–21.
9. Tefferi A. Nilotinib treatment-associated accelerated atherosclerosis: when is the risk justified? Vol. 27, Leukemia. England; 2013. p. 1939–40.
10. Muller CP, Wagner AU, Maucher C, et al. Hypocholesterolemia, an unfavorable feature of prognostic value in chronic myeloid leukemia. Eur J Haematol. 1989 Sep;43(3):235–9.
11. Wehmeier A, Daum I, Jamin H, et al. Incidence and clinical risk factors for bleeding and thrombotic complications in myeloproliferative disorders. A retrospective analysis of 260 patients. Ann Hematol. 1991 Aug;63(2):101–6.
12. van der Hoogt CC, de Haan W, Westerterp M, et al. Fenofibrate increases HDL-cholesterol by reducing cholesteryl ester transfer protein expression. J Lipid Res. 2007 Aug;48(8):1763–71.
13. de Haan W, van der Hoogt CC, Westerterp M, et al. Atorvastatin increases HDL cholesterol by reducing CETP expression in cholesterol-fed APOE*3-Leiden.CETP mice. Atherosclerosis. 2008 Mar;197(1):57–63.
14. van der Hoorn JWA, de Haan W, Berbee JFP, et al. Niacin increases HDL by reducing hepatic expression and plasma levels of cholesteryl ester transfer protein in APOE*3Leiden.CETP mice. Arterioscler Thromb Vasc Biol. 2008 Nov;28(11):2016–22.
15. Ason B, van der Hoorn JWA, Chan J, et al. PCSK9 inhibition fails to alter hepatic LDLR, circulating cholesterol, and atherosclerosis in the absence of ApoE. J Lipid Res. 2014 Nov;55(11):2370–9.
16. Kuhnast S, van der Hoorn JWA, Pieterman EJ, et al. Alirocumab inhibits atherosclerosis, improves the plaque morphology, and enhances the effects of a statin. J Lipid Res. 2014 Oct;55(10):2103–12.
17. Kuhnast S, van der Tuin SJL, van der Hoorn JWA, et al. Anacetrapib reduces progression of atherosclerosis, mainly by reducing non-HDL-cholesterol, improves lesion stability and adds to the beneficial effects of atorvastatin. Eur Heart J. 2015 Jan;36(1):39–48.
18. Dewey FE, Gusarova V, Dunbar RL, et al. Genetic and Pharmacologic Inactivation of ANGPTL3 and Cardiovascular Disease. N Engl J Med. 2017 Jul;377(3):211–21.
19. de Vries-van der Weij J, de Haan W, Hu L, et al. Bexarotene induces dyslipidemia by increased very low-density lipoprotein production and cholesteryl ester transfer protein-mediated reduction of high-density lipoprotein. Endocrinology. 2009 May;150(5):2368–75.
20. van Vlijmen BJ, van 't Hof HB, Mol MJ, et al. Modulation of very low density lipoprotein production and clearance contributes to age- and gender- dependent hyperlipoproteinemia in apolipoprotein E3-Leiden transgenic mice. J Clin Invest. 1996 Mar;97(5):1184–92.
21. Groot PH, van Vlijmen BJ, Benson GM, et al. Quantitative assessment of aortic atherosclerosis in APOE*3 Leiden transgenic mice and its relationship to serum cholesterol exposure. Arterioscler Thromb Vasc Biol. 1996 Aug;16(8):926–33.

22. Trion A, de Maat MPM, Jukema JW, et al. No effect of C-reactive protein on early atherosclerosis development in apolipoprotein E*3-leiden/human C-reactive protein transgenic mice. Arterioscler Thromb Vasc Biol. 2005 Aug;25(8):1635–40.
23. Kleemann R, Verschuren L, van Erk MJ, et al. Atherosclerosis and liver inflammation induced by increased dietary cholesterol intake: a combined transcriptomics and metabolomics analysis. Genome Biol. 2007; 8(9):R200.
24. Verschuren L, Radonjic M, Wielinga PY, et al. Systems biology analysis unravels the complementary action of combined rosuvastatin and ezetimibe therapy. Pharmacogenet Genomics. 2012 Dec;22(12):837–45.
25. Kooistra T, Verschuren L, de Vries-van der Weij J, et al. Fenofibrate reduces atherogenesis in ApoE*3Leiden mice: evidence for multiple antiatherogenic effects besides lowering plasma cholesterol. Arterioscler Thromb Vasc Biol. 2006 Oct;26(10):2322–30.
26. Kuhnast S, van der Hoorn JWA, van den Hoek AM, et al. Aliskiren inhibits atherosclerosis development and improves plaque stability in APOE*3Leiden.CETP transgenic mice with or without treatment with atorvastatin. J Hypertens. 2012 Jan;30(1):107–16.
27. Post SM, Zoeteweij JP, Bos MH, et al. Acyl-coenzyme A:cholesterol acyltransferase inhibitor, avasimibe, stimulates bile acid synthesis and cholesterol 7alpha-hydroxylase in cultured rat hepatocytes and in vivo in the rat. Hepatology. 1999 Aug;30(2):491–500.
28. Delsing DJ, Offerman EH, van Duyvenvoorde W, et al. Acyl-CoA:cholesterol acyltransferase inhibitor avasimibe reduces atherosclerosis in addition to its cholesterol-lowering effect in ApoE*3-Leiden mice. Circulation. 2001 Apr;103(13):1778–86.
29. Stary HC, Chandler AB, Dinsmore RE, et al. A definition of advanced types of atherosclerotic lesions and a histological classification of atherosclerosis. A report from the Committee on Vascular Lesions of the Council on Arteriosclerosis, American Heart Association. Circulation. 1995 Sep;92(5):1355–74.
30. Landlinger C, Pouwer MG, Juno C, et al. The AT04A vaccine against proprotein convertase subtilisin/kexin type 9 reduces total cholesterol, vascular inflammation, and atherosclerosis in APOE*3Leiden.CETP mice. Eur Heart J. 2017 Aug;38(32):2499–507.
31. Kuhnast S, Louwe MC, Heemskerk MM, et al. Niacin Reduces Atherosclerosis Development in APOE*3Leiden. CETP Mice Mainly by Reducing NonHDL-Cholesterol. PLoS One. 2013;8(6):e66467.
32. Tan SY, Kan E, Lim WY, et al. Metronidazole leads to enhanced uptake of imatinib in brain, liver and kidney without affecting its plasma pharmacokinetics in mice. J Pharm Pharmacol. 2011 Jul;63(7):918–25.
33. Peng B, Hayes M, Resta D, et al. Pharmacokinetics and pharmacodynamics of imatinib in a phase I trial with chronic myeloid leukemia patients. J Clin Oncol. 2004 Mar;22(5):935–42.
34. European Medicines Agency. Scientific Discussion on Tasigna I-N. No Title [Internet]. 2007. Available from: http://www.ema.europa.eu/docs/en_GB/document_library/EPAR_-_Scientific_Discussion/human/000798/WC500034398.pdf
35. European Medicines Agency. ANNEX I. Summary of product characteristics Iclusig INN-ponatinib. No Title [Internet]. Available from: http://www.ema.europa.eu/docs/en_GB/document_library/EPAR_-_Product_Information/human/002695/WC500145646.pdf
36. FDA. Clinical pharmacology and biopharmaceutics; Inclusig. [Internet]. 2012. Available from: https://www.accessdata.fda.gov/drugsatfda_docs/nda/2012/203469Orig1s000ClinPharmR.pdf
37. Gottardi M, Manzato E, Gherlinzoni F. Imatinib and hyperlipidemia. Vol. 353, The New England journal of medicine. United States; 2005. p. 2722–3.
38. Franceschino A, Tornaghi L, Benemacher V, et al. Alterations in creatine kinase, phosphate and lipid values in patients with chronic myeloid leukemia during treatment with imatinib. Vol. 93, Haematologica. Italy; 2008. p. 317–8.
39. Gologan R, Constantinescu G, Georgescu D, et al. Hypolipemiant besides antileukemic effect of imatinib mesylate. Leuk Res. 2009 Sep;33(9):1285–7.
40. Hochhaus A, Saglio G, Hughes TP, et al. Long-term benefits and risks of frontline nilotinib vs imatinib for chronic myeloid leukemia in chronic phase: 5-year update of the randomized ENESTnd trial. Leukemia. 2016 May;30(5):1044–54.
41. Libby P. Inflammation in atherosclerosis. Arterioscler Thromb Vasc Biol. 2012 Sep;32(9):2045–51.

42. Rea D, Mirault T, Cluzeau T, et al. Early onset hypercholesterolemia induced by the 2nd-generation tyrosine kinase inhibitor nilotinib in patients with chronic phase-chronic myeloid leukemia. Haematologica. 2014 Jul;99(7):1197–203.
43. Breccia M, Loglisci G, Cannella L, et al. Nilotinib therapy does not induce consistent modifications of cholesterol metabolism resulting in clinical consequences. Vol. 35, Leukemia research. England; 2011. p. e215-6.
44. Baroni S, Scribano D, Zuppi C, et al. Prognostic relevance of lipoprotein cholesterol levels in acute lymphocytic and nonlymphocytic leukemia. Acta Haematol. 1996;96(1):24–8.
45. Boren J, Cascante M, Marin S, et al. Gleevec (STI571) influences metabolic enzyme activities and glucose carbon flow toward nucleic acid and fatty acid synthesis in myeloid tumor cells. J Biol Chem. 2001 Oct;276(41):37747–53.
46. Lassila M, Allen TJ, Cao Z, et al. Imatinib attenuates diabetes-associated atherosclerosis. Arterioscler Thromb Vasc Biol. 2004 May;24(5):935–42.
47. Ballinger ML, Osman N, Hashimura K, et al. Imatinib inhibits vascular smooth muscle proteoglycan synthesis and reduces LDL binding in vitro and aortic lipid deposition in vivo. J Cell Mol Med. 2010 Jun;14(6B):1408–18.
48. El-Agamy DS. Nilotinib attenuates endothelial dysfunction and liver damage in high-cholesterol-fed rabbits. Hum Exp Toxicol. 2017 Nov;36(11):1131–45.
49. Hadzijusufovic E, Albrecht-Schgoer K, Huber K, et al. Nilotinib-induced vasculopathy: identification of vascular endothelial cells as a primary target site. Leukemia. 2017 Nov;31(11):2388–97.
50. Alhawiti N, Burbury KL, Kwa FA, et al. The tyrosine kinase inhibitor, nilotinib potentiates a prothrombotic state. Thromb Res. 2016 Sep;145:54–64.
51. Gover-Proaktor A, Granot G, Shapira S, et al. Ponatinib reduces viability, migration, and functionality of human endothelial cells. Leuk Lymphoma. 2017 Jun;58(6):1455–67.
52. Kang Z, Ji Y, Zhang G, et al. Ponatinib attenuates experimental pulmonary arterial hypertension by modulating Wnt signaling and vasohibin-2/vasohibin-1. Life Sci. 2016 Mar;148:1–8.
53. Loren CP, Aslan JE, Rigg RA, et al. The BCR-ABL inhibitor ponatinib inhibits platelet immunoreceptor tyrosine-based activation motif (ITAM) signaling, platelet activation and aggregate formation under shear. Thromb Res. 2015 Jan;135(1):155–60.
54. Xu Z, Lioi J, Mu J, et al. A multiscale model of venous thrombus formation with surface-mediated control of blood coagulation cascade. Biophys J. 2010 May;98(9):1723–32.
55. Elice F, Rodeghiero F. Hematologic malignancies and thrombosis. Thromb Res. 2012 Mar;129(3):360–6.
56. Simkovic M, Vodarek P, Motyckova M, et al. Venous thromboembolism in patients with chronic lymphocytic leukemia. Thromb Res. 2015 Dec;136(6):1082–6.
57. Falanga A. Thrombophilia in cancer. Semin Thromb Hemost. 2005 Feb;31(1):104–10.

5

The BCR-ABL1 tyrosine kinase inhibitors imatinib and ponatinib decrease plasma cholesterol through different effects on lipoprotein metabolism

Marianne G. Pouwer, Eveline Gart, Elsbet J. Pieterman, Ivana Bobeldijk-Pastorova, Martin Giera, J. Wouter Jukema, Hans M.G. Princen

Submitted

Abstract

Objectives: Chronic myeloid leukemia (CML) is treated with BCR-ABL1 tyrosine kinase inhibitors (TKIs), but modulations in plasma lipids occur. The objectives of this study were to evaluate the effect of three generations TKIs on plasma cholesterol and triglyceride (TG) metabolism and to investigate the underlying mechanism using APOE*3-Leiden.CETP mice, a model that mimics human lipoprotein metabolism.

Methods and results: Mice were fed a Western-type diet and were treated for 6 weeks with either imatinib, nilotinib or ponatinib at drug exposures relevant to CML patients. The effects on plasma and liver lipids, lipoprotein metabolism, and fecal lipid excretion were assessed. Imatinib decreased plasma non-high-density lipoprotein cholesterol (non-HDL-C) (-52%) and TG (-42%) mainly by reducing VLDL-TG and VLDL-apolipoprotein-B production, and reduced cholesterol ester (CE) content of the VLDL particles. This was accompanied by a reduction in the majority of the lipid classes (triacylglycerols, CEs, glycerophospholipids), including the pro-atherogenic sphingolipids, as determined by lipidomics analysis. Ponatinib decreased plasma non-HDL-C levels (-26%) by lowering intestinal cholesterol absorption. Moreover, ponatinib reduced the CE content in the liver and in the VLDL particles. Nilotinib did not affect lipoprotein metabolism.

Conclusions: Our data confirm the lipid-lowering effects of imatinib in CML-patients and provide an explanation by showing that imatinib and ponatinib affect lipoprotein metabolism through distinct mechanisms.

Introduction

BCR-ABL1 tyrosine kinase inhibitors (TKIs) are the standard of care for treatment of chronic myeloid leukemia (CML). The first line TKI imatinib is effective and safe, but not all patients do have a complete cytogenetic response or develop drug resistance. Consequently, novel and more potent TKIs have been developed, e.g. nilotinib and ponatinib, the latter as the only TKI with activity against the T315I mutation. Unfortunately, cardiovascular safety issues including ischemic heart disease and progressive arterial occlusive disease (PAOD) have been reported with nilotinib and ponatinib (1–4), which preferentially developed in those patients having a (very) high cardiovascular risk according to the SCORE chart (5,6).

Several studies describe plasma lipid modulations in CML-patients during TKI treatment. Imatinib consistently decreases plasma cholesterol, and even normalization in hypercholesterolemic CML-patients has been reported (7–10). Retrospective analysis of phase III studies revealed a lower incidence of cardiovascular events in patients treated with imatinib relative to patients treated without TKIs (11). In contrast, several studies with nilotinib reported increased plasma cholesterol levels (1,10,12,13), although these findings are not consistent (14). Data on ponatinib are scarce but one study reported no alterations in plasma lipids (10).

It is worth noting that in the setting of CML, both indirect effects of the underlying disease as well as direct effects of TKI-treatment may modulate cardiovascular risk factors, including plasma lipid levels. Therefore, we have previously investigated the (patho) physiology of the decreased cardiovascular risk by imatinib and the increased cardiovascular risk by nilotinib and ponatinib using a mouse model without CML, the APOE*3-Leiden.CETP mouse (15). At similar drug exposures as in CML-patients, we found that imatinib reduced plasma cholesterol and triglyceride (TG) levels, decreased atherosclerotic lesion size and improved lesion stability, all in line with the reported lipid reductions and improved cardiovascular outcome in CML-patients during imatinib treatment (7–11). Furthermore, ponatinib reduced plasma cholesterol levels and atherosclerosis progression, whereas nilotinib did not affect plasma lipid levels or atherosclerosis. Interestingly, nilotinib and ponatinib adversely affected genes involved in coagulation and increased plasma levels of FVII (ponatinib) and FVIIa (nilotinib) (15), important factors in the pathogenesis of atherothrombotic events. These findings suggest that not enhanced atherosclerosis progression, but changes in coagulation are related to the observed cardiotoxicity by nilotinib and ponatinib.

The lipid-modulating effects of imatinib are well described, but there are no reports that provide a mechanistical explanation for the observed effects. Also, little is known about the ability of ponatinib to affect lipoprotein metabolism, and the inconsistent effects of nilotinib on plasma lipids in CML-patients require further investigation. Therefore, the aim of this study was to investigate the mechanism underlying the ability of these TKIs

to affect lipid homeostasis. As in our previous study, we used the APOE*3-Leiden.CETP mouse model, since these mice, like humans, have a delayed clearance of apolipoprotein-B (apoB)-containing lipoproteins and express cholesteryl ester transfer protein (CETP), resulting in a lipoprotein profile similar as in patients with familial dysbetalipoproteinemia, and a human-like lipoprotein metabolism (16). This mouse model responds to all hypolipidemic drugs used in the clinic similarly as patients (17–19) and has been widely used to study the effect of drugs and other compounds on atherosclerosis (18–21), lipoprotein metabolism (22–26) and cardiovascular safety (27), including our previous study with BCR-ABL1 inhibitors (15).

Materials and methods

Animals

Eighty female APOE*3-Leiden.CETP transgenic mice on a C57BL/6 background (9 - 12 weeks of age) were obtained from the breeding facility of the Netherlands Organization of Applied Scientific Research (TNO), Leiden, the Netherlands. In this study, 4 groups of 16 - 17 mice were used, and per treatment group the mice were divided into two groups of each 8 - 9 mice as two different endpoint experiments were performed (**Table 1**). The number of mice was based on our experience from previous studies and was calculated using a probability of 0.05. We expected to have a variance of 18% in the endpoint experiments (VLDL clearance or VLDL production), a minimal difference of 50% and a two-sided test with 95% confidence interval, which resulted in 8 animals per experiment. Since, it is known that approximately 20% of the APOE*3-Leiden.CETP mice do not respond properly to the Western-type diet with respect to increasing their plasma cholesterol (TC) and TG (i.e. low-responders), the study initially started with 80 mice. Mice were fed a semi-synthetic diet, containing 15% (w/w) saturated fat from cacao butter and 0.15% (w/w) cholesterol (Western-type diet [WTD]; Altromin, Tiel, the Netherlands) for 3 weeks, and subsequently the low-responder mice were selected based on TC and TG levels and removed from the study prior to allocation into groups (**Table 1**). Since there were less low-responders as predicted, 67 mice were randomized according to body weight, age, plasma TC, and TG levels in 4 groups of 16 - 17 mice. The mice entered the study in a staggered way of 1 week apart with two batches of each 8 - 9 mice per group. During the study, mice were group-housed (4 - 5 mice per cage) under standard conditions with a 12-h light-dark cycle and had free access to food and water. Body weight, food intake and clinical signs of discomfort were monitored regularly during the study. The care and use of all mice in this study was carried out at the animal facility of TNO in accordance with national and EU ethical regulations. Animal experiments were approved by the Institutional Animal Care and Use Committee of TNO under registration number 3682.

Table 1 Study design

Time (weeks)	**All mice (n = 80)**	
-3 to 0	Run-in/acclimatization on a Western type diet	
0	Selection and exclusion of low-responders (n = 13)	
0	Matching in 4 groups based on plasma cholesterol, triglycerides, age and body weight	
Time (weeks)	**In life phase (4 groups of 16 - 17 mice)**	
0, 3, 6	Body weight, food intake and plasma parameters	
5	Fecal neutral sterols and bile acids	
5	Cholesterol absorption	
6	Lipidomics	
Time (weeks)	**End-experiment 1 (n = 8 per group)**	**End-experiment 2 (n = 8 - 9 per group)**
6	VLDL clearance	VLDL production
	Hepatic lipid content	

After a run-in period of 3 weeks on a Western-type diet mice were matched in 4 groups of each 16 17 mice and were treated for 6 weeks with 3 generations TKIs, imatinib (150 mg/kg BID), nilotinib (30 mg/kg QD for the first 3 weeks and 10 mg/kg QD during the last 3 weeks) or ponatinib (10 mg/kg QD first 3 weeks and 3 mg/kg QD last 3 weeks). After 6 weeks, mice were divided into 8 - 9 mice per group per experiment to assess VLDL clearance and VLDL production. Abbreviations: VLDL, very-low-density-lipoprotein

Experimental design

Upon randomization, mice received, based on the results of a previous pharmacokinetic (PK) study (15), an once-daily oral gavage with nilotinib (30 mg/kg), ponatinib (10 mg/kg), or a twice-daily gavage with imatinib (150 mg/kg) for 3 weeks to confirm our previous findings on plasma lipids (15), after which the doses were reduced for nilotinib (10 mg/kg) and ponatinib (3 mg/kg) to match better with relevant human doses (15). Doses and dose intervals were based on data obtained from a previously performed PK study (15). All The TKIs were suspended in 5% carboxymethyl cellulose (CMC) and all mice except the imatinib group received a second oral gavage with the vehicle (5% CMC). Body weight, food intake, plasma TC, TG, and high-density lipoprotein-cholesterol (HDL-C) were measured throughout and non-HDL-C was calculated by subtracting HDL-C from TC. Feces were collected in week 5 for the determination of bile acids and fecal neutral sterols. Lipidomics analysis was carried out in 4-hour fasted plasma of 8 mice per treatment group from week 6. After 6 weeks of treatment, two different endpoint experiments were performed: (I) very-low density-lipoprotein (VLDL)-like particle clearance was determined in 8 mice per treatment group, and (II) VLDL production and *de novo* apoB synthesis was

assessed in 8 - 9 mice per treatment group as described previously (26). Hepatic lipid content was analyzed in mice of experiment 1 (**Table 1**).

Plasma biochemical analysis

Plasma samples were collected in week 0, 3 and 6 after a 4-hour fast. Plasma TC and TG were determined using enzymatic kits (TC: Roche/Hitachi, catalogue# 11491458216, TG: Roche/Hitachi, catalogue# 11730711216) according to the manufacturer's protocols. HDL-C was measured after precipitation as described previously (21). Alanine aminotransferase (ALT) and aspartate aminotransferase (AST) enzymatic activity was measured by reflectance photometry using a Reflotron® Plus analyzer (Hoffman-La Roche, Basel, Switzerland).

Excretion of fecal sterols and bile acids

Fecal excretion of bile acids and neutral sterols was determined in feces, collected per cage during a 48- to 72-hour time period at three consecutive time points at week 5, by gas chromatographic analysis as described by Post et al (28).

In vivo clearance of VLDL-like particles

Mice (8 per treatment group) were fasted for 4 hours and injected in the tail vein with VLDL-like particles (80 nm) containing 3H-labelled fatty acids (FA) (as glycerol tri[3H]-oleate, [3H]-TO) and 14C-labelled cholesteryl oleate (as [14C]-cholesteryl oleate, [14C]-CO). At t=2, 5, 10 and 15 minutes post-injection, blood was collected to determine the plasma decay of [3H]-TO and [14C]-CO. At 15 minutes, mice were euthanized by cervical dislocation and perfused with heparin 10 U/mL in ice-cold PBS for 5 minutes. Organs (i.e. small intestine, right kidney, heart, spleen, lung, brown adipose tissue (BAT), gonadal white adipose tissue (gWAT), subcutaneous WAT (sWAT), femoral muscle and liver) were harvested and saponified overnight in 500 µl Solvable (Perkin-Elmer, Wellesley, MA) to determine [3H]-TO and [14C]-CO uptake. Retention of radioactivity in the saponified tissues was measured as % of the injected dose, and the half-life of VLDL-[3H]-TO and VLDL-[14C]-CO was calculated from the slope after linear fitting of semi-logarithmic decay curves as described previously (22,25,26,29).

Hepatic VLDL-TG and VLDL-apoB production

Mice (8 - 9 per treatment group) were fasted for 4 hours prior to the start of the experiment. During the experiment, mice were sedated with acepromazine-midazolam-fentanyl intraperitoneally [6.25 mg/kg acepromazine (Ceva Santé Animale), 6.25 mg/kg midazolam (Actavis), and 0.3125 mg/kg fentanyl (Bipharma)]. At t=0 minutes, blood was taken via tail bleeding and mice were intravenously (IV) injected with 100 µl phosphate buffered saline (PBS) containing 20 µCi Trans[35S]-labelled methionine/cysteine (ICN Biomedicals, Irvine, CA) to measure *de novo* apoB synthesis. After 30 minutes, the mice received a Triton WR1339 IV injection (500 mg/kg body weight), which inhibits lipoprotein lipase (LPL)

mediated lipolysis, thereby blocking VLDL clearance. Blood samples were drawn at 0, 15, 30, 60 and 90 minutes after Triton WR1339 injection and used for determination of the plasma TG concentration. After 90 minutes, the animals were sacrificed by cervical dislocation and blood was collected by heart puncture for subsequent isolation of VLDL by density-gradient ultracentrifugation. [35S]-apoB was measured in the VLDL fraction after apoB-specific precipitation, and VLDL-apoB production rate was calculated as disintegration per minute (dpm)/h, as previously reported (22,25,26,29). The free cholesterol (FC), cholesterol ester (CE), TG and phospholipid (PPL) content of the VLDL particles was determined using the kits "Cholesterol CHOD-PAP" (Roche, Mannheim, Germany), "Free cholesterol E" (Instruchemie, Delfzijl, the Netherlands), "Triglycerides GPO-PAP" (Roche, Mannheim, Germany), and "Phospholipids" (Instruchemie, Delfzijl, the Netherlands), respectively.

Hepatic lipid analysis

Frozen liver tissue samples of lobus sinister lateralis hepatis were homogenized at 4°C in phosphate-buffered saline, and the protein content was measured using a Lowry protein assay. Lipids were extracted, separated by high-performance thin-layer chromatography on silica gel plates, stained as described previously (30), and analyzed with ChemiDoc Touch Imaging System (Bio-Rad). TG, CE and FC content were quantified using Image-lab version 5.2.1 software (Bio-Rad) and expressed per mg liver protein.

Lipidomics analysis in plasma

Lipidomics analysis was carried out in 4-hour fasted plasma collected at week 6 of 8 mice per treatment group on the commercial Lipidyzer platform, according to the manufacturer's instructions (Sciex).

Excluded data

Of one mouse, a TC/non-HDL-C value misses (t=0 weeks) and of three mice, a HDL-C/non-HDL-C value misses (control t=0 weeks, 1 mouse; imatinib t=3 weeks, 1 mouse; ponatinib t=6 weeks, 1 mouse) as there was not enough plasma to measure TC and/or HDL-C. Six mice were excluded from analysis of the VLDL clearance experiment because the VLDL-like particles containing [3H]-TO and [14C]-CO, were not fully intravenously injected as confirmed by the absence of [14C]-CO in plasma collected at t=0 minutes (control, 1 mouse; nilotinib, 2 mice), or because the clearance curve showed aberrant results (i.e. higher [14C]-CO levels compared to the previous time point) (ponatinib, 3 mice). Four mice were excluded from the VLDL-TG production experiment: in two mice the [35S]-label was not fully intravenously injected demonstrated by absence of [35S]-decay in the plasma (control, 1 mouse; nilotinib, 1 mouse) and two mice were excluded as there was no plasma left to measure [35S]-decay (imatinib, 1 mouse; ponatinib, 1 mouse).

Data and statistical analysis

Data are presented as means ± SEM. A Kruskal–Wallis test was used to determine the significance of differences between the groups. Significance of differences of the individual groups with the control was calculated nonparametrically using a Mann–Whitney U-test. The lipidomics data were analyzed using a one-way ANOVA, and when the significance level of F was $P < 0.05$, a Dunnett's post hoc test was used to compare the treatment groups with the control group. IBM SPSS v24.0 was used for all analyses and P values < 0.05 were considered statistically significant. The data and statistical analysis comply with the recommendations on experimental design and analysis in pharmacology (31).

Results

Plasma drug concentrations

Based on data of our previously performed PK study (15) treatment with imatinib (150 mg/kg, BID), nilotinib (10 mg/kg, QD) and ponatinib (3 mg/kg, QD) resulted in similar drug exposures as reported in CML-patients (15).

Safety aspects of TKI treatment

No clinical signs of deviant behavior were noted in any treatment group. TKI treatment did not affect food intake or body weight in the mice (**Table 2**). Plasma ALT and AST, measured after 3 and 6 weeks of treatment, showed no aberrant results (**Table 2**). Mean body weight, food intake, ALT and AST were similar for mice of experiment 1 (VLDL clearance) and experiment 2 (VLDL production) for each treatment group (**Table 2**). Analogous to this short-term study, no adverse/toxic side-effects of the drugs were noted during long-term (16 weeks) exposure to the same doses for imatinib (150 mg/kg, BID), nilotinib (30 and 10 mg/kg, QD) and ponatinib (10 and 3 mg/kg, QD), as reported previously (15).

The effect of TKI treatment on plasma lipids

Imatinib and ponatinib decreased plasma cholesterol

The effect of TKI treatment on plasma lipids was assessed throughout the study (**Figure 1 and Table 2**). Imatinib markedly decreased plasma TC (**Figure 1A**), non-HDL-C (i.e. apoB-containing lipoproteins) (**Figure 1B**) and TG (**Figure 1C**) levels after 3 and 6 weeks of treatment, and ponatinib decreased plasma TC and non-HDL-C levels (**Figure 1A and C**). Nilotinib reduced plasma TG after 6 weeks of treatment (**Figure 1C**). These data confirm our previous findings (15) and correspond with the lipid-lowering properties of imatinib in patients (7–10).

Table 2 Overview of body weight, food intake and plasma parameters of mice in experiment 1 and 2

Experiment 1									
		Control		**Imatinib**		**Nilotinib**		**Ponatinib**	
Dose	*mg/kg*	-		150		30	10	10	3
Time	*weeks*	3	6	3	6	3	6	3	6
Body weight	*gram*	19.9±0.7	20.1±0.9	20.3±1.1	20.3±1.0	20.6±1.9	21.4±2.6	20.8±2.0	20.9±2.3
Food intake	*gram/mouse/day*	2.4±0.0	2.1±0.1	2.3±0.0	2.1±0.1	2.4±0.1	2.2±0.0	2.4±0.0	2.0±0.1
TC	*mmol/L*	17.6±2.2	13.3±2.8	7.2±1.9*	6.2±2.0*	15.9±4.1	11.3±3.1	10.5±1.8*	8.4±1.7*
HDL-C	*mmol/L*	1.0±0.4	0.8±0.2	0.6±0.2	0.5±0.1*	0.7±0.3	0.6±0.2	0.7±0.2	0.6±0.1
Non-HDLC	*mmol/L*	17.0±2.1	12.5±2.8	6.8±2.1*	5.7±2.1*	15.2±3.9	10.7±2.9	9.8±1.8*	7.7±1.8*
TG	*mmol/L*	4.6±1.3	4.3±1.5	1.5±0.6*	2.2±0.8*	4.4±1.2	2.5±1.1*	3.3±1.0	3.5±1.2
ALT	*U/L*	45	33	54	32	41	32	43	31
AST	*U/L*	109	88	98	79	128	72	145	82
Experiment 2									
		Control		**Imatinib**		**Nilotinib**		**Ponatinib**	
Dose	*mg/kg*	-		150		30	10	10	3
Time	*weeks*	3	6	3	6	3	6	3	6
Body weight	*gram*	20.3 ± 1.5	20.9±1.7	20.5±0.6	20.9±0.8	19.5±1.4	20.2±1.5	19.9±1.3	20.9±1.4
Food intake	*gram/mouse/day*	2.4±0.4	2.3±0.2	2.4±0.0	2.5±0.4	2.2±0.1	2.1±0.1	2.3±0.1	2.1±0.1
TC	*mmol/L*	14.6±4.4	11.9±4.3	8.3±2.7*	6.5±1.9*	13.0±4.3	10.9±2.2	8.7 ±1.8*	10.5±2.0
HDL-C	*mmol/L*	0.6 0.2	0.5±0.1	0.4±0.1*	0.5±0.2	0.6±0.3	0.6±0.2	0.8±0.5	0.6±0.3
Non-HDL-C	*mmol/L*	13.9±4.2	11.4±4.3	7.9±2.7*	6.1±1.9*	12.4±4.2	10.3±2.2	7.9±1.7*	9.9±2.0
TG	*mmol/L*	3.7±1.9	2.9±1.3	3.1±1.1	2.0±0.7	4.4±2.2	2.8±0.9	4.7±1.9	3.4±1.4
ALT	*U/L*	40	36	52	29	42	30	46	27
AST	*U/L*	138	120	119	96	119	93	135	113

Mice received a Western-type diet and were treated for 6 weeks with 3 generations TKIs, imatinib (150 mg/kg BID), nilotinib (30 mg/kg QD for the first 3 weeks and 10 mg/kg QD during the last 3 weeks) or ponatinib (10 mg/kg QD first 3 weeks and 3 mg/kg QD last 3 weeks). All parameters were measured after 3 and 6 weeks of treatment. Food intake was measured per cage and ALT and AST were measured in plasma pooled per group. After 6 weeks, two different endpoint experiments were performed. In Experiment 1 VLDL clearance was assessed, and experiment 2 determined VLDL production. (n=7-8 mice per experiment). *p<0.05 as compared to the control group. Abbreviations: TC, total cholesterol; HDL, high-density-lipoprotein; TG, triglycerides; ALT, alanine transaminase; AST, aspartate transaminase

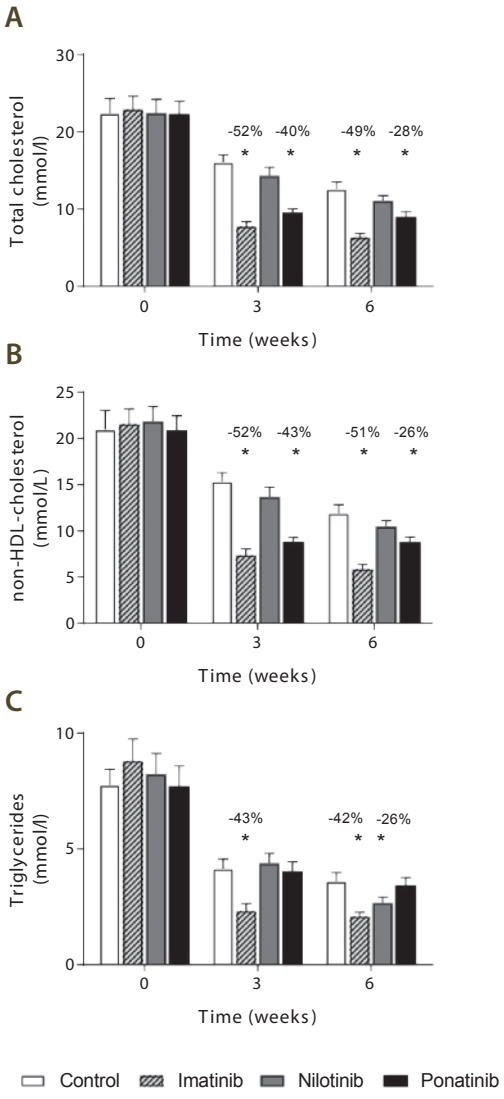

Figure 1 Imatinib and ponatinib decrease plasma lipids. Mice received a Western-type diet and were treated for 6 weeks with 3 generations TKIs, imatinib (150 mg/kg BID), nilotinib (30 mg/kg QD for the first 3 weeks and 10 mg/kg QD during the last 3 weeks) or ponatinib (10 mg/kg QD first 3 weeks and 3 mg/kg QD last 3 weeks). At baseline (t0) and after 3 and 6 weeks of intervention, 4-h fasted blood was taken and plasma was assayed for TC (A), non-HDL C (B) and TG (C). Non-HDL-C was calculated by subtracting HDL-C from TC. Data are presented as means + SEM. n=16-17 per group. *p<0.05 as compared to the control group. Abbreviations: TC, total cholesterol; (non)-HDL-C, high-density lipoprotein-cholesterol; TG, triglycerides

The effect of TKI treatment on lipoprotein and lipid metabolism

Imatinib decreased de novo VLDL synthesis and CE content of VLDL lipoproteins

Plasma VLDL levels are defined by the balance between VLDL production and VLDL clearance. We first determined the clearance and tissue uptake of glycerol tri[3H]oleate ([3H]-TO), representing FFAs and TGs, and [14C]cholesteryl oleate ([14C]-CO) by several organs at t=6 weeks in experiment 1. The clearance and tissue uptake of [3H]TO (**Figure 2A-B**) and of [14C]CO (**Figure 2C-D**) were not affected by TKI treatment, indicating that the lipid-modulating effects of imatinib and ponatinib cannot be explained by an increased VLDL clearance.

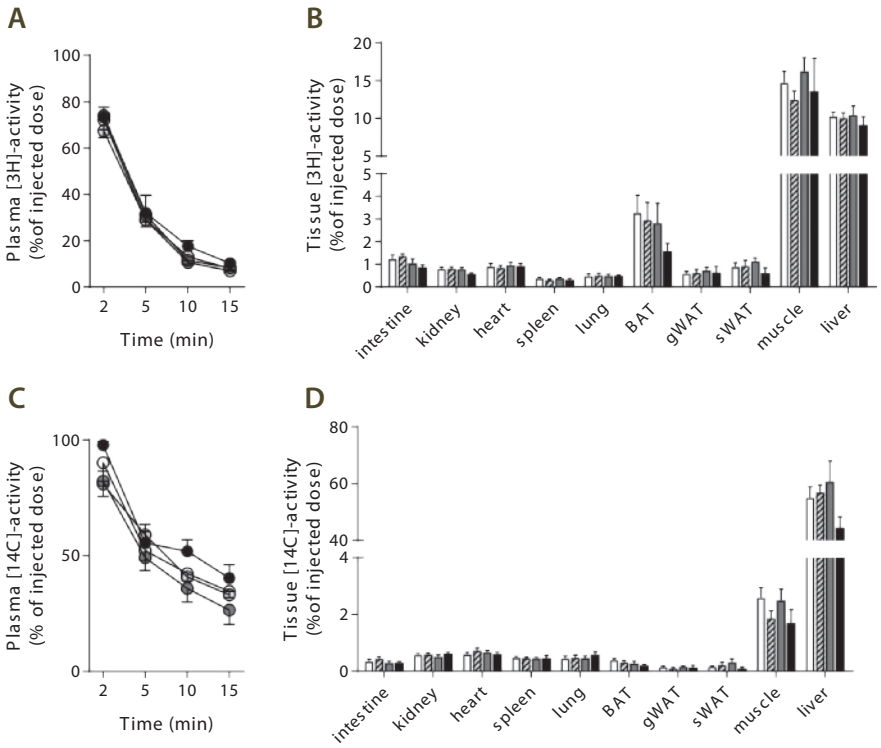

Figure 2 TKI treatment does not affect VLDL clearance and uptake. At t=6 weeks, 4-h fasted mice in experiment 1 were injected with glycerol tri[3H]oleate ([3H]TO) and [14C]cholesteryl oleate ([14C]CO)-labeled emulsion particles. [3H]TO plasma decay was plotted (A) and clearance of ([3H]TO) in individual organs was determined (B). [14C]CO plasma decay was plotted (C) and clearance of [14C]CO in individual organs was determined (D). Data are represented as mean ± SEM (n=5-8 per group). Abbreviations: Intestine, small intestine; BAT, brown adipose tissue; gWAT, gonadal white adipose tissue; sWAT, subcutaneous white adipose tissue; muscle, muscle femoralis

Next, we determined the VLDL-TG and VLDL-apoB production rate and the composition of the VLDL particles. Imatinib reduced VLDL-TG production (**Figure 3A-B**) and *de novo* VLDL-apoB synthesis (**Figure 3C**). Consequently, the TG production per apoB was not affected by imatinib (**Figure 3D**), indicating that the number of newly synthesized VLDL particles is decreased. Furthermore, imatinib and ponatinib decreased the amount of CE in the VLDL particles (**Figure 3E**). In contrast, nilotinib did not affect VLDL production. Altogether, these data demonstrate that imatinib reduced plasma TC and TG levels by decreasing the number of newly synthesized VLDL particles and the CE content of the VLDL particles, whereas ponatinib decreased the CE content of the particles.

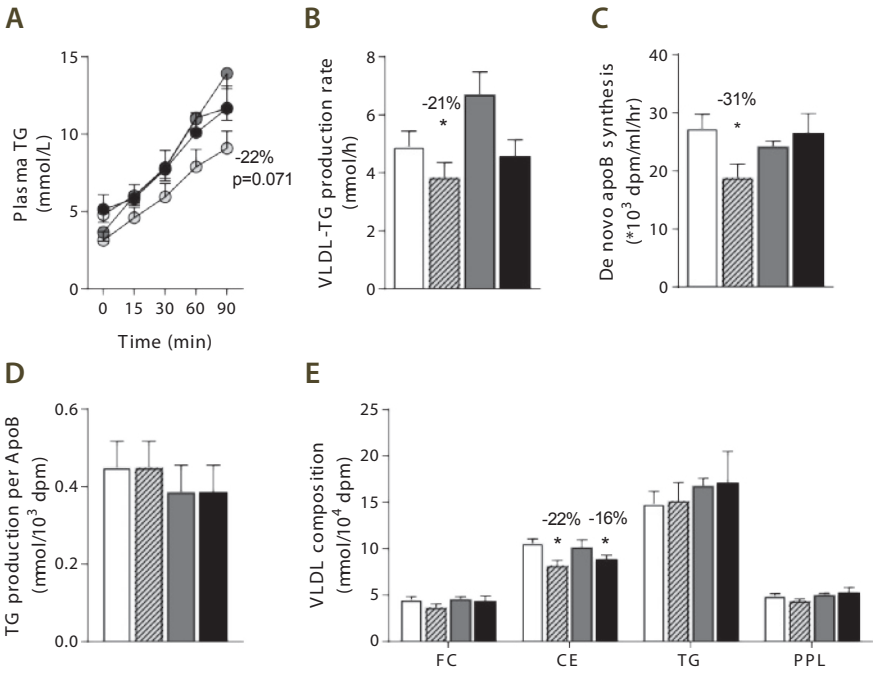

Figure 3 Imatinib decreases de novo VLDL-apoB production. At t=6 weeks, 4-h fasted mice in experiment 2 were injected with Tran[35S]-label and Triton after which blood samples were drawn up to 90 minutes. Plasma VLDL-TGs were plotted (A) and used to calculate the TG production rate (B) from the slope of individual curves. Ninety minutes after Triton injection plasma was used to isolate VLDL by ultracentrifugation, and the rate of de novo apoB synthesis was determined (C). Next, we calculated the TG production per apoB (D) and determined the lipid composition of the isolated VLDL particles (E). Data are represented as mean ± SEM (n=7-9 per group). *p<0.05 as compared to the control group. Abbreviations: FC, free cholesterol; CE, cholesterol ester; TG, triglycerides; PPL, phospholipids; apoB, apolipoprotein B.

Ponatinib decreased hepatic CE content and cholesterol absorption

Because a decreased VLDL-apoB particle production rate may be the result of changes in hepatic lipid metabolism, we determined hepatic lipid content and fecal excretion of bile acids and neutral sterols.

Imatinib did not affect hepatic lipid content (**Figure 4A**), indicating that the reduced VLDL particle production does not result in hepatic lipid accumulation, nor is the consequence of reduced availability of lipids for VLDL synthesis. Interestingly, ponatinib decreased hepatic CE content (**Figure 4A**), which may be related to reduced intestinal cholesterol absorption (30,32). Therefore, we measured fecal neutral sterol excretion and

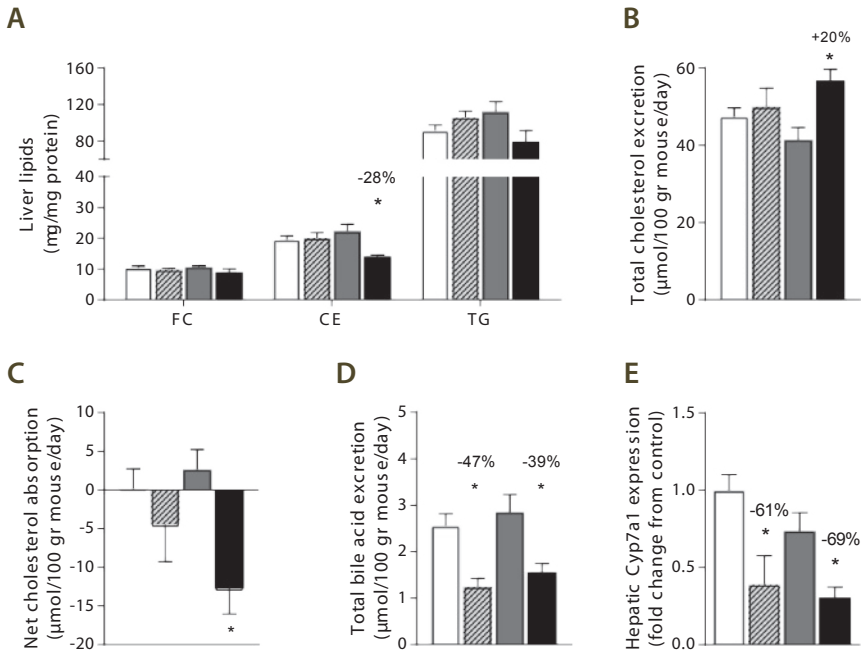

Figure 4 Ponatinib decreases hepatic CE content, bile acid excretion and cholesterol absorption. At t=6 weeks, livers were isolated from mice in experiment 1 and hepatic lipid content per mg liver protein was assessed (A). At t=5 weeks, feces from both experiments were collected per cage during a 48-72h period at 3 consecutive time points, in which neutral sterol excretion (B) was determined using gas chromatography. Total cholesterol balance (C) was calculated by subtracting fecal cholesterol excretion from dietary cholesterol intake. Bile acids (D) were determined in feces using gas chromatography, and Cyp7a1 mRNA expression was measured in the liver (E). Data are represented as mean + SEM (n=8 mice per group; n=4 cages and 3 time points per group). *p<0.05 as compared to the control group. Abbreviations: FC, free cholesterol; CE, cholesterol ester; TG, triglycerides.

calculated the net cholesterol absorption by subtracting the fecal neutral sterol excretion from the average dietary cholesterol intake (**Figure 4C**). Indeed, ponatinib increased the total cholesterol excretion (**Figure 4B**), thereby decreasing the net cholesterol absorption by 12.7 µmol/100 gram mouse per day (**Figure 4C**). Imatinib and nilotinib did not affect intestinal cholesterol absorption (**Figure 4C**). In addition, both imatinib and ponatinib reduced bile acid excretion (**Figure 4D**), via downregulation of the expression of *Cholesterol 7alpha-hydroxylase* (*Cyp7a1*), encoding the rate-limiting enzyme in bile acid synthesis (**Figure 4E**). Altogether, these data indicate that ponatinib reduced intestinal cholesterol uptake and consequently hepatic CE content, whereas imatinib did not affect hepatic lipid storage.

Plasma lipidomics analysis

Imatinib reduced the majority of lipid classes in plasma

Bioactive lipids, in particular sphingolipids including ceramides, are major regulators of lipid homeostasis (33) and together with (lyso-)glycerophospholipids play a role in atherogenesis (34–36). Therefore, we performed lipidomic analyses of plasma samples to identify characteristic molecular lipid changes of TKI treatment. Concentrations of almost all lipid classes were reduced by imatinib (**Figure 5A**), and the reductions in CE (-62%) and triacylglycerols (TAG) (-60%) were comparable with the observed reductions in plasma cholesterol (-49%) and TG (-42%) at 6 weeks of treatment (**Figure 1A and C**). These decreases were accompanied by reductions in the concentrations of glycerophospholipids (phosphatidylcholines and phosphatidylethanolamines), a subgroup of lipids that form the outer layer of lipoproteins, but are also recognized for their role in atherosclerosis development (36). Moreover, imatinib reduced the concentration of the pro-atherogenic sphingomyelins (-49%), ceramides (-55%), hexosylceramides (-50%) and lysophosphatidylcholines (LPC) (-45%) (**Figure 5A**). In contrast, ponatinib only reduced the concentration of CE by 38% (**Figure 5C**), in line with the decrease in plasma TC, without affecting TAG, phospholipids or sphingolipids. Nilotinib did not affect any of the lipid classes (**Figure 5B**). Normalization for plasma non-HDL-C levels revealed that the majority of the observed changes was associated with plasma non-HDL-C levels (**Figure 5 D-F**), except for the concentration of FFA in imatinib-treated mice, which was increased by 100% per µM non-HDL-C (**Figure 5D**) as expected, since FFA is bound to albumin and not present as such in lipoproteins. Collectively, the combined reduction in CE, TAG and phospholipids by imatinib confirms our finding that the drug decreases the number of VLDL particles, while the decreased concentration of sphingomyelins is in accordance with a more favorable cardiovascular profile of imatinib. The absolute concentrations for each lipid class quantified in mouse plasma are presented in **Table 3**.

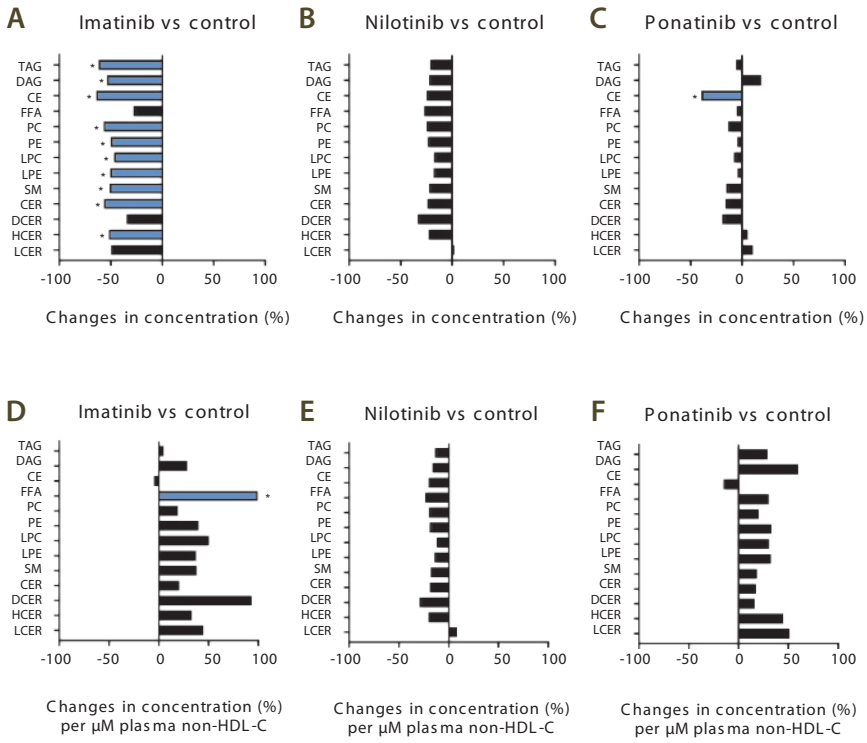

Figure 5 Differences in lipid class concentrations in plasma of mice treated with imatinib and ponatinib. After 6 weeks of treatment, 4-h fasted blood was taken, lipids were extracted from the plasma and the concentration (nmol/gram plasma) of 13 lipid classes was determined by MS/MS. The mean changes in concentration (%) for each lipid class compared to the control group are depicted for imatinib (A), nilotinib (B) or ponatinib (C). Next, the mean change in concentration (%) per µM plasma non-HDL cholesterol was calculated for each lipid class compared to the control group and depicted for imatinib (D), nilotinib (E) and ponatinib (F). Significance of differences between the treatment groups versus control was calculated using an one-way ANOVA with Dunnett post-hoc test using the data of which the means are depicted in **Table 3**. (n=8 mice per group). *p<0.05 as compared to the control group with significant changes shown in blue bars. Abbreviations: Non-HDL-C, non-high density-lipoprotein cholesterol; TAG, triacylglycerols; DAG, diacylglycerols; CE, cholesteryl esters; FFA, free fatty acids; PC, phosphatidylcholines; PE, phosphatidylethanolamines; LPC, lyso-phosphatidylcholines; LPE, lyso-phosphatidylethanolamines; SM, sphingomyelins; CER, ceramides; DCER, dihydroceramides; HCER, hexosylceramides; LCER, lactosylceramides.

Table 3 Plasma concentrations of lipid classes

	Concentration (nmol/gram plasma)			
Lipid class	**Control**	**Imatinib**	**Nilotinib**	**Ponatinib**
TAG	3697 ± 1798	1478 ± 901*	2979 ± 825	3551 ± 1926
DAG	52.6 ± 21.0	25.3 ± 13.3*	41.7 ± 5.9	62.4 ± 24.5
CE	10905 ± 4036	4092 ± 1012*	8407 ± 2383	6800 ± 2435*
FFA	1352 ± 474	1001 ± 151	1008 ± 177	1309 ± 388
PC	3854 ± 1237	1724 ± 503*	2973 ± 551	3411 ± 1246
PE	117.6 ± 39.2	60.8 ± 15.4*	91.8 ± 13.7	114.8 ± 46.6
LPC	1035 ± 345	571 ± 134*	871 ± 162	974 ± 299
LPE	13.3 ± 5.1	6.8 ± 1.7*	11.2 ± 1.9	13.0 ± 5.1
SM	1086 ± 385	550 ± 164*	862 ± 171	940 ± 345
CER	19.1 ± 7.4	8.6 ± 3.3*	14.9 ± 2.6	16.4 ± 6.0
DCER	1.9 ± 0.8	1.3 ± 0.7	1.3 ± 0.3	1.5 ± 0.4
HCER	18.9 ± 8.3	9.4 ± 2.6*	14.9 ± 3.7	19.9 ± 7.0
LCER	1.1 ± 0.7	0.6 ± 0.3	1.1 ± 0.2	1.2 ± 0.5

After 6 weeks of treatment lipidomic analysis was performed in 4-hour fasted blood (n=8 mice per group). *p<0.05 as compared to the control group. Abbreviations: TAG, triacylglycerols; DAG, diacylglycerols; CE, cholesteryl esters; FFA, free fatty acids; PC, phosphatidylcholines; PE, phosphatidylethanolamines; LPC, lyso-phosphatidylcholines; LPE, lyso-phosphatidylethanolamines; SM, sphingomyelins; CER, ceramides; DCER, dihydroceramides; HCER, hexosylceramides; LCER, lactosylceramides.

Discussion

To our knowledge, this is the first *in vivo* study that investigated the effects of three different BCR-ABL1 tyrosine kinase inhibitors on lipoprotein metabolism, of which the results are summarized in **Table 4**. We confirm the lipid-lowering ability of imatinib as reported in CML patients, and provide evidence using APOE*3-Leiden.CETP mice that this is caused by a reduction of the VLDL particle production and CE content of the VLDL particles. This observation is supported by lipidomics analysis showing a reduction of glycerophospholipids in the plasma, which form the outer layer of the VLDL particles. The decreased concentration of the pro-atherogenic sphingomyelins, ceramides and (lyso-)phospholipids further contributes to the favorable cardiovascular safety profile of imatinib (11,15). Ponatinib also reduced plasma cholesterol, but the identified mechanism of action differed from imatinib. A decrease of intestinal cholesterol absorption led to a reduction of hepatic CE content, an accumulative process as long-term (16-week) exposure to ponatinib further decreased hepatic lipid content, including FC and TG (15). As a consequence

Table 4 Summary of the (cardio)metabolic effects of imatinib, nilotinib and ponatinib in APOE*3-Leiden.CETP mice

	Effects in APOE*3-Leiden.CETP mice		
	Imatinib	**Nilotinib**	**Ponatinib**
Plasma parameters			
Total cholesterol	↓		↓
Non-HDL cholesterol	↓		↓
Triglycerides	↓	↓*1	
Pro-atherogenic sphingolipids	↓		
Lipoprotein metabolism			
VLDL particle production rate	↓		
CE content of the VLDL particles	↓		↓
Hepatic lipid content			↓
Intestinal lipid absorption			↓
Cardiovascular safety effects*2			
Atherosclerosis progression	↓		↓
Coagulation		↑	↑

Mice received a Western-type diet and were treated for 6 weeks with 3 generations TKIs, imatinib (150 mg/kg BID), nilotinib (30 mg/kg QD for the first 3 weeks and 10 mg/kg QD during the last 3 weeks) or ponatinib (10 mg/kg QD first 3 weeks and 3 mg/kg QD last 3 weeks). Plasma parameters were measured after 3 and 6 weeks of treatment. Intestinal lipid absorption was measured after 5 weeks of treatment, and the parameters regarding lipoprotein metabolism were measured at end-point. *1 reduced at t=6 weeks, not at t=3 weeks. *2 The effects on atherosclerosis and coagulation were determined in our previous study (15).

of the limited substrate availability for lipoprotein synthesis, the CE content of the VLDL particles was reduced. In contrast to imatinib, the VLDL-TG production rate was maintained and thus, plasma TG levels were not affected. Ponatinib did not additionally reduce sphingolipids, which contributes to the pro-atherogenic profile of the drug (2,3). Importantly, nilotinib had no effect on lipoprotein metabolism and it is reasonable to believe that the lipid elevations reported with nilotinib in CML-patients (1,10,12,13,37) are caused by response to treatment rather than being a direct effect of off-target (kinase) inhibition.

In CML-patients, it is challenging to distinguish between disease-related lipid modulation or off-target effects of TKI treatment on lipoprotein metabolism. Reduced caloric intake and increased energy requirements imposed by tumor growth may result in reduced plasma cholesterol and TG levels at the moment of diagnosis (38), whereas good response to treatment increases plasma lipid levels again (39,40). In addition, early versus late diagnosis, individual patient characteristics, the presence of one or more risk factors, and previous or current treatment with other TKIs or drugs may affect plasma cholesterol

levels. To exclusively focus on the off-target effects of TKI-treatment, we have used a mouse model without CML, but with a human-like lipoprotein metabolism, the APOE*3-Leiden. CETP mouse model. Unlike wildtype rodents, these mice have a delayed apoE-LDLR-mediated clearance pathway of atherogenic apoB-containing lipoproteins and express CETP (16), and develop hypercholesterolemia upon a Western-type diet. This well-characterized model has been widely used to study lipoprotein metabolism (22,24–26,41) and responds similarly as humans do to hypolipidemic drugs used in the clinic, including statins, fibrates, niacin and PCSK9-inhibitors (18,19,25,42,43). To further improve the translatability of our results, the dose and dose interval of the treatments were based on data of our previously performed PK study (15), resulting in drug concentrations similar as in CML-patients. The lipid-lowering effects of imatinib and ponatinib were induced within 3 weeks and the magnitude of the changes in plasma lipid levels were consistent with our previous observations in APOE*3-Leiden.CETP mice (15). Moreover, the lipid-lowering properties of imatinib are in line with findings in CML-patients (7–10).

Cardiovascular safe profile of imatinib

Our previous study suggested that the lower incidence of cardiovascular events in patients treated with imatinib (11) are the result of reduced plasma lipids and atherosclerosis progression without adverse pro-thrombotic effects as observed with other TKIs (15). In this study, we provide evidence that this is the result of reduced VLDL particle synthesis, illustrated by the decreased (I) VLDL-TG and VLDL-apoB production, (II) CE content of the VLDL particles, and (III) the concentration plasma glycerophospholipids. In line with our findings, *de novo* fatty acid synthesis is reduced when myeloid tumor cells are treated with imatinib (44), pointing towards decreased VLDL particle production.

Parallel to the lipid-modulating effects, imatinib decreased the concentration of pro-atherogenic sphingolipids, amphiphilic molecules that are associated with lipoproteins, of which VLDL and LDL contain most of the sphingomyelins and ceramides (34). Relevant pro-atherogenic processes that are promoted by sphingomyelins and ceramides include lipoprotein aggregation, induction of macrophage foam cell formation, plaque instability and stimulation of pro-inflammatory responses (reviewed in (34,45)). Moreover, imatinib reduced the concentration LPCs, which increase endothelial inflammation (36) and activate signal-transduction cascades involved in the initiation and progression of atherosclerosis (46). Plasma concentrations of ceramides and sphingomyelins are elevated in patients with unstable angina pectoris and acute myocardial infarction (47), specific ceramides are associated with plaque instability and cardiovascular death (48,49), and some LPC species are identified as diagnostic markers for myocardial infarction (50), indicating that the lipid-associated reduction in sphingolipids as observed in our study is relevant for CML-patients treated with imatinib. The reduction of plasma TC, TG and pro-atherogenic sphingolipids may all have contributed to the reduced atherosclerosis development (15) and the favorable cardiac profile in CML-patients (11).

Cardiovascular toxic effects of nilotinib and ponatinib

In contrast to the cardiovascular safe profile of imatinib, the second and third line BCR-ABL1 tyrosine kinase inhibitors nilotinib and ponatinib increase the onset of arterial occlusive events (1–4,12), especially in those patients having a high or very high cardiovascular risk according to the SCORE chart that includes sex, age, smoking habits, systolic blood pressure and TC levels (5,6). Nilotinib did not directly affect lipoprotein metabolism and the lipid elevations reported in nilotinib-treated CML-patients are probably related to response to treatment (39,40). Nevertheless, these elevations may add to the cardiovascular risk (reviewed in (2)), and it is therefore recommended to monitor plasma cholesterol levels when subscribing nilotinib.

Interestingly, ponatinib decreased plasma TC levels by reducing intestinal cholesterol absorption and we previously reported that such a decrease was correlated to reduced atherosclerosis progression (15). Despite, these favorable processes are probably dominated by several negative effects. The decrease in plasma cholesterol and subsequently reduced atherosclerosis development in APOE*3-Leiden.CETP mice was less pronounced with ponatinib as compared to imatinib (15), and therefore might be abolished by response to treatment in patients. In addition, whereas imatinib reduced the concentration of pro-atherogenic glycerophospholipids in the plasma, this was not observed with ponatinib. More importantly, however, we and others have shown that both nilotinib and ponatinib increase blood coagulability (15,51–54), essential in the pathogenesis of atherothrombotic events. These findings, together with the observation of the strongly increased risk in patients predisposed with adverse traditional cardiovascular risk factors (2,5,6) underline the importance to carefully monitor patients during nilotinib and ponatinib treatment.

Acknowledgments

The authors thank Wim Duyvenvoorde, Nanda Keijzer, Anita van Nieuwkoop, Nicole Worms, Jessica Snabel, Christa Ruiter and Joline Attema for their excellent technical assistance.

Disclosures

JWJ received research grants from and was speaker on (CME-accredited) meetings sponsored by Amgen, Astellas, Astra-Zeneca, Daiichi Sankyo, Lilly, Merck-Schering-Plough, Pfizer, Roche, Sanofi-Aventis, the Netherlands Heart Foundation, the Interuniversity Cardiology Institute of the Netherlands, and the European Community Framework KP7 Program. MGP, EG, EJP and HMGP have nothing to disclose.

Funding

This work was supported by an allowance for TKI-LSH from the Ministry of Economic Affairs in the Netherlands (TKI1413P01) and the TNO research program "Preventive Health Technologies".

References

1. Castagnetti F, Breccia M, Gugliotta G, et al. Nilotinib 300 mg twice daily: an academic single-arm study of newly diagnosed chronic phase chronic myeloid leukemia patients. Haematologica. 2016 Oct;101(10):1200–7.
2. Moslehi JJ, Deininger M. Tyrosine Kinase Inhibitor-Associated Cardiovascular Toxicity in Chronic Myeloid Leukemia. J Clin Oncol. 2015 Dec;33(35):4210–8.
3. Valent P, Hadzijusufovic E, Schernthaner G-H, et al. Vascular safety issues in CML patients treated with BCR/ABL1 kinase inhibitors. Blood. 2015 Feb;125(6):901–6.
4. Cortes JE, Kim D-W, Pinilla-Ibarz J, et al. A phase 2 trial of ponatinib in Philadelphia chromosome-positive leukemias. N Engl J Med. 2013 Nov;369(19):1783–96.
5. Assuncao PM, Lana TP, Delamain MT, et al. Cardiovascular Risk and Cardiovascular Events in Patients With Chronic Myeloid Leukemia Treated With Tyrosine Kinase Inhibitors. Clin Lymphoma Myeloma Leuk. 2019 Mar;19(3):162–6.
6. Caocci G, Mulas O, Abruzzese E, et al. Arterial occlusive events in chronic myeloid leukemia patients treated with ponatinib in the real-life practice are predicted by the Systematic Coronary Risk Evaluation (SCORE) chart. Hematol Oncol. 2019 Mar;
7. Gottardi M, Manzato E, Gherlinzoni F. Imatinib and hyperlipidemia. Vol. 353, The New England journal of medicine. United States; 2005. p. 2722–3.
8. Franceschino A, Tornaghi L, Benemacher V, et al. Alterations in creatine kinase, phosphate and lipid values in patients with chronic myeloid leukemia during treatment with imatinib. Vol. 93, Haematologica. Italy; 2008. p. 317–8.
9. Gologan R, Constantinescu G, Georgescu D, et al. Hypolipemiant besides antileukemic effect of imatinib mesylate. Leuk Res. 2009 Sep;33(9):1285–7.
10. Rea D, Mirault T, Cluzeau T, et al. Early onset hypercholesterolemia induced by the 2nd-generation tyrosine kinase inhibitor nilotinib in patients with chronic phase-chronic myeloid leukemia. Haematologica. 2014 Jul;99(7):1197–203.
11. Giles FJ, Mauro MJ, Hong F, et al. Rates of peripheral arterial occlusive disease in patients with chronic myeloid leukemia in the chronic phase treated with imatinib, nilotinib, or non-tyrosine kinase therapy: a retrospective cohort analysis. Leukemia. 2013 Jun;27(6):1310–5.
12. Kim TD, Rea D, Schwarz M, et al. Peripheral artery occlusive disease in chronic phase chronic myeloid leukemia patients treated with nilotinib or imatinib. Leukemia. 2013 Jun;27(6):1316–21.
13. Hochhaus A, Saglio G, Hughes TP, et al. Long-term benefits and risks of frontline nilotinib vs imatinib for chronic myeloid leukemia in chronic phase: 5-year update of the randomized ENESTnd trial. Leukemia. 2016 May;30(5):1044–54.
14. Breccia M, Loglisci G, Cannella L, et al. Nilotinib therapy does not induce consistent modifications of cholesterol metabolism resulting in clinical consequences. Vol. 35, Leukemia research. England; 2011. p. e215-6.
15. Pouwer MG, Pieterman EJ, Verschuren L, et al. The BCR-ABL1 Inhibitors Imatinib and Ponatinib Decrease Plasma Cholesterol and Atherosclerosis, and Nilotinib and Ponatinib Activate Coagulation in a Translational Mouse Model. Front Cardiovasc Med. 2018;5:55.
16. Princen HMG, Pouwer MG, Pieterman EJ. Comment on "Hypercholesterolemia with consumption of PFOA-laced Western diets is dependent on strain and sex of mice" by Rebholz S.L. et al. Toxicol. Rep. 2016 (3) 46-54. Toxicol reports. 2016;3:306–9.
17. Zadelaar S, Kleemann R, Verschuren L, et al. Mouse models for atherosclerosis and pharmaceutical modifiers. Arterioscler Thromb Vasc Biol. 2007 Aug;27(8):1706–21.
18. Dewey FE, Gusarova V, Dunbar RL, et al. Genetic and Pharmacologic Inactivation of ANGPTL3 and Cardiovascular Disease. N Engl J Med. 2017 Jul;377(3):211–21.
19. Kuhnast S, van der Hoorn JWA, Pieterman EJ, et al. Alirocumab inhibits atherosclerosis, improves the plaque morphology, and enhances the effects of a statin. J Lipid Res. 2014 Oct;55(10):2103–12.
20. Ason B, van der Hoorn JWA, Chan J, et al. PCSK9 inhibition fails to alter hepatic LDLR, circulating cholesterol, and atherosclerosis in the absence of ApoE. J Lipid Res. 2014 Nov;55(11):2370–9.
21. Kuhnast S, van der Tuin SJL, van der Hoorn JWA, et al. Anacetrapib reduces progression of atherosclerosis, mainly by reducing non-HDL-cholesterol, improves lesion stability and adds to the beneficial effects of atorvastatin. Eur Heart J. 2015 Jan;36(1):39–48.

22. Bijland S, Rensen PCN, Pieterman EJ, et al. Perfluoroalkyl sulfonates cause alkyl chain length-dependent hepatic steatosis and hypolipidemia mainly by impairing lipoprotein production in APOE*3-Leiden CETP mice. Toxicol Sci. 2011 Sep;123(1):290–303.
23. de Haan W, van der Hoogt CC, Westerterp M, et al. Atorvastatin increases HDL cholesterol by reducing CETP expression in cholesterol-fed APOE*3-Leiden.CETP mice. Atherosclerosis. 2008 Mar;197(1):57–63.
24. van der Hoogt CC, de Haan W, Westerterp M, et al. Fenofibrate increases HDL-cholesterol by reducing cholesteryl ester transfer protein expression. J Lipid Res. 2007 Aug;48(8):1763–71.
25. van der Hoorn JWA, de Haan W, Berbee JFP, et al. Niacin increases HDL by reducing hepatic expression and plasma levels of cholesteryl ester transfer protein in APOE*3Leiden.CETP mice. Arterioscler Thromb Vasc Biol. 2008 Nov;28(11):2016–22.
26. Pouwer MG, Pieterman EJ, Chang S-C, et al. Dose effects of ammonium perfluorooctanoate on lipoprotein metabolism in APOE*3-Leiden.CETP mice. Toxicol Sci. 2019 Jan;
27. de Vries-van der Weij J, de Haan W, Hu L, et al. Bexarotene induces dyslipidemia by increased very low-density lipoprotein production and cholesteryl ester transfer protein-mediated reduction of high-density lipoprotein. Endocrinology. 2009 May;150(5):2368–75.
28. Post SM, de Crom R, van Haperen R, et al. Increased fecal bile acid excretion in transgenic mice with elevated expression of human phospholipid transfer protein. Arterioscler Thromb Vasc Biol. 2003 May;23(5):892–7.
29. Geerling JJ, Boon MR, van der Zon GC, et al. Metformin lowers plasma triglycerides by promoting VLDL-triglyceride clearance by brown adipose tissue in mice. Diabetes. 2014 Mar;63(3):880–91.
30. Post SM, Zoeteweij JP, Bos MH, et al. Acyl-coenzyme A:cholesterol acyltransferase inhibitor, avasimibe, stimulates bile acid synthesis and cholesterol 7alpha-hydroxylase in cultured rat hepatocytes and in vivo in the rat. Hepatology. 1999 Aug;30(2):491–500.
31. Curtis MJ, Alexander S, Cirino G, et al. Experimental design and analysis and their reporting II: updated and simplified guidance for authors and peer reviewers. Vol. 175, British journal of pharmacology. England; 2018. p. 987–93.
32. Volger OL, van der Boom H, de Wit EC, et al. Dietary plant stanol esters reduce VLDL cholesterol secretion and bile saturation in apolipoprotein E*3-Leiden transgenic mice. Arterioscler Thromb Vasc Biol. 2001 Jun;21(6):1046–52.
33. Worgall TS. Sphingolipid synthetic pathways are major regulators of lipid homeostasis. Adv Exp Med Biol. 2011;721:139–48.
34. Hornemann T, Worgall TS. Sphingolipids and atherosclerosis. Atherosclerosis. 2013 Jan;226(1):16–28.
35. Hui DY. Intestinal phospholipid and lysophospholipid metabolism in cardiometabolic disease. Curr Opin Lipidol. 2016 Oct;27(5):507–12.
36. Li Y-F, Li R-S, Samuel SB, et al. Lysophospholipids and their G protein-coupled receptors in atherosclerosis. Front Biosci (Landmark Ed. 2016 Jan;21:70–88.
37. Iurlo A, Orsi E, Cattaneo D, et al. Effects of first- and second-generation tyrosine kinase inhibitor therapy on glucose and lipid metabolism in chronic myeloid leukemia patients: a real clinical problem? Oncotarget. 2015 Oct;6(32):33944–51.
38. Muller CP, Wagner AU, Maucher C, et al. Hypocholesterolemia, an unfavorable feature of prognostic value in chronic myeloid leukemia. Eur J Haematol. 1989 Sep;43(3):235–9.
39. Baroni S, Scribano D, Zuppi C, et al. Prognostic relevance of lipoprotein cholesterol levels in acute lymphocytic and nonlymphocytic leukemia. Acta Haematol. 1996;96(1):24–8.
40. Ghalaut VS, Pahwa MB, Sunita, et al. Alteration in lipid profile in patients of chronic myeloid leukemia before and after chemotherapy. Clin Chim Acta. 2006 Apr;366(1–2):239–42.
41. de Haan W, de Vries-van der Weij J, van der Hoorn JWA, et al. Torcetrapib does not reduce atherosclerosis beyond atorvastatin and induces more proinflammatory lesions than atorvastatin. Circulation. 2008 May;117(19):2515–22.
42. van De Poll SW, Romer TJ, Volger OL, et al. Raman spectroscopic evaluation of the effects of diet and lipid-lowering therapy on atherosclerotic plaque development in mice. Arterioscler Thromb Vasc Biol. 2001 Oct;21(10):1630–5.
43. Kooistra T, Verschuren L, de Vries-van der Weij J, et al. Fenofibrate reduces atherogenesis in ApoE*3Leiden mice: evidence for multiple antiatherogenic effects besides lowering plasma cholesterol. Arterioscler Thromb Vasc Biol. 2006 Oct;26(10):2322–30.

44. Boren J, Cascante M, Marin S, et al. Gleevec (STI571) influences metabolic enzyme activities and glucose carbon flow toward nucleic acid and fatty acid synthesis in myeloid tumor cells. J Biol Chem. 2001 Oct;276(41):37747–53.
45. Iqbal J, Walsh MT, Hammad SM, et al. Sphingolipids and Lipoproteins in Health and Metabolic Disorders. Trends Endocrinol Metab. 2017 Jul;28(7):506–18.
46. Matsumoto T, Kobayashi T, Kamata K. Role of lysophosphatidylcholine (LPC) in atherosclerosis. Curr Med Chem. 2007;14(30):3209–20.
47. Pan W, Yu J, Shi R, et al. Elevation of ceramide and activation of secretory acid sphingomyelinase in patients with acute coronary syndromes. Coron Artery Dis. 2014 May;25(3):230–5.
48. Cheng JM, Suoniemi M, Kardys I, et al. Plasma concentrations of molecular lipid species in relation to coronary plaque characteristics and cardiovascular outcome: Results of the ATHEROREMO-IVUS study. Atherosclerosis. 2015 Dec;243(2):560–6.
49. Laaksonen R, Ekroos K, Sysi-Aho M, et al. Plasma ceramides predict cardiovascular death in patients with stable coronary artery disease and acute coronary syndromes beyond LDL-cholesterol. Eur Heart J. 2016 Jul;37(25):1967–76.
50. Ward-Caviness CK, Xu T, Aspelund T, et al. Improvement of myocardial infarction risk prediction via inflammation-associated metabolite biomarkers. Heart. 2017 Aug;103(16):1278–85.
51. Alhawiti N, Burbury KL, Kwa FA, et al. The tyrosine kinase inhibitor, nilotinib potentiates a prothrombotic state. Thromb Res. 2016 Sep;145:54–64.
52. Loren CP, Aslan JE, Rigg RA, et al. The BCR-ABL inhibitor ponatinib inhibits platelet immunoreceptor tyrosine-based activation motif (ITAM) signaling, platelet activation and aggregate formation under shear. Thromb Res. 2015 Jan;135(1):155–60.
53. Kang Z, Ji Y, Zhang G,et al. Ponatinib attenuates experimental pulmonary arterial hypertension by modulating Wnt signaling and vasohibin-2/vasohibin-1. Life Sci. 2016 Mar;148:1–8.
54. Hadzijusufovic E, Albrecht-Schgoer K, Huber K, et al. Nilotinib-induced vasculopathy: identification of vascular endothelial cells as a primary target site. Leukemia. 2017 Nov;31(11):2388–97.

6

Dose effects of ammonium perfluorooctanoate on lipoprotein metabolism in APOE*3-Leiden.CETP mice

Marianne G. Pouwer, Elsbet J. Pieterman, Shu-Ching Chang, Geary W. Olsen, Martien P.M. Caspers, Lars Verschuren, J. Wouter Jukema, Hans M. G. Princen

Toxicol Sci. 2019 Apr 1;168(2):519-534

Abstract

Objectives: Epidemiological studies have reported positive associations between serum PFOA and total and non-high-density lipoprotein cholesterol (non-HDL-C) although the magnitude of effect of PFOA on cholesterol lacks consistency. The objectives of this study were to evaluate the effect of PFOA on plasma cholesterol and triglyceride metabolism at various plasma PFOA concentrations relevant to humans, and to elucidate the mechanisms using APOE*3-Leiden.CETP mice, a model with a human-like lipoprotein metabolism.

Methods and results: APOE*3-Leiden.CETP mice were fed a Western-type diet with PFOA (10, 300, 30 000 ng/g/d) for 4-6 weeks. PFOA exposure did not alter plasma lipids in the 10 and 300 ng/g/d dietary PFOA dose groups. At 30 000 ng/g/d, PFOA decreased plasma triglycerides (TG), total cholesterol (TC) and non-HDL-C, whereas HDL-C was increased. The plasma lipid alterations could be explained by decreased very low-density lipoprotein (VLDL) production and increased VLDL clearance by the liver through increased lipoprotein lipase activity. The concomitant increase in HDL-C was mediated by decreased cholesteryl ester transfer activity and changes in gene expression of proteins involved in HDL metabolism. Hepatic gene expression and pathway analysis confirmed the changes in lipoprotein metabolism that were mediated for a major part through activation of the peroxisome proliferator-activated receptor (PPAR)α.

Conclusions: Our data confirmed the findings from a phase 1 clinical trial in humans that demonstrated high serum or plasma PFOA levels resulted in lower cholesterol levels. The study findings do not show an increase in cholesterol at environmental or occupational levels of PFOA exposure, thereby indicating these findings are associative rather than causal.

Introduction

Salts of perfluorooctanoic acid (PFOA) were widely used as an emulsifier in the manufacture of fluoropolymers. Because PFOA is extremely stable (due to strong carbon-fluorine bond strength) and nonflammable, it cannot be readily degraded by strong acids, alkalis, or oxidizing agents; and as a result, it persists in the environment and is detected ubiquitously in humans and wildlife (1).

In general populations with ambient exposures or a community exposed to environmental levels of PFOA, several cross-sectional epidemiological studies have reported associations of serum PFOA with increased serum concentrations of total cholesterol (TC) and low-density lipoprotein cholesterol (LDL-C) in adults and children (2–8). However, the magnitude of effect on cholesterol appears to be less in more highly exposed occupational workers (9–16). In addition, there has been no reported increased risk for coronary artery disease incidence related to PFOA exposure in an exposed community (17) or in occupational cohorts when using internal referent comparisons (18,19).

Several studies have evaluated the effect of PFOA on plasma lipids, including mice (20–22), rats (20,23), and monkeys (24). In general, plasma lipids were either lowered or unchanged under these toxicological study conditions. These findings were consistent with one of the known toxicodynamic properties of PFOA in which it can activate nuclear receptor peroxisome proliferator-activated receptor alpha (PPARα) and subsequently leads to increased fatty acid (FA) oxidation and an overall lowering of serum/plasma lipid levels (25–27). The activation of PPARα is the operative mechanism of fibrate drugs that reduce serum/plasma lipids in both laboratory animals and humans (28,29). In a phase 1 clinical trial study, PFOA was investigated as an antitumor agent due to its ability to inhibit PIM kinase activity (30). These patients received weekly ammonium PFOA doses that ranged between 50 and 1200 mg for 6 weeks. A reduction in plasma TC levels (LDL, not HDL-C) occurred at plasma PFOA concentrations between 420 and 565 µM (175 000–230 000 ng/mL). Albeit the exact mechanism was not fully elucidated, the finding reported by Convertino et al. (30) was consistent with the toxicodynamic property of PFOA described previously where hypolipidemic responses were observed in laboratory animals (20,22,23).

It is worth noting that, unlike humans, rodent lipoprotein metabolism is characterized by fast clearance of apoB-containing lipoproteins and the absence of cholesteryl ester transfer protein (CETP) resulting in a higher proportion of HDL-C relative to LDL-C (31). CETP is responsible for transferring cholesterol ester (CE) from HDL-C to the apoB-containing lipoproteins in exchange for triglycerides (TG). In contrast, human and nonhuman primates have a higher proportion of LDL-C relative to HDL-C due to the presence of CETP (31). Given the difference in lipid-handling that can hamper the extrapolation of rodent lipid data to human (31), we undertook this study to evaluate the effects of PFOA on lipid metabolism using the APOE*3-Leiden.CETP mouse model. This genetically engineered

mouse model was designed to mimic the human lipoprotein metabolism with CETP expression and a delayed apoB clearance (31). It has been widely used to study the effect of drugs on atherosclerosis (32–35), cardiovascular safety (36,37), and lipid metabolism (38–40). Therefore, the objectives of the study reported herein are to (I) evaluate the effect of PFOA on plasma cholesterol at different PFOA concentrations that had been reported in human observational and experimental studies; and (II) elucidate the mechanism for the hypolipidemic responses with PFOA exposures, including hepatic gene expression and pathway analysis.

Materials and methods

Animals

Sixty-four male APOE*3-Leiden.CETP transgenic mice of 7–12 weeks (experiment 1) and 6–10 weeks (experiment 2) of age at the start of the experiment were used in this study. Mice were housed under standard conditions with a 12-h light-dark cycle and had free access to food and water. When fasting was required, only food was removed for the length specified by the study protocol. Body weight, food intakes, and clinical signs of behavior were monitored regularly during the study. Animal experiments were approved by the Institutional Animal Care and Use Committee of The Netherlands Organization for Applied Research (TNO) under registration number 3682. All procedures involving animals were conformed to Guide for the Care and Use of Laboratory Animals (41).

Human plasma samples

Plasma from healthy anonymized donors was obtained after their written informed consent from Sanquin blood bank (the Netherlands), in accordance with the Declaration of Helsinki.

Materials

PFOA ammonia salt (FC-143, lot 332) was provided by 3M Company (St Paul, Minnesota). It consisted of 77.6% linear and 22% branched (12.6% internal monomethyl (nonalpha), 9% isopropyl, 0.2% tert-butyl, 0.1% gem-dimethyl, and 0.1% alpha monomethyl). This test material, a white solid, was 97.99% pure and was stored at room temperature. All other chemicals were reagent-grade.

Study design

In this study, mice were fed a semisynthetic Western-type diet (WTD) for 4 weeks of a dietary run-in (acclimation) period prior to group allocation (**Figure 1**). The semisynthetic WTD consisted of 0.25% cholesterol (wt/wt), 1% corn oil (wt/wt), and 14% bovine fat (wt/wt; Hope Farms, Woerden, The Netherlands).

	Time (weeks)	-4	-3	-2	-1	0	1	2	3	4	5	6
Experiment 1 **n=8 mice per group**	**Control**	Run-in/acclimatization on a WTD				Matching BW, FI Plasma TC, TG, HDL-C FFA, glycerol				BW, FI Plasma TC, TG, HDL-C FFA, glycerol, ALT	HL + LPL activity EchoMRI Collection of feces	BW, FI Plasma TC, TG, HDL-C FFA, glycerol, ALT CETP activity VLDL production **Sacrifice**
	10 ng/kg/d											
	300 ng/kg/d											
	30 000 ng/kg/d											
Experiment 2 **n=8 mice per group**	**Control**	Run-in/acclimatization on a WTD				Matching BW, FI Plasma TC, TG, HDL-C				BW, FI Plasma TC, TG, HDL-C,ALT VLDL clearance **Sacrifice** Hepatic lipids and pathology Transcriptome analysis		
	10 ng/kg/d											
	300 ng/kg/d											
	30 000 ng/kg/d											

Figure 1 Study set-up. At the end of the 4-week run-in period (t=0 weeks), mice were randomized into 4 groups based on age, body weight, and baseline plasma TC, TG, and HDL-C levels measured at the end of the run-in period. Upon randomization, mice were either fed with WTD alone (control group) or WTD containing ammonium PFOA at 10, 300, or 30 000 ng/g/d (n=8 mice per dose group). Abbreviations: BW, body weight; CETP, cholesteryl ester transfer protein; FFA, free fatty acids; FI, food intake; HDL-C, high-density lipoprotein cholesterol; HL, hepatic lipase; LPL, lipoprotein lipase; MRI, magnetic resonance imaging; TC, total cholesterol; TG, triglycerides; VLDL, very-low-density lipoprotein; WTD, Western-type diet.

For test material administration, ammonium PFOA was incorporated into this WTD at either 10, 300, or 30 000 ng/g/d (verification by liquid chromatography-tandem mass spectrometry [LC-MS/MS]). These dietary PFOA doses were chosen to achieve serum or plasma PFOA concentrations that had been reported in human observational or experimental studies. At the end of 4–6 weeks of dietary PFOA treatment at either 10, 300, or 30 000 ng/g/d, the mice were aimed to achieve comparable plasma PFOA levels found in the mid-Ohio river valley residents whose drinking water was contaminated with PFOA (ie, environmental exposure), fluorochemical production workers (ie, occupational exposure), or laboratory toxicological studies where reduced serum/plasma lipids were observed (ie, toxicological exposure), respectively.

Experiment 1 (6-week dietary treatment containing ammonium PFOA)

At the end of the 4-week run-in period (t=0 weeks), mice were randomized into 4 four groups based on age, body weight, and baseline plasma TC, TG, and HDL-C levels measured at the end of run-in period (n = 8 mice per dose group) after a 4-h fast by tail vein bleeding. Upon randomization, mice were fed with the WTD alone (control group) or WTD containing ammonium PFOA at either 10, 300, or 30 000 ng/g/d for 6 weeks (**Table 1**). Body weight and food intakes were monitored and recorded throughout the study for all mice. At the end of week 4, plasma TC, TG, free fatty acids (FFA), glycerol and alanine aminotransferase (ALT) were measured in blood samples from 4-h fasted mice collected by tail vein bleeding. At the end of week 5, hepatic lipase (HL) and lipoprotein lipase (LPL) activities were determined in plasma (after heparin injection). In addition, total fat mass was determined by EchoMRI image and 48–72 h feces were collected to measure excretion of bile acids and neutral sterols. At the end of week 6, in addition to plasma TC, TG, FFA, glycerol, and ALT determination, very low-density lipoprotein (VLDL) production was measured for all mice (**Figure 1**). Aliquots of plasma samples (approximately 20 µl) were collected from mice at week 0, 4, and 6 for PFOA concentration determination by LC-MS/MS. All mice were euthanized at the end of week 6, and perigonadal white adipose tissue (pWAT) and brown adipose tissue (BAT) were weighed.

Experiment 2 (4-week dietary treatment containing ammonium PFOA)

Similar to experiment 1, at the end of the 4-week run-in period (t=0 weeks), mice were randomized into 4 groups based on age, body weight, and baseline plasma TC, TG and HDL-C levels measured at the end of the run-in period (n=8 mice per dose group) after a 4-hour fast by tail vein bleeding. Upon randomization, mice were either fed with WTD alone (control group) or WTD containing ammonium PFOA at 10, 300, or 30 000 ng/g/d similar to experiment 1 described above (**Table 1**). Body weight and food intakes were monitored and recorded throughout the study for all mice. At the end of week 4, plasma TC, TG and ALT enzyme activity were measured for all mice in addition to VLDL-clearance evaluation. Aliquots of plasma samples (approximately 20 µl) were collected from mice at

Table 1 Dietary PFOA intake and mean plasma concentrations of PFOA

		Control	10 ng/g/d PFOA	300 ng/g/d PFOA	30000 ng/g/d PFOA
	[PFOA] in diet (ng/g)	<0.5	9 ± 1	273 ± 12	26 380 ± 683
Experiment 1	Dietary PFOA intake (ng/g bw/day)	0.0	10	291	30 238
	Plasma [PFOA], t=4 weeks (ng/mL)	<1.0	49 ± 4	1 350 ± 88	90 663 ± 8 867
	Plasma [PFOA], t=6 weeks (ng/mL)	5 ± 1	65 ± 7	1 524 ± 54	144 000 ± 13 406
Experiment 2	Dietary PFOA intake (ng/g bw/day)	0.0	10	298	29 476
	Plasma [PFOA], t=4 weeks (ng/mL)	<1.0	51 ± 5	1 395 ± 100	93 713 ± 4 827

Mice received a Western-type diet without or with 10, 300 or 30 000 ng/g/d PFOA, for 6 weeks (experiment 1) or 4 weeks (experiment 2). Dietary and plasma PFOA concentrations were measured by LC-MS/MS and dietary PFOA intake was calculated. Data are presented as mean ± SD. (n=8 mice per group, n=6 dietary samples).

week 0 and 4 for PFOA concentration determination by LC-MS/MS. In experiment 2, all mice were euthanized on week 4 for liver-related analysis, including microscopic evaluation, detailed hepatic lipid profiling, and transcriptome analysis (**Figure 1**).

Determination of serum and dietary concentrations of PFOA

Dietary PFOA concentrations were determined by LC-MS/MS. Briefly, one gram of each dietary sample (sampled from top, middle, and bottom of the bag) were pulverized and followed by addition of 50% methanol in water (9 mL). After overnight incubation at room temperature on a roller shaker, samples were then sonicated for 15 min followed by centrifugation (2500 × g, 5 min). One hundred microliters of the top layer was transferred to a new tube which contained a fixed amount of the stable isotope-labeled internal standard (13C-PFOA), followed by the addition of 1 N formic acid (1 mL) and 100 µl of saturated ammonium sulfate. The solution was mixed by vortexing and then subjected to solid phase extraction (SPE) with Phenomenex Strata-X 3-ml SPE columns and LC-MS/MS according to the method described in Ehresman et al. (42). Serum PFOA concentrations were also determined by LC-MS/MS as described previously (42).

Plasma biochemical analysis

EDTA plasma samples were collected in week 0, 4, and 6 after a 4-h fast. Plasma TC, TG, FFA, and free glycerol were determined using enzymatic kits (TC: Roche/Hitachi, Mannheim,

Germany, catalogue# 11491458216 TG: Roche/Hitachi, catalogue# 11730711216, FFA: Wako diagnostics, Richmond, USA, catalogue# 434-91795 and 436-91995, free glycerol: Sigma-Aldrich, St. Louis, USA, catalogue# F6428) according to the manufacturer's protocols. HDL-C was measured after precipitation as described previously (35). Non-HDL-C levels were calculated by subtracting HDL-C from TC. The distribution of cholesterol over plasma lipoproteins was determined in group-wise pooled plasma by fast protein liquid chromatography (FPLC) (43). ALT enzymatic activity was measured by reflectance photometry using a Reflotron® Plus analyzer (Hoffman-La Roche, Mannheim, Germany).

CETP activity assay

Differences in CETP activity between APOE*3-Leiden.CETP mice and humans may affect the magnitude of the PFOA-induced increase of plasma HDL-C. Therefore, endogenous CETP activity was measured in human and mouse plasma with a fluorescent assay using donor liposomes enriched with nitrobenzoxadiazole-labeled cholesteryl esters (RB-CETP, Roar Biomedical, New York, New York) as described previously (44).

Hepatic VLDL-TG and VLDL-apoB production

All mice were fasted for 4 h prior to the start of the experiment. During the experiment, mice were sedated with acepromazine-midazolam-fentanyl intraperitoneally [6.25 mg/kg acepromazine (Ceva Santé Animale B.V., Naaldwijk, The Netherlands), 6.25 mg/kg midazolam (Actavis, Baarn, The Netherlands), and 0.3125 mg/kg fentanyl (Bipharma B.V., Almere, The Netherlands)]. At t=0 min, blood was taken via tail bleeding and mice were intravenously (IV) injected with 100 µl phosphate-buffered saline (PBS) containing 20 µCi Trans^{35}S-labeled methionine/cysteine (ICN Biomedicals, Irvine, California) to measure de novo apoB synthesis. After 30 min, the mice received a Triton WR1339 IV injection (500 mg/kg body weight), which inhibits LPL-mediated lipolysis, thereby blocking VLDL clearance. Blood samples were drawn at 0, 15, 30, 60, and 90 min after Triton WR1339 injection and used for determination of the plasma TG concentration. After 90 min, the animals were sacrificed by cervical dislocation and blood was collected by heart puncture for subsequent isolation of VLDL by density-gradient ultracentrifugation. ^{35}S-apoB was measured in the VLDL fraction after apoB-specific precipitation, and VLDL-apoB production rate was calculated as disintegration per minute (dpm)/h, as previously reported (40,45,46).

In vivo clearance of VLDL-like particles

All mice were fasted for 4 h and injected in the tail vein with VLDL-like particles (80 nm) containing 3H-labeled FA (as glycerol tri[3H]-oleate, [3H]-TO) and 14C-labeled cholesteryl oleate (as [14C]-cholesteryl oleate, [14C]-CO). At t=2, 5, 10, and 15 min post-injection, blood was collected to determine the plasma decay of [3H]-TO and [14C]-CO. At 15 min, mice were euthanized by cervical dislocation and perfused with heparin 10 U/mL in ice-cold

PBS for 5 min. Organs (ie, liver, subcutaneous WAT [sWAT], BAT, spleen, lung and skeletal femoral muscle) were harvested and saponified overnight in 500 µl Solvable (Perkin-Elmer, Wellesley, Massachusetts) to determine [3H]-TO and [14C]-CO uptake. Retention of radioactivity in the saponified tissues was measured as % of the injected dose and the half-life of VLDL-[3H]-TO and [14C]-CO was calculated from the slope after linear fitting of semilogarithmic decay curves as described previously (40,45,46).

HL and lipoprotein lipase assay

Lipolytic activity of both LPL and HL was determined at t=5 weeks. To liberate LPL from the endothelium, 4-h fasted mice were injected IV with heparin (0.1 U/g body weight; Leo Pharmaceutical Products BV, Weesp, The Netherlands) and blood was collected after 20 min. Postheparin plasma was incubated with 0.2 ml of TG substrate mixture containing triolein (4.6 mg/mL) and [3H]-TO (2.5 µCi/mL) for 30 min at 37°C in the presence or absence of 1 M NaCl, which completely inhibits LPL activity, to estimate both the HL and LPL activity. The LPL activity was calculated as the fraction of total triacylglycerol hydrolase activity that was inhibited by the presence of 1 M NaCl and is expressed as the amount of FFAs released per hour per mL of plasma (45,47).

Liver histology

Liver samples (lobus sinister medialis hepatis) were collected, fixed in formalin and paraffin embedded, and sections (3 µm) were stained with hematoxylin and eosin (HE). The level of macrovesicular and microvesicular steatosis and hypertrophy relative to the total liver area was determined by a board-certified pathologist and expressed as the percentage of total liver area. Inflammation was scored by counting the number of aggregates of inflammatory cells per mm^2. Inflammatory aggregates, as marker of liver inflammation, are defined as a cluster, not a row, of ≥ 5 inflammatory cells (48).

Hepatic lipid analysis

Liver tissue samples of lobus sinister lateralis hepatis were homogenized in phosphate-buffered saline, and the protein content was measured using a Lowry protein assay. Lipids were extracted as described previously (49), separated by high-performance thin-layer chromatography on silica gel plates, stained and analyzed with ChemiDoc Touch Imaging System (Bio-Rad Laboratories Inc, Hercules, USA). TG, CE, and free cholesterol (FC) content were quantified using Image-lab version 5.2.1 software (Bio-Rad Laboratories Inc, Hercules, USA) and expressed per mg liver protein.

Excretion of fecal sterols and bile acids

Fecal excretion of neutral sterols and bile acids was determined in feces, collected during a 48- to 72-h time period at 2 consecutive time points at week 5, by gas chromatographic analysis as described previously (47).

Hepatic gene expression and pathway analysis

Total RNA was extracted from the liver using the RNAbee isolation kit (Tel-Test Inc., Friendswood, USA, catalogue# CS-105B) and the Nucleospin RNA II mini spin kit (Macherey-Nagel GmbH & Co, Düren, Germany, catalogue# 740.955.50). Total RNA concentration was determined spectrophotometrically using Nanodrop 1000 (Isogen Life Science, De Meern, The Netherlands), and RNA quality was assessed using the 2100 Bioanalyzer (Agilent Technologies, Amstelveen, The Netherlands). The NEBNext Ultra Directional RNA Library Prep Kit for Illumina was used to process the samples according to the protocol "NEBNext Ultra Directional RNA Library Prep Kit for Illumina" (NEB #E7420S/L). Strand-specific messenger RNA sequencing libraries were generated and sequenced at GenomeScan (Leiden, The Netherlands). The libraries were multiplexed, clustered, and sequenced on an Illumina NextSeq 500 with a single-read 75-cycle sequencing protocol, 15 million reads per sample. The genome reference and annotation file Mus_Musculus.GRCm38 was used for analysis in FastA and GTF format. The reads were aligned to the reference sequence using Tophat 2.0.14 combined with Bowtie 2.1.0, and based on the mapped read locations and the gene annotation. HTSeq-count version 0.6.1p1 was used to count how often a read was mapped on the transcript region. Selected differentially expressed genes (DEGs) were used as an input for pathway and upstream regulator analysis through Ingenuity Pathway Analysis suite (www.ingenuity.com; Accessed November 2016). Calculated p-values <0.01 were used as threshold for significance in all analysis except for those in the 30 000 ng/g/d dose group for which we used the adjusted p-value of <0.05, the latter indicating a higher level of stringency. Gene set enrichment analysis was used to highlight the most important processes and pathways ranked based on their p-value of overlap (37,45,48).

Statistical analysis

Data are presented as means ± SD. A Kruskal–Wallis test was used to determine the significance of differences between the groups. Significance of differences of the individual groups with the control was calculated nonparametrically using a Mann–Whitney U-test and the rejection criteria were adjusted using a Bonferroni–Holm correction. IBM SPSS v24.0 was used for all analyses. p-Values ≤0.05 were considered statistically significant.

Results

Clinical observations and food intakes

No clinical signs of abnormal behavior were noted in any treatment group during the study. There was no PFOA treatment-related mortality observed in the study and PFOA dietary treatment did not appear to affect food intakes in the mice. Four mice died in experiment 1 due to anesthetic complications (2 mice in 10 ng/g/d, 1 mouse in 300 ng/g/d, and 1 mouse in 30 000 ng/g/d) and this was not considered to be treatment related.

Dietary and plasma concentrations of PFOA

Dietary PFOA concentrations were determined for each dose group and based on 5–6 samples per dose group. The mean dietary PFOA concentrations were 8.5 ± 0.8, 273.0 ± 11.6, and 26 380 ± 683.3 ng/g for the 10, 300, and 30 000 ng/g/d dose groups, respectively, which represented 89.1 ± 8.6%, 95.0 ± 4.0%, and 91.8 ± 2.4% of the target doses (**Table 1**). Based on body weight and food intake, these dietary PFOA intakes are approximately 10, 300 and 30 000 ng/g/d, respectively (**Table 1**).

Mean plasma PFOA concentrations were measured in all animals from both experiments and are presented in **Table 1**. In both experiments, there were dose-dependent increases in plasma PFOA concentrations. After 4 weeks of dietary PFOA exposures, plasma PFOA concentrations in either experiment 1 or experiment 2 were very similar; they were at 49–51 ng/mL (from 10 ng/g dose group), 1350–1395 ng/mL (from 300 ng/g dose group), and 90 663–93 713 ng/mL (from 30 000 ng/g/d dose group). In experiment 1, plasma PFOA concentrations continued to increase through week 6 (**Table 1**).

Body weight and liver weight

In experiment 1, there was a statistically significant decrease in body weight of the 30 000 ng/g/d dose group mice at t=4 weeks (–10%, $p<0.01$) and at t=6 weeks (–18%, $p<0.001$) when compared with control. The body weight reduction was not observed in week 4 in experiment 2 (**Table 2**). There was also a statistically significant increase in liver weight from the 30 000 ng/g/d group in experiment 1 (+150%, $p<0.001$) and in experiment 2 (+190%, $p<0.001$), but not with the 10 or 300 ng/g/d dietary dose (**Table 2**).

The effect of PFOA on plasma lipids

PFOA decreased plasma TC and TG and increased HDL-C

PFOA exposure did not alter plasma lipids at 10 and 300 ng/g/d dietary PFOA dose groups, respectively (**Figure 2A–D**). In contrast, at 30 000 ng/g/d dietary dose group where plasma PFOA reached 144 000 ng/mL after 6 weeks of dietary PFOA exposure, it decreased plasma TG (–72%, $p<0.001$) (**Figure 2A**), TC (–33%, $p<0.001$) (**Figure 2B**), and non-HDL-C (–69%, $p<0.001$) (**Figure 2C**) relative to controls. There was a concomitant increase in HDL-C (+130%, $p<0.001$) (**Figure 2D**). The lipoprotein profile at this high PFOA exposure

Table 2 Body weight, food intake, liver weight, and plasma parameters of mice in experiment 1 and experiment 2

	Experiment 1 (t=4 weeks)			
	Control	**10 ng/g/d**	**300 ng/g/d**	**30 000 ng/g/d**
Body weight (gram)	28.9 ± 1.9	28.5 ± 2.5	28.5 ± 2.4	25.9 ± 1.1**
Food intake (gram/day/mouse)	2.8 ± 0.1	3.0 ± 0.4	2.8 ± 0.3	2.8 ± 0.3
Liver weight (gram)	*NA*	*NA*	*NA*	*NA*
Liver weight (% of body weight)	*NA*	*NA*	*NA*	*NA*
ALT (U/L)	145 ± 84	83 ± 27	217 ± 151	437 ± 112***
TC (mmol/L)	6.2 ± 0.9	6.8 ± 1.5	5.9 ± 1.1	4.3 ± 0.7**
HDL-C (mmol/L)	1.8 ± 0.3	1.5 ± 0.3	1.7 ± 0.3	3.6 ± 0.5***
non-HDL-C (mmol/L)	4.4 ± 0.9	5.3 ± 1.4	4.2 ± 1.1	0.7 ± 0.2***
TG (mmol/L)	1.7 ± 0.4	1.6 ± 0.3	1.2 ± 0.2	0.3 ± 0.0***
	Experiment 1 (t=6 weeks)			
	Control	**10 ng/g/d**	**300 ng/g/d**	**30 000 ng/g/d**
Body weight (gram)	30.2 ± 1.9	28.9 ± 3.0	29.6 ± 2.4	25.5 ± 1.0***
Food intake (gram/day/mouse)	3.0 ± 0.1	2.9 ± 0.4	3.0 ± 0.4	2.6 ± 0.3
Liver weight (gram)	1.4 ± 0.1	1.4 ± 0.3	1.5 ± 0.3	3.5 ± 0.2***
Liver weight (% of body weight)	4.5 ± 0.3	4.8 ± 0.5	5.2 ± 0.6	13.6 ± 0.1***
ALT (U/L)	95 ± 27	118 ± 70	123 ± 90	740 ± 161**
TC (mmol/L)	7.6 ± 1.3	6.9 ± 1.5	7.8 ± 2.7	5.1 ± 0.6***
HDL-C (mmol/L)	1.4 ± 0.3	1.5 ± 0.4	1.5 ± 0.2	3.2 ± 0.3***
non-HDL-C (mmol/L)	6.3 ± 1.4	5.4 ± 1.2	6.3 ± 2.7	2.0 ± 0.5***
TG (mmol/L)	1.8 ± 0.4	1.5 ± 0.4	1.5 ± 0.4	0.5 ± 0.0***
	Experiment 1 (t=4 weeks)			
	Control	**10 ng/g/d**	**300 ng/g/d**	**30 000 ng/g/d**
Body weight (gram)	27.6 ± 1.9	28.7 ± 2.5	28.3 ± 1.6	25.8 ± 1.9
Food intake (gram/day/mouse)	2.7 ± 0.2	3.0 ± 0.2	2.9 ± 0.1	2.6 ± 0.1
Liver weight (gram)	1.3 ± 0.1	1.4 ± 0.1	1.5 ± 0.1	3.8 ± 0.3***
Liver weight (% of body weight)	4.9 ± 0.4	4.8 ± 0.4	5.2 ± 0.2	14.8 ± 0.6***
ALT (U/L)	178 ± 52	211 ± 118	533 ± 950	553 ± 81**
TC (mmol/L)	6.1 ± 0.7	6.4 ± 1.5	6.0 ± 1.1	4.9 ± 1.2
HDL-C (mmol/L)	2.4 ± 0.4	2.2 ± 0.3	2.0 ± 0.2	4.5 ± 0.9***
non-HDL-C (mmol/L)	3.7 ± 0.9	4.3 ± 1.5	4.0 ± 1.1	0.3 ± 0.2***
TG (mmol/L)	1.5 ± 0.5	1.6 ± 0.5	1.5 ± 0.2	0.4 ± 0.1***

Mice received a Western-type diet without or with 10, 300 or 30 000 ng/g/d PFOA for 6 weeks in experiment 1 or for 4 weeks in experiment 2. All parameters were measured individually, except for food intake which was measured per cage. Data are presented as mean ± SD (n=8 per group, n=5–7 per group for ALT, n=3–4 cages per group). **p<0.01, ***p <0.001 as compared with the control group. Abbreviations: ALT, alanine transaminase; HDL-C, high-density lipoprotein cholesterol; NA, not applicable; non-HDL-C, non-high-density lipoprotein cholesterol; TC, total cholesterol; TG, triglycerides.

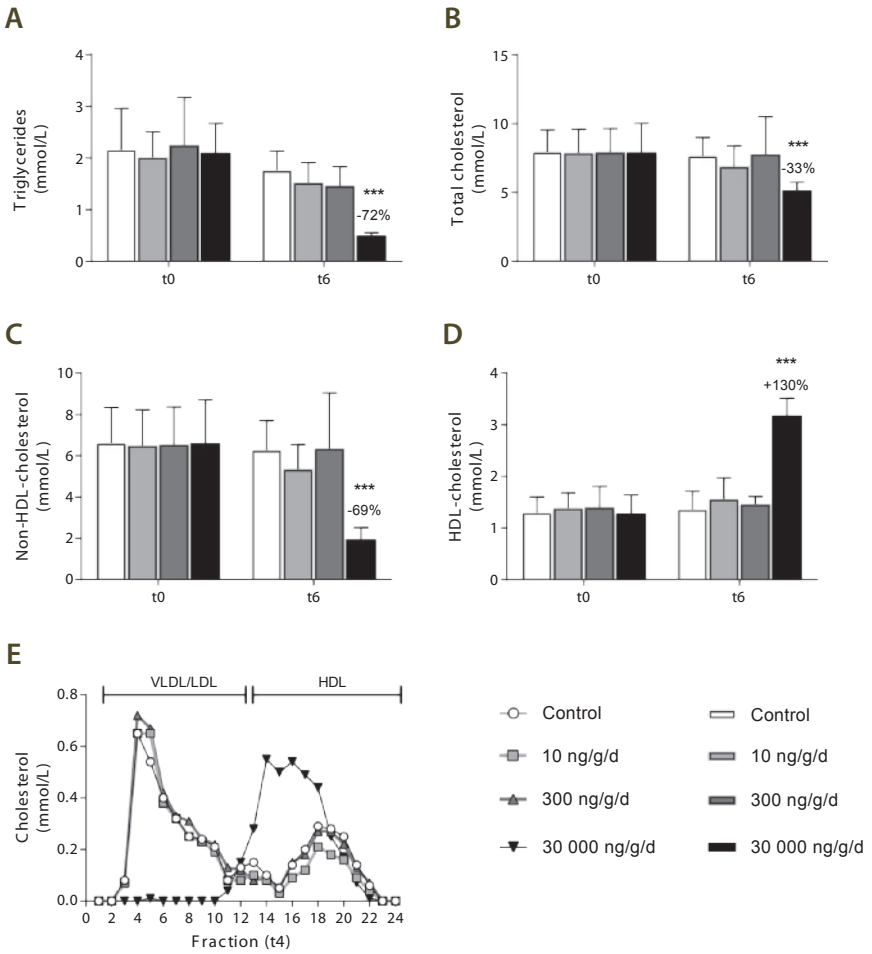

Figure 2 PFOA at low dose does not alter plasma lipids. Mice received a Western-type diet without or with 10, 300 or 30 000 ng/g/d PFOA. At baseline (t0) and after 6 weeks of exposure (t6), 4-h fasted blood was taken and plasma was assayed for TG (A), TC (B), non-HDL-C (C), and HDL-C (D). After 4 weeks of intervention, cholesterol distribution over lipoproteins was determined by FPLC in group-wise pooled plasma (E). Data are presented as means + SD (n=8 per group). ***$p < .001$ as compared with the control group. Abbreviations: FPLC, fast protein liquid chromatography; HDL-C, high-density lipoprotein cholesterol; VLDL/LDL, (very) low-density lipoprotein.

exhibited a distribution pattern where most cholesterol was confined to large cholesterol ester-rich HDL (43) and almost none in VLDL-LDL (non-HDL) (**Figure 2E**).

PFOA decreased plasma FFA, plasma glycerol, pWAT, and BAT weight

After 6 weeks of PFOA exposure at the high dietary dose of 30 000 ng/g/d, total body fat mass (–66%, p<0.01), pWAT (–61%, p<0.01), and intrascapular BAT (–47%, p<0.001) were decreased compared with control (**Table 3**). These observations were accompanied by decreased plasma FFAs (–48%, <0.001) and glycerol levels (–42%, p<0.001) (**Table 3**), both of which are primarily derived from TG lipolysis in adipose tissue.

Table 3 PFOA decreases plasma FFAs, plasma glycerol and body fat

	Control	10 ng/g/d	300 ng/g/d	30 000 ng/g/d
Total body fat (gram)	3.5 ± 1.9	2.8 ± 0.9	3.3 ± 1.2	1.2 ± 0.3**
pWAT (gram)	0.8 ± 0.3	0.7 ± 0.3	0.6 ± 0.2	0.3 ± 0.1**
BAT (gram)	0.15 ± 0.03	0.13 ± 0.02	0.12 ± 0.02	0.08 ± 0.03**
FFA (mmol/L)	0.9 ± 0.1	0.9 ± 0.1	0.8 ± 0.2	0.5 ± 0.1***
Free glycerol (mmol/L)	0.4 ± 0.1	0.3 ± 0.0	0.3 ± 0.1	0.1 ± 0.0***

Mice received a Western-type diet without or with 10, 300 or 30 000 ng/g/d PFOA. In experiment 1, total body fat was measured by EchoMRI at week 5. At week 6, blood samples were taken after a 4-hour fast and plasma was assayed for FFAs and glycerol. At the end of experiment 1, BAT and pWAT were collected and weighted. Data are presented as mean ± SD (n=6-8 per group). ** P< 0.01, *** P<0.001 as compared to the control group. Abbreviations: pWAT, perigonadal white adipose tissue; BAT, brown adipose tissue; FFAs, free fatty acids; MRI, magnetic resonance imaging

PFOA increased plasma HDL-C levels by reducing CETP activity

Because high dose of PFOA at 30 000 ng/g/d did result in increased plasma HDL-C levels and HDL size (**Figure 2D and E**), we investigated whether this was caused by reduction of CETP activity. Indeed, PFOA significantly reduced CE transfer activity by 20% (p<0.01) in plasma of APOE*3-Leiden.CETP mice (**Figure 3A**). When we compared the CETP activity in plasma of the control APOE*3-Leiden.CETP mice with the activity in human plasma, we found a 7.5-fold higher activity in mice (**Figure 3B**). Taken together, the HDL-raising effect observed in this mouse model with PFOA treatment appears to be a consequence of the reduced CETP activity. This effect might be less pronounced in humans due to substantially lower CETP activity as illustrated in **Figure 3B**.

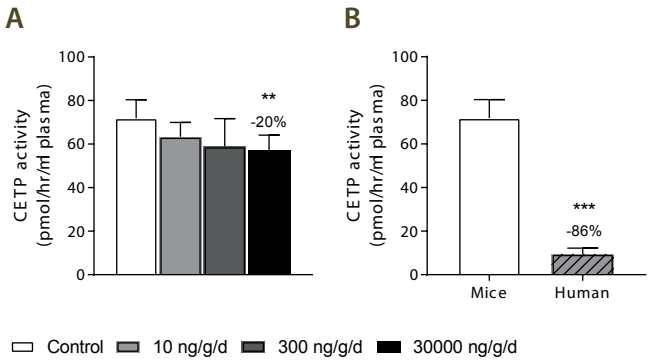

Figure 3 PFOA at high dose increases HDL-C by reducing CETP activity. Mice received a Western-type diet without or with PFOA in 3 different doses, 10, 300 and 30 000 ng/g/d. After 6 weeks of PFOA exposure in experiment 1, CETP activity was determined (A), and the activity in mice of the control group was compared with the activity in human plasma samples (B). Data are represented as mean + SD (n=6–8 mice per group and n=4 human plasma samples). **p<0.01 as compared with the control group and ***p<0.001 as compared with control APOE*3-Leiden.CETP mice. Abbreviations: CETP, cholesteryl ester transfer protein.

The effect of PFOA on hepatic lipoprotein and lipid metabolism

PFOA decreased hepatic VLDL-production rate

Because a decreased VLDL production may contribute to the overall TC- and TG-lowering effects, the VLDL production rate was determined in mice after 6 weeks of PFOA exposure. The VLDL-TG production rate was markedly decreased (–87%, p<0.001) by high dose PFOA exposure (30 000 ng/g/d dietary dose group) (**Figure 4A and B**) and a similar decrease was observed in the VLDL-apoB production rate (–86%, p<0.001) (**Figure 4C**). When normalized by apoB, the overall TG production rate per apoB was similar across all dose groups (**Figure 4D**), indicating that PFOA reduced the production rate of VLDL particles but did not alter the ratio between TG to apoB. These findings also provide an explanation for the marked reduction in total fat and pWAT and intrascapular BAT mass, and the correspondingly decreased plasma FFAs and glycerol levels through a reduced supply of VLDL-TG-derived FFAs for storage in adipose tissue. In contrast, VLDL production was not affected by either 10 or 300 ng/g/d dietary PFOA dose groups.

PFOA increased plasma VLDL clearance through enhanced LPL activity

Plasma VLDL-TG levels are defined by the balance between VLDL-TG production and VLDL-TG clearance, hence this part of the experiment evaluated the plasma clearance and tissue uptakes of [3H]-TO- and [14C]-CO-labeled VLDL-like particles after 4 weeks of PFOA exposure. At 10 or 300 ng/g/d dietary PFOA exposures, VLDL clearance was not affected

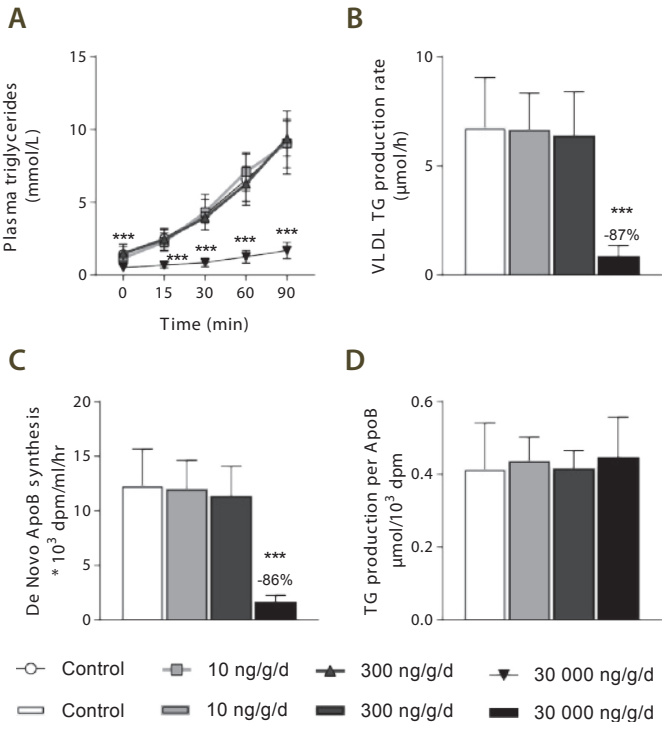

Figure 4 PFOA at high dose decreases VLDL-TG production and apoB synthesis. Mice received a Western-type diet without or with 10, 300 or 30 000 ng/g/d PFOA. After 6 weeks, 4-h fasted mice of experiment 1 were injected with Tran^{35}S-label and Triton after which blood samples were drawn up to 90 min. Plasma VLDL-TGs (A) were plotted and used to calculate the rate of TG production (B) from the slope of the individual curves. Ninety minutes after Triton injection plasma was used to isolate VLDL by ultracentrifugation, and the rate of de novo ApoB synthesis was determined (C). The TG production per apoB was then calculated (D). Data are represented as mean ± SD (n=6–8 per group). ***p<0.001 as compared with the control group. Abbreviations: apoB, apolipoprotein B; TG, triglycerides; VLDL, very low-density lipoproteins.

(**Figure 5**). The uptake of [3H]-TO, representing FFAs and TGs, was increased by the high dose dietary PFOA treatment as indicated by decreased plasma [3H]-TO at t=15 min (–49%, p<0.05; **Figure 5A**), resulting in a significantly decreased half-life time (–30%, p<0.05; **Figure 5B**) relative to control. This effect was mainly due to increased [3H]-TO uptake by the liver (+54%, p<0.05), sWAT (+180%, p<0.01) and BAT (+90%, p<0.01; **Figure 5C**). The uptake of [14C]-CO, representing cholesteryl oleate, was not affected by PFOA exposure (**Figure 5D–F**).

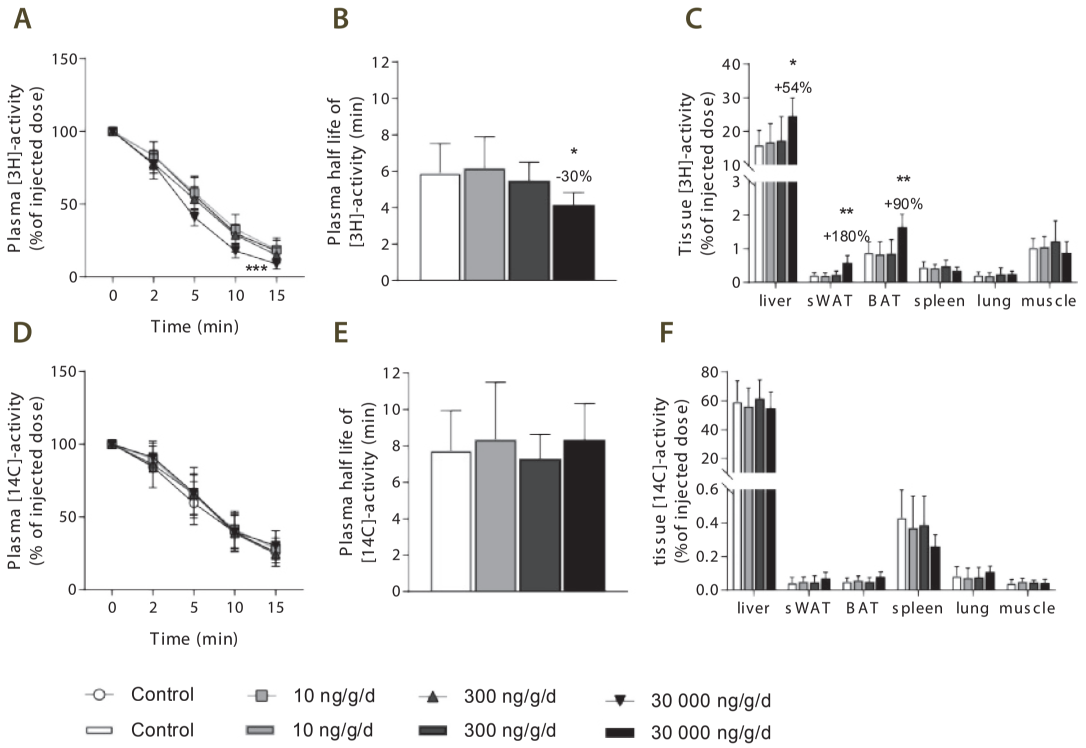

Figure 5 PFOA at high dose increases VLDL clearance mainly due to increased hepatic uptake. Mice received a Western-type diet without or with 10, 300 or 30 000 ng/g/d PFOA. After 4 weeks, 4-h fasted mice of experiment 2 were injected with glycerol tri[3H]-oleate ([3H]-TO) and [14C]-cholesteryl oleate ([14C]-CO)-labeled VLDL-like particles. [3H]-TO plasma decay was plotted (A) and used to calculate the rate of [3H]-TO uptake (B). Clearance of [3H]-TO in individual organs was determined (C). [14C]-CO plasma decay was plotted (D) and used to calculate the rate of [14C]-CO uptake (E). Clearance of [14C]-CO in individual organs was determined (F). Data are represented as mean ± SD (n=6–7 per group).*p<0.05, **p<0.01, and ***p<0.001 as compared with the control group. Abbreviations: BAT, brown adipose tissue; muscle, femoral muscle; sWAT, subcutaneous white adipose tissue; VLDL, very low-density lipoproteins.

Because these data are consistent with increased lipolytic processing of VLDL particles, lipolytic activities (LPL and HL) were evaluated in experiment 1. After 5 weeks of PFOA exposure, mice were injected with heparin to liberate LPL from the endothelium, and LPL and HL activities were measured in plasma samples. HL activity was not affected by PFOA in any treatment group, but LPL activity was increased by the high PFOA dose at 30 000 ng/g/d (+39%, $p < 0.05$) (**Figure 6**), providing an explanation for the increased FFA uptake by the liver and the adipose tissues. Collectively, these data indicate that high PFOA dose at 30 000 ng/g/d increased the hepatic uptake of FFAs, which together with the reduced VLDL production contributed to the decreased plasma lipid levels.

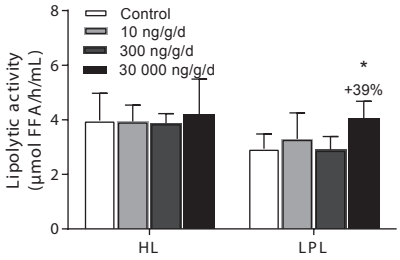

Figure 6 PFOA at high dose increases LPL activity. Mice received a Western-type diet without or with 10, 300 or 30 000 ng/g/d PFOA. After 5 weeks, 4-h fasted mice of experiment 1 were injected with heparin (0.1 U/g body weight) and postheparin plasma was collected. Plasma was incubated with a [3H]-TO-containing substrate mixture in the absence or presence of 1M NaCl, to estimate both the HL and LPL activity. Data are represented as mean + SD (n=5–8 per group). *$p<0.05$ as compared with the control group. Abbreviations: FFA, free fatty acids; HL, hepatic lipase; LPL, lipoprotein lipase; NaCl, sodium chloride.

PFOA resulted in hepatic hypertrophy without altering hepatic lipid contents

Consistent with previous findings in rodents (50,51) and monkeys (24), high dose PFOA at 30 000 ng/g/d resulted in increased ALT (**Table 2**) and hepatic hypertrophy, which was absent in control mice and was minimally observed in the 2 lower PFOA dose groups (**Figure 7A**). Because the decreased VLDL-TG production rate and increased VLDL clearance may be the result of changes in hepatic lipid metabolism, we evaluated liver pathology and measured hepatic lipid content and fecal excretion of bile acids and neutral sterols. Microscopically, macrovesicular steatosis was not observed with PFOA exposure (**Figure 7A**). While there was no microvesicular steatosis present in livers of control mice or in mice administered with the high PFOA dose group at 30 000 ng/g/d, a low amount (<5% of total liver area) of the liver area consisted of microvesicular steatosis (2.3 ± 5.2% and 4.7 ± 12.3%) in mice treated with 10 and 300 ng/g/d PFOA, respectively. The

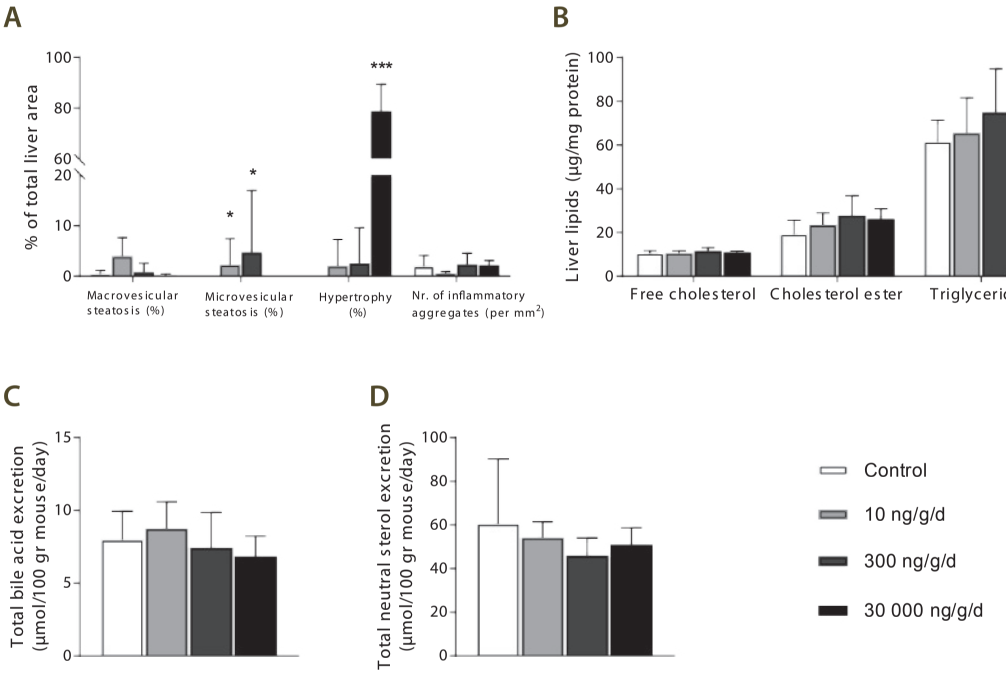

Figure 7 PFOA at high dose induces hepatic hypertrophy. Mice received a Western-type diet without or with 10, 300 or 30 000 ng/g/d PFOA. After 4 weeks of PFOA exposure in experiment 2, livers were histologically analyzed for macrovesicular and microvesicular steatosis, hypertrophy and the number of inflammatory aggregates per mm^2 (A), and hepatic lipid content per mg liver protein was measured (B). After 5 weeks of PFOA exposure in experiment 1, feces were collected per cage during a 48–72 h period at 2 consecutive time points, in which bile acid excretion (C) and neutral sterol excretion (D) were determined using gas chromatography. Data are represented as mean + SD (n=6–7 per group and n=6–8 collection points per group). *p <0.05 and ***p <0.001 as compared with the control group.

number of inflammatory aggregates per mm^2, defined as a cluster of ≥5 infiltrating inflammatory cells (48), was not affected by any of the dietary PFOA groups.

Hepatic FC, CE, and TG contents were also not altered by any of the PFOA doses (**Figure 7B**). Similarly, no changes were observed in the excretion of bile acids (which are solely produced by the liver) and neutral sterols (**Figure 7C and D**). These data indicate that the decreased rate in VLDL-TG production is not explained by reduced availability of liver lipids for VLDL synthesis.

PFOA affected hepatic expression of genes involved in TG and cholesterol metabolism

To further investigate the mechanism by which PFOA affects lipid metabolism, gene expression of selected genes related to TG and cholesterol metabolism was determined in the liver as central organ in lipid metabolism. There were no significant changes in hepatic expression of lipid-related genes at the 2 lower PFOA dose groups. All significantly DEGs related to lipid metabolism in the liver mediated by the 30 000 ng/g/d PFOA dose group are depicted in **Table 4**. Although LPL expression in the liver is low as compared with heart, muscle, and adipose tissue, this PFOA exposure increased the expression of *Lpl* and decreased *Apoc3* expression, which is in line with the increased LPL activity and VLDL-TG clearance. Genes involved in FA/TG synthesis and VLDL assembly (*Scd3, Acss1, Scd2, Acsl3, Acsl4, Acsl5, Acsl1, Fasn, Acaca, Acss2,* and *Mttp*), FA β-oxidation (*Acss1, Ehhadh, Cpt1b, Acca1b, Acox1, Acsl3, Acsl4, Acsl5, Acsl1, Acca1a,* and *Acss2*), and uptake, transport, and binding of FAs (*Slc27a1, Fabp4, Cd36, Slc27a4,* and *Fabp1)* were increased. Collectively, these data indicate that PFOA in the liver increases FA oxidation, binding and activation, and mobilizes FA for TG synthesis and secretion as VLDL. Most likely, the latter 2 pathways are surpassed by increased FA uptake and transport. Additionally, the expression of *Apob* was decreased, which provides an explanation for the decreased VLDL-apoB formation.

PFOA affected hepatic expression of genes involved in HDL-C metabolism

High dose PFOA at 30 000 ng/g/d affected genes involved in HDL-C metabolism by decreasing the expression of *Apoa1* (the major gene in the formation of HDL), *Scarb1* (the principle gene in HDL-C clearance), and *Lipc* (plays a role in remodeling of HDL), and by increasing the expression of *Pltp* (which plays an important role in the remodeling of HDL by facilitating phospholipid transfer to HDL during its maturation from discoidal HDL into spherical HDL) (**Table 4**). Thus, together with the decreased CETP activity, changes in gene expression leading to reduced HDL-C uptake and formation of larger particles have contributed to the increased plasma HDL-C plasma levels and HDL size.

Table 4 The effect of 30 000 ng/g/d PFOA dose on hepatic expression of genes encoding proteins and transcription factors involved in TG and cholesterol metabolism

TG metabolism			
Protein	**Gene**	**Fold change**	**Padj**
Lipolysis			
LPL	*Lpl*	4.3	<0.001
HL	*Lipc*	0.5	<0.001
APOC3	*Apoc3*	0.5	<0.001
APOA5	*Apoa5*	0.4	<0.001
Fatty acid/TG synthesis			
SCD	*Scd3*	157.6	<0.001
ACS	*Acss1*	39.4	<0.001
SCD	*Scd2*	18.4	<0.001
ACS	*Acsl3*	2.5	<0.001
ACS	*Acsl4*	2.3	<0.001
ACS	*Acsl5*	2.3	<0.001
ACS	*Acsl1*	2.1	<0.001
FAS	*Fasn*	2.1	0.001
ACC	*Acaca*	1.9	0.001
ACS	*Acss2*	1.7	0.010
DGAT1	*Dgat1*	1.4	0.030
ACS	*Acsm3*	0.7	0.020
DGAT2	*Dgat2*	0.7	0.030
SREBP1a/c	*Srebf1*	0.7	0.040
ACS	*Acsm1*	0.6	<0.001
ACS	*Acsm5*	0.6	0.002
ACS	*Acsl6*	0.1	0.006
Beta oxidation			
ACS	*Acss1*	39.4	<0.001
bifunctional enzyme	*Ehhadh*	34.3	<0.001
CPT1	*Cpt1b*	4.6	<0.001
thiolase	*Acaa1b*	3.0	<0.001
ACO	*Acox1*	2.6	<0.001
ACS	*Acsl3*	2.5	<0.001
ACS	*Acsl4*	2.3	<0.001
ACS	*Acsl5*	2.3	<0.001
ACS	*Acsl1*	2.1	<0.001
thiolase	*Acaa1a*	1.7	<0.001
ACS	*Acss2*	1.7	0.010
ACO	*Acox3*	0.7	0.010
ACS	*Acsm3*	0.7	0.020
ACS	*Acsm1*	0.6	<0.001
ACS	*Acsm5*	0.6	0.002
PGC1alpha	*Ppargc1a*	0.6	0.007
ACS	*Acsl6*	0.1	0.006
FA uptake, transport, binding			
FATP	*Slc27a1*	9.8	<0.001
FABP	*Fabp4*	8.6	<0.001
CD36	*Cd36*	7.5	<0.001
FATP	*Slc27a4*	2.8	<0.001
FABP	*Fabp1*	1.7	0.010
FATP	*Slc27a5*	0.6	<0.001
FABP	*Fabp2*	0.5	<0.001
VLDL assemblage/formation			
MTTP	*Mttp*	1.5	0.020
APOB	*Apob*	0.8	0.050
Cholesterol metabolism			
Protein	**Gene**	**Fold change**	**Padj**
HDL maturation			
LCAT	*Lcat*	0.6	<0.001
HDL formation and remodeling/ destabilisation			
APOA1	*Apoa1*	0.2	<0.001
PLPT	*Plpt*	3.2	<0.001
HL	*Lipc*	0.5	<0.001
HDL uptake			
SRB1	*Scarb1*	0.5	<0.001

Table 4 Continued

Synthesis			
HMGCS	*Hmgcs1*	2.8	<0.001
HMG CoA synthase	*Hmgcs2*	1.7	0.001
Storage			
ACAT2	*Acat2*	1.6	0.001
ACAT1	*Acat1*	1.5	0.020
Uptake			
VLDLR	*Vldlr*	32.0	<0.001
LRP	*Lrp11*	2.5	0.002
LRP	*Lrp1*	0.6	0.010
SORT-1	*Sort1*	0.5	0.004
LRP	*Lrp2*	0.2	0.002
Metabolism			
BSEP	*Abcb11*	0.5	<0.001
NTCP	*Slc10a1*	0.3	<0.001
CYP7A	*Cyp7a1*	0.2	<0.001
IBAT	*Slc10a2*	0.1	0.001
Excretion			
ABCG5	*Abcg5*	0.6	0.010
Transcription factors			
Protein	**Gene**	**Fold change**	**Padj**
HNF4A	*Hnf4a*	1.6	0.001
PGC1alpha	*Ppargc1a*	0.6	0.007
CAR	*Nr1i3*	0.6	0.009

Mice received a Western type diet without or with 30 000 ng/g/d PFOA and livers were collected after a 4-hour fast after the VLDL-clearance experiment (experiment 2) at t=4 weeks. Total RNA was extracted from liver of individual mice (n=8 mice per group) and gene expression analysis was performed using the Illumina Nextseq 500. A selection of genes involved in lipid metabolism is depicted with only those DEGs with an adjusted P-value <0.05. Data represent fold change as compared with the control. Abbreviations: Padj, adjusted P-value; TG, triglycerides; FA, fatty acids; VLDL, very-low-density-lipoprotein; HDL, high-density-lipoprotein.

PFOA regulated pathways related to lipid and xenobiotic metabolism, coagulation, and inflammation

To further investigate the mechanism by which PFOA affects lipid metabolism and to explore its effect on other biological processes, pathway analysis was performed in the liver. The total number of DEGs was assessed (**Table 5**) and used to identify overlap between the various treatments and PFOA-specific molecular responses.

There were no statistically significant changes in gene transcripts in the liver with the low PFOA dose group at 10 ng/g/d. In silico prediction of transcription factor activity in the liver (**Table 6**), based on the DEGs (padj <0.05), predicted activation of genes regulated by PPARα (p=1E-75, Z-score 6.5) at 30 000 ng/g/d PFOA dose. This dose of PFOA also activated the transcription factor PXR (Nr1i2), a nuclear receptor that functions as sensor of endobiotic and xenobiotic substances. Analysis of the magnitude of the effect of PFOA on these 2 master regulators of PFOA-induced gene expression showed that these upstream regulators are activated in the order PPARα ≥ PXR.

In addition to modulation of lipid and xenobiotic metabolism, the 30 000 ng/g/d PFOA dose displayed significantly regulated pathways related to coagulation and inflammation (**Table 7**). With the 300 ng/g/d PFOA dose group, there were also statistically

Table 5 The number of DEGs in the liver

	pval<			padj<		
	0.05	**0.01**	**0.001**	**0.05**	**0.01**	**0.001**
Control vs 10 ng/g/d	293	63	12	2	2	1
Control vs 300 ng/g/d	1109	379	103	20	4	3
Control vs 30 000 ng/g/d	5170	3603	2364	3379	2370	1640

Mice received a Western-type diet without or with 10, 300 or 30 000 ng/g/d PFOA, mRNA was isolated from liver tissue, and after further processing next generation sequencing analysis was performed. The table indicates the number of DEGs when compared to control. DEGs depicted in green were used for the pathway analysis in IPA (n=8 mice per group). Padj <0.05 indicates a higher level of stringency as compared to Pval <0.01. Abbreviations: DEGs, differentially expressed genes; pval, p-value; padj, adjusted p-value; IPA, ingenuity pathway analysis.

Table 6 In silico prediction of transcription factor activity based on the expression changes of known target genes at 30 000 ng/g/d PFOA dose

	Upstream regulator	**Activation state**	***Z*-score**	**P of overlap**
PPAR	Peroxisome proliferator-activated receptor α (PPARα)	activated	6.5	1E-75
HNF1A	Hepatocyte nuclear factor 1 homeobox A	inhibited	-3.6	1E-26
HNF4A	Hepatocyte nuclear factor 4 alpha	inhibited	-2.4	1E-25
ESR1	Estrogen receptor 1	activated	2.4	1E-25
NFE2L2	Nuclear factor, erythroid 2 like 2	activated	3.3	1E-22
NR1L2	Pregnane X receptor (PXR)	activated	5.4	1E-20

Mice received a Western type diet without or with 30 000 ng/g/d PFOA, mRNA was isolated from liver tissue and gene expression analysis was performed using the Illumina Nextseq 500. To determine the activation status of transcription factors, an upstream regulator analysis was performed. A positive Z-score >2 indicates activation and a negative Z-score <-2 inhibition. All DEGs with an adjusted P-value <0.05 were used for the analysis (n=8 mice per group).

significant changes in the gene transcripts related to hepatic activation of inflammation and immune responses (**Table 7**). Because the biological processes of inflammation and immune response are complex (52) and involve various organs other than liver, the biological significance of these gene transcripts, as they relate to the assessment of cardiovascular risk, remains unclear.

Table 7 Hepatic pathways significantly regulated at 30 000 ng/g/d PFOA dose

30 000 ng/g/d PFOA		300 ng/g/d PFOA	
Canonical pathway	**P-value**	**Canonical pathway**	**P-value**
FXR/RXR activation	1E-15	Phagosome formation	1E-7
LPS/IL-1 mediated inhibition of RXR function	1E-13	Leukocyte extravasation signaling	1E-6
Stearate biosynthesis I (animals)	1E-11	Role of pattern recognition receptors in recognition	1E-6
Fatty acid β-oxidation I	1E-10	Role of NFAT in regulation of the immune response	1E-6
Coagulation system	1E-10	Production of nitric oxide and reactive oxygen species	1E-6
LXR/RXR activation	1E-9	FCγ receptor-mediated phagocytosis in macrophages	1E-5
Acute Phase Response Signaling	1E-8	Dendritic cell maturation	1E-5
Tryptophan degradation III (Eukaryotic)	1E-7	Natural killer cell signaling	1E-5
Superpathway of citrulline metabolism	1E-7	Virus entry via endocytic pathways	1E-5
Complement system	1E-7	CD28 signaling in T helper cells	1E-5
Intrinsic prothrombin activation pathway	1E-6	IL-8 signaling	1E-5
Estrogen biosynthesis	1E-6	TREM1 signaling	1E-4
Bile acid biosynthesis, neutral pathway	1E-6	CTLA4 signaling in cytotoxic T lymphocytes	1E-4
Role of tissue factor in cancer	1E-6	Macropinocytosis signaling	1E-4
Isoleucine degradation I	1E-6	T cell receptor signaling	1E-4
Glutathione-mediated detoxification	1E-6	NF-κB activation by viruses	1E-4
Atherosclerosis signaling	1E-6	Tec kinase signaling	1E-4
Glutaryl-CoA degradation	1E-5	Reelin signaling in neurons	1E-4
Triacylglycerol biosynthesis	1E-5	Granulocyte adhesion and diapedesis	1E-4
Aryl hydrocarbon receptor signaling	1E-5	fMLP signaling in neutrophils	1E-4
Citrulline biosynthesis	1E-5	Epoxysqualene biosynthesis	1E-4
Nicotine degradation III	1E-5	Endothelin-1 signaling	1E-4
Xenobiotic metabolism signaling	1E-5	CD40 signaling	1E-4
Superpathway of melatonin degradation	1E-5	Inflammasome pathway	1E-3
PXR/RXR activation	1E-5	PKCL signaling in T lymphocytes	1E-3

Mice received a Western type diet without or with 30 000 ng/g/d PFOA or 300 ng/g/d, mRNA was isolated from liver tissue and gene expression analysis was performed. Differentially expressed genes (DEGs) (**Table 5**) were used as input for pathway analysis through ingenuity pathway analysis (IPA) suite. All DEGs with an adjusted P-value <0.05 were used for the analysis of the 30 000 ng/g/d dose group, and all DEGs with an P-value <0.01 were used for the analysis of the 300 ng/g/d PFOA dose group. The top 25 most relevant canonical pathways are shown (n=8 mice per group). Abbreviations: FXR, farnesoid X receptor; RXR, retinoid X receptor; LPS, lipopolysaccharides; LXR, liver X receptor; PXR, pregnane X receptor; DEGs, differentially expressed genes.

Discussion

In this study, we have investigated the effects of 3 different doses of PFOA on plasma lipid levels and lipid metabolism in APOE*3-Leiden.CETP mice, a mouse model with a human-like lipoprotein metabolism (31). At the end of the study, the low dose group at 10 ng/g/d resulted in a mean plasma PFOA concentration of approximately 50 ng/mL, which is similar to the range reported in a community population in the mid-Ohio river valley area that had known PFOA exposure in its drinking water (median 27 ng/mL, mean 80 ng/mL) (8). Likewise, the mid-dose group at 300 ng/g/d resulted in a plasma concentration of approximately 1500 ng/mL which is within the range reported in different occupational studies among fluorochemical production workers (9,10,12,15). At 30 000 ng/g/d PFOA achieved a plasma concentration that approached the level reported in the phase 1 clinical trial where a decrease in total cholesterol was clearly observed to occur (30).

This differentiation of plasma PFOA concentrations is a major strength of this study to understand lipid-related associations, or lack of, in human observational and experimental studies. Plasma PFOA concentrations were translatable to the human exposure scenarios and we conclude that, using the APOE*3-Leiden.CETP mouse model, plasma PFOA levels at either 50 ng/mL (community drinking water exposed) or 1500 ng/mL (occupationally exposed) did not alter plasma lipids. PFOA exposure did decrease plasma TG, TC, and non-HDL-C levels and increased HDL-C level when plasma PFOA concentrations reached 90 663 ng/mL (at the end of the 4-week treatment) or 144 000 ng/mL (at the end of the 6-week treatment). We have demonstrated that environmentally and occupationally relevant PFOA exposures did not affect plasma lipids or lipoprotein metabolism using this mouse model. Our data are consistent with the findings by Convertino et al. (30) that high serum or plasma PFOA levels resulted in lower cholesterol levels. Our current study data do not show an increase in cholesterol at environmental or occupational levels of PFOA exposure as shown in some observational epidemiological studies, suggesting these findings are likely associative rather than causal.

Consistent with our data, toxicological PFOA concentrations (>30 000 ng/g/d or 0.02% wt/wt) in mice and rats decreased plasma TC (20,22,23). While the major lipid in wild-type rodents are limited to HDL-C, it is interesting that cholesterol contained in the HDL-C fraction was reported to be increased in C57BL/6 and BALB/c mice fed a high cholesterol and high fat diet containing PFOA (560 µg/kg/d) (21). However, given the inherent difference in rodent lipid metabolism (vs human), it is difficult to extrapolate these results to the human situation, emphasizing the importance to select an animal model resembling human lipid metabolism (31). The APOE*3-Leiden.CETP mouse used in our study is a well-characterized model for its human-like lipoprotein metabolism with delayed apoE-LDLR clearance and expression of CETP, and these characteristics are absent in wild-type rodents, including C57BL/6 and BALB/c mice.

Unlike wild-type rodents, nonhuman primates and humans express CETP. Butenhoff et al., (24) found no effect on lipid levels when cynomolgus monkeys were administered with daily oral doses of PFOA for 6 months (24). In that study, serum PFOA concentration approximated 158 000 ± 100 000 ng/mL; however, there was no distinction made between cholesterol in non-HDL-C or HDL-C hence precluding direct comparison with the present data. In humans, Convertino et al. (30) reported a decline in TC and LDL-C with high (toxicological exposure) plasma concentrations of PFOA, however, unlike our study, they did not observe any change in HDL-C. This discrepancy could be due to the higher CETP activity measured in APOE*3-Leiden.CETP mouse plasma than human (**Figure 3B**). The concomitant increase in HDL-C observed in our study resulted from downregulation of CE transfer activity in plasma by PPARα activation (of which PFOA has been shown to be an activator), the strong downregulation of *Scarb1* (the principle gene in HDL-C clearance) and *Lipc* (plays a role in remodeling of HDL), and by the increased expression of *Pltp* (resulting in formation of larger HDL particles) (39,53,54).

Most reports studying the effects of PFOA in experimental animals do not provide a mechanistic explanation for the observed changes in lipoprotein metabolism. Our studies revealed that high PFOA exposure decreased (V)LDL levels by severely impairing the production of VLDL and increasing VLDL clearance by the liver through increased LPL-mediated lipolytic activity, accompanied by hepatomegaly with cellular hypertrophy. Gene expression and pathway analysis confirmed that lipid metabolism was regulated by PFOA mainly through activation of PPARα. Although not evaluated in this study, the hepatocellular hypertrophy is likely reversible, as has been reported in rats (50) and monkeys (24).

The increased VLDL clearance accompanied by augmented uptake of FFAs by the liver and LPL-expressing organs, such as sWAT and BAT, can be explained by upregulation of *Lpl* and downregulation of an inhibitor of LPL (*Apoc3*), resulting in increased plasma LPL activity. The strongly decreased VLDL-TG and VLDL-apoB production rate (equally diminished by as much as 85%) is not caused by PPARα activation as fenofibrate enhances VLDL-TG secretion (28) or by reduced availability of lipids for VLDL synthesis because hepatic lipid content was not reduced by PFOA. More likely, PFOA prevents VLDL particle formation and secretion from the liver by reduced apoB *de novo* synthesis caused by decreased *Apob* mRNA expression. In line with this contention, treatment of cultured rat hepatocytes with PFOA decreased the VLDL secretion through disturbance of the association of apoB48 with VLDL particles, a process independent of PPARα (55), and toxicological PFOA exposure reduced apob100 mRNA expression in BALB/c mice (56) as well. Therefore, we conclude that at toxicological PFOA exposure the decreased plasma TC and TG levels result from increased VLDL clearance and diminished VLDL-TG and VLDL-apoB production, the latter caused by a reduced supply of apoB substrate which is essential for the assemblage of the VLDL particles.

Fecal neutral sterol and bile acid excretion, the latter as marker of hepatic bile acid synthesis, were not affected by PFOA despite a decrease in Cyp7a1 mRNA expression,

indicating that there is sufficient supply of substrate for bile acid synthesis. Consistently, we found no changes in hepatic lipid content, implying that despite reduced VLDL production, hepatic cholesterol and TG homeostasis is maintained. In contrast, the mass of adipose tissue was decreased in spite of enhanced plasma lipolytic activity. LPL-mediated delivery of VLDL-TG–derived FA is a strong determinant of WAT mass and obesity (57). However, the reduced VLDL-TG production limits the availability of substrate for LPL on peripheral tissues, leading to less FA delivery to WAT and skeletal muscle. This can explain the reduced pWAT mass induced by toxicological PFOA exposure, accompanied by a reduction of plasma FFAs and glycerol that are mainly derived from TG lipolysis in adipose tissue.

Gene expression and pathway analysis revealed that FA oxidation and individual genes involved therein, all under control of PPARα, were enhanced, in line with previous reports in mice (58), rat (50) and human hepatocytes (25,59). In silico prediction of transcription factor activity predicted PPARα as the principal transcription factor regulated by toxicological PFOA not only based on the regulation of lipid metabolism-related genes, but of all DEGs in the liver. Upstream regulator analysis also predicted the involvement of the xenosensor receptor PXR (*Nr1l2*) in the regulation of biological processes, whereas CAR (*Nr1l3*) mediated processes were affected to a much lesser extent, in line with literature (26). Next to its role in xenobiotic metabolism, PXR activation is also involved in lipid metabolism, as it reduces the hepatic expression of *Apoa1*, *Lcat*, and *Hl*, players in the formation, maturation, and remodeling of HDL-C in APOE*3-Leiden.CETP mice (38) as also observed in the present study. While accumulation of TG and cholesterol in the liver can be induced by constitutive PXR expression (60) or the PXR agonist PCN (38), it was not observed in our study, most likely because the PXR-induced effect was negated by the strong PPARα activation, leading to decreased hepatic lipid content in APOE*3-Leiden. CETP mice (28), provoked at the applied PFOA exposure at high (toxicological) level.

At 30 000 ng/g/d PFOA, inflammation-related gene pathways were observed to have statistically significant changes. Activation of both PPARα and PXR is known to attenuate the inflammatory response (61–63), and toxicological exposure to PFOA has been reported to reduce inflammatory pathways and responses (64–67). In contrast, PFOA at 300 ng/g/d upregulated pathways involved in inflammatory and immune response processes. The physiological consequences hereof, however, are unknown and require further research.

In conclusion, we have demonstrated that in APOE*3-Leiden.CETP mice, dietary PFOA exposure at 30 000 ng/g/d reduced plasma TG and TC levels by affecting VLDL-TG production through decreased apoB synthesis and by increasing VLDL clearance. This was not observed with lower PFOA doses. Our data confirmed the findings from a phase 1 clinical trial in humans that demonstrated high serum or plasma PFOA levels resulted in lower cholesterol levels. The study findings do not show an increase in cholesterol at environmental or occupational levels of PFOA exposure, thereby indicating these findings are associative rather than causal.

Acknowledgments

We thank Nicole Worms, Nanda Keijzer, Anita van Nieuwkoop, Wim van Duyvenvoorden, Jessica Snabel, Christa de Ruiter, and Joline Attema for their excellent technical assistance.

Disclosures

Nothing to disclose.

Funding

This work was supported by 3M Company and S.C.C. and G.W.O. are employees of 3M. 3M was involved in the study design and preparation of the manuscript (S.C.C. and G.W.O.), but had no role in data collection apart from determination of dietary and serum concentrations of PFOA.

References

1. Lau C, Anitole K, Hodes C,et al. Perfluoroalkyl acids: a review of monitoring and toxicological findings. Toxicol Sci. 2007 Oct;99(2):366–94.
2. Eriksen KT, Raaschou-Nielsen O, McLaughlin JK, et al. Association between plasma PFOA and PFOS levels and total cholesterol in a middle-aged Danish population. PLoS One. 2013;8(2):e56969.
3. Frisbee SJ, Shankar A, Knox SS, et al. Perfluorooctanoic acid, perfluorooctanesulfonate, and serum lipids in children and adolescents: results from the C8 Health Project. Arch Pediatr Adolesc Med. 2010 Sep;164(9):860–9.
4. Geiger SD, Xiao J, Ducatman A, et al. The association between PFOA, PFOS and serum lipid levels in adolescents. Chemosphere. 2014 Mar;98:78–83.
5. Jain RB, Ducatman A. Associations between lipid/lipoprotein levels and perfluoroalkyl substances among US children aged 6-11 years. Environ Pollut. 2018 Dec;243(Pt A):1–8.
6. Liu H-S, Wen L-L, Chu P-L, et al. Association among total serum isomers of perfluorinated chemicals, glucose homeostasis, lipid profiles, serum protein and metabolic syndrome in adults: NHANES, 2013-2014. Environ Pollut. 2018 Jan;232:73–9.
7. Nelson JW, Hatch EE, Webster TF. Exposure to polyfluoroalkyl chemicals and cholesterol, body weight, and insulin resistance in the general U.S. population. Environ Health Perspect. 2010 Feb;118(2):197–202.
8. Steenland K, Tinker S, Frisbee S, et al. Association of perfluorooctanoic acid and perfluorooctane sulfonate with serum lipids among adults living near a chemical plant. Am J Epidemiol. 2009 Nov;170(10):1268–78.
9. Costa G, Sartori S, Consonni D. Thirty years of medical surveillance in perfluooctanoic acid production workers. J Occup Environ Med. 2009 Mar;51(3):364–72.
10. Olsen GW, Zobel LR. Assessment of lipid, hepatic, and thyroid parameters with serum perfluorooctanoate (PFOA) concentrations in fluorochemical production workers. Int Arch Occup Environ Health. 2007 Nov;81(2):231–46.
11. Olsen GW, Burris JM, Burlew MM, et al. Plasma cholecystokinin and hepatic enzymes, cholesterol and lipoproteins in ammonium perfluorooctanoate production workers. Drug Chem Toxicol. 2000 Nov;23(4):603–20.
12. Olsen GW, Burris JM, Burlew MM, et al. Epidemiologic assessment of worker serum perfluorooctanesulfonate (PFOS) and perfluorooctanoate (PFOA) concentrations and medical surveillance examinations. J Occup Environ Med. 2003 Mar;45(3):260–70.
13. Olsen GW, Ehresman DJ, Buehrer BD, et al. Longitudinal assessment of lipid and hepatic clinical parameters in workers involved with the demolition of perfluoroalkyl manufacturing facilities. J Occup Environ Med. 2012 Aug;54(8):974–83.
14. Sakr CJ, Kreckmann KH, Green JW, et al. Cross-sectional study of lipids and liver enzymes related to a serum biomarker of exposure (ammonium perfluorooctanoate or APFO) as part of a general health survey in a cohort of occupationally exposed workers. J Occup Environ Med. 2007 Oct;49(10):1086–96.
15. Sakr CJ, Leonard RC, Kreckmann KH, et al. Longitudinal study of serum lipids and liver enzymes in workers with occupational exposure to ammonium perfluorooctanoate. J Occup Environ Med. 2007 Aug;49(8):872–9.
16. Steenland K, Fletcher T, Savitz DA. Epidemiologic evidence on the health effects of perfluorooctanoic acid (PFOA). Environ Health Perspect. 2010 Aug;118(8):1100–8.
17. Steenland K, Zhao L, Winquist A. A cohort incidence study of workers exposed to perfluorooctanoic acid (PFOA). Occup Environ Med. 2015 May;72(5):373–80.
18. Raleigh KK, Alexander BH, Olsen GW, et al. Mortality and cancer incidence in ammonium perfluorooctanoate production workers. Occup Environ Med. 2014 Jul;71(7):500–6.
19. Steenland K, Woskie S. Cohort mortality study of workers exposed to perfluorooctanoic acid. Am J Epidemiol. 2012 Nov;176(10):909–17.
20. Loveless SE, Finlay C, Everds NE, et al. Comparative responses of rats and mice exposed to linear/branched, linear, or branched ammonium perfluorooctanoate (APFO). Toxicology. 2006 Mar;220(2–3):203–17.
21. Rebholz SL, Jones T, Herrick RL, et al. Hypercholesterolemia with consumption of PFOA-laced Western diets is dependent on strain and sex of mice. Toxicol reports. 2016;3:46–54.
22. Xie Y, Yang Q, Nelson BD, et al. The relationship between liver peroxisome proliferation and adipose tissue atrophy induced by peroxisome proliferator exposure and withdrawal in mice. Biochem Pharmacol. 2003 Sep;66(5):749–56.

23. Haughom B, Spydevold O. The mechanism underlying the hypolipemic effect of perfluorooctanoic acid (PFOA), perfluorooctane sulphonic acid (PFOSA) and clofibric acid. Biochim Biophys Acta. 1992 Sep;1128(1):65–72.
24. Butenhoff J, Costa G, Elcombe C, et al. Toxicity of ammonium perfluorooctanoate in male cynomolgus monkeys after oral dosing for 6 months. Toxicol Sci. 2002 Sep;69(1):244–57.
25. Buhrke T, Kruger E, Pevny S, et al. Perfluorooctanoic acid (PFOA) affects distinct molecular signalling pathways in human primary hepatocytes. Toxicology. 2015 Jul;333:53–62.
26. Elcombe CR, Elcombe BM, Foster JR, et al. Hepatocellular hypertrophy and cell proliferation in Sprague-Dawley rats following dietary exposure to ammonium perfluorooctanoate occurs through increased activation of the xenosensor nuclear receptors PPARalpha and CAR/PXR. Arch Toxicol. 2010 Oct;84(10):787–98.
27. Takacs ML, Abbott BD. Activation of mouse and human peroxisome proliferator-activated receptors (alpha, beta/delta, gamma) by perfluorooctanoic acid and perfluorooctane sulfonate. Toxicol Sci. 2007 Jan;95(1):108–17.
28. Bijland S, Pieterman EJ, Maas ACE, et al. Fenofibrate increases very low density lipoprotein triglyceride production despite reducing plasma triglyceride levels in APOE*3-Leiden.CETP mice. J Biol Chem. 2010 Aug;285(33):25168–75.
29. Staels B, Maes M, Zambon A. Fibrates and future PPARalpha agonists in the treatment of cardiovascular disease. Nat Clin Pract Cardiovasc Med. 2008 Sep;5(9):542–53.
30. Convertino M, Church TR, Olsen GW, et al. Stochastic Pharmacokinetic-Pharmacodynamic Modeling for Assessing the Systemic Health Risk of Perfluorooctanoate (PFOA). Toxicol Sci. 2018 May;163(1):293–306.
31. Princen HMG, Pouwer MG, Pieterman EJ. Comment on "Hypercholesterolemia with consumption of PFOA-laced Western diets is dependent on strain and sex of mice" by Rebholz S.L. et al. Toxicol. Rep. 2016 (3) 46-54. Toxicol reports. 2016;3:306–9.
32. Ason B, van der Hoorn JWA, Chan J, et al. PCSK9 inhibition fails to alter hepatic LDLR, circulating cholesterol, and atherosclerosis in the absence of ApoE. J Lipid Res. 2014 Nov;55(11):2370–9.
33. Dewey FE, Gusarova V, Dunbar RL, et al. Genetic and Pharmacologic Inactivation of ANGPTL3 and Cardiovascular Disease. N Engl J Med. 2017 Jul;377(3):211–21.
34. Kuhnast S, van der Hoorn JWA, Pieterman EJ, et al. Alirocumab inhibits atherosclerosis, improves the plaque morphology, and enhances the effects of a statin. J Lipid Res. 2014 Oct;55(10):2103–12.
35. Kuhnast S, van der Tuin SJL, van der Hoorn JWA, et al. Anacetrapib reduces progression of atherosclerosis, mainly by reducing non-HDL-cholesterol, improves lesion stability and adds to the beneficial effects of atorvastatin. Eur Heart J. 2015 Jan;36(1):39–48.
36. de Vries-van der Weij J, de Haan W, Hu L, et al. Bexarotene induces dyslipidemia by increased very low-density lipoprotein production and cholesteryl ester transfer protein-mediated reduction of high-density lipoprotein. Endocrinology. 2009 May;150(5):2368–75.
37. Pouwer MG, Pieterman EJ, Verschuren L, et al. The BCR-ABL1 Inhibitors Imatinib and Ponatinib Decrease Plasma Cholesterol and Atherosclerosis, and Nilotinib and Ponatinib Activate Coagulation in a Translational Mouse Model. Front Cardiovasc Med. 2018;5:55.
38. de Haan W, de Vries-van der Weij J, Mol IM, et al. PXR agonism decreases plasma HDL levels in ApoE3-Leiden. CETP mice. Biochim Biophys Acta. 2009 Mar;1791(3):191–7.
39. van der Hoogt CC, de Haan W, Westerterp M, et al. Fenofibrate increases HDL-cholesterol by reducing cholesteryl ester transfer protein expression. J Lipid Res. 2007 Aug;48(8):1763–71.
40. van der Hoorn JWA, de Haan W, Berbee JFP, et al. Niacin increases HDL by reducing hepatic expression and plasma levels of cholesteryl ester transfer protein in APOE*3Leiden.CETP mice. Arterioscler Thromb Vasc Biol. 2008 Nov;28(11):2016–22.
41. ILAR. National Research Council (US) Committee for the Update of the Guide for the Care and Use of Laboratory Animals. Guide for the Care and Use of Laboratory Animals. National Academies Press (US), Washington, DC.; 2011.
42. Ehresman DJ, Froehlich JW, Olsen GW, et al. Comparison of human whole blood, plasma, and serum matrices for the determination of perfluorooctanesulfonate (PFOS), perfluorooctanoate (PFOA), and other fluorochemicals. Environ Res. 2007 Feb;103(2):176–84.
43. Kooistra T, Verschuren L, de Vries-van der Weij J, et al. Fenofibrate reduces atherogenesis in ApoE*3Leiden mice: evidence for multiple antiatherogenic effects besides lowering plasma cholesterol. Arterioscler Thromb Vasc Biol. 2006 Oct;26(10):2322–30.

44. Gautier T, Tietge UJF, Boverhof R, et al. Hepatic lipid accumulation in apolipoprotein C-I-deficient mice is potentiated by cholesteryl ester transfer protein. J Lipid Res. 2007 Jan;48(1):30–40.
45. Bijland S, Rensen PCN, Pieterman EJ, et al. Perfluoroalkyl sulfonates cause alkyl chain length-dependent hepatic steatosis and hypolipidemia mainly by impairing lipoprotein production in APOE*3-Leiden CETP mice. Toxicol Sci. 2011 Sep;123(1):290–303.
46. Geerling JJ, Boon MR, van der Zon GC, et al. Metformin lowers plasma triglycerides by promoting VLDL-triglyceride clearance by brown adipose tissue in mice. Diabetes. 2014 Mar;63(3):880–91.
47. Post SM, de Crom R, van Haperen R, et al. Increased fecal bile acid excretion in transgenic mice with elevated expression of human phospholipid transfer protein. Arterioscler Thromb Vasc Biol. 2003 May;23(5):892–7.
48. Liang W, Verschuren L, Mulder P, et al. Salsalate attenuates diet induced non-alcoholic steatohepatitis in mice by decreasing lipogenic and inflammatory processes. Br J Pharmacol. 2015 Nov;172(22):5293–305.
49. Post SM, Zoeteweij JP, Bos MH, et al. Acyl-coenzyme A:cholesterol acyltransferase inhibitor, avasimibe, stimulates bile acid synthesis and cholesterol 7alpha-hydroxylase in cultured rat hepatocytes and in vivo in the rat. Hepatology. 1999 Aug;30(2):491–500.
50. Butenhoff JL, Bjork JA, Chang S-C, et al. Toxicological evaluation of ammonium perfluorobutyrate in rats: twenty-eight-day and ninety-day oral gavage studies. Reprod Toxicol. 2012 Jul;33(4):513–30.
51. Yang B, Zou W, Hu Z, et al. Involvement of oxidative stress and inflammation in liver injury caused by perfluorooctanoic acid exposure in mice. Biomed Res Int. 2014;2014:409837.
52. P. Parham. The Immune System. Ww Norton & Co., New York, New York, USA; 2014.
53. Guerin M, Bruckert E, Dolphin PJ, et al. Fenofibrate reduces plasma cholesteryl ester transfer from HDL to VLDL and normalizes the atherogenic, dense LDL profile in combined hyperlipidemia. Arterioscler Thromb Vasc Biol. 1996 Jun;16(6):763–72.
54. Wang Y, van der Tuin S, Tjeerdema N, et al. Plasma cholesteryl ester transfer protein is predominantly derived from Kupffer cells. Hepatology. 2015 Dec;62(6):1710–22.
55. Okochi E, Nishimaki-Mogami T, Suzuki K, et al. Perfluorooctanoic acid, a peroxisome-proliferating hypolipidemic agent, dissociates apolipoprotein B48 from lipoprotein particles and decreases secretion of very low density lipoproteins by cultured rat hepatocytes. Biochim Biophys Acta. 1999 Mar;1437(3):393–401.
56. Hui Z, Li R, Chen L. The impact of exposure to environmental contaminant on hepatocellular lipid metabolism. Gene. 2017 Jul;622:67–71.
57. Voshol PJ, Rensen PCN, van Dijk KW, et al. Effect of plasma triglyceride metabolism on lipid storage in adipose tissue: studies using genetically engineered mouse models. Biochim Biophys Acta. 2009 Jun;1791(6):479–85.
58. Das KP, Wood CR, Lin MT, et al. Perfluoroalkyl acids-induced liver steatosis: Effects on genes controlling lipid homeostasis. Toxicology. 2017 Mar;378:37–52.
59. Bjork JA, Butenhoff JL, Wallace KB. Multiplicity of nuclear receptor activation by PFOA and PFOS in primary human and rodent hepatocytes. Toxicology. 2011 Oct;288(1–3):8–17.
60. Zhou J, Zhai Y, Mu Y, et al. A novel pregnane X receptor-mediated and sterol regulatory element-binding protein-independent lipogenic pathway. J Biol Chem. 2006 May;281(21):15013–20.
61. Bougarne N, Weyers B, Desmet SJ, et al. Molecular Actions of PPARalpha in Lipid Metabolism and Inflammation. Endocr Rev. 2018 Oct;39(5):760–802.
62. Kleemann R, Gervois PP, Verschuren L, et al. Fibrates down-regulate IL-1-stimulated C-reactive protein gene expression in hepatocytes by reducing nuclear p50-NFkappa B-C/EBP-beta complex formation. Blood. 2003 Jan;101(2):545–51.
63. Wallace K, Cowie DE, Konstantinou DK, et al. The PXR is a drug target for chronic inflammatory liver disease. J Steroid Biochem Mol Biol. 2010 May;120(2–3):137–48.
64. Guruge KS, Yeung LWY, Yamanaka N, et al. Gene expression profiles in rat liver treated with perfluorooctanoic acid (PFOA). Toxicol Sci. 2006 Jan;89(1):93–107.
65. Rosen MB, Abbott BD, Wolf DC, et al. Gene profiling in the livers of wild-type and PPARalpha-null mice exposed to perfluorooctanoic acid. Toxicol Pathol. 2008 Jun;36(4):592–607.
66. Rosen MB, Schmid JR, Corton JC, et al. Gene Expression Profiling in Wild-Type and PPARalpha-Null Mice Exposed to Perfluorooctane Sulfonate Reveals PPARalpha-Independent Effects. PPAR Res. 2010;2010.
67. Corsini E, Avogadro A, Galbiati V, et al. In vitro evaluation of the immunotoxic potential of perfluorinated compounds (PFCs). Toxicol Appl Pharmacol. 2011 Jan;250(2):108–16.

7

The APOE*3-Leiden heterozygous glucokinase knockout mouse as novel translational disease model for type 2 diabetes, dyslipidemia, and diabetic atherosclerosis

Marianne G. Pouwer*, Suvi E. Heinonen*, Margareta Behrendt, Anne-Christine Andréasson, Arianne van Koppen, Aswin L. Menke, Elsbet J. Pieterman, Anita M. van den Hoek, J. Wouter Jukema, Brendan Leighton, Ann-Cathrine Jönsson-Rylander, Hans M. G. Princen

*These authors contributed equally

J Diabetes Res. 2019 Feb 21;2019:9727952

Abstract

Objectives: There is a lack of predictive preclinical animal models combining atherosclerosis and type 2 diabetes. APOE*3-Leiden (E3L) mice are a well-established model for diet-induced hyperlipidemia and atherosclerosis, and glucokinase$^{+/-}$ (GK$^{+/-}$) mice are a translatable disease model for glucose control in type 2 diabetes. The respective mice respond similarly to lipid-lowering and antidiabetic drugs as humans. The objective of this study was to evaluate/characterize the APOE*3-Leiden.Glucokinase$^{+/-}$ (E3L.GK$^{+/-}$) mouse as a novel disease model to study the metabolic syndrome and diabetic complications.

Methods and results: Female E3L.GK$^{+/-}$, E3L, and GK$^{+/-}$ mice were fed fat- and cholesterol-containing diets for 37 weeks, and plasma parameters were measured throughout. Development of diabetic macro- and microvascular complications was evaluated. Cholesterol and triglyceride levels were significantly elevated in E3L and E3L.GK$^{+/-}$ mice compared to GK$^{+/-}$ mice, whereas fasting glucose was significantly increased in E3L.GK$^{+/-}$ and GK$^{+/-}$ mice compared to E3L. Atherosclerotic lesion size was increased 2.2-fold in E3L.GK$^{+/-}$ mice as compared to E3L ($p=0.037$), which was predicted by glucose exposure ($R^2=0.636$; $p=0.001$). E3L and E3L.GK$^{+/-}$ mice developed NASH with severe inflammation and fibrosis which, however, was not altered by introduction of the defective GK phenotype, whereas mild kidney pathology with tubular vacuolization was present in all three phenotypes.

Conclusions: We conclude that the E3L.GK$^{+/-}$ mouse is a promising novel diet-inducible disease model for investigation of the etiology and evaluation of drug treatment on diabetic atherosclerosis.

Introduction

The metabolic syndrome consists of a cluster of cardiovascular risk factors, including abdominal obesity, elevated blood pressure, elevated fasting plasma glucose, high serum triglycerides, and low high-density lipoprotein (HDL) levels, and drives the global epidemics of type 2 diabetes (T2D) and cardiovascular disease (CVD). Diabetes increases the CVD risk about twofold (1–3), which is the leading cause of death worldwide, and aggravates nonalcoholic steatohepatitis (NASH) (4) and diabetic nephropathy (5). These comorbidities emphasize the need for antidiabetic treatments that are effective against both T2D and associated cardiovascular complications.

Animal models can be used to learn more about the underlying pathology of diabetic complications and the effect of pharmacological interventions thereon, and a wide range of mouse models combining atherosclerosis and diabetes are described (6). Most available models are dyslipidemic mice, e.g., apoE$^{-/-}$ and LDLr$^{-/-}$ mice, with chemically (STZ) or genetically (ob/ob, db/db, and IRS2$^{-/-}$) induced diabetes (6). Although these models are widely used in biomedical research and drug development, they do not sufficiently reflect human disease. First, deficiency of the *Apoe* or *Ldlr* gene and STZ treatment result in extreme hyperlipidemia and hyperglycemia, respectively, and may result in overestimation of the contribution of hyperglycemia to diabetic complications. Besides, STZ treatment is difficult to control and creates a type 1 diabetic-like condition. Second, commonly used animal models of T2D (ob/ob and db/db mice) have a wide but unstable hyperglycemic range (7,8) and are monogenic models of obesity thereby inducing hyperglycemia, which weakens their translatable value as obesity is seldom caused by a monogenic mutation (7,9). Last, apoE$^{-/-}$ and LDLr$^{-/-}$ mice do not respond well to lipid-lowering drugs used in the clinic (10,11), making these models unsuitable in the development of novel therapeutic strategies against hyperlipidemia and vascular complications.

The objective of this study was to develop a translational mouse model for the metabolic syndrome and diabetic complications by combining diet-induced dyslipidemia and hyperglycemia, with plasma levels translatable to the human situation: the APOE*3-Leiden.Glucokinase$^{+/-}$ mouse (E3L.GK$^{+/-}$). We have generated the E3L.GK$^{+/-}$ mouse by cross-breeding dyslipidemic APOE*3-Leiden (E3L) mice with hyperglycemic heterozygous glucokinase knockout (GK$^{+/-}$) mice. The E3L mouse was initially developed as an animal model for mixed dyslipoproteinemia and was generated by the introduction of a DNA construct obtained from a patient with Familial Dysbetalipoproteinemia (FD) or type III hyperlipoproteinemia containing the human *APOE*3LEIDEN* and *APOC1* genes (12). Apoc1 is an inhibitor of lipoprotein lipase (LPL) and inhibits lipolysis of triglyceride-rich lipoproteins. The E*3-Leiden mutation results in a dysfunctional protein with reduced binding to the low-density lipoprotein receptor (LDLr) which leads to impaired clearance of triglyceride- and cholesterol-rich lipoproteins (chylomicron and VLDL remnants), thereby mimicking the slow clearance observed in humans, particularly in FD patients. E3L

mice are prone to develop hyperlipidemia and atherosclerosis upon feeding a Western-type diet containing saturated fat and cholesterol (13), and they respond similarly as humans do to lipid-modulating interventions that are being used in the clinic (e.g., statins, fibrates, niacin, and PCSK9 inhibitors) (11,14–22).

Glucokinase (GK) catalyzes the first and rate-limiting step in glycolysis, phosphorylation of glucose to glucose-6-phosphate, and acts as a "glucose sensor" in controlling glucose-stimulated insulin secretion (23). Loss of function mutations in the *GK* gene in man results in persistent hyperglycemia, referred to as maturity-onset diabetes of the young type 2 (MODY2) (24,25). Various transgenic animals with global or tissue-specific GK knockouts have been generated, each with specific characteristics with respect to metabolic control (26). In this study, we used the global heterozygous GK knockout mouse, which has reduced GK activity in both liver and pancreatic β-cells (26). $GK^{+/-}$ mice are moderately hyperglycemic when on chow, become diabetic on a high-fat diet (HFD) (26), and respond well to glucose-lowering therapeutic agents (e.g., metformin, sitagliptin, insulin, and exendin-4) (8,27).

Materials and methods

Animals and breeding

10–23-week old female E3L, $GK^{+/-}$, and E3L.$GK^{+/-}$ mice (n=6-10/sex/genotype) were used in the study. Both E3L and $GK^{+/-}$ mice are bred on a C57BL/6J background. Since homozygous E3L mice are not viable in utero, these mice are bred heterozygously by breeding E3L X C57BL/6J. $GK^{+/-}$ mice are bred heterozygously ($GK^{+/-}$ X C57BL/6J) as described previously (26), because the homozygous deletion of GK is postnatally lethal. E3L.$GK^{+/-}$ mice were generated by cross-breeding E3L mice with $GK^{+/-}$ mice, thereby generating 27 to 40% offspring of each genotype. Mice were crossed once and were not backcrossed. E3L mice are huApoE3Leiden-huApoC1 double transgenic mice, with both genes located on one genomic DNA construct (12), and therefore, the presence of the E3L phenotype was evaluated by genotyping for *APOC1*. The presence of the $GK^{+/-}$ phenotype was evaluated by qPCR as described previously (26). Females were used because E3L females are more responsive to dietary cholesterol and fat than males. E3L females have a higher VLDL production than males (28) resulting in higher plasma total cholesterol (TC) and triglyceride (TG) levels and development of atherosclerosis (12,29). All mice were housed under standard conditions with a 12 h light-dark cycle and had free access to food and water. Body weight was monitored regularly during the study. Animal experiments were approved by the Regional Animal Ethics Committee for Experimental Animals, Göteborg University. All *in vivo* activities were carried out conforming to the Swedish Animal Welfare Act and regulations SJVFS 2012: 26.

Experimental design and analyses

First, mice were fed a semisynthetic diet, containing saturated fat with 15% (w/w) cacao butter (Western-type diet (WTD); Hope Farms, Woerden, the Netherlands) and 0.15% cholesterol for 7 weeks to study the effect of a mildly lipid-elevating diet on plasma lipid and glucose levels. Subsequently, this diet was supplemented with 10% glucose in the drinking water in weeks 6–7 to investigate whether dietary glucose did modulate these plasma levels. During the following 30 weeks, mice were fed a WTD + 1.0% cholesterol to induce atherosclerosis (20) (**Figure 1**). EDTA blood samples were drawn after a 4-hour fast, and plasma parameters were evaluated at different time points throughout the study. The last blood sample was drawn at week 36, and all animals were sacrificed by CO_2 inhalation at week 37. Plasma TC, TG, glucose, and insulin were measured throughout the study, and HbA1c was measured at week 36. TC and glucose exposure were calculated by adding up for all intervals the products of the mean cholesterol or glucose level during that interval times the duration of that interval and expressed as mmol/L*weeks. Lipoprotein profiles, alanine transaminase (ALT), and aspartate transaminase (AST) were measured in group wise-pooled unfasted sacrifice plasma. Urinary albumin:creatinine levels were measured in spot urine collected in week 36. Hepatic lipid content was analyzed in homogenized, snap-frozen liver samples as described previously (30). Heart and aorta, liver, and kidneys were collected for histopathological analysis of atherosclerosis, NAFLD/NASH and liver fibrosis, and diabetic nephropathy.

Biochemical analyses

Plasma TC and TG were determined throughout the study using enzymatic colorimetric methods (TC: kit no. A11A01634, Horiba ABX, France and TG: kit no. 12146029, Roche Diagnostics GmbH, Germany) according to the manufacturer's protocols and TC exposure was calculated. HDL-C was measured after precipitation of apoB-containing particles (31). The distribution of cholesterol over plasma lipoproteins was determined in group wise-pooled unfasted sacrifice plasma by fast protein liquid chromatography (FPLC) (32). Blood glucose and HbA1C levels were measured in one drop of blood obtained from the

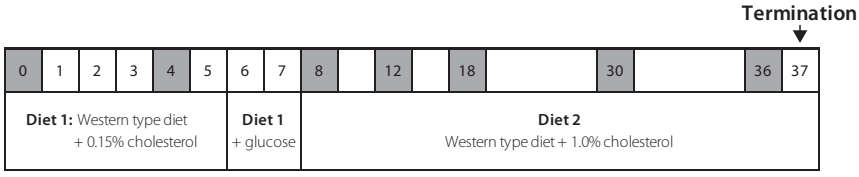

Figure 1 Study design. Female E3L.GK$^{+/-}$, E3L, and GK$^{+/-}$ mice were fed different diets throughout the study. Blood samples were drawn at weeks 0, 4, 8, 12, 18, 30, and 36 as depicted in grey. All mice were sacrificed at week 37. +glucose: 10% glucose drinking water.

tail in awake mice, using Accu-Chek (Roche, REF 05599415370) and HbA1C Now+ (Bayer, REF81611409-3038), respectively, and total glucose exposure was then calculated. Plasma insulin levels were measured with a radioimmunoassay (SRI-13K, Millipore Corporation, USA) on a 1470 Automatic Gamma Counter (PerkinElmer, USA). Plasma ALT and AST were determined using a spectrophotometric assay (Boehringer Reflotron system) in group wise-pooled samples. Urinary albumin and creatinine levels were determined using the mouse albumin ELISA kit (ALPCO, Salem, USA) and the creatinine kit (Exocell, Philadelphia, USA). All assays were performed according to manufacturer's instruction. Hepatic lipid content was analyzed in homogenized, snap-frozen liver samples and analyzed with TINA2.09 software (Raytest Isotopen Meβgeräte, Straubenhardt, Germany).

Histological assessment of atherosclerosis

Hearts were fixed in formalin, embedded in paraffin and sectioned perpendicular to the axis of the aorta. Serial cross sections (5 µm thick with intervals of 50 µm) were stained with hematoxylin-phloxine-saffron (HPS) for histological analysis. The average total lesion area per cross-section was then calculated (31,33). For determination of lesion severity the lesions were classified into five categories according to the American Heart Association classification (34): 0) no lesion, I) early fatty streak, II) regular fatty streak, III) mild plaque, IV) moderate plaque, and V) severe plaque. Lesion composition was determined for the type III-V lesions as a percentage of lesion area after immunostaining with anti-human alpha-actin (1:400; PROGEN Biotechnik GmbH, Germany. Cat#:61001) for smooth muscle cells (SMC), anti-mouse Mac-3 (1:50; BD Pharmingen, the Netherlands. Cat#: 550292) for macrophages and Sirius Red staining for collagen. Necrotic area and cholesterol clefts were measured after HPS staining. Lesion stability index was calculated as described previously (31,33). In each segment used for lesion quantification, the number of monocytes adhering to the endothelium was counted after immunostaining with AIA 31240 antibody (1:1000; Accurate Chemical and Scientific, New York, New York, USA. Cat#: J1857) (31). Lesion areas were measured using Cell D imaging software (Olympus Soft Imaging Solutions).

Histological assessment of liver steatosis and fibrosis

Liver samples (lobus sinister medialis hepatis) were collected from non-fasted mice, fixed in formalin and paraffin embedded, and sections (3 µm) were stained with hematoxylin and eosin (HE) and Sirius Red. Hepatic steatosis was scored blinded by a board-certified pathologist in HE-stained cross-sections using an adapted grading system of human NASH (35,36). Hepatic fibrosis was identified using Sirius Red stained slides and evaluated using an adapted grading system of human NASH (35,37), in which the presence of pathological collagen staining was scored as either absent (0), observed within perisinusoidal/perivenular or periportal area (1), within both perisinusoidal and periportal areas (2), bridging fibrosis (3) or cirrhosis (4). In addition, liver fibrosis (expressed as the

percentage of the total liver tissue area) was quantified automatically using ImageJ software (version 1.48, NIH, Bethesda, MD, USA) (38).

Histological assessment of diabetic nephropathy

Left kidneys were fixed in formalin, embedded in paraffin and sections (3 µm) were stained with HE, Masson's trichrome (MTC), periodic acid–Schiff (PAS) and immunohistochemically for nephrin. Nephrin was stained using a Ventana Discovery with an antibody raised in guinea pig (ab6698, Abcam) diluted 1:1000, Link Rb@GP (Abcam) diluted 1:500, followed by OmniMap@Rb HRP (ROCHE) and ChromoMap DAB-kit (Roche) was used to detect the positive reaction. Sections were finally counterstained with HE (Roche). An overall score based on the combination of all evaluated parameters was determined blinded by a board-certified pathologist where 0 indicates no change in morphology and 5 indicates severe morphological changes. Vacuolized tubuli were scored as 0 indicating that no vacuolized tubuli are present, 1 indicating small and few vacuoles and 2 indicating large and many vacuoles. Sections stained with HE were evaluated for the presence of renal damage focusing on glomerular damage, including mesangial matrix expansion, and tubule-interstitial damage, including interstitial inflammation, fibrosis and tubular abnormalities, as central causes for loss of kidney function. MTC was used for detection of fibrosis, PAS for scoring of matrix expansion and protein deposition in the tubuli, and nephrin for confirmation of matrix expansion and deletion of nephrin.

Statistical analysis

The E3L.GK$^{+/-}$ phenotype was compared to E3L and GK$^{+/-}$, and significance of differences was calculated parametrically using a one-way ANOVA with Dunnett's post hoc test. Differences in plasma parameters between the different time points were calculated for each genotype using a one-way ANOVA with a Bonferroni post hoc test. Significance of differences between the E3L.GK$^{+/-}$ and E3L mice in atherosclerotic lesion number, severity, and composition was calculated using an independent sample *t*-test. A multiple regression analysis was performed to predict the effect of variables on lesion size, and linear regression was used to assess correlations between variables. SPSS 22.0 for Windows was used for statistical analysis. Values are presented as means ± SD. All reported p-values < 0.05 were considered statistically significant.

Results

Safety aspects

No clinical signs of deviant behavior were noted in any of the phenotypes. From week 0 to 36, all three phenotypes gained 5 ± 2 gram body weight (**Table 1**). Plasma pooled per group showed lower AST and ALT values as markers of hepatocellular damage in GK$^{+/-}$ mice when compared to E3L.GK$^{+/-}$ and E3L (**Table 1**). One mouse was terminated during the study based on human end-point criteria.

Table 1 Biochemical parameters in E3L. GK$^{+/-}$, E3L and GK$^{+/-}$ mice

	E3L.GK$^{+/-}$	E3L	GK$^{+/-}$
Weight gain (g)	5 ± 2	5 ± 2	5 ± 2
Weight gain (% of body weight at t=0)	23 ± 6	24 ± 6	24 ± 11
Liver weight (g)	1.9 ± 0.3†	2.0 ± 0.4	1.4 ± 0.3
Liver weight (% of body weight at t=36)	8 ± 1††	8 ± 2	6 ± 1
Cholesterol (mmol/L)	14 ± 3†††	12 ± 3	2 ± 1
Triglycerides (mmol/L)	2.0 ± 0.8†††	1.7 ± 0.4	0.5 ± 0.1
Glucose (mmol/L)	10 ± 1***	8 ± 1	12 ± 2
Insulin (ng/mL)	0.4 ± 0.3	0.1 ± 0.1	0.2 ± 0.1
HbA1c (%)	5.1 ± 0.6**	4.3 ± 0.2	5.4 ± 0.4
ALT (U/L)	272	199	30
AST (U/L)	660	402	125
Urinary albumin:creatinin	19 ± 11	16 ± 2	31 ± 34

All depicted parameters are measured at week 36, except for liver weight (week 37). ** P<0.01, *** P<0.001 when compared to E3L; †P<0.05, †† P<0.01, ††† P<0.001 when compared to GK+/- . Data are presented as means ± SD (n = 8-10 per group and insulin n=4-8 per group).

Plasma parameters for metabolic disease and response to diets

E3L.GK$^{+/-}$ mice are hyperlipidemic and hyperglycemic

Plasma TC and TG levels in E3L.GK$^{+/-}$ mice were similar to E3L mice and increased by 540% (TC) and 450% (TG) when compared to GK$^{+/-}$ mice (**Figure 2A and B**), resulting in a significantly increased cholesterol exposure (mmol/L*weeks) (+316%, p<0.001) (**Figure 2D**). Cholesterol in the E3L and E3L.GK$^{+/-}$ mice was mainly contained in VLDL and LDL, and in GK$^{+/-}$ in HDL (**Figure 2C**). Glucose levels were significantly elevated at all time points except at t=4 weeks when compared to E3L mice (**Figure 2E**). Total glucose exposure (mmol/L*weeks) was 429 ± 60, 299 ± 14 and 492 ± 52 mmol/L for E3L.GK$^{+/-}$, E3L and GK$^{+/-}$, respectively, and significantly increased in E3L.GK$^{+/-}$ when compared to E3L mice (+40%,

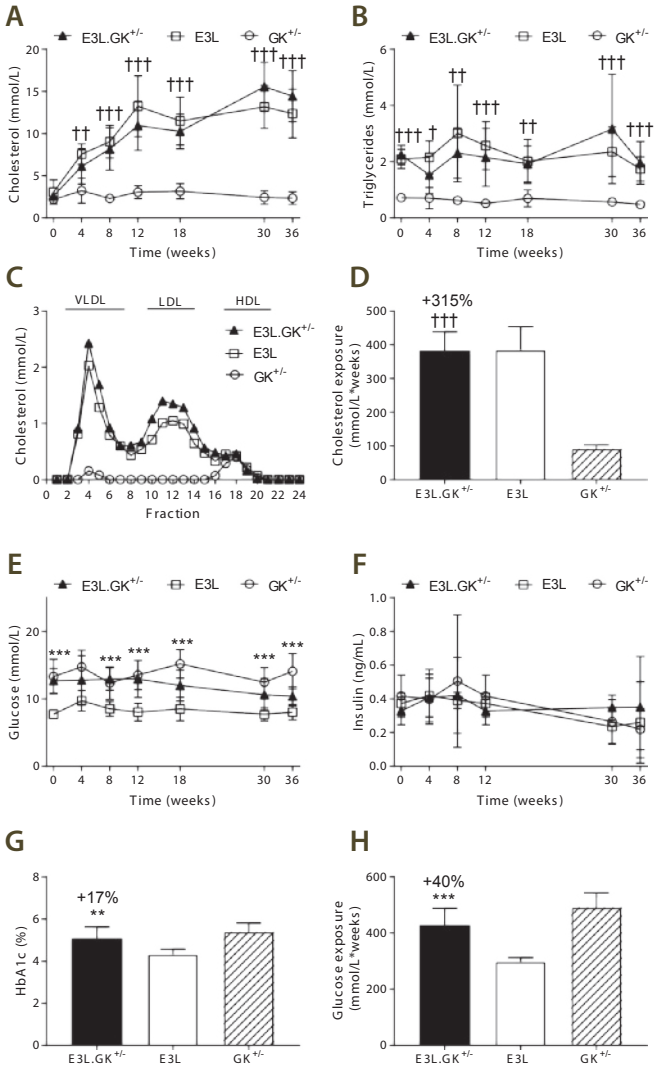

Figure 2 E3L.GK+/– mice have comparable lipid levels and higher glucose levels as E3L mice. Plasma cholesterol (A) and triglycerides (B) were measured throughout the study. Lipoprotein profiles were assessed by FPLC lipoprotein separation in group wise-pooled unfasted sacrifice plasma (C). Cholesterol exposure over time was calculated as mmol/L*weeks (D). Plasma glucose (E) and insulin (F) were measured throughout, HbA1c (%) was measured at week 36 (G), and glucose exposure was calculated as mmol/L*weeks (H). Data are presented as means ± SD (n=8-10 per group and for insulin n=4-8 per group). E3L.GK+/– compared to E3L. *p<0.05, **p<0.01, and ***p<0.001; E3L.GK+/– compared to GK+/–: †p<0.05, ††<0.01, and ††† p<0.001. Abbreviations: FPLC, fast protein liquid chromatography; HbA1c, hemoglobine A1c.

p<0.001) (**Figure 2H**). Insulin levels did not differ between the strains (**Figure 2F**). HbA1c was increased by 17% when compared to E3L mice (p=0.005) (**Figure 2G**). In conclusion, these data show that E3L.GK$^{+/-}$ combine both adverse phenotypes with increased lipid levels as in E3L mice and mildly elevated glucose levels as of GK$^{+/-}$ mice.

Plasma cholesterol levels are modulated by the diet in E3L.GK$^{+/-}$ and E3L mice

Different diets were used in this study to evaluate the response of the mouse model to dietary interventions. Plasma TC, but not TG, increased in both E3L.GK$^{+/-}$ and E3L mice when switched from a chow diet (t=0 weeks) to a WTD with 0.15% cholesterol added (+143%, p=0.038; +173%, p=0.001), whereas plasma lipid levels were not affected in GK$^{+/-}$ mice (**Table 2**). Plasma glucose and insulin levels were not affected by the WTD with 0.15% cholesterol added, except for glucose which increased in E3L mice (+26%, p=0.010). Adding 10% glucose to the drinking water further increased plasma TC levels: when compared to t=0 weeks (chow) TC levels increased by 215% in E3L.GK$^{+/-}$ mice (p=0.001) and by 224% in E3L mice (p<0.001). However, this increase was not significant when compared to t=4 (WTD with 0.15% cholesterol) (**Table 2** Increasing the amount of cholesterol in the diet to 1.0%, further increased plasma TC levels in E3L.GK$^{+/-}$ and E3L mice when compared to t=0 and when compared to t=8 (+89%, p<0.001; +43%, p=0.013). Insulin levels dropped in E3L mice at t=36 weeks when compared to t=0 weeks (-60%, p=0.020) and t=8 weeks (-66%, p=0.010), whereas this effect was less pronounced in GK$^{+/-}$ mice (-41%, p=0.081 compared to t=8 weeks), and absent in E3L.GK$^{+/-}$ mice. Interestingly, plasma glucose levels in E3L.GK$^{+/-}$ and GK$^{+/-}$ mice were not modulated by glucose in the drinking water, indicating that despite reduced glucokinase activity (26) the mice maintain their glucose homeostasis at increased glucose supply. Altogether, these data show that plasma lipids can be modulated in the E3L.GK$^{+/-}$ mouse model, as in E3L mice, whereas the elevated glucose levels on chow are not further increased by these dietary interventions.

Diabetic macro- and microvascular complications in E3L.GK$^{+/-}$ mice

Atherosclerotic lesion size and severity are aggravated in E3L.GK$^{+/-}$ mice

One of the most important diabetic complications is increased risk for CVD (1–3) and therefore, we assessed atherosclerotic lesion size, lesion severity and plaque phenotype, as marker of vulnerability to rupture, in the aortic root. E3L mice developed 0.4 ± 0.5 mild (I-II), 3.6 ± 2.3 moderate (III) and 1.6 ± 1.8 severe (IV-V) lesions per cross-section. The number of severe lesions was significantly increased in E3L.GK$^{+/-}$ mice (2.8-fold; p=0.038) (**Figure 3A**). When lesion severity was depicted as the percentage of total plaque area that consisted of mild or severe lesions, there was no difference between E3L and E3L.GK$^{+/-}$ mice (**Figure 3B**). However, the total atherosclerotic lesion size was significantly increased by 2.2-fold in the E3L.GK$^{+/-}$ mice (68 ± 42 *1000 μm^2) as compared to E3L (32 ± 29 *1000 μm^2) (p=0.037) (**Figure 3C**). There were no lesions visible in the GK$^{+/-}$ mice (**Figure 3C**). The plaque composition was analyzed in the type III-V lesions, as illustrated by representative images

Table 2 Plasma cholesterol levels are modulated by the diet in E3L.GK$^{+/-}$ and E3L mice

Diet at time of plasma sample		Chow	WTD + 0.15% cholesterol		WTD + 0.15% cholesterol and 10% glucose drinking water			WTD + 1.0% cholesterol		
Time (weeks)		*0*	*4*		*8*			*36*		
			mmol/L[*1]	relative to t=0 (%)	mmol/L[*1]	relative to t=0 (%)	relative to t=4 (%)	mmol/L[*1]	relative to t=0 (%)	relative to t=8 (%)
TC	E3L.GK$^{+/-}$	2.6 ± 0.3	6.1 ± 2.1*	143	8.2 ± 2.5**	215	64	14.4 ± 3.0***/†††	463	89
	E3L	3.1 ± 1.5	7.6 ± 1.2**	173	9.0 ± 1.9***	224	20	12.4 ± 2.9***/†	353	43
	GK$^{+/-}$	2.2 ± 0.4	3.2 ± 1.5	60	2.3 ± 0.3	9	-20	2.3 ± 0.8	11	4
TG	E3L.GK$^{+/-}$	2.2 ± 0.3	1.5 ± 0.7	-30	2.3 ± 0.9	3	95	2.0 ± 0.8	-14	-5
	E3L	2.1 ± 0.3	2.2 ± 0.6	5	3.0 ± 1.7	45	45	1.7 ± 0.4	-15	-28
	GK$^{+/-}$	0.7 ± 0.0	0.7 ± 0.4	-2	0.6 ± 0.1	-14	1	0.5 ± 0.1	-33	-19
Glucose	E3L.GK$^{+/-}$	12.7 ± 1.8	12.8 ± 3.6	1	13.0 ± 1.7	4	7	10.4 ± 1.4	-19	-17
	E3L	7.7 ± 0.7	9.7 ± 1.5*	26	8.5 ± 1.1	11	-10	8.0 ± 1.2	5	-4
	GK$^{+/-}$	13.3 ± 2.6	14.7 ± 2.5	14	12.4 ± 2.4	-6	-14	14.1 ± 2.6	9	17
Insulin	E3L.GK$^{+/-}$	0.3 ± 0.1	0.4 ± 0.1	30	0.4 ± 0.2	43	8	0.4 ± 0.3	-13	9
	E3L	0.4 ± 0.1	0.4 ± 0.2	15	0.4 ± 0.0	7	3	0.1 ± 0.1*/†	-60	-66
	GK$^{+/-}$	0.4 ± 0.1	0.4 ± 0.1	3	0.5 ± 0.4	32	24	0.2 ± 0.1	-42	-41

The response of plasma lipids, glucose and insulin to the different diets was evaluated. Data are presented as means ± SD (n=8-10 per group and insulin n=4-8 per group). * P<0.05, ** P<0.01, *** P<0.001 when compared to T = 0 weeks; †P<0.05, ††† P<0.001 when compared to previous time point. [*1] Insulin (ng/mL). Abbreviations: WTD, western type diet.

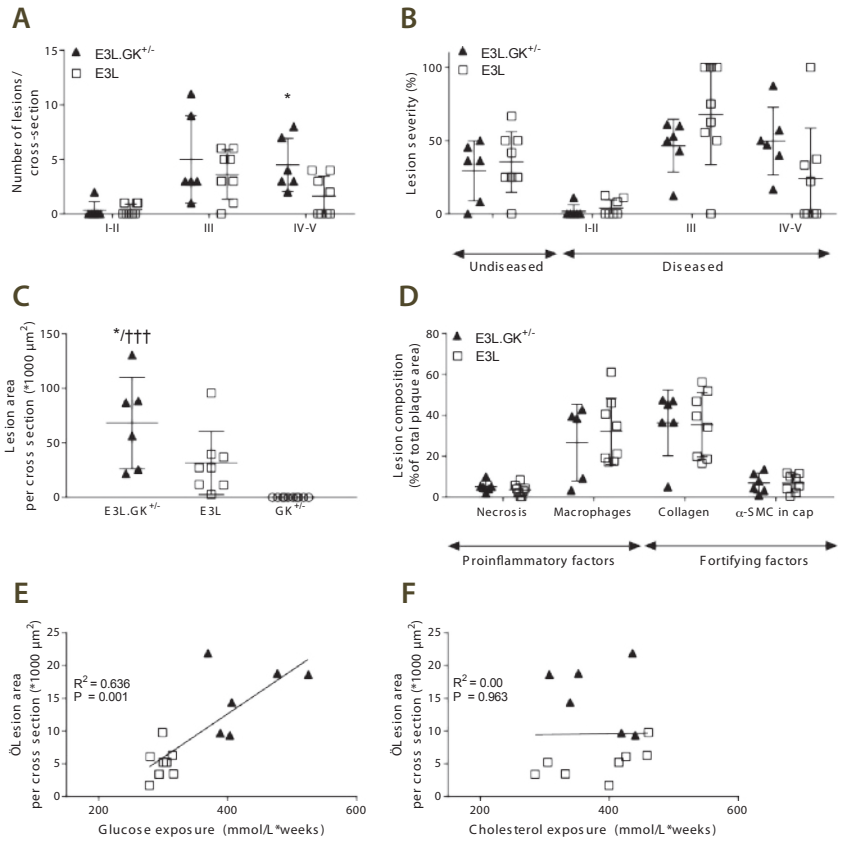

Figure 3 Atherosclerotic lesion size and severity are aggravated in E3L.GK$^{+/-}$ mice which is correlated to glucose exposure. The number of lesions (A), lesion severity classified as mild (type I-II lesions), moderate (type III) and severe (type IV and V) lesions (B), and atherosclerotic lesion size per cross-section (C). Necrotic and macrophage content as pro-inflammatory factors, and αSMCs and collagen as fortifying factors, were determined in type III-V lesions and expressed as percentage of total plaque area (D). Linear regression analyses were performed on the square root of the lesion area plotted against glucose exposure (E) or cholesterol exposure (F). Data are presented as means ± SD (n = 6-8 per group).*P<0.05 when compared to E3L; ††† P<0.001 when compared to GK$^{+/-}$.

in **Figure 4**. There were no significant differences between E3L.GK$^{+/-}$ and E3L mice in plaque composition (**Figure 3D**), plaque stability index or monocyte adherence to the endothelium (data not shown). Collectively, these data show that atherosclerotic lesion size is aggravated in E3L.GK$^{+/-}$ as compared to E3L mice without affecting plaque composition and monocyte adherence.

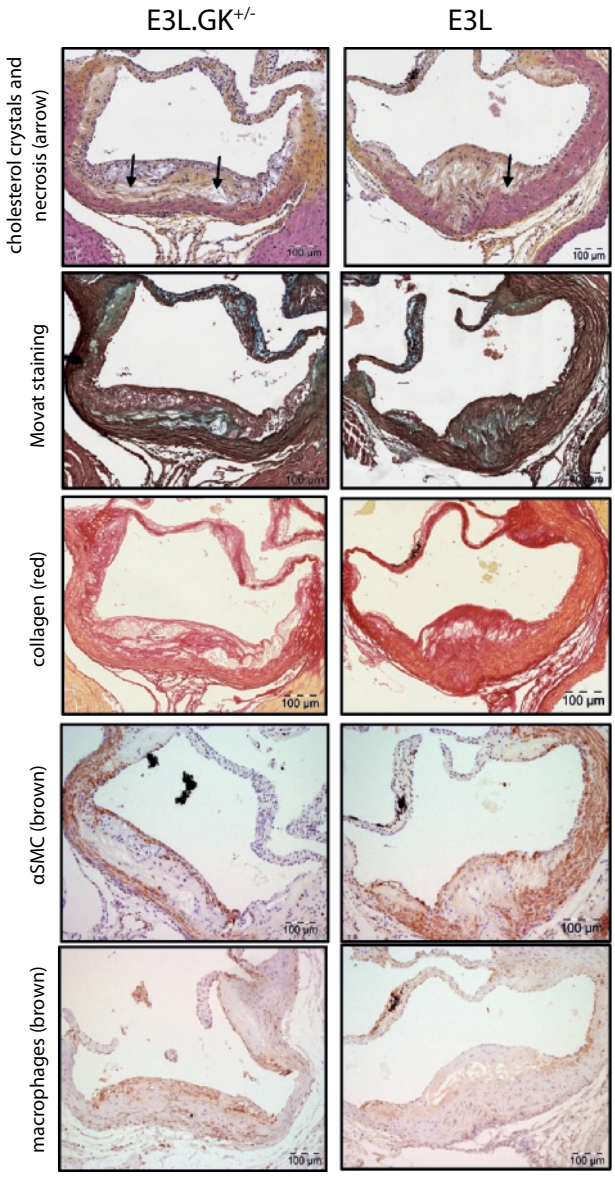

Figure 4 Plaque composition in a severe plaque of a E3L and E3L.GK$^{+/-}$ mouse. Representative images of HPS staining, Movat staining, Sirius red staining for collagen, immunostaining with α-actin for SMCs and immunostaining with Mac-3 for macrophages. The arrows depict necrotic areas, including cholesterol clefts. Abbreviations: HPS, hematoxylin-phloxine-saffron; SMCs, smooth muscle cells.

Elevated plasma glucose levels contribute to the increased development of atherosclerosis in E3L.GK$^{+/-}$ mice

To explore the contribution of the elevated plasma glucose levels to the increased lesion size, a multiple regression analysis was performed with cholesterol and glucose exposure as covariates after square root transformation of the lesion area. Lesion size was predicted only by glucose exposure ($p<0.001$). In addition, univariate regression analysis showed a clear association of lesion size with glucose exposure ($R^2=0.636$, $p=0.001$) (**Figure 3E**) but not with cholesterol exposure (**Figure 3F**), pointing towards an important role for glucose in the accelerated atherosclerosis development in E3L.GK$^{+/-}$ mice.

The GK$^{+/-}$ phenotype does not aggravate hepatic steatosis, inflammation or fibrosis

NAFLD/NASH is strongly associated with the metabolic syndrome and type 2 diabetes (39,40). To assess whether the GK$^{+/-}$ phenotype worsens the development of NASH, liver sections were examined for hepatic steatosis, inflammation and fibrosis, and liver lipid content was measured. Hepatic macrosteatosis did not differ between the phenotypes (**Figure 5A**), whereas hepatic microsteatosis was significantly elevated by 2.7-fold ($p=0.003$) in E3L.GK$^{+/-}$ mice when compared to GK$^{+/-}$ (**Figure 5B**), and both E3L.GK$^{+/-}$ and E3L had severe liver inflammation which was 6.8-fold increased ($p<0.001$) in E3L.GK$^{+/-}$ relative to GK$^{+/-}$ (**Figure 5C**). Furthermore, mean fibrosis stage in E3L.GK$^{+/-}$ was significantly elevated when compared to GK$^{+/-}$ (2.3-fold, $p<0.001$) (**Figure 5D**), as well as the percentage Sirius red positive area of total liver area (6.1-fold, $p=0.011$) (**Figure 5E**). Liver lipids did not differ between the phenotypes (**Figure 5F-H**). Representative images are shown (**Figure 5I-N**). Collectively, these data show that E3L and E3L.GK$^{+/-}$ mice, but not GK$^{+/-}$, develop NASH with severe inflammation and fibrosis, which is not worsened by increased glucose levels. This indicates a dominant role for the combination of the E3L phenotype and dietary cholesterol in the progression of NASH and liver fibrosis.

Mild kidney pathology is present in all three phenotypes

Diabetic nephropathy is becoming an increasingly important cause of morbidity and mortality worldwide and is related to the increasing prevalence of type 2 diabetes. Therefore, kidneys were analyzed for the presence of renal damage focusing on glomerular damage, including mesangial matrix expansion, and tubulo-interstitial damage, including interstitial inflammation, fibrosis and tubular abnormalities, as central causes for loss of kidney function. Nephrin staining was performed to study renal filtration barrier function. There were no differences in inflammation, fibrosis (data not shown), mesangial matrix expansion (**Figure 6A**) or nephrin score (**Figure 6B**) between the phenotypes. Abnormal tubular structures were observed in all three phenotypes but were most pronounced in GK$^{+/-}$ mice, wherein the tubuli showed vacuolization (**Figure 6C**). The pathological changes did not affect permeability in the glomerulus, as measured by the urinary albumin:creatinine ratio (**Table 1**). Altogether, we can conclude that mild pathological changes are present, which are not aggravated in E3L.GK$^{+/-}$ mice.

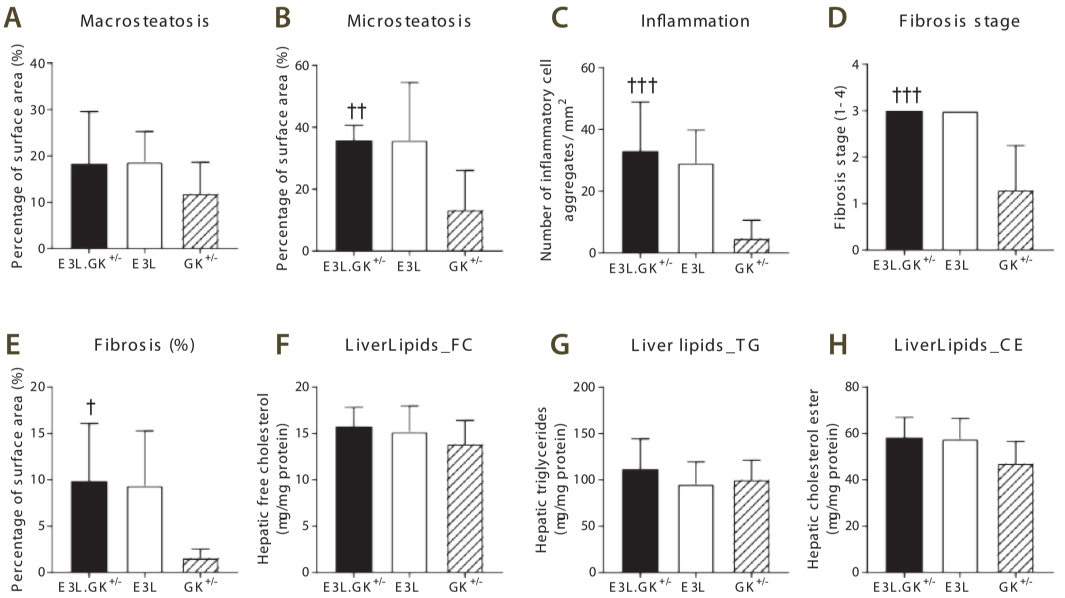

Figure 5 The GK phenotype does not aggravate hepatic steatosis, inflammation or fibrosis in E3L mice. Macrovesicular steatosis (A) and microvesicular steatosis (B) as percentage of total liver area was determined. The number of inflammatory cell aggregates were counted per mm^2 (C). Fibrosis grade (1-4) was scored (D) and percentage of area positive for Sirius Red was measured in ImageJ (E). Intrahepatic free cholesterol (F), intrahepatic triglycerides (G) and intrahepatic cholesterol esters (H) were analyzed by HPTLC. Representative images of HE (I-K) and Sirius Red (L-N) staining at a 5x magnification. Data are presented as means ± SD (n = 6-10 per group). † P<0.05, †† P<0.01, ††† P<0.001 when compared to $GK^{+/-}$. Abbreviations: HPTLC, high-performance thin-layer chromatography; HE, hematoxylin-eosin.

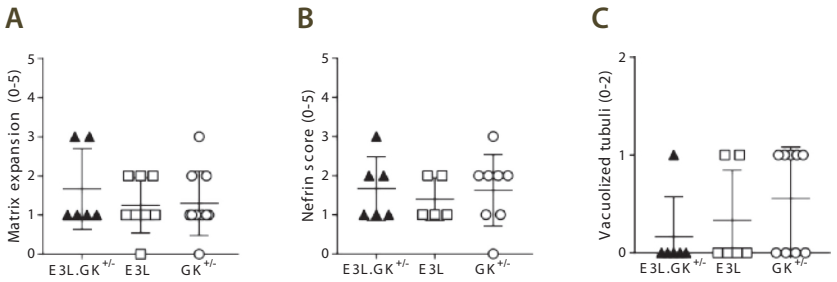

Figure 6 Mild matrix expansion and vacuolized tubuli in all phenotypes. Presence of matrix expansion (A), nephrin score (B) and vacuolized tubuli (C) was scored in a range of 0-5. Data are presented as means ± SD (n = 7-10 per group). .

Discussion

In the present study, we evaluated the E3L.GK$^{+/-}$ mouse as an animal model for diet-induced hyperlipidemia and hyperglycemia and the pathological consequences thereof. We showed that plasma lipids can be titrated to desired and for humans relevant levels by adding cholesterol and fat to the diet, and that these levels remain stable for a long period (up to 37 weeks). In addition, E3L.GK$^{+/-}$ mice were mildly hyperglycemic and developed more atherosclerosis than E3L mice, which was related to the higher glucose levels in the E3L.GK$^{+/-}$ mice. E3L and E3L.GK$^{+/-}$ mice both developed hepatic steatosis with severe inflammation and fibrosis, which, however, was not altered by introduction of the defective GK phenotype, whereas only mild kidney pathology with tubular vacuolization was present in all three phenotypes.

Translatability of animal models is essential when investigating the pathogenesis of diabetic complications and evaluating drug treatment thereon. Plasma cholesterol and glucose levels in the diet-induced E3L.GK$^{+/-}$ mouse model were similar to levels in patients with increased cardiovascular risk (2,41). Partial deletion of the *Gk* gene in the E3L mice did not affect the response of plasma lipids to dietary modulation, and in both E3L.GK$^{+/-}$ and E3L mice plasma cholesterol levels raised similarly upon feeding a WTD with increasing amounts of cholesterol. Interestingly, glucose and insulin levels were not affected by the diet, but remained stable representing mild hyperglycemia in E3L.GK$^{+/-}$ and GK$^{+/-}$ mice (10.4 ± 1.4 mmol/L and 14.1 ± 2.6 mmol/L at end-point, respectively). In contrast, glucose levels in male GK$^{+/-}$ mice increase over time on a high-fat diet with plasma levels reaching 18.9 ± 1.0 mmol/L and impaired glucose tolerance (8,26). This gender difference may be explained by the C57BL/6J background of the E3L and GK$^{+/-}$ transgenic mice. Upon a high-fat diet, insulin and glucose levels increase over time in C57BL/6J males, consistent

with insulin resistance and glucose intolerance, whereas C57BL/6J females have normal serum insulin concentrations and glucose levels remain constant (42). Estrogens affect different metabolic pathways in the glucose hemostasis (43), thereby protecting against the risk of developing type 2 diabetes in both pre-menopausal women (44) and mice (43).

We observed a markedly increased atherosclerotic lesion size in E3L.GK$^{+/-}$ as compared to E3L mice which was highly significantly correlated with glucose exposure (R^2=0.636, p=0.001), suggesting a pro-atherogenic role of glucose in the development of atherosclerosis. Indeed, it is known that prolonged exposure to hyperglycemia negatively affects the endothelium, vascular smooth muscle cells and macrophages, and it increases thrombosis while impairing fibrinolysis, leading to formation of atherosclerotic plaques (45). This may explain the association of diabetes type 2/hyperglycemia with cardiovascular disease as found in both humans (1,2,45,46) and hyperglycemic mice (6), including E3L.GK$^{+/-}$ mice.

In the present study, both the hyperglycemic GK$^{+/-}$ mice as well as the hyperlipidemic E3L and E3L.GK$^{+/-}$ mice developed hepatic steatosis, in line with the pathogenesis of NAFLD wherein both metabolic overload and hyperlipidemia contribute to the accumulation of triglycerides and cholesterol in the liver. Interestingly, E3L and E3L.GK$^{+/-}$, but not GK$^{+/-}$ mice, developed extensive inflammation and hepatic fibrosis, pointing towards a role for cholesterol in the transition of NAFLD to NASH. Consistent with this view, when cholesterol is supplied to HFD diet, E3L mice develop NASH and liver fibrosis as well (47), and E3L and E3L.CETP mice have been shown to be established diet-induced NASH and liver fibrosis models (47,48). In a previous study with E3L mice, an increased amount of hepatic cholesterol crystals was found and intrahepatic free cholesterol levels were positively correlated with the number of inflammatory aggregates and the expression of hepatic pro-inflammatory and pro-fibrotic genes (49). Similarly, it has been shown that accumulation of free cholesterol leading to the formation of cholesterol crystals in hepatocyte lipid droplets may trigger the progression of simple steatosis to NASH both in patients and in mice (50). Since no additional effects of glucose were observed on hepatic inflammation or fibrosis in E3L.GK$^{+/-}$ mice, we suggest that hyperlipidemia rather than hyperglycemia is an initiator of hepatic inflammation and fibrosis.

Chronic kidney disease is a largely irreversible disease characterized by tubulointerstitial inflammation, fibrosis, and glomerulosclerosis. The present study describes only mild kidney pathology without microalbuminuria in all three phenotypes. In addition to risk factors investigated in this study (hyperglycemia and dyslipidemia), hypertension plays a central role in renal injury through increasing renal tubular reabsorption and causing a hypertensive shift of renal-pressure natriuresis (5). Studies on nephropathic patients showed that decreased blood pressure reduced the incidence of renal events and improved kidney function (51,52). In the present study blood pressure was not measured. However, it is known that E3L mice do not develop hypertension upon a WTD, but do respond to anti-hypertensive treatment (15,17), and although there are no reports in GK$^{+/-}$ mice, GK deficiency in humans does not aggravate blood pressure (25).

Previously, the GK$^{+/-}$ApoE$^{-/-}$ mouse model has been developed as model combining hyperlipidemia and hyperglycemia, which had impaired glucose tolerance and a minimal increase of atherosclerosis relative to ApoE$^{-/-}$ mice (53). A disadvantage of this model is the ApoE$^{-/-}$ background. ApoE$^{-/-}$ mice are, like LDLR$^{-/-}$ mice, a severe model for hyperlipidemia, and due to the absence of a functional apoE-LDLR-mediated clearance pathway these mice do not respond well to lipid-lowering drugs (e.g. statins (10), PCSK9 inhibitors (11)) and therefore cannot be used for the evaluation of combination treatment. In contrast, E3L mice are very suited to study lipoprotein metabolism and lipid modulation (10,54).

In **Figure 7** we give an overview of all registered cholesterol- and glucose-lowering drugs that have been evaluated in E3L and GK$^{+/-}$ mice, respectively. E3L mice respond similarly as humans do to lipid lowering agents, including statins, fibrates, niacin and PCSK9-inhibitors (11,14–22), whereas glucose levels are successfully reduced in GK$^{+/-}$ mice by standard therapeutic agents as insulin, metformin, exendin-4 and GKAs at doses corresponding to therapeutic drug levels in man (8,27). Although these interventions have not been assessed in E3L.GK$^{+/-}$ mice yet, we carefully speculate about the effects and discuss how the model can be of value for future research. As E3L.GK$^{+/-}$ mice have similar lipid and glucose levels as their parent models, and respond in a similar way to dietary modulations, we propose that both lipid and glucose lowering agents will be effective in the combined model. Also, we propose that E3L.GK$^{+/-}$ mice can be used to examine interactions between glucose and lipid metabolism, e.g. how statin treatment increases the risk of diabetes incidence (55). Last, atherosclerosis development and CV safety can be evaluated in the E3L.GK$^{+/-}$ model, which is especially interesting regarding the currently unknown mechanisms by which glucose-lowering agents (e.g. empagliflozin, liraglutide, semaglutide) improve CV outcome (56–58).

Altogether, we conclude that the E3L.GK$^{+/-}$ mouse is a promising translatable diet-inducible model, combining dyslipidemia and hyperglycemia with human-like plasma cholesterol and glucose levels and aggravated atherosclerosis, to study the etiology of diabetic atherosclerosis and for the evaluation of lipid-lowering and anti-diabetic drugs and their combination thereon.

Acknowledgements

The authors thank Erik Offerman (TNO) and Marlieke Geerts (Leiden University Medical Centre, Leiden, the Netherlands) for their excellent technical assistance.

Disclosures

JWJ received research grants from and was speaker on (CME-accredited) meetings sponsored by Amgen, Astellas, Astra-Zeneca, Daiichi Sankyo, Lilly, Merck-Schering-Plough, Pfizer, Roche, Sanofi-Aventis, the Netherlands Heart Foundation, the Interuniversity Cardiology Institute of the Netherlands, and the European Community Framework KP7 Program. MB, ACA and ACJR are employees of AstraZeneca and SHE and BL were employees

of AstraZeneca during the execution of the study. MGP, AvK, ALM, EJP, AMvdH and HMGP have nothing to disclose.

Funding

This work was supported in part by AstraZeneca, Mölndal, Sweden, the TNO research program "Preventive Health Technologies" and the European Union Seventh Framework Programme (FP7/2007-2013) grant nr. 602936 (CarTarDis project).

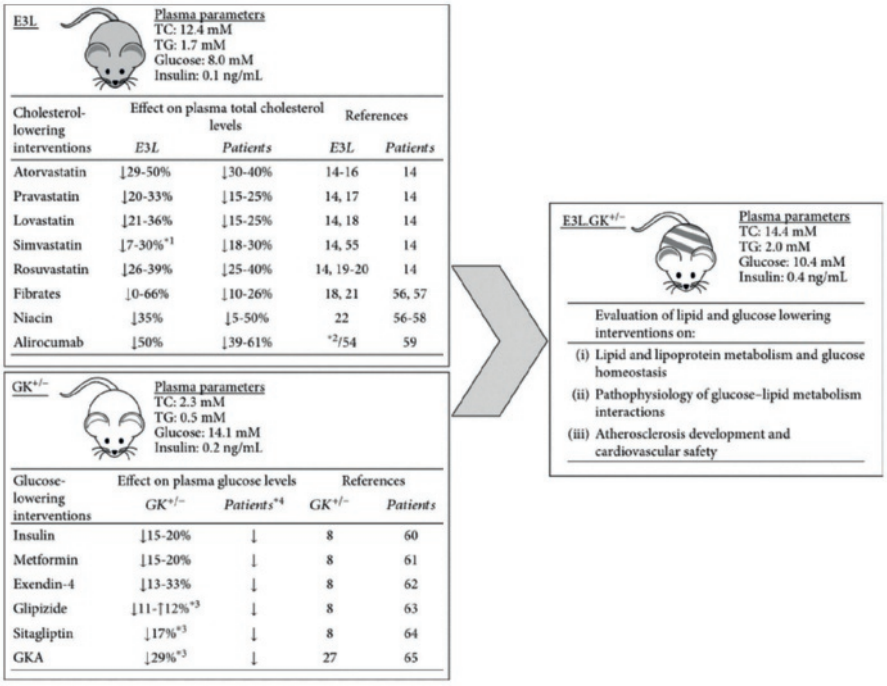

Figure 7 Overview of intervention studies with cholesterol- and glucose-lowering drugs performed in the E3L and GK+/- mouse models. The effects of cholesterol-lowering interventions on plasma TC levels were evaluated in E3L mice in long-term (5-28 weeks) exposure studies. The effects of glucose-lowering interventions on free-feeding blood glucose profiles were evaluated in GK+/- mice after single or repeated*3 dosing. In all studies, mice where fed a high fat or high fat/cholesterol containing diet. Data are extrapolated from published studies (see references). The depicted plasma parameters were measured at end-point in the present study. *1: Data shown of both APOE*3-Leiden and APOE*3-Leiden.CETP mice. *2: Unpublished. See reference 58 for data obtained from APOE*3-Leiden.CETP mice. *3: Repeated dosing. *4: As doses in diabetic patients are generally adapted to reach the desired plasma glucose level of < 8 mM, reductions are not depicted as percentages. Abbreviations: TC, total cholesterol; TG, triglycerides; GKA, glucokinase activator

References

1. Barengo NC, Katoh S, Moltchanov V, et al. The diabetes-cardiovascular risk paradox: results from a Finnish population-based prospective study. Eur Heart J. 2008 Aug;29(15):1889–95.
2. Sarwar N, Gao P, Seshasai SRK, et al. Diabetes mellitus, fasting blood glucose concentration, and risk of vascular disease: a collaborative meta-analysis of 102 prospective studies. Lancet (London, England). 2010 Jun;375(9733):2215–22.
3. Bae JC, Cho NH, Suh S, et al. Cardiovascular disease incidence, mortality and case fatality related to diabetes and metabolic syndrome: A community-based prospective study (Ansung-Ansan cohort 2001-12). J Diabetes. 2015 Nov;7(6):791–9.
4. Tarantino G, Saldalamacchia G, Conca P, et al. Non-alcoholic fatty liver disease: further expression of the metabolic syndrome. J Gastroenterol Hepatol. 2007 Mar;22(3):293–303.
5. Maric C, Hall JE. Obesity, metabolic syndrome and diabetic nephropathy. Contrib Nephrol. 2011;170:28–35.
6. Heinonen SE, Genove G, Bengtsson E, et al. Animal models of diabetic macrovascular complications: key players in the development of new therapeutic approaches. J Diabetes Res. 2015;2015:404085.
7. Lindstrom P. The physiology of obese-hyperglycemic mice [ob/ob mice]. ScientificWorldJournal. 2007 May;7:666–85.
8. Baker DJ, Atkinson AM, Wilkinson GP, et al. Characterization of the heterozygous glucokinase knockout mouse as a translational disease model for glucose control in type 2 diabetes. Br J Pharmacol. 2014 Apr;171(7):1629–41.
9. King AJF. The use of animal models in diabetes research. Br J Pharmacol. 2012 Jun;166(3):877–94.
10. Zadelaar S, Kleemann R, Verschuren L, et al. Mouse models for atherosclerosis and pharmaceutical modifiers. Arterioscler Thromb Vasc Biol. 2007 Aug;27(8):1706–21.
11. Ason B, van der Hoorn JWA, Chan J, et al. PCSK9 inhibition fails to alter hepatic LDLR, circulating cholesterol, and atherosclerosis in the absence of ApoE. J Lipid Res. 2014 Nov;55(11):2370–9.
12. van den Maagdenberg AM, Hofker MH, Krimpenfort PJ, et al. Transgenic mice carrying the apolipoprotein E3-Leiden gene exhibit hyperlipoproteinemia. J Biol Chem. 1993 May;;268(14):10540–5.
13. van Vlijmen BJ, van den Maagdenberg AM, Gijbels MJ, et al. Diet-induced hyperlipoproteinemia and atherosclerosis in apolipoprotein E3-Leiden transgenic mice. J Clin Invest. 1994 Apr;93(4):1403–10.
14. van de Steeg E, Kleemann R, Jansen HT, et al. Combined analysis of pharmacokinetic and efficacy data of preclinical studies with statins markedly improves translation of drug efficacy to human trials. J Pharmacol Exp Ther. 2013 Dec;347(3):635–44.
15. Delsing DJM, Jukema JW, van de Wiel MA, et al. Differential effects of amlodipine and atorvastatin treatment and their combination on atherosclerosis in ApoE*3-Leiden transgenic mice. J Cardiovasc Pharmacol. 2003 Jul;42(1):63–70.
16. Verschuren L, Kleemann R, Offerman EH, et al. Effect of low dose atorvastatin versus diet-induced cholesterol lowering on atherosclerotic lesion progression and inflammation in apolipoprotein E*3-Leiden transgenic mice. Arterioscler Thromb Vasc Biol. 2005 Jan;25(1):161–7.
17. van der Hoorn JWA, Kleemann R, Havekes LM, et al. Olmesartan and pravastatin additively reduce development of atherosclerosis in APOE*3Leiden transgenic mice. J Hypertens. 2007 Dec;25(12):2454–62.
18. van Vlijmen BJ, Pearce NJ, Bergo M, et al. Apolipoprotein E*3-Leiden transgenic mice as a test model for hypolipidaemic drugs. Arzneimittelforschung. 1998 Apr;48(4):396–402.
19. Delsing DJM, Post SM, Groenendijk M, et al. Rosuvastatin reduces plasma lipids by inhibiting VLDL production and enhancing hepatobiliary lipid excretion in ApoE*3-leiden mice. J Cardiovasc Pharmacol. 2005 Jan;45(1):53–60.
20. Kleemann R, Princen HMG, Emeis JJ, et al. Rosuvastatin reduces atherosclerosis development beyond and independent of its plasma cholesterol-lowering effect in APOE*3-Leiden transgenic mice: evidence for antiinflammatory effects of rosuvastatin. Circulation. 2003 Sep;108(11):1368–74.
21. Kooistra T, Verschuren L, de Vries-van der Weij J, et al. Fenofibrate reduces atherogenesis in ApoE*3Leiden mice: evidence for multiple antiatherogenic effects besides lowering plasma cholesterol. Arterioscler Thromb Vasc Biol. 2006 Oct;26(10):2322–30.
22. van der Hoorn JWA, de Haan W, Berbee JFP, et al. Niacin increases HDL by reducing hepatic expression and plasma levels of cholesteryl ester transfer protein in APOE*3Leiden.CETP mice. Arterioscler Thromb Vasc Biol. 2008 Nov;28(11):2016–22.

23. Postic C, Shiota M, Niswender KD, et al. Dual roles for glucokinase in glucose homeostasis as determined by liver and pancreatic beta cell-specific gene knock-outs using Cre recombinase. J Biol Chem. 1999 Jan;274(1):305–15.
24. Fajans SS, Bell GI, Bowden DW, et al. Maturity onset diabetes of the young (MODY). Diabet Med. 1996 Sep;13(9 Suppl 6):S90-5.
25. Velho G, Blanche H, Vaxillaire M, et al. Identification of 14 new glucokinase mutations and description of the clinical profile of 42 MODY-2 families. Diabetologia. 1997 Feb;40(2):217–24.
26. Gorman T, Hope DCD, Brownlie R, et al. Effect of high-fat diet on glucose homeostasis and gene expression in glucokinase knockout mice. Diabetes Obes Metab. 2008 Sep;10(10):885–97.
27. Baker DJ, Wilkinson GP, Atkinson AM, et al. Chronic glucokinase activator treatment at clinically translatable exposures gives durable glucose lowering in two animal models of type 2 diabetes. Br J Pharmacol. 2014 Apr;171(7):1642–54.
28. van Vlijmen BJ, van 't Hof HB, Mol MJ, et al. Modulation of very low density lipoprotein production and clearance contributes to age- and gender- dependent hyperlipoproteinemia in apolipoprotein E3-Leiden transgenic mice. J Clin Invest. 1996 Mar;97(5):1184–92.
29. Trion A, de Maat MPM, Jukema JW, et al. No effect of C-reactive protein on early atherosclerosis development in apolipoprotein E*3-leiden/human C-reactive protein transgenic mice. Arterioscler Thromb Vasc Biol. 2005 Aug;25(8):1635–40.
30. Post SM, Zoeteweij JP, Bos MH, et al. Acyl-coenzyme A:cholesterol acyltransferase inhibitor, avasimibe, stimulates bile acid synthesis and cholesterol 7alpha-hydroxylase in cultured rat hepatocytes and in vivo in the rat. Hepatology. 1999 Aug;30(2):491–500.
31. Kuhnast S, van der Tuin SJL, van der Hoorn JWA, et al. Anacetrapib reduces progression of atherosclerosis, mainly by reducing non-HDL-cholesterol, improves lesion stability and adds to the beneficial effects of atorvastatin. Eur Heart J. 2015 Jan;36(1):39–48.
32. Westerterp M, van der Hoogt CC, de Haan W, et al. Cholesteryl ester transfer protein decreases high-density lipoprotein and severely aggravates atherosclerosis in APOE*3-Leiden mice. Arterioscler Thromb Vasc Biol. 2006 Nov;26(11):2552–9.
33. Kuhnast S, van der Hoorn JWA, van den Hoek AM, et al. Aliskiren inhibits atherosclerosis development and improves plaque stability in APOE*3Leiden.CETP transgenic mice with or without treatment with atorvastatin. J Hypertens. 2012 Jan;30(1):107–16.
34. Stary HC, Chandler AB, Dinsmore RE, et al. A definition of advanced types of atherosclerotic lesions and a histological classification of atherosclerosis. A report from the Committee on Vascular Lesions of the Council on Arteriosclerosis, American Heart Association. Circulation. 1995 Sep;92(5):1355–74.
35. Kleiner DE, Brunt EM, Van Natta M, et al. Design and validation of a histological scoring system for nonalcoholic fatty liver disease. Hepatology. 2005 Jun;41(6):1313–21.
36. Liang W, Menke AL, Driessen A, et al. Establishment of a general NAFLD scoring system for rodent models and comparison to human liver pathology. PLoS One. 2014;9(12):e115922.
37. Tiniakos DG, Vos MB, Brunt EM. Nonalcoholic fatty liver disease: pathology and pathogenesis. Annu Rev Pathol. 2010;5:145–71.
38. Morrison MC, Mulder P, Salic K, et al. Intervention with a caspase-1 inhibitor reduces obesity-associated hyperinsulinemia, non-alcoholic steatohepatitis and hepatic fibrosis in LDLR-/-.Leiden mice. Int J Obes (Lond). 2016 Sep;40(9):1416–23.
39. Kotronen A, Yki-Jarvinen H, Mannisto S, et al. Non-alcoholic and alcoholic fatty liver disease - two diseases of affluence associated with the metabolic syndrome and type 2 diabetes: the FIN-D2D survey. BMC Public Health. 2010 May;10:237.
40. Lim H-W, Bernstein DE. Risk Factors for the Development of Nonalcoholic Fatty Liver Disease/Nonalcoholic Steatohepatitis, Including Genetics. Clin Liver Dis. 2018 Feb;22(1):39–57.
41. Di Angelantonio E, Sarwar N, Perry P, et al. Major lipids, apolipoproteins, and risk of vascular disease. JAMA. 2009 Nov;302(18):1993–2000.
42. Pettersson US, Walden TB, Carlsson P-O, et al. Female mice are protected against high-fat diet induced metabolic syndrome and increase the regulatory T cell population in adipose tissue. PLoS One. 2012;7(9):e46057.
43. Louet J-F, LeMay C, Mauvais-Jarvis F. Antidiabetic actions of estrogen: insight from human and genetic mouse models. Curr Atheroscler Rep. 2004 May;6(3):180–5.

44. Crespo CJ, Smit E, Snelling A, et al. Hormone replacement therapy and its relationship to lipid and glucose metabolism in diabetic and nondiabetic postmenopausal women: results from the Third National Health and Nutrition Examination Survey (NHANES III). Diabetes Care. 2002 Oct;25(10):1675–80.
45. Laakso M, Kuusisto J. Insulin resistance and hyperglycaemia in cardiovascular disease development. Nat Rev Endocrinol. 2014 May;10(5):293–302.
46. Roussel R, Steg PG, Mohammedi K,et al. Prevention of cardiovascular disease through reduction of glycaemic exposure in type 2 diabetes: A perspective on glucose-lowering interventions. Diabetes Obes Metab. 2018 Feb;20(2):238–44.
47. Liang W, Verschuren L, Mulder P, et al. Salsalate attenuates diet induced non-alcoholic steatohepatitis in mice by decreasing lipogenic and inflammatory processes. Br J Pharmacol. 2015 Nov;172(22):5293–305.
48. Zimmer M, Bista P, Benson EL, et al. CAT-2003: A novel sterol regulatory element-binding protein inhibitor that reduces steatohepatitis, plasma lipids, and atherosclerosis in apolipoprotein E*3-Leiden mice. Hepatol Commun. 2017 Jun;1(4):311–25.
49. Morrison MC, Liang W, Mulder P, et al. Mirtoselect, an anthocyanin-rich bilberry extract, attenuates non-alcoholic steatohepatitis and associated fibrosis in ApoE(*)3Leiden mice. J Hepatol. 2015 May;62(5):1180–6.
50. Ioannou GN, Haigh WG, Thorning D, et al. Hepatic cholesterol crystals and crown-like structures distinguish NASH from simple steatosis. J Lipid Res. 2013 May;54(5):1326–34.
51. Bakris GL, Williams M, Dworkin L, et al. Preserving renal function in adults with hypertension and diabetes: a consensus approach. National Kidney Foundation Hypertension and Diabetes Executive Committees Working Group. Am J Kidney Dis. 2000 Sep;36(3):646–61.
52. de Galan BE, Perkovic V, Ninomiya T, et al. Lowering blood pressure reduces renal events in type 2 diabetes. J Am Soc Nephrol. 2009 Apr;20(4):883–92.
53. Adingupu DD, Heinonen SE, Andreasson A-C, et al. Hyperglycemia Induced by Glucokinase Deficiency Accelerates Atherosclerosis Development and Impairs Lesion Regression in Combined Heterozygous Glucokinase and the Apolipoprotein E-Knockout Mice. J Diabetes Res. 2016;2016:8630961.
54. Princen HMG, Pouwer MG, Pieterman EJ. Comment on "Hypercholesterolemia with consumption of PFOA-laced Western diets is dependent on strain and sex of mice" by Rebholz S.L. et al. Toxicol. Rep. 2016 (3) 46-54. Toxicol reports. 2016;3:306–9.
55. Sattar N, Preiss D, Murray HM, et al. Statins and risk of incident diabetes: a collaborative meta-analysis of randomised statin trials. Lancet (London, England). 2010 Feb;375(9716):735–42.
56. Zinman B, Wanner C, Lachin JM, et al. Empagliflozin, Cardiovascular Outcomes, and Mortality in Type 2 Diabetes. N Engl J Med. 2015 Nov;373(22):2117–28.
57. Marso SP, Daniels GH, Brown-Frandsen K, et al. Liraglutide and Cardiovascular Outcomes in Type 2 Diabetes. N Engl J Med. 2016 Jul;375(4):311–22.
58. Marso SP, Bain SC, Consoli A, et al. Semaglutide and Cardiovascular Outcomes in Patients with Type 2 Diabetes. N Engl J Med. 2016 Nov;375(19):1834–44.

8

Inflammatory cytokine Oncostatin M induces endothelial activation in macro- and microvascular endothelial cells and in APOE*3-Leiden.CETP mice

Danielle van Keulen, Marianne G. Pouwer, Gerard Pasterkamp, Alain J. van Gool, Maarten D. Sollewijn Gelpke, Hans M. G. Princen, Dennie Tempel

PLoS One. 2018 Oct 1;13(10):e0204911

Abstract

Objectives: Endothelial activation is involved in many chronic inflammatory diseases, such as atherosclerosis, and is often initiated by cytokines. Oncostatin M (OSM) is a relatively unknown cytokine that has been suggested to play a role in both endothelial activation and atherosclerosis. We comprehensively investigated the effect of OSM on endothelial cell activation from different vascular beds and in APOE*3-Leiden.CETP mice.

Methods and results: Human umbilical vein endothelial cells, human aortic endothelial cells and human microvascular endothelial cells cultured in the presence of OSM express elevated MCP-1, IL-6 and ICAM-1 mRNA levels. Human umbilical vein endothelial cells and human aortic endothelial cells additionally expressed increased VCAM-1 and E-selectin mRNA levels. Moreover, ICAM-1 membrane expression is increased as well as MCP-1, IL-6 and E-selectin protein release. A marked increase was observed in STAT1 and STAT3 phosphorylation indicating that the JAK/STAT pathway is involved in OSM signaling. OSM signals through the LIF receptor alfa (LIFR) and the OSM receptor (OSMR). siRNA knockdown of the LIFR and the OSMR revealed that simultaneous knockdown is necessary to significantly reduce MCP-1 and IL-6 secretion, VCAM-1 and E-selectin shedding and STAT1 and STAT3 phosphorylation after OSM stimulation. Moreover, OSM administration to APOE*3-Leiden.CETP mice enhances plasma E-selectin levels and increases ICAM-1 expression and monocyte adhesion in the aortic root area. Furthermore, *Il-6* mRNA expression was elevated in the aorta of OSM treated mice.

Conclusions: OSM induces endothelial activation *in vitro* in endothelial cells from different vascular beds through activation of the JAK/STAT cascade and *in vivo* in APOE*3-Leiden.CETP mice. Since endothelial activation is an initial step in atherosclerosis development, OSM may play a role in the initiation of atherosclerotic lesion formation.

Introduction

The endothelium is involved in many processes including maintenance of the endothelial barrier function, prevention of spontaneous blood clot formation, inflammatory cell recruitment upon injury and regulation of the vascular tone (1–3). Impairment of one or more of these functions is often referred to as endothelial dysfunction, and may lead to the development of atherosclerosis, angiogenesis in cancer, vascular leakage, infectious diseases or stroke (4).

Although endothelial dysfunction is often described as the inability to dilate vessels, endothelial dysfunction is also characterized by endothelial activation, which is marked by increased cytokine release, adhesion molecule expression and endothelial permeability. The released cytokines attract leukocytes to the site of the activated endothelium, where the leukocytes bind to the endothelial barrier, which is enabled by enhanced adhesion molecule expression. Firmly adhered leukocytes then migrate through the endothelial barrier into the underlying tissue (5).

The process of endothelial activation can occur both, locally on well-known predilection sites and systemically, and is often triggered by traditional cardiovascular risk factors such as hypercholesterolemia, hypertension, smoking or diabetes and is initiated by inflammatory cytokines. One such a cytokine, which was first discovered in the cancer field, is oncostatin M (OSM). This relatively unexplored cytokine is an interleukin-6 (IL-6) family member that can signal through the leukemia inhibitory factor receptor (LIFR) and the OSM receptor (OSMR), which are both dependent on heterodimerization with the gp130 receptor to form a functional receptor complex (6). OSM is upregulated in multiple chronic inflammatory diseases including periodontitis, rheumatoid arthritis and inflammatory bowel diseases and is known to induce angiogenesis and smooth muscle cell proliferation and migration, both processes that are involved in atherosclerosis development (7–16). Other pro-inflammatory cytokines that promote angiogenesis, smooth muscle cell proliferation and endothelial activation, such as TNFα and IL-18, have already been proven to accelerate atherosclerosis (17–24). Furthermore, OSM is found in human carotid atherosclerotic plaques and in the intima and media of atherosclerotic mice (16).

Based on these findings and on the knowledge that endothelial cells are very high expressers of OSM receptors (25), we hypothesized that OSM may be involved in atherosclerosis development partially by inducing endothelial activation as a first step in the development of atherosclerosis. In this study, we incubated human endothelial cells with OSM to investigate if OSM induces systemic or local endothelial activation. As the cell heterogeneity among endothelial cells is huge (26,27) and endothelial cells from different vascular beds show different responses/ behave different to physiological stimuli (28,29), we tested the effect of OSM in endothelial cells derived from multiple vascular beds, human umbilical vein endothelial cells (HUVECs), human aortic endothelial cells (HAECs) and human microvascular endothelial cells (HMEC-1). Of which HAECs are the most

suitable endothelial cell type to study atherosclerosis development as atherosclerosis mainly affects the medium and large-sized arteries (30). To validate our findings in cultured endothelial cells in vivo, we administered OSM to APOE*3-Leiden.CETP mice, a translational mouse model for hyperlipidemia and atherosclerosis (31,32). The mildly pro-inflammatory state that is present in this animal model of hyperlipidemia makes it a suitable model to investigate the role of OSM in atherosclerosis prone conditions. We found that OSM induces endothelial activation in all different investigated human endothelial cell types and in mice after chronic administration and identified the JAK/STAT pathway as a key player in this process.

Materials and methods

Cell culture

Two different batches of pooled primary human umbilical vein endothelial cells (HUVECs, Lonza, the Netherlands), a single batch of primary human aortic endothelial cells from one single donor (HAECs, ATCC, Manassas, VA, USA) and a human dermal microvascular endothelial cell line (HMEC-1, ATCC, Manassas, VA, USA) were cultured in EBM®-2 medium (Lonza, Walkersville, MD) supplemented with EGMTM-2 SingleQuots® (Lonza, Walkersville, MD) under normoxic conditions (21% O_2). Throughout the study, passage 6 was used for HUVECs and HAECs, while passage 27 was used for the HMEC-1 cell line. All experiments were performed in 70% subconfluent HUVECs, HAECs, or HMEC-1 cells. After each experiment, cells and conditioned medium were collected for subsequent RNA or protein analysis. Repetitive experiments were only started if the previous experiment had been finished.

In vitro RNA expression

Human OSM (R&D systems, Minneapolis, MN) was added to HUVECs, HAECs and HMEC-1 cells in a concentration range from 0–20 ng/mL. After 3 or 6 hours, RNA was isolated with the NucleoSpin® RNA kit (Macherey-Nagel, Düren, Germany) according to the manufacturer's protocol. Isolated RNA (500 ng) was reverse transcribed into cDNA with the qSCript™ cDNA Synthesis Kit (Quanta Biosciences, Beverly, MA) and analyzed by real-time fluorescence assessment of SYBR Green signal (iQ™ SYBR® Green Supermix, Bio-Rad, Hercules, CA) in the CFX96™ Real-Time Detection System (Bio-Rad, Hercules, CA). Each sample was measured in duplicates. Primers were designed for the human genes of interest, sequences are listed in **Table 1**. mRNA levels were analyzed and corrected for the housekeeping gene ACTB. Experiments were repeated 4–7 times.

In vitro cytokine release

To determine the effect of OSM on endothelial activation, HUVECs, HAECs or HMEC-1 cells were incubated with 5 ng/mL OSM. 3h and 6h after OSM treatment, conditioned medium was collected. To investigate the effect of OSM on endothelial activation after siRNA knockdown of the LIFR and OSMR, siRNA transfected HUVECs were treated with 5 ng/mL OSM 48h post transfection. 6h after OSM treatment conditioned medium was collected. Conditioned medium was analyzed with the ProcartaPlex Mix&Match Human 6-plex (Thermo Fisher, Waltham, MA) according to the manufacturer's protocol and measured on the Bio-plex® 200 system (Bio-Rad, Hercules, CA) to determine the release of MCP-1, IL-6, soluble E-selectin, soluble P-selectin and soluble VCAM-1. Experiments were repeated 3–7 times.

Table 1 Primer sets for qPCR analysis

Gene	Species	Direction	Primer sequence (5'-3')
MCP-1	Human	Forward	TGGAATCCTGAACCCACTTCT
		Reverse	CAGCCAGATGCAATCAATGCC
IL-6	Human	Forward	AGTGAGGAACAAGCCAGAGC
		Reverse	GTCAGGGGTGGTTATTGCAT
ICAM-1	Human	Forward	TTGAACCCCACAGTCACCTAT
		Reverse	CCTCTGGCTTCGTCAGAATCA
VCAM-1	Human	Forward	TGGGAAAAACAGAAAAGAGGTG
		Reverse	GTCTCCAATCTGAGCAGCAA
E-SELECTIN	Human	Forward	AAGCCTTGAATCAGACGGAA
		Reverse	TCCCTCTAGTTCCCCAGATG
ACTB	Human	Forward	GATCGGCGGCTCCATCCTG
		Reverse	GACTCGTCATACTCCTGCTTGC
Mcp-1	Murine	Forward	TTAAAAACCTGGATCGGAACCAA
		Reverse	GCATTAGCTTCAGATTTACGGGT
Il-6	Murine	Forward	CTATACCACTTCACAAGTCGGA
		Reverse	GAATTGCCATTGCACAACTCTTT
Icam-1	Murine	Forward	TCCGCTACCATCACCGTGTAT
		Reverse	TAGCCAGCACCGTGAATGTG
Hprt	Murine	Forward	TCAGGAGAGAAAGATGTGATTGA
		Reverse	CAGCCAACACTGCTGAAACA

Flow cytometry

5 ng OSM was added to HUVECs, HAECs, or HMEC-1 cells for 18h. Cells were washed with PBS and detached with accutase. Subsequently, cells were fixed with 1% PFA and incubated with 2.5 µL antibodies/ 1,000,000 cells against VCAM-1, ICAM-1, P-selectin and, E-selectin all obtained from Thermo Fisher. The experiment was repeated 3 times.

siRNA transfection

Knockdown of LIFR and OSMR was achieved by transfection with a mix of 4 specific siRNA sequences directed against the human mRNA sequence (SMARTpool siGENOME, GE Dharmacon, Lafayette, CO) in 70% subconfluent HUVEC cultures. Cells were incubated for 1 hour in a small volume of EGM-2 medium supplemented with DharmaFECT 1 (GE Dharmacon, Lafayette, CO) according to manufacturer's instructions. After 2 hours cells were supplemented with extra EGM-2 medium to complement medium volumes. As controls, HUVECs were transfected with a mix of 4 scrambled, non-targeting siRNAs (siSham Smartpool; GE Dharmacon, Lafayette, CO). siRNA transfected HUVECs were treated with OSM 48h after siRNA transfection.

Western blot

HUVECs were lysed with cOmplete™ Lysis-M, EDTA-free reagent (Sigma Aldrich, Saint Louis, MO) for 15 minutes on ice. Next, protein concentration was determined with the Pierce™ BCA protein Assay Kit (Thermo Scientific, Waltham, MA). The protein sample was treated with NuPAGE™ Sample Reducing Agent (Thermo Scientific, Waltham, MA) and NuPAGE™ LDS Sample Buffer (Thermo Scientific, Waltham, MA). Subsequently, the solution was boiled at 70°C for 10 minutes. Samples were loaded on a Bolt™ 4–12% Bis-Tris Plus gel (Thermo Scientific, Waltham, MA), run for 50 minutes at 160V and transferred to an iBlot®2 PVDF Stack (Thermo Scientific, Waltham, MA) with the iBlot®2 Gel Transfer Device (Thermo Scientific, Waltham, MA). Blots were incubated with the primary antibody overnight at 4°C. Subsequently, blots were incubated with the appropriate secondary antibody conjugated with horseradish peroxidase (HRP) for 1h at RT. Peroxidase labeled antibodies were detected with Chemiluminescent Peroxidase Substrate (Sigma, Saint Louis, MO).

Animals and treatments

Thirty-two female APOE*3-Leiden.CETP transgenic mice (15–22 weeks of age) were used. The number of animals per group was calculated with Java Applets for Power and Sample Size [Computer software], from http://homepage.stat.uiowa.edu/~rlenth/Power/index.html using a one-way ANOVA with a probability of 0.05 and a Dunnett's correction, a SD of 20%, a power of 80% and a minimal expected difference of 35%. Mice were housed under standard conditions with a 12h light-dark cycle and had free access to food and water. Body weight, food intake and clinical signs of behavior were monitored regularly during the study. Mice received a Western type diet (WTD) (a semi-synthetic diet containing

15 w/w% cacao butter and 0.15% dietary cholesterol, Altromin, Tiel, the Netherlands). At t=0 weeks, after a run-in period of 3 weeks, mice were matched based on plasma total cholesterol levels, plasma triglyceride levels, body weight, and age in 4 groups of 8 mice. Two mice died during the diet intervention period, 1 in the 1 µg/kg/day OSM group and 1 in the 10 µg/kg/day OSM group. At t=7 weeks, an ALZET® Osmotic Pump Type 1004 (4-week release duration, Durect, Cupertino, CA) containing either 1, 3 or 10 µg/kg/day murine OSM (R&D systems, Minneapolis, MN) or PBS was placed subcutaneously in the flank. Doses were based on previous studies, which gave a single or double injection of 5–50 µg/kg OSM resulting in local increased permeability, edema, swelling, infiltration of immune cells, increased serum VEGF levels and increased angiopoietin 2 expression (33–36). All solutions, also PBS of control group, contained 1% mouse serum to prevent OSM from sticking to plastics. Prior to surgery, mice received the analgesic Carprofen (5 mg/kg s.c.) and were anesthetized with isoflurane (induction 4%, maintenance 2%). At t=10 weeks, mice were euthanized by gradual CO_2 inhalation (6 L/min in a 20 Liter container). CO_2 flow was maintained for a minimum of 1 minute after respiration ceased (as observed by lack of respiration and faded eye color). Death was confirmed by exsanguination (via heart puncture). Hearts were isolated for immunohistochemistry in the aortic root and aortas were isolated for RNA expression analysis. EDTA blood samples were drawn after a 4 hour fast at t=0 and t=10 weeks. All animal experiments were performed conform the guidelines from Directive 2010/63/EU of the European Parliament on the protection of animals used for scientific purposes or the NIH guidelines. The care and use of all mice in this study was carried out at the animal facility of The Netherlands Organization for Applied Research (TNO) in accordance with the ethical review committee "TNO-DEC" under the registration number 3683. Animal experiments were approved by the Institutional Animal Care and Use Committee of TNO under registration number TNO-202.

Plasma parameters

Plasma cholesterol and triglycerides were measured spectrophotometrically with enzymatic assays (Roche diagnostics). The inflammatory markers, E-selectin and monocyte chemoattractant protein 1 (MCP-1) were measured with ELISA kits from R&D. Plasma alanine transaminase (ALT) and aspartate transaminase (AST) were determined using a spectrophotometric assay (Boehringer Reflotron system) in group wise-pooled samples from sacrifice plasma. All assays were performed according to the manufacturer's instruction.

Histological assessment of vascular inflammation

Vascular inflammation was assessed in the aortic root area as reported previously by Landlinger et al. (37) in control mice and mice receiving 10 µg/kg/day OSM. Briefly, the aortic root was identified by the appearance of aortic valve leaflets and serial cross-sections

of the entire aortic root area (5 µm thick with intervals of 50 µm) were mounted on 3-aminopropyl triethoxysilane-coated slides and stained with hematoxylin-phloxine-saffron (HPS). Each section consisted of 3 segments (separated by the valves) and in 4 sections ICAM-1 expression and the number of monocytes adhering to the activated endothelium was counted after immunostaining with mouse monoclonal ICAM-1 antibody (Santa Cruz) and AIA 31240 antibody (Accurate Chemical and Scientific) respectively . One mouse from the control group was excluded from analysis due to a technical error, resulting in 7 and 8 mice per group.

RNA isolation murine tissue

To isolate RNA from aortic tissue, RA1 lysis buffer (Macherey-Nagel, Düren, Germany) containing 1% DTT was added to the tissue, which was cut in tiny pieces and subsequently minced. RNA was isolated with the RNeasy® Plus Micro Kit (Qiagen, Hilden, Germany) according to the RNeasy Fibrous Tissue Mini Kit protocol (Qiagen, Hilden, Germany). Isolated RNA (500 ng) was reverse transcribed into cDNA with the qSCript™ cDNA Synthesis Kit (Quanta Biosciences, Beverly, MA) and analyzed by real-time fluorescence assessment of SYBR Green signal (iQ™ SYBR® Green Supermix, Bio-Rad, Hercules, CA) in the CFX96™ Real-Time Detection System (Bio-Rad, Hercules, CA). Each sample was measured in duplicates. Primers were designed for the murine genes of interest, sequences are listed in **Table 1**. mRNA levels were analyzed and corrected for the housekeeping gene *Hprt*. RNA isolation was unsuccessful in one mouse from the 3 µg/kg/day OSM group resulting in 6, 7 and 8 mice per group.

Statistical analysis

qPCR data was analyzed according to the ΔΔCt method, statistical tests were performed on ΔCt values. Two-way ANOVA was used to analyze in vitro data to take into account day-to-day variation of the experiments. Not normally (Gaussian) distributed parameters were transformed with the natural logarithm or in case of undetectable values analyzed with the appropriate non-parametric test. Dose-dependency was determined by a Pearson correlation. All statistical analyses were performed in SPSS statistics version 21.0. A two-tailed p-value of 0.05 was regarded statistically significant in all analyses. Graphs were made in GraphPad Prism version 7.02 for Windows (GraphPad Software, La Jolla California USA, www.graphpad.com).

Results

OSM induces endothelial activation in human endothelial cells

To investigate whether OSM induces endothelial activation, we first examined cytokine mRNA expression in HUVECs, HAECs and HMEC-1 cells treated with 5 ng/mL OSM for 3 or 6 hours. OSM treatment was found to increase mRNA expression of the cytokines *MCP-1* ($p<0.01$) and *IL-6* ($p<0.001$) in HUVECs, HAECs ($p<0.001$) and HMEC-1 cells ($p<0.001$) at both 3h and 6h time points (**Figure 1A–F**). Since these cytokines are released by activated endothelial cells, we next measured MCP-1 and IL-6 protein concentrations in conditioned medium of OSM treated HUVECs, HAECs and HMEC-1 cells. Both MCP-1 ($p<0.05$) and IL-6 (<0.001) release were increased in OSM treated HUVECs, HAECs ($p<0.05$ and $p<0.01$ respectively) and HMEC-1 cells ($p<0.001$) at both time points (**Figure 1G–L**). Subsequently, we measured adhesion molecule expression, which is another feature of endothelial activation. *ICAM-1* mRNA expression was increased by OSM treatment in HUVECs ($p<0.001$) and HAECs ($p<0.01$) again at both 3h and 6h time points and in HMEC-1 cells 3h after addition of OSM ($p<0.01$)(**Figure 2A–C**). *VCAM-1* mRNA expression was upregulated in HUVECs at 3h ($p=0.008$) and in HAECs at both 3h and 6h ($p<0.001$)(**Figure 2D and E**). Moreover, we observed an upregulation in *E-selectin* mRNA expression in both HUVECs and HAECs at both 3h and 6h ($p<0.001$ and $p<0.05$)(**Figure 2F and G**), while *VCAM-1* and *E-selectin* mRNA levels were too low expressed in HMEC-1 cells. In addition, ICAM-1 membrane expression was increased in HUVECs ($p<0.05$), HAECs ($p<0.05$) and HMEC-1 cells ($p<0.05$) (**Figure 2H–J**), but not membrane expression of VCAM-1, P-selectin or E-selectin (data not shown). Since these adhesion molecules can also be shed upon endothelial activation (38), we measured P-selectin, E-selectin, soluble VCAM-1 and soluble ICAM-1 levels in conditioned medium. Soluble VCAM-1 was upregulated in conditioned medium of HUVECs 6h after OSM addition ($p<0.05$) and in HAECs at both 3h and 6h post OSM addition ($p<0.01$) (**Figure 2K and L**). Soluble VCAM-1 was not detectable in conditioned medium of HMEC-1 cells. Additionally, E-selectin levels were upregulated at both time points in conditioned medium of OSM treated HUVECs ($p<0.05$) and HAECs ($p<0.01$) and 6h post OSM addition in HMEC-1 cells ($p<0.05$) (**Figure 2M–O**). P-selectin levels were not detectable. Overall, these results indicate that OSM consistently induces endothelial activation in vitro in the different human endothelial cell types. Therefore, subsequent mechanistic studies were conducted in HUVECs.

JAK/STAT signaling is involved in OSM induced endothelial activation

IL-6 family members signal through the Janus kinase/signal transducers and activators of transcription (JAK/STAT) pathway, a pathway that is often involved in cytokine and growth factor signaling (39–41). Therefore, we investigated whether this pathway is also involved in OSM induced endothelial activation. STAT1 and STAT3 phosphorylation were markedly increased ($p<0.05$) (**Figure 3**) upon addition of OSM indicating that the JAK/STAT pathway is involved in OSM induced endothelial activation as well.

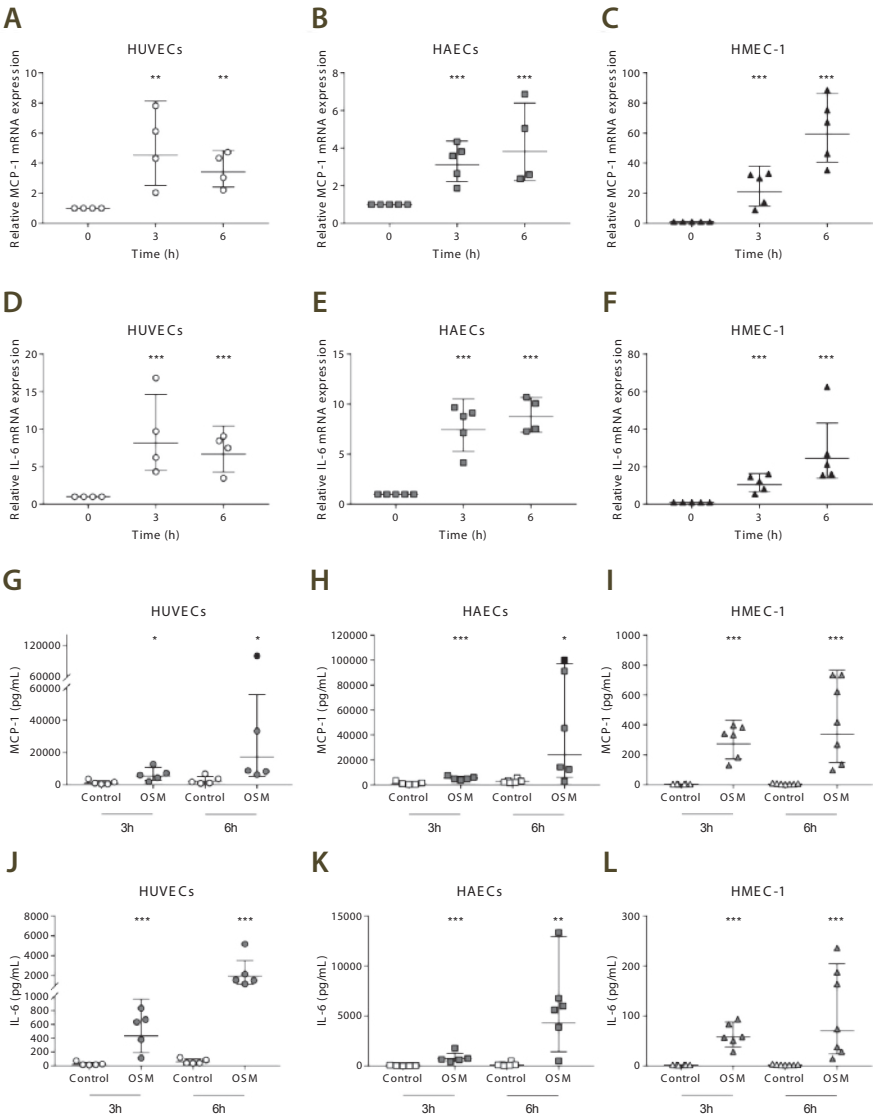

Figure 1 OSM increases cytokine release in different endothelial cells. HUVECs, HAECs and HMEC-1 cells were incubated with 5 ng/mL OSM for the indicated period of time. All values are relative values compared to control, which was given an arbitrary value of 1. Values were normalized to ACTB and calculated with the ΔΔCt method. (A-F). MCP-1 and IL-6 release was measured in conditioned medium of HUVECs, HAECs and HMEC-1 cells incubated with 5 ng/mL OSM for 3 or 6h. Values too high to measure were arbitrarily set on 100,000 and are indicated with ● or ■. (G-L). All data represent geometric mean ± geometric SD. *p<0.05 **p<0.01 ***p<0.001 compared to control (n = 4–7).

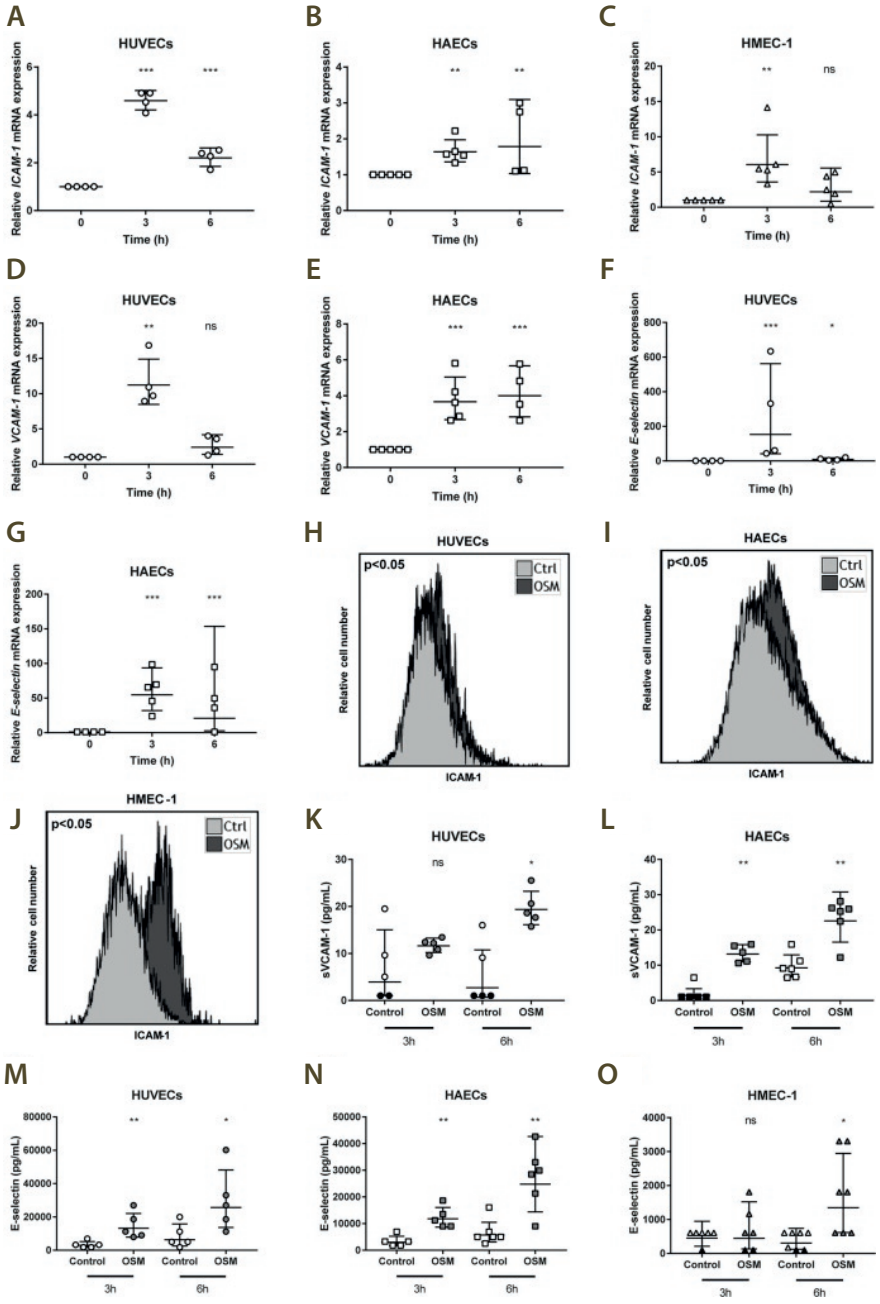

Figure 2 OSM increases adhesion molecule expression and release in different endothelial cells. HUVECs, HAECs and HMEC-1 cells were incubated with 5 ng/mL OSM for the indicated period of time.

All values are relative values compared to control, which was given an arbitrary value of 1. Values were normalized to *ACTB* and calculated with the ΔΔCt method. (A-C). ICAM-1 membrane expression was determined in HUVECs, HAECs and HMEC-1 cells treated with 5 ng/mL OSM for 18h. (D-F). Shedding of VCAM-1 and E-selectin was determined in conditioned medium of HUVECs, HAECs and HMEC-1 cells treated with 5 ng/mL OSM for 3 or 6h by measuring soluble VCAM-1 and E-selectin. Soluble VCAM-1 values too low to measure were arbitrarily set on 1 and are indicated with ● or ■. Soluble E-selectin values too low to measure were arbitrarily set on 100 and are indicated with ▲. (G-K). All data represent geometric mean ± geometric SD, except for flow cytometry data which shows a representative histogram of control and OSM treated cells (n = 3–7). *p<0.05 **p<0.01 ***p<0.001 compared to control, ns = not significant.

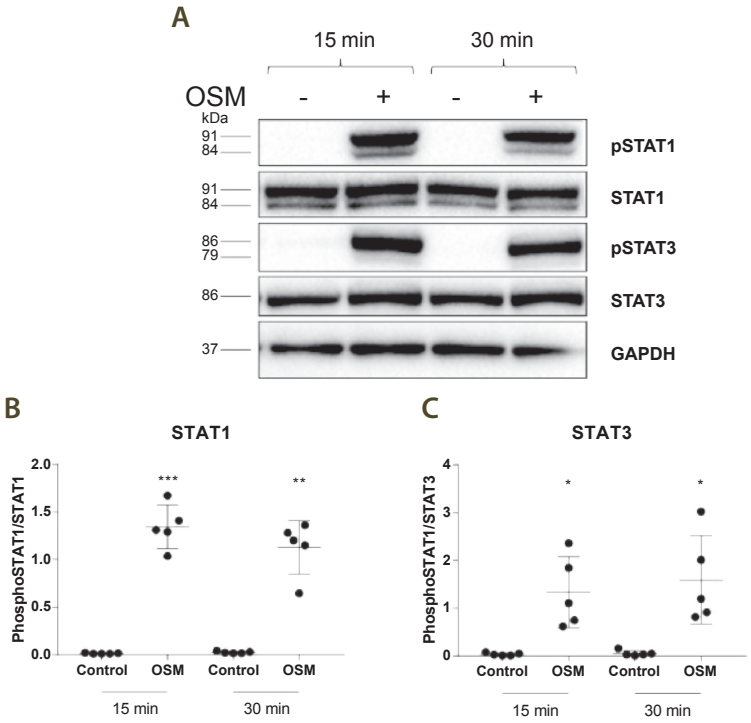

Figure 3 JAK/STAT pathway is involved in OSM induced endothelial activation. HUVECs were incubated with 5 ng/mL OSM for 15 or 30 min. A representative picture shows STAT1 phosphorylation at Tyr701, STAT1, STAT3 phosphorylation at Tyr705, STAT3 and GAPDH (A). Bar graphs show relative STAT1 and STAT3 phosphorylation (B,C). Data represent mean ± SD (n = 5). *p<0.05 **p<0.01 ***p<0.001 compared to control.

OSM induces endothelial activation by simultaneous signaling through the LIFR and OSMR

As OSM can signal through both the OSMR and the LIFR, a siRNA knockdown was performed to investigate which of these receptors is involved in OSM induced endothelial activation. *LIFR* mRNA expression was decreased to 25 ± 6% (mean ± SD), and *OSMR* mRNA expression to 52 ± 15%. Simultaneous knockdown resulted in a decrease of the *LIFR* to 31 ± 8% and of the *OSMR* to 45 ± 11% (**Figure 4A and B**). Single knockdown of *LIFR* did significantly decrease MCP-1 ($p=0.019$) and IL-6 secretion ($p = 0.005$), but not VCAM-1 or E-selectin shedding. Single knockdown of *OSMR* did only decrease IL-6 secretion ($p<0.001$), while MCP-1 secretion was significantly increased ($p=0.007$). VCAM-1 and E-selectin shedding were both not significantly changed. Double knockdown did not only decrease IL-6 ($p<0.001$) and MCP-1 ($p<0.001$) secretion, but also VCAM-1 ($p=0.009$) and E-selectin ($p<0.001$) shedding compared to non-targeting siRNA treated cells (**Figure 4C and D**). A similar effect was observed for STAT1 and STAT3 phosphorylation, which was only reduced by double knockdown ($p<0.05$) compared to control (**Figure 4E and F**). Altogether, these data indicate that OSM signals through LIFR and OSMR simultaneously in human endothelial cells.

OSM induces an inflammatory response in APOE*3-Leiden.CETP mice

To investigate whether OSM activates the endothelium in vivo as well, hyperlipidemic APOE*3-Leiden.CETP mice were administered OSM for 3 weeks. No clinical signs of deviant behavior and no significant effects on food intake were noted in any treatment group as compared to control. Plasma ALT and AST, measured at end-point as safety markers, showed no aberrant results (**Table 2**). Also, no significant difference in body weight, triglyceride, or cholesterol levels were observed compared to control (**Figure 5A–C**). As endothelial activation goes hand in hand with a pro-inflammatory response, plasma levels of inflammatory markers MCP-1 and E-selectin were measured. Plasma MCP-1 tended to be increased ($p=0.107$) and plasma E-selectin was increased ($p<0.001$) in mice treated with 10 µg/kg/day OSM compared to the control group (**Figure 5D and E**).

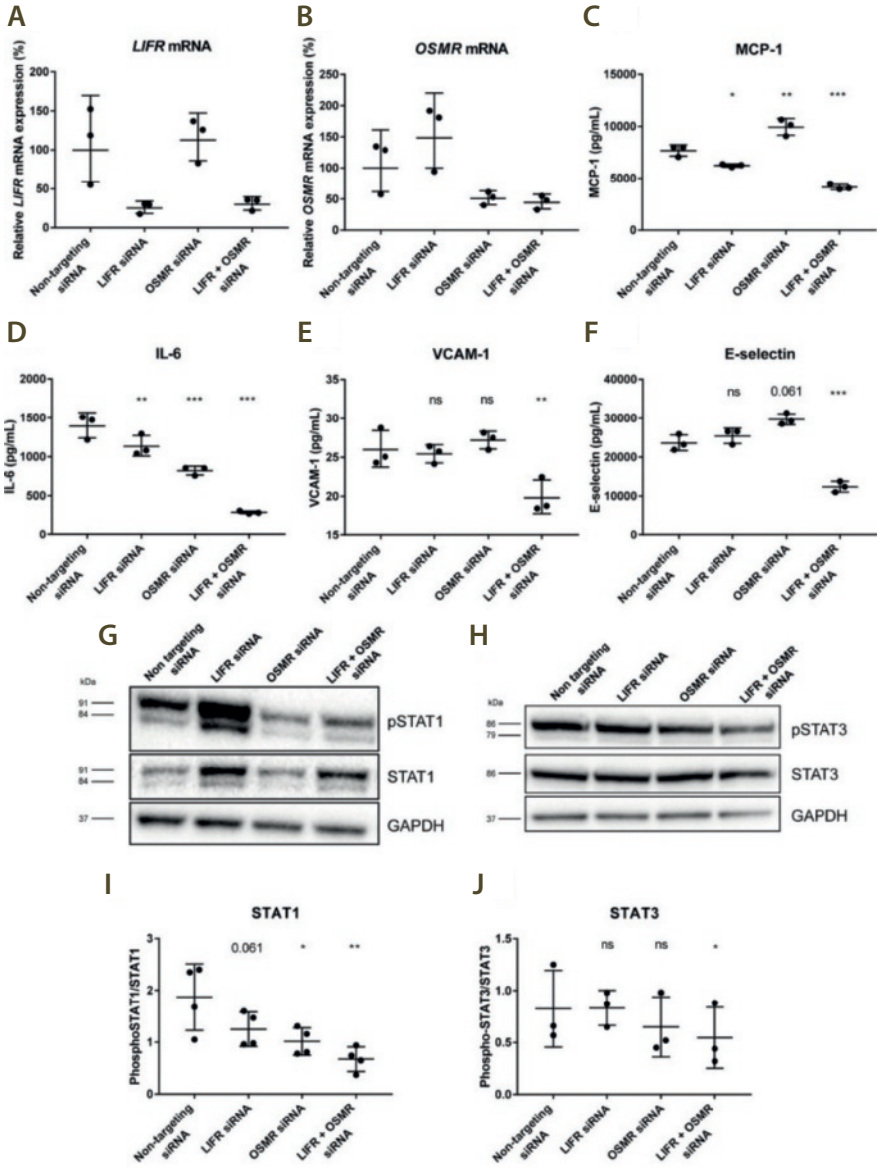

Figure 4 Simultaneous downregulation of *LIFR* and *OSMR* decreases IL-6 and MCP-1 release and prevents STAT1 and STAT3 phosphorylation. *LIFR* (A) and *OSMR* (B) mRNA expression levels were downregulated by siRNA transfection in HUVECs. 48h post transfection, HUVECs were treated with 5 ng/mL OSM for 6h to determine IL-6 and MCP-1 secretion and VCAM-1 and E-selectin shedding (C-F) or for 15 min to determine STAT1 and STAT3 phosphorylation (G-J). All data represent mean ± SD (n = 3–4). *p<0.05 **p<0.01 compared to control, ns = not significant.

Table 2 Average food intake and ALT and AST levels in mice

	Dose *µg/kg/day*	**Food intake** *(g/mouse/day)*	**ALT** *(U/L)*	**AST** *(U/L)*
Control	-	2.4 ± 0.2	53.1	324
OSM	1	2.7 ± 0.4	52.5	333
OSM	3	2.4 ± 0.3	92.1	669
OSM	10	2.4 ± 0.3	59.4	293

Food intake is measured per cage (n=2-4 mice per cage) and ALT and AST is measured in plasma pooled per group. Abbreviations: ALT, alanine aminotransferase; AST, aspartate aminotransferase

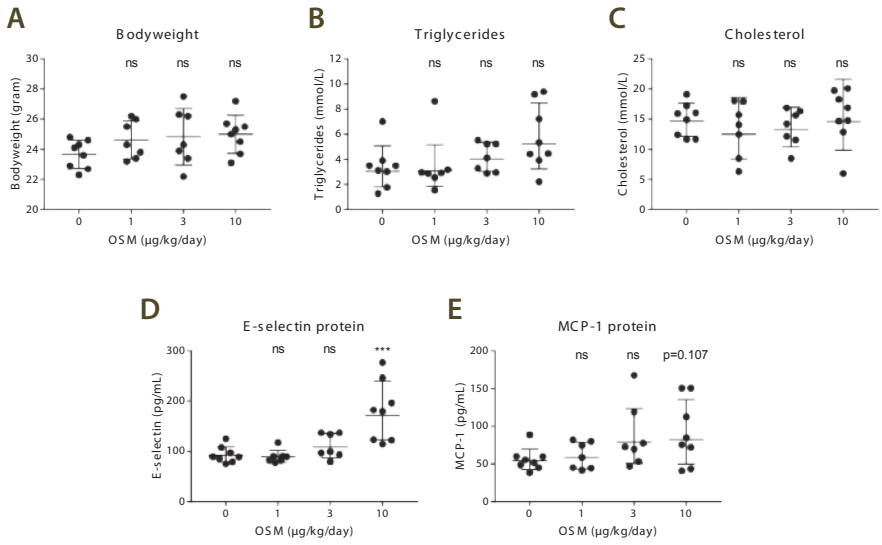

Figure 5 OSM enhances plasma levels of inflammatory markers in APOE*3-Leiden.CETP mice treated with OSM. After 3 weeks of OSM treatment, body weight (A), triglyceride (B), cholesterol (C), E-selectin (D) and MCP-1 (E) levels were measured and compared to control mice. All data represent geometric mean ± geometric SD, except for body weight which represents mean ± SD (n = 7–8). ***p<0.001 compared to control, ns = not significant.

OSM induces endothelial activation in the vasculature of APOE*3-Leiden.CETP mice

To further investigate if OSM is able to induce endothelial activation, the aortic root area was examined for relevant markers. ICAM-1 protein expression tended to be elevated from 39 ± 15% (mean ± SD) to 59 ± 22% (p=0.067) and an increase in monocyte adhesion to the activated endothelium was observed from 5.7 ± 3.0 to 10.3 ± 4.7 monocytes (mean ± SD, p<0.05) in mice treated with 10 µg/kg/day OSM (**Figure 6**). Furthermore, aortic mRNA expression analysis revealed a dose-dependent increase in *Il-6* expression (p<0.001) and *Icam-1* expression tended to be increased in the 1 µg/kg/day and 10 µg/kg/day OSM treated groups (p=0.101 and p=0.133, respectively) compared to control. *Mcp-1* mRNA expression was not enhanced (**Figure 7**). These results show that OSM does not only induce endothelial activation *in vitro*, but also *in vivo* in a hyperlipidemic mouse model.

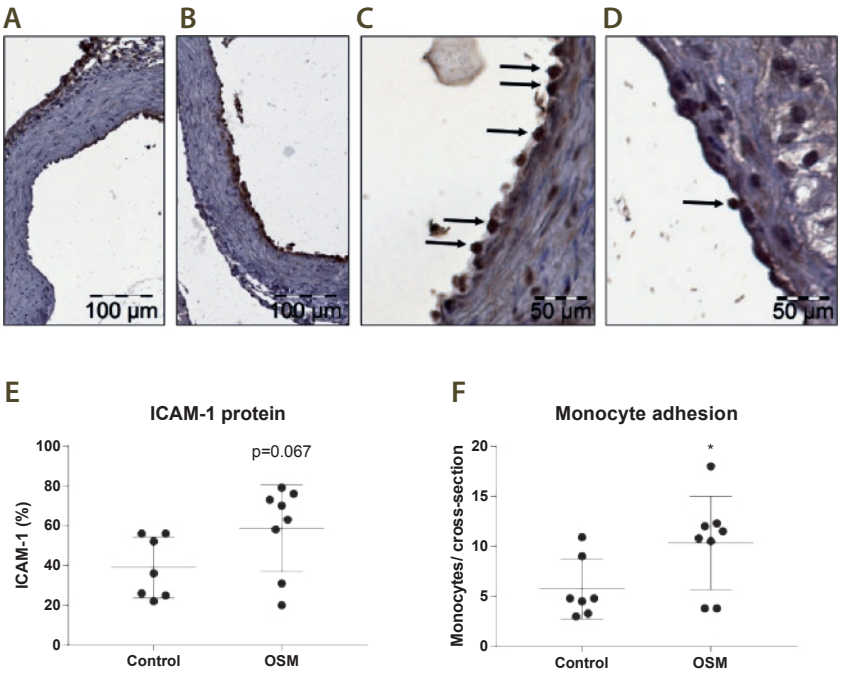

Figure 6 OSM increases ICAM-1 expression and monocyte adherence in the aortic root area in OSM treated APOE*3-Leiden.CETP. Representative pictures showing the endothelial ICAM-1 expression (brown staining) in a control (A) and a 10 µg/kg/day OSM treated (B) mouse and monocyte adherence (arrows) in a control (C) and a 10 µg/kg/day OSM treated (D) mouse. Endothelial ICAM-1 expression was determined as percentage of the endothelial surface in the cross-sections (E) and adhering monocytes were counted per cross-section after staining with AIA 31240 (F). Data represent mean ± SD (n = 7–8). Data represent mean ± SD. *p<0.05.

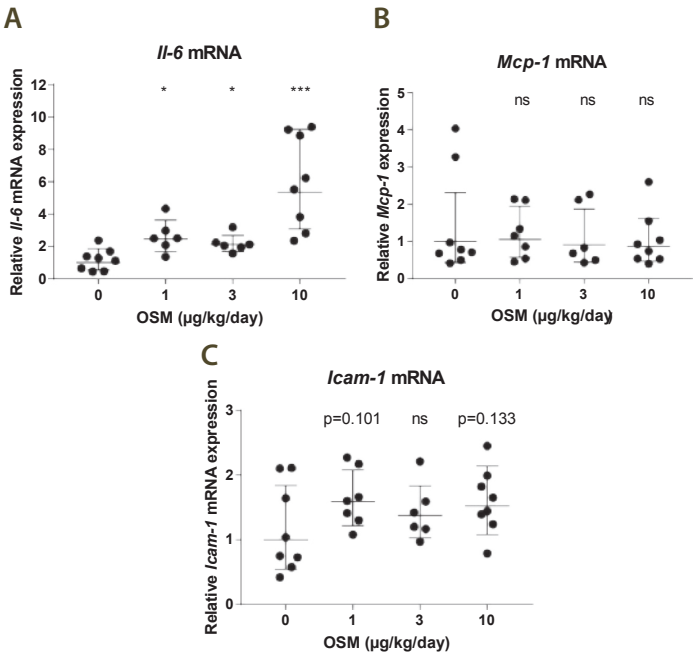

Figure 7 OSM increases *Il-6* mRNA expression in aortic tissue of APOE*3-Leiden.CETP mice treated with OSM. After 3 weeks of OSM treatment, mRNA was isolated from the aorta and analyzed by qPCR. *Il-6* (A), *Mcp-1* (B) and *Icam-1* (C) mRNA expression were quantified. All values are relative values compared to the control group, which was given an arbitrary value of 1. Values were normalized to *Hprt* and calculated with the ΔΔCt method. Data represent geometric mean ± geometric SD (n = 6–8). All values were compared to control. *p<0.05 ***p<0.001 compared to control, ns = not significant.

Discussion

The present study demonstrates that OSM induces endothelial activation in cultured human endothelial cells as well as *in vivo* in APOE*3-Leiden.CETP mice. The data show increased release of inflammatory markers and adhesion molecule expression, both features of endothelial activation. Furthermore, OSM increased monocyte adhesion in the aortic root area, as functional marker of endothelial activation.

We studied OSM induced endothelial activation in vitro by investigating the effect of OSM in three different types of human endothelial cells. Our data add to and expand on previous data that showed that OSM increases IL-6, IL-8 and MCP-1 secretion, ICAM-1 and VCAM-1 membrane expression and PMN adhesion to endothelial cells in vitro (34,42,43). Consistently, increased VCAM-1 and E-selectin shedding was observed in all three

endothelial cell types. ICAM-1 is an important adhesion molecule in monocyte binding as ICAM-1$^{-/-}$ endothelial cells show a strong attenuation in monocyte binding compared to control endothelial cells (44). Although we did not observe an increase in membrane E-selectin and VCAM-1 expression, OSM did increase soluble E-selectin and VCAM-1. Soluble VCAM-1 was previously shown to serve as a monocyte chemoattractant agent and soluble E-selectin enhances leukocyte migration and binding to endothelial cells (45,46). Taken together, these observations show that OSM induces different biomarkers of endothelial activation in cultured endothelial cells.

Previous short term *in vivo* studies in healthy wildtype mice with OSM administered for only 6 to 24 hours have shown signs of acute endothelial activation, such as increased angiopoietin 2 expression in cardiac tissue, increased plasma VEGF levels and increased permeability and infiltration of inflammatory cells (33–36). It is important to note that publicly available datasets show that *Osmr* and *Lifr* mRNA are expressed in aortic endothelial cells from mice as well (data accessible at NCBI GEO database (47), accession GSE114805 and (48), accession GSE115618).

The aim of the present study was to investigate the effect of chronic OSM exposure on endothelial activation in a hyperlipidemic mouse model, the APOE*3-Leiden.CETP mouse. This mouse model features elevated lipid levels, representing humans with hyperlipidemia and mild chronic inflammation who have an increased risk of developing atherosclerosis (31,32,37). We found that OSM tended to increase plasma MCP-1 and significantly increased plasma E-selectin, both markers of activated or dysfunctional endothelium (5,49) after 3 weeks of chronic OSM administration. Moreover, mRNA expression of *Il-6* was increased dose-dependently in aortic tissue of OSM treated mice. We also observed a trend towards increased ICAM-1 expression in the aortic root of OSM treated mice and a markedly enhanced monocyte binding as functional marker of activated endothelium, thus demonstrating augmented endothelial activation. ICAM-1 expression and adhesion of monocytes are strongly related, as previous studies show increased monocyte binding upon enhanced ICAM-1 expression and decreased monocyte binding upon reduced ICAM-1 expression (44,50). Collectively, these findings provide evidence that OSM does not only induce endothelial activation *in vitro*, but also *in vivo* on top of the inflammatory state that is present in hyperlipidemic mice, resulting in increased monocyte recruitment and adherence.

Even though, endothelial cells are directly activated by OSM *in vitro*, it is important to note that the *in vivo* situation is much more complex and other cell types may have contributed to the observed effects as well. For instance, the increase in plasma MCP-1 and cardiac *Il-6* expression can partly be caused by fibroblasts or smooth muscle cells, as these two cell types also show increased IL-6 and MCP-1 expression upon OSM treatment in vitro (51,52). Furthermore, OSM can promote growth factor and cytokine release in cell types other than endothelial cells, these released growth factors and cytokines can in turn

activate the endothelium, thereby inducing indirect endothelial activation (51–53). An example of such a growth factor is vascular endothelial growth factor (VEGF), which can be upregulated by OSM in multiple cell types (35,54–56) and is known to induce endothelial activation by increasing adhesion molecule expression and leukocyte adhesion (57).

Although our *in vivo* study was not aimed at and was too short to investigate whether chronic OSM exposure aggravates atherosclerosis, our results do give clues that OSM may be involved in the initiation of the atherosclerotic process. Some of the diverse hallmarks of endothelial activation that we observed, have previously been associated with atherosclerosis development in humans (49,58). Further indications come from reports showing that OSM is present in both murine and human plaques (16), and higher mRNA expression levels of OSM in PBMCs derived from coronary artery disease patients compared to healthy individuals (59). Moreover, a recent paper showed that prevention of OSM signaling, as opposed to stimulation of OSM signaling in our study, in OSMR-$\beta^{-/-}$ApoE$^{-/-}$ mice resulted in less and smaller atherosclerotic lesions and less macrophages compared to ApoE$^{-/-}$ mice (60).

Other studies have shown that partial inhibition of endothelial activation by knockdown of E-selectin, P-selectin, ICAM-1 or MCP-1 attenuates atherosclerosis development in mice (61,62). Therefore, lowering of plasma OSM levels or intervention in OSM signaling might be worth investigating as a possible future approach in the treatment of atherosclerosis.

As it is currently unknown which of the OSM receptors is involved in OSM induced endothelial activation, we performed a siRNA knockdown of the *LIFR* and the *OSMR*. Single knockdown experiments showed that solely *LIFR* or *OSMR* downregulation is not sufficient to prevent OSM induced endothelial activation or JAK/STAT signaling. Only simultaneous knockdown of both receptors was able to dramatically decrease IL-6 and MCP-1 release, VCAM-1 and E-selectin shedding and STAT1 and STAT3 phosphorylation. Hence, it is essential to block both receptors simultaneously or to target OSM when considering intervening in OSM signaling as a possible future therapy. Targeting both receptors or OSM itself could be a relative safe approach since OSM$^{-/-}$ mice are viable and healthy (63).

Taken together, our comprehensive study provides new evidence that OSM induces activation of human endothelial cells from different vascular beds and in APOE*3-Leiden. CETP mice chronically treated with OSM. Moreover, we provided data indicating both receptors for OSM as well as OSM itself as potential therapeutic targets in atherosclerosis and other chronic inflammatory diseases in which endothelial activation is involved such as rheumatoid arthritis, abnormal angiogenesis and thrombosis (64–67).

Acknowledgments

The authors thank Erik Offerman (TNO), Eveline Gart (TNO) and Stephanie van der Voorn (UMCU) for their excellent technical assistance.

Disclosures

Nothing to disclose.

Funding

This work was supported by the European Union Seventh Framework Programme (FP7/2007-2013) [grant number 602936] (CarTarDis project). The funders had no role in study design, data collection and analysis, decision to publish, or preparation of the manuscript. Quorics B.V provided support in the form of salaries for authors DVK and DT, and Molecular Profiling Consulting provided salary for MDSG but did not have any additional role in the study design, data collection and analysis, decision to publish, or preparation of the manuscript.

References

1. Sandoo A, van Zanten JJCSV, Metsios GS, et al. The endothelium and its role in regulating vascular tone. Open Cardiovasc Med J. 2010 Dec;4:302–12.
2. Rajendran P, Rengarajan T, Thangavel J, et al. The vascular endothelium and human diseases. Int J Biol Sci. 2013;9(10):1057–69.
3. Wu KK, Thiagarajan P. Role of endothelium in thrombosis and hemostasis. Annu Rev Med. 1996;47:315–31.
4. Hadi HAR, Carr CS, Al Suwaidi J. Endothelial dysfunction: cardiovascular risk factors, therapy, and outcome. Vasc Health Risk Manag. 2005;1(3):183–98.
5. Szmitko PE, Wang C-H, Weisel RD,et al. New markers of inflammation and endothelial cell activation: Part I. Circulation. 2003 Oct;108(16):1917–23.
6. Mosley B, De Imus C, Friend D, et al. Dual oncostatin M (OSM) receptors. Cloning and characterization of an alternative signaling subunit conferring OSM-specific receptor activation. J Biol Chem. 1996 Dec;271(51):32635–43.
7. O'Kane CM, Elkington PT, Friedland JS. Monocyte-dependent oncostatin M and TNF-alpha synergize to stimulate unopposed matrix metalloproteinase-1/3 secretion from human lung fibroblasts in tuberculosis. Eur J Immunol. 2008 May;38(5):1321–30.
8. Brown TJ, Lioubin MN, Marquardt H. Purification and characterization of cytostatic lymphokines produced by activated human T lymphocytes. Synergistic antiproliferative activity of transforming growth factor beta 1, interferon-gamma, and oncostatin M for human melanoma cells. J Immunol. 1987 Nov;139(9):2977–83.
9. Cross A, Edwards SW, Bucknall RC, et al. Secretion of oncostatin M by neutrophils in rheumatoid arthritis. Arthritis Rheum. 2004 May;50(5):1430–6.
10. Hui W, Bell M, Carroll G. Detection of oncostatin M in synovial fluid from patients with rheumatoid arthritis. Ann Rheum Dis. 1997 Mar;56(3):184–7.
11. Pradeep AR, S TM, Garima G, et al. Serum levels of oncostatin M (a gp 130 cytokine): an inflammatory biomarker in periodontal disease. Biomarkers Biochem Indic Expo response, susceptibility to Chem. 2010 May;15(3):277–82.
12. West NR, Hegazy AN, Owens BMJ, et al. Oncostatin M drives intestinal inflammation and predicts response to tumor necrosis factor-neutralizing therapy in patients with inflammatory bowel disease. Nat Med. 2017 May;23(5):579–89.
13. Vasse M, Pourtau J, Trochon V, et al. Oncostatin M induces angiogenesis in vitro and in vivo. Arterioscler Thromb Vasc Biol. 1999 Aug;19(8):1835–42.
14. Camare C, Pucelle M, Negre-Salvayre A, et al. Angiogenesis in the atherosclerotic plaque. Redox Biol. 2017 Aug;12:18–34.
15. Shi N, Chen S-Y. Mechanisms simultaneously regulate smooth muscle proliferation and differentiation. J Biomed Res. 2014 Jan;28(1):40–6.
16. Albasanz-Puig A, Murray J, Preusch M, et al. Oncostatin M is expressed in atherosclerotic lesions: a role for Oncostatin M in the pathogenesis of atherosclerosis. Atherosclerosis. 2011 Jun;216(2):292–8.
17. Tenger C, Sundborger A, Jawien J, et al. IL-18 accelerates atherosclerosis accompanied by elevation of IFN-gamma and CXCL16 expression independently of T cells. Arterioscler Thromb Vasc Biol. 2005 Apr;25(4):791–6.
18. Reddy VS, Valente AJ, Delafontaine P, et al. Interleukin-18/WNT1-inducible signaling pathway protein-1 signaling mediates human saphenous vein smooth muscle cell proliferation. J Cell Physiol. 2011 Dec;226(12):3303–15.
19. Amin MA, Rabquer BJ, Mansfield PJ, et al. Interleukin 18 induces angiogenesis in vitro and in vivo via Src and Jnk kinases. Ann Rheum Dis. 2010 Dec;69(12):2204–12.
20. Jing Y, Ma N, Fan T, et al. Tumor necrosis factor-alpha promotes tumor growth by inducing vascular endothelial growth factor. Cancer Invest. 2011 Aug;29(7):485–93.
21. Zhang Y, Yang X, Bian F, et al. TNF-alpha promotes early atherosclerosis by increasing transcytosis of LDL across endothelial cells: crosstalk between NF-kappaB and PPAR-gamma. J Mol Cell Cardiol. 2014 Jul;72:85–94.
22. Stamatiou R, Paraskeva E, Gourgoulianis K, et al. Cytokines and growth factors promote airway smooth muscle cell proliferation. ISRN Inflamm. 2012;2012:731472.
23. Morel JC, Park CC, Woods JM, et al. A novel role for interleukin-18 in adhesion molecule induction through NF kappa B and phosphatidylinositol (PI) 3-kinase-dependent signal transduction pathways. J Biol Chem. 2001 Oct;276(40):37069–75.

24. Mako V, Czucz J, Weiszhar Z, et al. Proinflammatory activation pattern of human umbilical vein endothelial cells induced by IL-1beta, TNF-alpha, and LPS. Cytometry A. 2010 Oct;77(10):962–70.
25. Brown TJ, Rowe JM, Liu JW, et al. Regulation of IL-6 expression by oncostatin M. J Immunol. 1991 Oct;147(7):2175–80.
26. Langenkamp E, Molema G. Microvascular endothelial cell heterogeneity: general concepts and pharmacological consequences for anti-angiogenic therapy of cancer. Cell Tissue Res. 2009 Jan;335(1):205–22.
27. Aird WC. Endothelial cell heterogeneity. Cold Spring Harb Perspect Med. 2012 Jan;2(1):a006429.
28. Scott DW, Vallejo MO, Patel RP. Heterogenic endothelial responses to inflammation: role for differential N-glycosylation and vascular bed of origin. J Am Heart Assoc. 2013 Jul;2(4):e000263.
29. Wang Q, Pfeiffer GR 2nd, Stevens T, et al. Lung microvascular and arterial endothelial cells differ in their responses to intercellular adhesion molecule-1 ligation. Am J Respir Crit Care Med. 2002 Sep;166(6):872–7.
30. Falk E. Pathogenesis of atherosclerosis. J Am Coll Cardiol. 2006 Apr;47(8 Suppl):C7-12.
31. Dewey FE, Gusarova V, Dunbar RL, et al. Genetic and Pharmacologic Inactivation of ANGPTL3 and Cardiovascular Disease. N Engl J Med. 2017 Jul;377(3):211–21.
32. Kuhnast S, van der Hoorn JWA, Pieterman EJ, et al. Alirocumab inhibits atherosclerosis, improves the plaque morphology, and enhances the effects of a statin. J Lipid Res. 2014 Oct;55(10):2103–12.
33. Sugaya M, Fang L, Cardones AR, et al. Oncostatin M enhances CCL21 expression by microvascular endothelial cells and increases the efficiency of dendritic cell trafficking to lymph nodes. J Immunol. 2006 Dec;177(11):7665–72.
34. Modur V, Feldhaus MJ, Weyrich AS, et al. Oncostatin M is a proinflammatory mediator. In vivo effects correlate with endothelial cell expression of inflammatory cytokines and adhesion molecules. J Clin Invest. 1997 Jul;100(1):158–68.
35. Rega G, Kaun C, Demyanets S, et al. Vascular endothelial growth factor is induced by the inflammatory cytokines interleukin-6 and oncostatin m in human adipose tissue in vitro and in murine adipose tissue in vivo. Arterioscler Thromb Vasc Biol. 2007 Jul;27(7):1587–95.
36. Rychli K, Kaun C, Hohensinner PJ, et al. The inflammatory mediator oncostatin M induces angiopoietin 2 expression in endothelial cells in vitro and in vivo. J Thromb Haemost. 2010 Mar;8(3):596–604.
37. Landlinger C, Pouwer MG, Juno C, et al. The AT04A vaccine against proprotein convertase subtilisin/kexin type 9 reduces total cholesterol, vascular inflammation, and atherosclerosis in APOE*3Leiden.CETP mice. Eur Heart J. 2017 Aug;38(32):2499–507.
38. Pigott R, Dillon LP, Hemingway IH, et al. Soluble forms of E-selectin, ICAM-1 and VCAM-1 are present in the supernatants of cytokine activated cultured endothelial cells. Biochem Biophys Res Commun. 1992 Sep;187(2):584–9.
39. Rawlings JS, Rosler KM, Harrison DA. The JAK/STAT signaling pathway. J Cell Sci. 2004 Mar;117(Pt 8):1281–3.
40. Scheller J, Chalaris A, Schmidt-Arras D, et al. The pro- and anti-inflammatory properties of the cytokine interleukin-6. Biochim Biophys Acta. 2011 May;1813(5):878–88.
41. Heinrich PC, Behrmann I, Muller-Newen G, et al. Interleukin-6-type cytokine signalling through the gp130/Jak/STAT pathway. Biochem J. 1998 Sep;334 (Pt 2:297–314.
42. Ruprecht K, Kuhlmann T, Seif F, et al. Effects of oncostatin M on human cerebral endothelial cells and expression in inflammatory brain lesions. J Neuropathol Exp Neurol. 2001 Nov;60(11):1087–98.
43. Modur V, Li Y, Zimmerman GA, Prescott SM, et al. Retrograde inflammatory signaling from neutrophils to endothelial cells by soluble interleukin-6 receptor alpha. J Clin Invest. 1997 Dec;100(11):2752–6.
44. Kevil CG, Patel RP, Bullard DC. Essential role of ICAM-1 in mediating monocyte adhesion to aortic endothelial cells. Am J Physiol Cell Physiol. 2001 Nov;281(5):C1442-7.
45. Tokuhira M, Hosaka S, Volin M V, et al. Soluble vascular cell adhesion molecule 1 mediation of monocyte chemotaxis in rheumatoid arthritis. Arthritis Rheum. 2000 May;43(5):1122–33.
46. Kang S-A, Blache CA, Bajana S, et al. The effect of soluble E-selectin on tumor progression and metastasis. BMC Cancer. 2016 May;16:331.
47. Natarelli L, Geissler C, Csaba G, et al. miR-103 promotes endothelial maladaptation by targeting lncWDR59. Nat Commun. 2018 Jul;9(1):2645.
48. McDonald AI, Shirali AS, Aragon R, et al. Endothelial Regeneration of Large Vessels Is a Biphasic Process Driven by Local Cells with Distinct Proliferative Capacities. Cell Stem Cell. 2018 Aug;23(2):210–225.e6.
49. Reynolds HR, Buyon J, Kim M, et al. Association of plasma soluble E-selectin and adiponectin with carotid plaque in patients with systemic lupus erythematosus. Atherosclerosis. 2010 Jun;210(2):569–74.

50. Zhao W, Feng H, Guo S, et al. Danshenol A inhibits TNF-alpha-induced expression of intercellular adhesion molecule-1 (ICAM-1) mediated by NOX4 in endothelial cells. Sci Rep. 2017 Oct;7(1):12953.
51. Dumas A, Lagarde S, Laflamme C, et al. Oncostatin M decreases interleukin-1 beta secretion by human synovial fibroblasts and attenuates an acute inflammatory reaction in vivo. J Cell Mol Med. 2012 Jun;16(6):1274–85.
52. Schnittker D, Kwofie K, Ashkar A, et al. Oncostatin M and TLR-4 ligand synergize to induce MCP-1, IL-6, and VEGF in human aortic adventitial fibroblasts and smooth muscle cells. Mediators Inflamm. 2013;2013:317503.
53. Pugin J, Ulevitch RJ, Tobias PS. A critical role for monocytes and CD14 in endotoxin-induced endothelial cell activation. J Exp Med. 1993 Dec;178(6):2193–200.
54. Foglia B, Cannito S, Morello E, et al. Oncostatin M induces increased invasiveness and angiogenesis in hepatic cancer cells through HIF1α-related release of VEGF-A. Dig Liver Dis Elsevier. 2017;49(e5 10.1016/j.dld.2017.01.013).
55. Fossey SL, Bear MD, Kisseberth WC, et al. Oncostatin M promotes STAT3 activation, VEGF production, and invasion in osteosarcoma cell lines. BMC Cancer. 2011 Apr;11:125.
56. Weiss TW, Simak R, Kaun C, et al. Oncostatin M and IL-6 induce u-PA and VEGF in prostate cancer cells and correlate in vivo. Anticancer Res. 2011 Oct;31(10):3273–8.
57. Kim I, Moon S-O, Hoon Kim S, et al. VEGF Stimulates Expression of ICAM-1, VCAM-1 and E-Selectin through Nuclear Factor-κ B Activation in Endothelial Cells. JBC Pap [Internet]. 2000; Available from: http://www.jbc.org.ezproxy.leidenuniv.nl:2048/
58. Mudau M, Genis A, Lochner A, et al. Endothelial dysfunction: the early predictor of atherosclerosis. Cardiovasc J Afr. 2012 May;23(4):222–31.
59. Kapoor D, Trikha D, Vijayvergiya R, et al. Conventional therapies fail to target inflammation and immune imbalance in subjects with stable coronary artery disease: a system-based approach. Atherosclerosis. 2014 Dec;237(2):623–31.
60. Zhang X, Li J, Qin J-J, et al. Oncostatin M receptor beta deficiency attenuates atherogenesis by inhibiting JAK2/STAT3 signaling in macrophages. J Lipid Res. 2017 May;58(5):895–906.
61. Collins RG, Velji R, Guevara N V, et al. P-Selectin or intercellular adhesion molecule (ICAM)-1 deficiency substantially protects against atherosclerosis in apolipoprotein E-deficient mice. J Exp Med. 2000 Jan;191(1):189–94.
62. Gosling J, Slaymaker S, Gu L, et al. MCP-1 deficiency reduces susceptibility to atherosclerosis in mice that overexpress human apolipoprotein B. J Clin Invest. 1999 Mar;103(6):773–8.
63. Esashi E, Ito H, Minehata K, et al. Oncostatin M deficiency leads to thymic hypoplasia, accumulation of apoptotic thymocytes and glomerulonephritis. Eur J Immunol. 2009 Jun;39(6):1664–70.
64. Kisucka J, Chauhan AK, Patten IS, et al. Peroxiredoxin1 prevents excessive endothelial activation and early atherosclerosis. Circ Res. 2008 Sep;103(6):598–605.
65. Rajashekhar G, Willuweit A, Patterson CE, et al. Continuous endothelial cell activation increases angiogenesis: evidence for the direct role of endothelium linking angiogenesis and inflammation. J Vasc Res. 2006;43(2):193–204.
66. Wilder RL, Case JP, Crofford LJ, et al. Endothelial cells and the pathogenesis of rheumatoid arthritis in humans and streptococcal cell wall arthritis in Lewis rats. J Cell Biochem. 1991 Feb;45(2):162–6.
67. Zwaginga JJ, Sixma JJ, de Groot PG. Activation of endothelial cells induces platelet thrombus formation on their matrix. Studies of new in vitro thrombosis model with low molecular weight heparin as anticoagulant. Arteriosclerosis. 1990;10(1):49–61.

9

Oncostatin M reduces atherosclerosis development in APOE*3-Leiden.CETP mice and is associated with increased survival probability in humans

Danielle van Keulen, Marianne G. Pouwer, Valur Emilsson, Ljubica Perisic Matic, Elsbet J. Pieterman, Ulf Hedin, Vilmundur Gudnason, Lori L. Jennings, Kim Holmstrøm, Boye S. Nielsen, Gerard Pasterkamp, Jan H.N. Lindeman, Alain J. van Gool, Maarten D. Sollewijn Gelpke, Hans M. G. Princen*, Dennie Tempel*

*These authors contributed equally

PLoS One. 2019 Aug 28;14(8):e0221477

Abstract

Objectives: Previous studies indicate a role for Oncostatin M (OSM) in atherosclerosis and other chronic inflammatory diseases for which inhibitory antibodies are in development. However, to date no intervention studies with OSM have been performed, and its relation to coronary heart disease (CHD) has not been studied.

Methods and Results: Gene expression analysis on human normal arteries (n=10) and late stage/advanced carotid atherosclerotic arteries (n=127) and in situ hybridization on early human plaques (n=9) showed that OSM, and its receptors, OSM receptor (OSMR) and Leukemia Inhibitory Factor Receptor (LIFR) are expressed in normal arteries and atherosclerotic plaques. Chronic OSM administration in APOE*3-Leiden.CETP mice (n=15/group) increased plasma E-selectin levels and monocyte adhesion to the activated endothelium independently of cholesterol but reduced the amount of inflammatory Ly-6C^{High} monocytes and atherosclerotic lesion size and severity. Using aptamer-based proteomics profiling assays high circulating OSM levels were shown to correlate with post incident CHD survival probability in the AGES–Reykjavik study (n=5457).

Conclusions: Chronic OSM administration in APOE*3-Leiden.CETP mice reduced atherosclerosis development. In line, higher serum OSM levels were correlated with improved post incident CHD survival probability in patients, suggesting a protective cardiovascular effect.

Introduction

Cytokines have an indisputable role in all stages of atherosclerosis development. In the initial stages of the disease, cytokines induce endothelial activation leading to endothelial adhesion molecule expression and leukocyte recruitment to the activated endothelium. In later stages of the disease, cytokines are involved in smooth muscle cell (SMC) migration, foam cell formation and enhanced MMP activity leading to plaque destabilization (1,2).

Similarly, a role for Oncostatin M (OSM) in atherosclerosis has been suggested (3,4). This cytokine is secreted by activated macrophages and neutrophils and signals through the Leukemia Inhibitory Factor Receptor (LIFR) and the OSM receptor (OSMR) (5–7). OSM induces endothelial activation by increasing cytokine release, adhesion molecule expression, and leukocyte adhesion to the activated endothelium in cultured endothelial cells (8–10). Moreover, OSM reduces vascular integrity of rat blood brain barrier endothelial cells and enhances angiogenesis (11,12). Next to its effects on the endothelium, OSM enhances SMC proliferation, migration and differentiation (4,12,13).

Additional evidence for this potential role of OSM in atherosclerosis, was provided by Albasanz-Puig et al., who showed that OSM is expressed in both murine and human atherosclerotic plaques (13). Furthermore, in ApoE$^{-/-}$ mice, OSMR deficiency attenuated atherosclerosis development and increased plaque stability (14).

Using a different approach, we recently demonstrated that short-term OSM administration (for 3 weeks) to APOE*3-Leiden.CETP mice increased plasma E-selectin levels, Interleukin (IL)-6 mRNA expression in the aorta and Intercellular Adhesion Molecule 1 (ICAM-1) expression and monocyte adherence to the activated endothelium in the aortic root (10). Collectively, these findings suggest that OSM may be involved in atherosclerosis development but so far this has never been studied.

The aim of this study is to investigate whether OSM is involved in atherosclerosis development in a humanized mouse model and in man. Therefore, we first investigated if OSM and its receptors are expressed in human normal and atherosclerotic arteries and if circulating OSM levels correlate with markers of endothelial activation in humans. Next, we explored the effect of long-term OSM administration on endothelial activation, atherosclerosis development and lesion composition in APOE*3-Leiden.CETP mice, a translational model for human lipoprotein metabolism and atherosclerosis development (15). Finally, we investigated if circulating OSM levels were associated with survival probability post coronary heart disease (CHD) in humans.

Materials and methods

Microarray on BiKE study material

Late stage/advanced atherosclerotic plaques were obtained from patients undergoing surgery for high grade (>50%) carotid stenosis and retained within the BiKE study. Normal artery controls were obtained from nine macroscopically disease-free iliac arteries and one aorta from organ donors without history of cardiovascular disease. All samples were collected with informed consent from patients or organ donor guardians. 127 plaques from BiKE patients and 10 normal arteries were analyzed by Affymetrix HGU133 plus 2.0 GeneChip microarrays. Robust multiarray average normalization was performed and processed gene expression data was transformed in $\log^2$-scale. The microarray dataset is available from Gene Expression Omnibus (GSE21545). The BiKE study cohort demographics, details of sample collection, processing, and analyses were previously described (16).

In situ hybridization (ISH) on SOCRATES study material

Early stage atherosclerotic lesions for in situ hybridization were obtained from the SOCRATES biobank (Leiden University Medical Center, the Netherlands). Details of this biobank have been described previously (17). Briefly, this biobank contains aortic wall patches obtained during kidney transplantation with grafts derived from cadaveric donors. Sample collection and handling were performed in accordance with the guidelines of the Medical and Ethical Committee in Leiden, the Netherlands, and the code of conduct of the Dutch Federation of Biomedical Scientific Societies (https://www.federa.org/?s=1&m=82&p=0&v=4#827). Chromogenic mRNA-ISH was essentially performed as previously described (18,19) on 9 atherosclerotic lesions from the SOCRATES biobank. For detection of the OSM, OSMR and LIFR mRNAs, ISH was performed in a Ventana Discovery ULTRA instrument (Ventana Medical Systems Inc., AZ, USA) using the ACD RNAscope® 2.5 Red Kit (Advanced Cell Diagnostics, Newark, CA, USA) and the mRNA Discovery ULTRA RED 4.0 procedure. RNAscope® 2.5 VS. Probes for Hs-OSM (#456389), Hs-OSMR-tv1 (#445699) and Hs-LIFR (#441029) were designed by the probe manufacturer (Advanced Cell Diagnostics). FFPE sections (5 µm) were applied to Superfrost Plus (Thermo Fisher Scientific) slides, and all operations including deparaffinization, pretreatment, ISH and counterstaining using hematoxylin were performed in a Ventana Discovery ULTRA instrument. Following the ISH-procedure in the Ventana instrument, slides were washed in lukewarm tap water with detergent until oil from the slides was fully removed. Subsequently, slides were washed in demineralized water, air dried and mounted in EcoMount mounting medium (Advanced Cell Diagnostics) prior to scanning in a bright-field whole-slide scanner (Axio Scan.Z1, Zeiss, Oberkochen Germany) using a 20x objective. The resulting digital images were inspected and regions of interest were selected.

Proteomics on AGES-Reykjavik study material

Association between OSM levels and IL-6, vascular cell adhesion molecule (VCAM)-1, P-selectin, E-selectin, ICAM-1 and Monocyte chemoattractant protein-1 (MCP-1) levels, and between OSM levels and survival were explored in the AGES-Reykjavik cohort (n=5457) (20), a single-center prospective population-based study of deeply phenotyped elderly European Caucasians (aged 66 through 96, mean age 75±6 years) who survived the 50-year-long prospective Reykjavik study. Phenotype description, patient numbers and other details related to the present study have been described previously (21). The AGES-Reykjavik study was approved by the NBC in Iceland (approval number VSN-00-063), the National Institute on Aging Intramural Institutional Review Board (USA), and the Data Protection Authority in Iceland. We applied a custom version of the Slow Off-rate Modified Aptamer (SOMAmer) platform targeting proteins known or predicted to be found in the extracellular milieu, including the predicted extracellular domains of single- and certain multi-pass transmembrane proteins, as previously described (21).

For survival analysis post CHD, we used 698 incident CHD cases exhibiting 307 deaths during the survival follow-up period of 12 years. Follow-up time for survival post incident CHD was defined as the time from 28 days after an incident CHD event until death from any cause or end of follow-up time.

Animals and treatments

Sixty-five female in-house bred APOE*3-Leiden.CETP transgenic mice (10-15 weeks of age) were used. Mice were housed under standard conditions with a 12h light-dark cycle and free access to food and water. Body weight, food intake and clinical signs of behavior were monitored regularly. Mice received a Western type diet (semi-synthetic containing 15 w/w% cacao butter and 0.15% dietary cholesterol, Altromin, Tiel, the Netherlands). At t=0 weeks, after a run-in period of 3 weeks, mice were matched based on body weight, age, plasma total cholesterol and E-selectin levels in 4 groups: a control group, and three intervention groups, two of which were treated with 10 or 30 µg/kg/day OSM for 16 weeks, and an initial priming group, which received 30 µg/kg/day OSM for the first 5.5 weeks only. All groups consisted of 15 mice except for the control group which had an additional 5 mice to monitor the atherosclerosis development. Five mice were removed from the study based on human end-point criteria and were excluded from all analyses: 2 mice in the 16 week 30 µg/kg/day OSM group and 1 in each of the other 3 groups. At t=0 weeks, an ALZET® Osmotic Pump Type 1004 (Durect, Cupertino, CA) containing either 10 or 30 µg/kg/day murine OSM (R&D systems, Minneapolis, MN) or the vehicle (PBS + 1% mouse serum) was placed subcutaneously in the flank and were replaced at t=5.5 and 11 weeks. Doses were based on our previous research (10). Prior to surgery, mice received the analgesic Carprofen (5 mg/kg s.c.) and were anesthetized with isoflurane (induction 4%, maintenance 2%). EDTA blood samples were drawn after a 4 hour fast at t=0, 4, 8, 12 and 16 weeks for determination of total cholesterol and inflammatory markers. At t=12 weeks,

4 mice from the control group were euthanized to assess atherosclerosis development for the determination of the end-point of the study. At t=16 weeks, mice were euthanized by gradual CO_2 inhalation. Death was confirmed by exsanguination (via heart puncture) and hearts were isolated. All animal experiments were performed conform the guidelines from Directive 2010/63/EU of the European Parliament on the protection of animals used for scientific purposes or the NIH guidelines. Approval was granted by the ethics committee on animal experiments (approval reference number DEC-3683) and the institutional animal welfare body (approval reference number TNO-255).

Plasma parameters

Plasma cholesterol was measured spectrophotometrically with enzymatic assays (Roche Diagnostics). E-selectin and MCP-1 were measured with ELISA kits from R&D (Minneapolis, MA, USA), and Serum Amyloid A (SAA) with an ELISA kit from Tridelta Development Limited (Maynooth, County Kildare, Ireland). All assays were performed according to the manufacturer's instructions.

Histological assessment of atherosclerosis and plaque composition

Atherosclerotic lesion area and severity were assessed in the aortic root area, as reported previously (22,23). Briefly, the aortic root was identified by the appearance of aortic valve leaflets, and serial cross-sections of the entire aortic root area (5 µm thick with intervals of 50 µm) were mounted on 3-aminopropyl triethoxysilane-coated slides and stained with haematoxylin-phloxine-saffron (HPS). For each mouse, the lesion area was measured in 4 subsequent sections. Each section consisted of 3 segments (separated by the valves). For determination of atherosclerotic lesion severity, the lesions were classified into five categories according to the American Heart Association (AHA) criteria (24): type 1 (early fatty streak), type 2 (regular fatty streak), type 3 (mild plaque), type 4 (moderate plaque), and type 5 (severe plaque). The total lesion area was calculated per cross-section. Due to a technical error one mouse of the OSM (30 µg/kg, 16 weeks) was excluded from analysis. Lesion severity was calculated as relative amount of type I-V lesions in which the lesion-free segments are included. From this, the relative amounts of lesion-free segments and diseased segments were calculated, and the relative amount of diseased segments was further subdivided into type I–V lesions, where types I-III refer to mild, and types IV-V to severe lesions. Lesion composition of type IV and V lesions was assessed after double immunostaining with anti-α smooth muscle actin (1:400; PROGEN Biotechnik GmbH, Germany) for smooth muscle cells (SMC), and anti-mouse MAC-3 (1:400; BD Pharmingen, the Netherlands) for macrophages. Anti-α smooth muscle actin was labeled with Vina green (Biocare Medical, Pacheco, USA), and MAC-3 with DAB (Vector laboratories, Burlingame, USA). After slides were scanned and analyzed, cover slips were detached overnight in xylene and Sirius Red staining for collagen was performed. The necrotic area was measured in the Sirius Red-stained slides. Lesion stability index, as the ratio of collagen

and αSMC area (i.e. stabilization factors) to macrophage and necrotic area (i.e. destabilization factors) was calculated as described previously (22). Lesion composition was assessed in all type IV-V lesions with a mean of 5.9 ± 3.1 lesions in control, 5.6 ± 2.5 lesions in OSM 10 µg/kg/d, 2.9 ± 2.0 lesions in OSM 30 µg/kg/d temporary and 2.8 ± 2.9 lesions in OSM 30 µg/kg/d. Eight mice were excluded from analysis as there were no type IV-V lesions present (n=1 in control; n=4 in OSM 30 µg/kg/d temporary and n=3 in OSM 30 µg/kg/d). In each segment used for lesion quantification, ICAM-1 expression and the number of monocytes adhering to the endothelium were counted after immunostaining with mouse monoclonal ICAM-1 antibody (1:400; Santa Cruz Biotechnology, Dallas, USA) and AIA 31240 antibody (1:500; Accurate Chemical and Scientific, New York, USA) respectively (25). NLRP3 expression in the macrophages was quantified after staining with rabbit polyclonal antibody to NLRP3 (1:400; Abcam, Cambridge, UK). All slides were scanned by an Aperio AT2 slide scanner (Leica Biosystems). Atherosclerotic area, monocyte adherence and ICAM-1 expression were measured in Image Scope (version 12-12-2015), and the area that stained positive for αSMA, MAC-3, Sirius Red and NLRP3 in the plaques was quantified automatically in Fiji (version 30-5-2017) using a threshold method.

Flow cytometry

To analyze the different monocyte subsets, 25 µL whole blood was incubated with antibodies against CD11b (APC-eFluor780-conjugated, eBioscience, San Diego, California, USA), Ly-6C (eFluor450-conjugated, eBioscience, San Diego, California, USA) and Ly-6G (A647-conjugated, Biolegend, San Diego, California, USA) for 30 min at RT. Erythrocytes were lysed with lysis buffer (deionized water with 168 mM ammonium chloride (Merck, Darmstadt, Germany), 9.99 mM potassium bicarbonate (Merck, Darmstadt, Germany) and 0.11 mM Na_2EDTA (Sigma-Aldrich, St. Louis, MO, USA)) for 10 min on ice and remaining erythrocytes were lysed with fresh lysis buffer for 5 min on ice. After washing, cells were fixed in 1% paraformaldehyde for 10 min on ice, measured with flow cytometry (Gallios, Beckman Coulter Fullerton, CA, USA) and analyzed with Kaluza Flow Analysis Software Version 2.1 (Beckman Coulter). Monocytes were defined as CD11b+Ly-6G-.

Statistics

BiKE transcriptomic dataset analyses were performed with GraphPad Prism 6 and Bioconductor software using a linear regression model adjusted for age and gender and a two-sided Student's t-test assuming non-equal deviation, with correction for multiple comparisons according to Bonferroni, as previously described (16). Data are presented as mean ± SD and adjusted $p<0.05$ was considered to indicate statistical significance.

Prior to protein data analyses, we applied a Box-Cox transformation on the proteins to improve normality, symmetry and to maintain all protein variables on a similar scale (21). For protein to protein correlation we used linear regression analysis. Given consistency in terms of sample handling including time from blood draw to processing, same personnel

handling all specimens and the ethnic homogeneity of the Icelandic population we adjusted only for age and sex in all our regression analyses.

Mouse data analyses were performed with GraphPad Prism 7.04 and IBM SPSS v25.0. Data are presented as mean ± SD. Normally (Gaussian) distributed mouse parameters were analyzed with a t-test or one-way ANOVA and not normally distributed mouse parameters with a Kruskal-Wallis test followed by a Mann-Whitney U test if significant. A significant difference between the 16 week 10 and 16 week 30 µg/kg/day groups was considered as a dose-dependent difference. The rejection criteria were adjusted using a Bonferroni-Holm correction. Correlation between plaque size and Ly-6C^{High} monocytes was tested with a Pearson correlation. A two-tailed p-value of 0.05 was regarded statistically significant in all analyses.

Cox proportional hazards regression was used for post incident CHD and Kaplan-Meier plots were applied to display survival data.

Results

mRNAs coding for OSM, OSMR and LIFR are present in human atherosclerotic plaques

To explore if OSM signaling can be involved in human plaque development, we first investigated if OSM mRNA and the mRNAs for the receptors for OSM, OSMR and LIFR, were present in late-stage human carotid plaques from the BiKE study. Gene expression analysis revealed presence of OSMR, LIFR and OSM mRNAs at low to moderate levels. mRNA expression of both receptors was significantly downregulated in plaques ($p<0.0001$) compared to normal arteries, while OSM expression was significantly increased ($p=0.003$) (**Figure 1A-C**). OSM mRNA expression positively correlated with macrophage markers and negatively with SMC markers (**Table 1**). Subsequent in situ hybridization confirmed the presence of OSMR, LIFR and OSM mRNAs in all investigated atherosclerotic plaque stages (**Figure 1D-O**), which is reflected in **Table 2**.

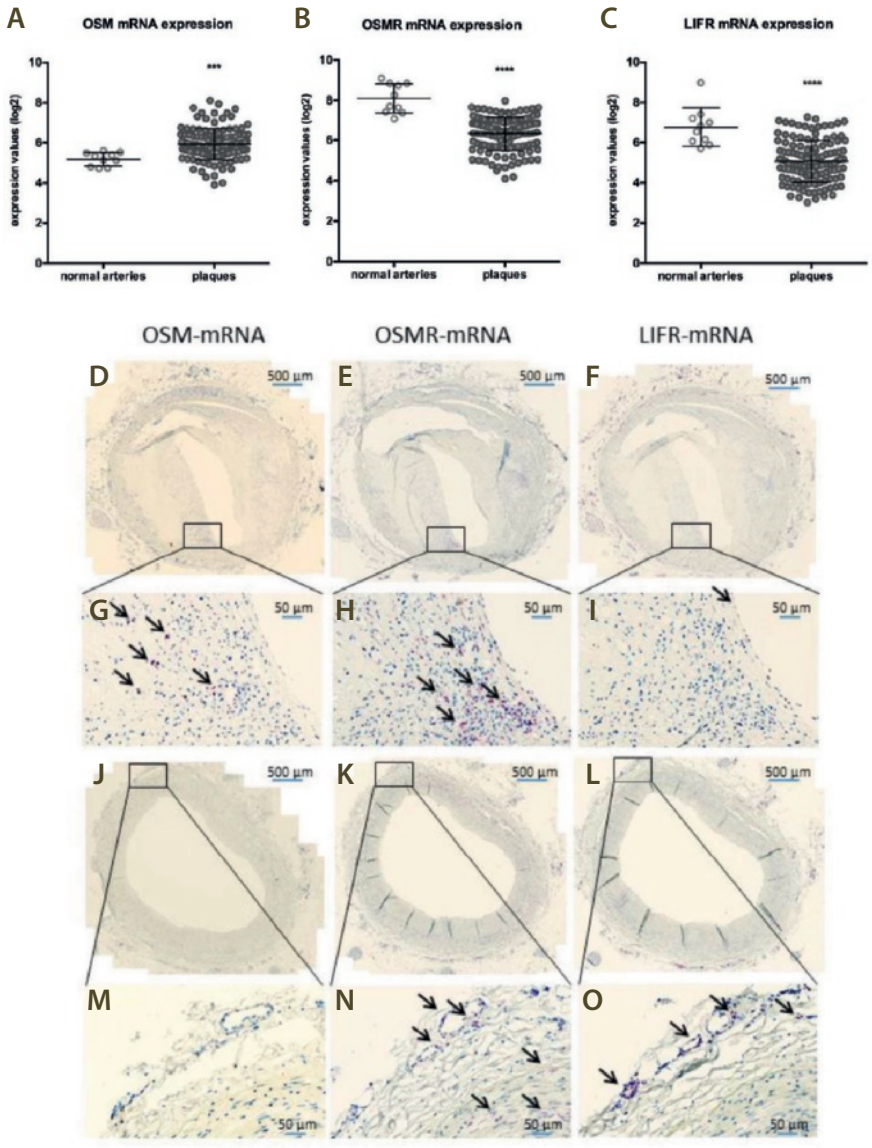

Figure 1 OSM, OSMR and LIFR mRNA expression is present in human atherosclerotic plaques. mRNA expression was measured in normal arteries and in carotid plaques by microarray analysis (A-C) and ISH was used to visualize OSM, OSMR and LIFR mRNA expression (red spots and shown by the black arrows) in two different stages of atherosclerosis development, the late fibroatheroma (D-I) and intimal xanthoma (J-O). ***p<0.001, ****p<0.0001. Abbreviations: ISH, in situ hybridization.

Table 1 Correlation between OSM and genes of interest in plaques

	Gene symbol	Pearson r	p-value	Significance level
Cell type markers				
Smooth muscle cells				
Myosin heavy chain 11	MYH11	-0.4327	< 0.0001	****
Smoothelin	SMTN	-0.4437	< 0.0001	****
Alpha smooth muscle actin	ACTA2	-0.3476	< 0.0001	****
Myocardin	MYOCD	-0.4119	< 0.0001	****
Transgelin	TAGLN	-0.3127	0.0004	***
Endothelial cells				
von Willebrand factor	VWF	0.1486	0.0967	ns
Pecam-1 (CD31)	PECAM1	0.3009	0.0006	***
Dendritic cells				
Itgax (CD11c)	ITGAX	0.4738	< 0.0001	****
Ly75 (CD205)	LY75	-0.03098	0.7295	ns
CD80	CD80	0.6013	< 0.0001	****
T Lymphocytes				
CD11b	ITGAM	0.4048	< 0.0001	****
ITGAL	ITGAL	0.5012	< 0.0001	****
CD27	CD27	0.107	0.233	ns
CD28	CD28	0.2859	0.0012	**
CD3 delta	CD3D	0.3678	< 0.0001	****
CD4	CD4	0.1078	0.2295	ns
CD8A	CD8A	0.2258	0.0107	*
PTPRC (CD45RA)	PTPRC	0.3758	< 0.0001	****
CD69	CD69	0.4909	< 0.0001	****
ITGAE	ITGAE	0.2827	0.0013	**
FABP4	FABP4	0.3884	< 0.0001	****
Macrophages				
CD83	CD83	0.5474	< 0.0001	****
CD86	CD86	0.4934	< 0.0001	****
CD163	CD163	0.4434	< 0.0001	****
TNFRSF9	TNFRSF9	0.3696	< 0.0001	****
CD40	CD40	0.3422	< 0.0001	****
CD36	CD36	0.4466	< 0.0001	****
Inflammation/ Apoptosis Calcification markers				
IL-1beta	IL1B	0.5657	< 0.0001	****
NFkB	NFKB1	0.1764	0.0481	*

Table 1 Continued

	Gene symbol	Pearson r	p-value	Significance level
Inflammation/ Apoptosis Calcification markers				
MCP-1	CCL2	0.5311	< 0.0001	****
Caspase-3	CASP3	0.2726	0.002	**
Caspase-7	CASP7	0.05738	0.5233	ns
Caspase-9	CASP9	0.2318	0.009	**
BCL2	BCL2	0.2761	0.0018	**
RANTES	CCL5	0.3821	< 0.0001	****
BMP4	BMP4	-0.1434	0.1091	ns
Extracellular matrix/ degradation				
MMP9	MMP9	0.4202	< 0.0001	****
TIMP1	TIMP1	0.3891	< 0.0001	****
Growth factors				
TGFB1	TGFB1	0.4113	< 0.0001	****
TGFA	TGFA	0.328	0.0002	***
IGF1	IGF1	0.256	0.0038	**
PDGFA	PDGFA	-0.02346	0.7943	ns
PDGFB	PDGFB	0.2417	0.0064	**
PDGFC	PDGFC	-0.2382	0.0072	**
PDGFD	PDGFD	-0.2889	0.001	**
Chemokines and receptors				
Interferon gamma	IFNG	0.2032	0.0225	*
IL2	IL2	0.2446	0.0058	**
IL4	IL4	0.03414	0.7043	ns
IL5	IL5	0.1947	0.0289	*
IL6	IL6	0.5659	< 0.0001	****
IL9	IL9	0.05453	0.5442	ns
IL10	IL10	0.4213	< 0.0001	****

Pearson correlation analyses were calculated from n=127 human plaque microarrays, p-values are corrected for multiple comparisons according to the Bonferroni method. Correlation considered weak if $r < 0.3$ moderate if $0.3 < r < 0.5$ and strong if $r > 0.5$. *p<0.05, **p<0.01, ***p<0.001, ****p<0.0001

Table 2 Quantification of ISH signal in various atherosclerotic plaque stages

		mRNA expression		
		OSM	OSMR	LIFR
Adaptive Intimal Thickening	**Neo-intima**	1	2	2
	Media	1	3	2
	Adventitia	1	3	3
Intimal Xanthoma	**Neo-intima**	1	2	2
	Media	0	2	3
	Adventitia	0	2	3
Pathological Intimal Thickening	**Neo-intima**	1	2	2
	Media	1	3	2
	Adventitia	1	3	3
Early Fibroatheroma	**Neo-intima**	2	2	2
	Media	1	2	2
	Adventitia	1	3	3
Late Fibroatheroma	**Neo-intima**	2	2	2
	Media	2	2	2
	Adventitia	1	2	4
Fibrous Calcified Plaque	**Neo-intima**	2	2	2
	Media	1	3	2
	Adventitia	1	3	2

The amount of ISH signal was scored in various atherosclerotic plaque stages. A general score and a single cell score was given. 0 = no signal, 1 = few cells expressing mRNA, 2 = low expression, 3 = moderate expression and 4 = high expression. Abbreviations: ISH, in situ hybridization.

OSM is associated with endothelial activation markers IL-6 and VCAM-1 in humans

We previously found that OSM induces endothelial activation both in vitro in human endothelial cells and in vivo in APOE*3-Leiden.CETP mice (10). To investigate if OSM can be linked with markers of endothelial activation in a human setting as well, we measured serum levels of OSM and several circulating endothelial activation markers in the AGES-Reykjavik study. OSM levels modestly correlated with IL-6 (β = 0.210, $p=5*10^{-56}$) and VCAM-1 (β = 0.130, $p=4*10^{-20}$) levels, but inversely with P-Selectin (β = -0.115, $p=5*10^{-17}$), E-Selectin (β = -0.092, $p=2*10^{-11}$) and ICAM-1 (β = -0.013, $p=5*10^{-7}$) levels (**Figure 2**). No correlation of OSM with MCP-1 was observed.

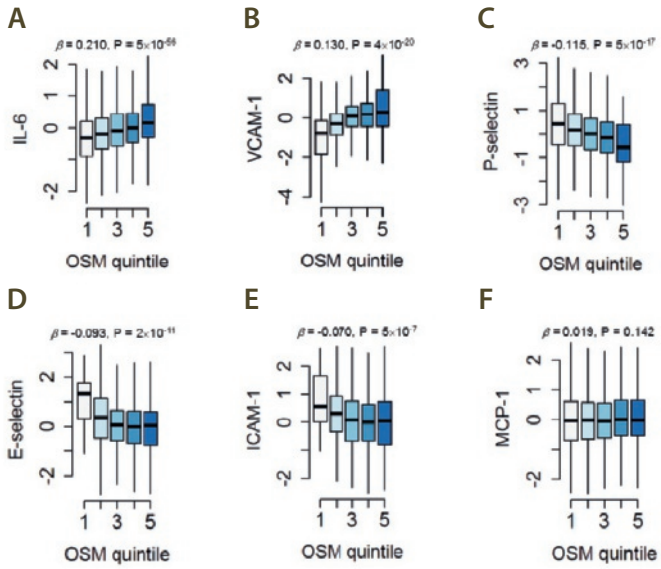

Figure 2 OSM is associated with endothelial activation markers. Association of serum IL-6 (A), VCAM-1 (B), P-selectin (C), E-selectin (D), ICAM-1 (E) and MCP-1 (F) levels (y-axis) with quintiles of increasing OSM serum levels (x-axis) using specific aptamers measured in 5457 subjects of the AGES cohort. Linear regression analyses were used to test for association.

Chronic exposure to OSM results in a pro-inflammatory vascular phenotype in APOE*3-Leiden.CETP mice

The above and our previous data (10) suggest a role for OSM in atherosclerosis development. Therefore, we performed a long-term study in which we administered OSM to APOE*3-Leiden.CETP mice for 16 weeks. To specifically investigate the effect of OSM on the initiation of atherosclerosis, we added an initial priming group that was treated with OSM only for the first 5.5 weeks of the study. As previous studies had a much shorter duration (ranging from 6 hours to 3 weeks), we first investigated if long-term OSM treatment persistently causes an inflammatory phenotype by measuring E-selectin, MCP-1 and SAA plasma levels, as markers of vessel wall, general and liver-derived inflammation. Treatment groups receiving either 10 µg/kg/day ($p=0.002$) or 30 µg/kg/day ($p<0.001$) OSM for 16 weeks showed markedly increased E-selectin levels at all time points and a dose-dependent increase at t=4 ($p<0.01$) and 8 weeks ($p<0.01$). The group receiving 5.5 weeks 30 µg/kg/day OSM treatment also showed markedly increased E-selectin levels at t=4 ($p<0.001$), though after discontinuation of OSM treatment, E-selectin levels dropped and declined to similar levels as the control group. MCP-1 and SAA levels did not differ between the OSM treated groups and control (**Figure 3A-C**). Also, no statistical difference

was observed in ICAM-1 expression at the endothelium in the aortic root area (**Figure 3D**). In contrast, monocyte adhesion, as functional marker of endothelial activation, in the aortic root area was increased from 4.9 ± 3.3 monocytes per cross-section in the control group to 17.9 ± 10.7 in the 16 weeks 30 µg/kg/day group (p=0.003) (**Figure 3E**). These results indicate that continuous OSM exposure results in a sustained pro-inflammatory vascular phenotype, even after 16 weeks of treatment.

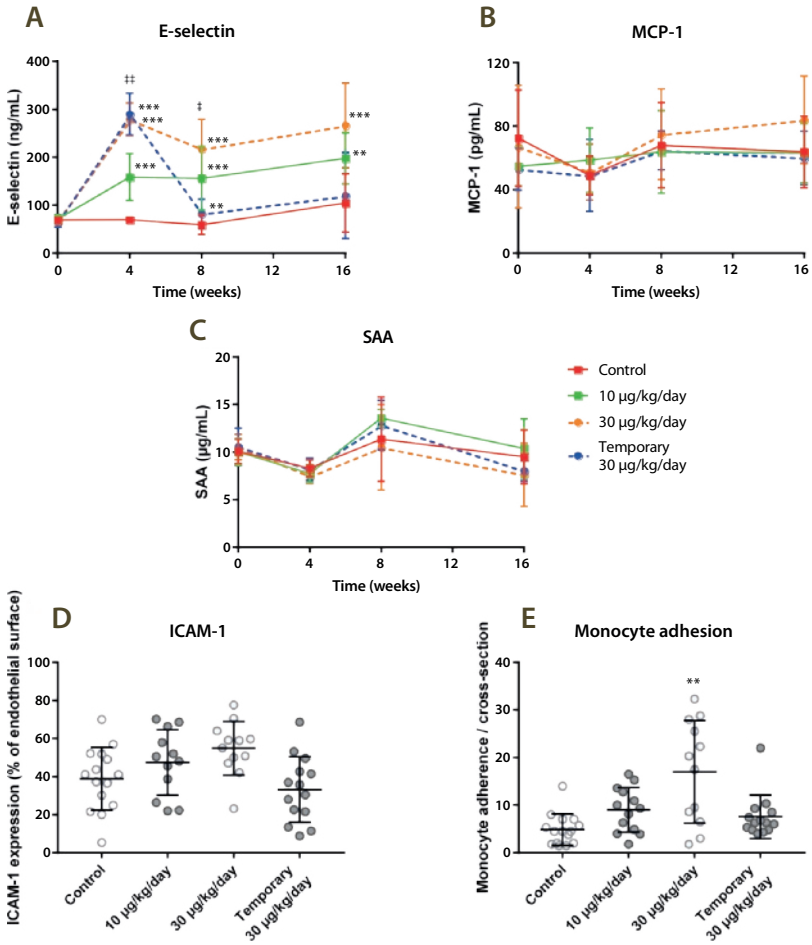

Figure 3 OSM induces a pro-inflammatory vascular phenotype in APOE*3-Leiden.CETP mice. Plasma E-selectin, MCP-1 and SAA (A-C) were measured at multiple time points during the study. Monocyte adhesion (D) and endothelial ICAM-1 expression were assessed per cross-section in the aortic root area (E). Data represent mean ± SD (n=12-20). ‡ p<0.05 compared to 10 µg/kg/day; **p<0.01 compared to control; ‡‡ p<0.01 compared to 10 µg/kg/day; ***p<0.001 compared to control.

OSM reduces atherosclerotic lesion area and severity in APOE*3-Leiden.CETP mice

Total plasma cholesterol levels, a risk factor for cardiovascular disease, did not differ between any of the groups (data not shown). Atherosclerotic lesion size and severity were investigated in the aortic root area of which representative pictures are shown in **Figure 4**. The control group had an average lesion size of 119 ± 64 *1000 μm^2. In the 5.5 week 30 μg/kg/day OSM group, plaque size was reduced by 59% (p=0.002) and in the 16 week 30 μg/kg/day OSM group by 58% (p=0.002), while the 16 week 10 μg/kg/day OSM treated group did not differ from the control (**Figure 5A**). The decrease in plaque area was dose-dependent (p=0.006). In the control group, 62 ± 27% of the lesions were classified as severe lesions, while only 23 ± 22% (p=0.001) and 26 ± 24% (p=0.002) of the lesions were severe in the 16 week 30 μg/kg/day and 5.5 week 30 μg/kg/day OSM treated group,

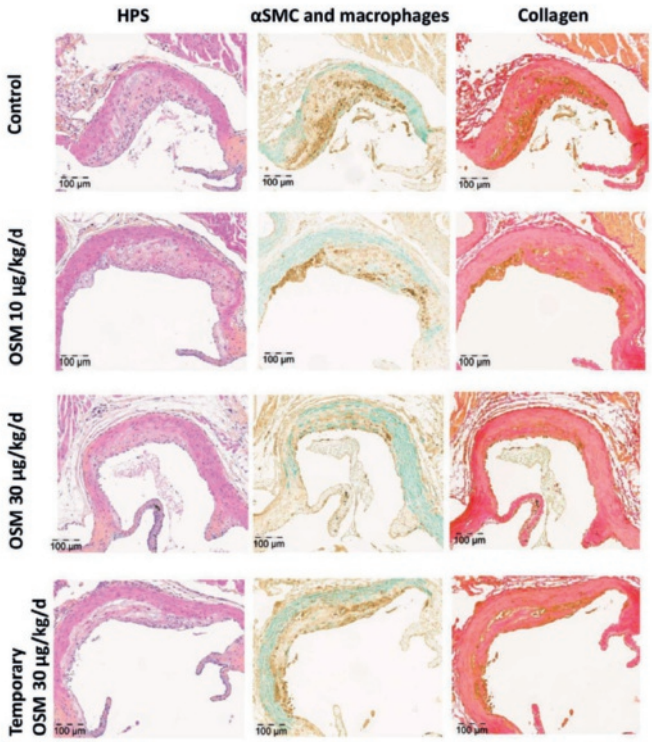

Figure 4 Effect of OSM on plaque composition in APOE*3-Leiden.CETP mice. Representative pictures showing severe lesion types (type IV and V) stained with HPS staining, SMC staining (green), macrophage staining (brown) and collagen staining (red) to determine the effect of OSM on the lesion composition.

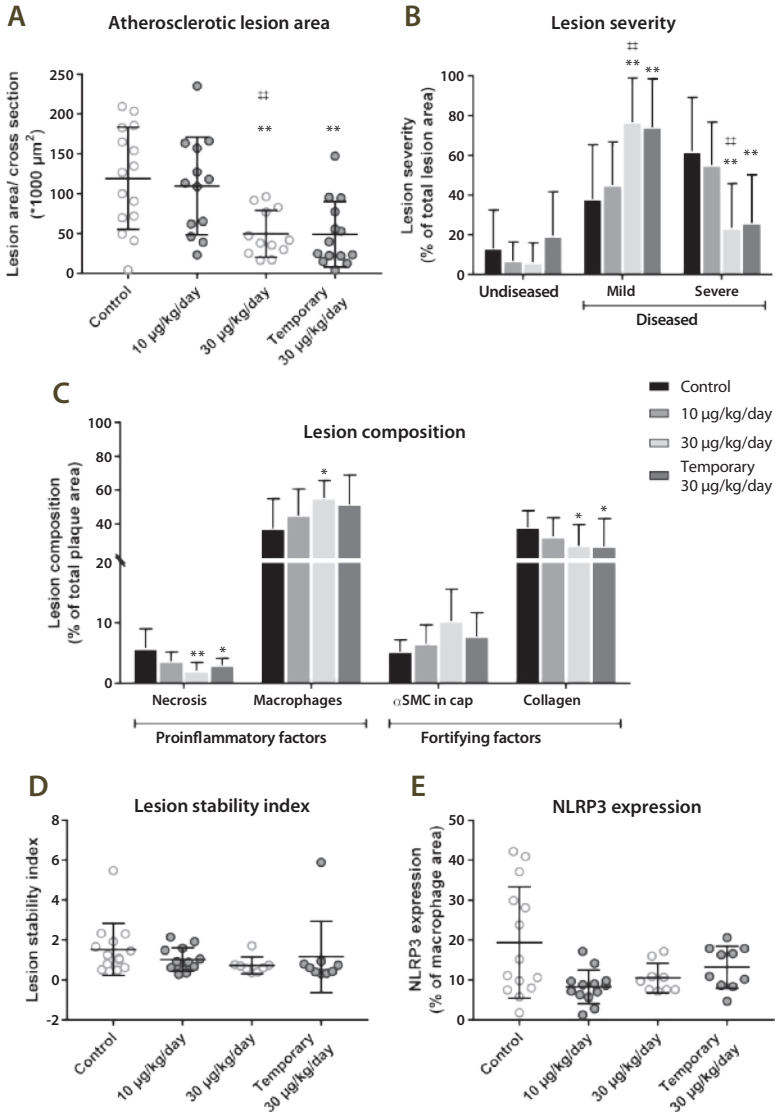

Figure 5 OSM reduces lesion size and severity in APOE*3-Leiden.CETP mice. The atherosclerotic lesion size was determined in the aortic root area (A) and the lesions were classified as mild (type I-III) or severe (IV and V) lesions (B). Furthermore, the amount of necrosis, macrophages, smooth muscle cells and collagen was quantified (C) and the lesion stability index was calculated by dividing the summed proportions of SMCs and collagen, as stabilizing factors, by the summed proportions of necrosis and macrophages, as destabilizing factors (D). Additionally, the amount of NLRP3 expression was examined as percentage of the macrophage area (E). Data represent mean ± SD (n=9-15). *p<0.05 **p<0.01 compared to control; ‡‡ p<0.01 compared to 10 µg/kg/day.

respectively. Again, the 16 week 10 µg/kg/day OSM treatment group did not differ from the control group. In line with plaque area, we observed a dose-dependent decrease in lesion severity (p=0.003) (**Figure 5B**). Collectively, these results show that early continuous exposure to OSM reduces atherosclerotic lesion size and severity independently from plasma cholesterol in APOE*3-Leiden.CETP mice.

OSM has no effect on the stability of severe lesions in APOE*3-Leiden.CETP mice

To assess the effect of OSM treatment on plaque stability of the severe lesions, we determined the amount of necrosis and macrophages, as indicators of unstable plaques and the amount of SMCs and collagen, as indicators of stable plaques (**Figure 5C**) in the severe lesions. Lesions in the control group consisted of 6 ± 3% necrosis, 37 ± 18% macrophages, 5 ± 2% SMCs and 38 ± 10% collagen. The amount of necrosis was decreased to 3 ± 1% in the 5.5 week 30 µg/kg/day OSM group (p=0.012) and to 2 ± 1% in the 16 week 30 µg/kg/day OSM group (p=0.01), while the macrophage content was slightly increased in the 16 week 30 µg/kg/day OSM group (55 ± 10%) (p=0.016) only. The collagen content was decreased in the 5.5 week 30 µg/kg/day OSM group to 28 ± 17% (p=0.012) and to 27 ± 13% in the 16 week 30 µg/kg/day OSM group (p=0.018). No difference was observed in SMC content. The plaque composition of the 16 week 10 µg/kg/day OSM group was similar as in the control group. No differences were observed in the plaque stability ratio between the control and OSM treated groups (**Figure 5D**). As the amount of macrophages is not necessarily a measure for macrophage activity, we measured the expression of the caspase-1-activating inflammasome protein NLRP3 as marker of macrophage activation (26). No significant difference was observed in NLRP3 expression in the plaque area (**Figure 5E**). In conclusion, although OSM does affect lesion composition by slightly increasing the amount of macrophages and decreasing the amount of necrosis and collagen, it does not affect overall plaque stability of the severe lesions.

OSM reduces the inflammatory Ly-6CHigh monocyte subset

No difference in the percentage of circulating CD11b+ cells was observed between the groups (**Figure 6A**). As the Ly-6C^{High} monocyte subset is linked to atherosclerosis development (27), we investigated the effect of OSM on the circulating monocyte subtype composition (**Figure 7**). In the control group 20.8 ± 6.5% of the monocytes belonged to the Ly-6C^{High} subset and 79.2 ± 6.5% to the Ly-6C$^{Low+Intermediate}$ subset. The amount of Ly-6C^{High} monocytes was decreased to 13.2 ± 3.8% in the 16 week 30 µg/kg/day OSM group (p=0.004) and the amount of Ly-6C$^{Low+Intermediate}$ monocytes increased to 86.8 ± 3.8% (p=0.004) (**Figure 6B and C**). The Ly-6C^{High} subset showed a positive correlation with lesion size (r=0.303, p=0.029), supporting a role of the Ly-6C^{High} monocytes in the development of atherosclerosis (**Figure 6D**). Thus, OSM decreases the percentage of Ly-6C^{High} monocytes which may contribute to the smaller atherosclerotic lesion size.

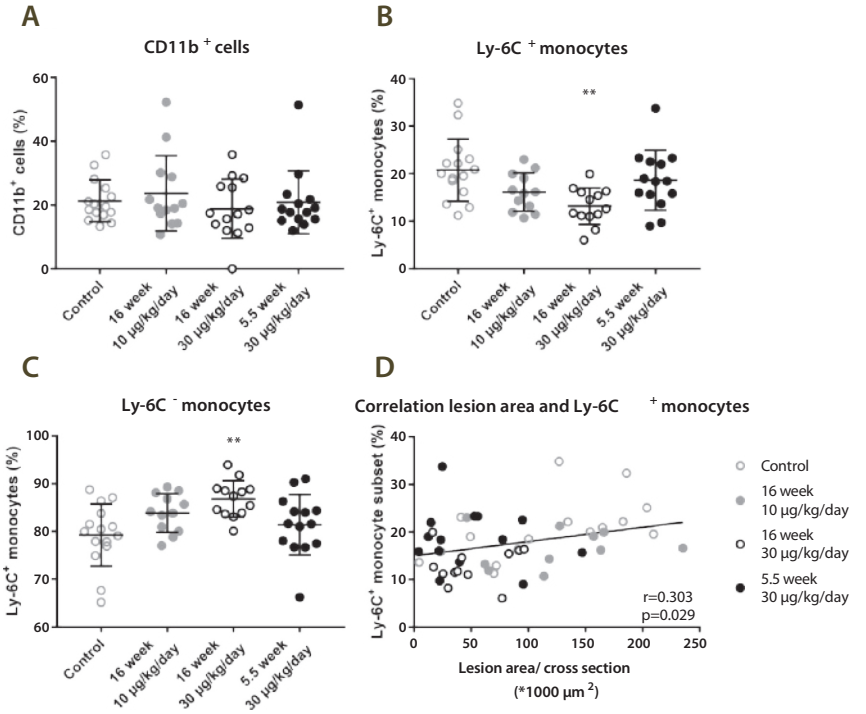

Figure 6 OSM reduces the percentage of circulating Ly-6C^{High} monocytes. No difference in percentage of CD11b+ cells was observed between the groups (A). But, APOE*3-Leiden.CETP mice treated with OSM have a higher percentage of circulating Ly-6C^{High} monocytes (B) and a lower percentage of circulating Ly-6C$^{Low+Intermediate}$ monocytes (C). The percentage of Ly-6C^{High} monocytes was correlated with an increased lesion size (D). Data represent mean ± SD (n=12-20). **p<0.01 compared to control.

Serum OSM levels are associated with increased post incident CHD in humans

We next explored if variable levels of OSM in the human circulation were associated with survival probability in the AGES-Reykjavik study. We found that higher serum OSM levels were associated with increased survival probability post incident CHD (HR=0.838, p=2*10^{-6}) (**Figure 8A**), also using adjusted survival curves for the Cox model (28) (**Figure 8B**). Thus, elevated levels of OSM predicted reduced mortality in humans.

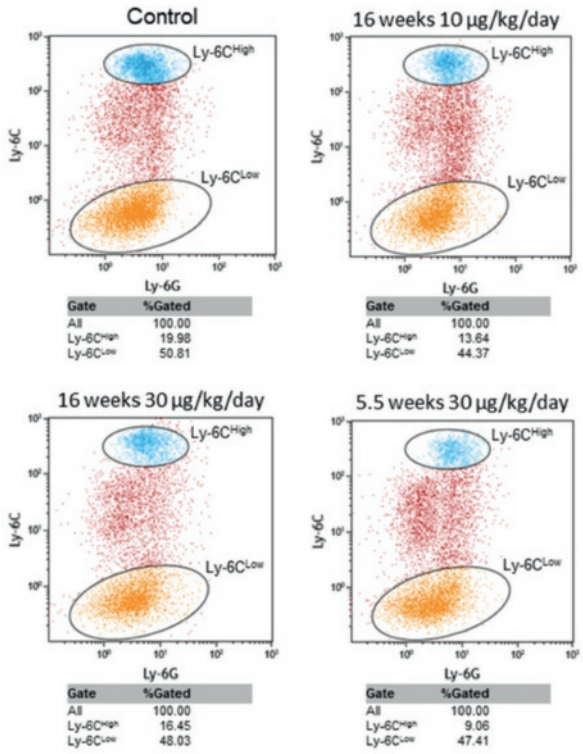

Figure 7 Representative pictures of the distribution of the Ly-6C monocyte subsets. Based on the Ly-6C expression, monocytes were distributed into 3 monocyte subsets, the Ly-6C^{Low}, Ly-6C^{Intermediate} and Ly-6C^{High} monocyte subset.

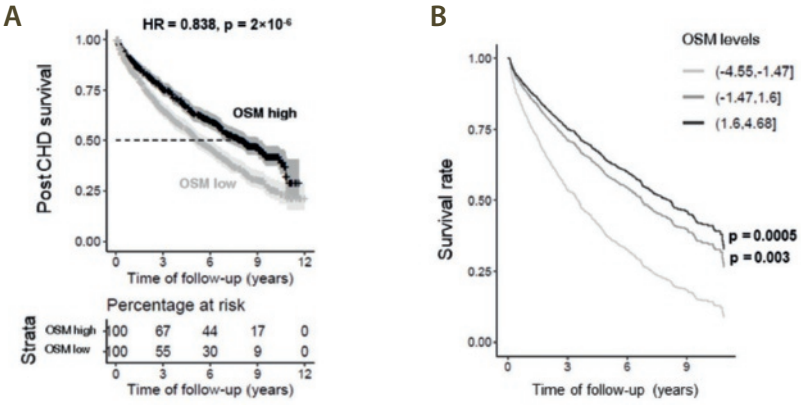

Figure 8 High OSM is associated with reduced post CHD mortality. Serum OSM levels of CHD patients were significantly associated with CHD related mortality rates when comparing the lower 25% quantile to the upper 75% quantile in OSM levels (hazard ratio (HR)=0.838, $p=2*10^{-6}$) (A), and in the adjusted survival curves for the Cox model for three groups of OSM protein levels (top vs. bottom HR=0.618, p=0.0005) (B).

Discussion

In the present study, we showed that mRNAs coding for OSM as well as its receptors, OSMR and LIFR, were expressed in human normal arteries and carotid atherosclerotic plaques. We demonstrated that serum OSM levels in humans were positively correlated with several but not with other well-known markers of endothelial activation. Chronic OSM administration to APOE*3-Leiden.CETP mice reduced atherosclerotic lesion size and severity even after initial priming. In line with these data, increased OSM levels in humans were associated with decreased post incident CHD mortality.

Extending the previous finding by Albasanz-Puig et al (13), who showed that OSM is present in both human and murine atherosclerotic plaques, we here demonstrated the presence of OSMR and LIFR mRNA in human normal and atherosclerotic arteries as well. The relatively higher OSMR and LIFR expression in normal arteries compared to atherosclerotic arteries may be explained by the high expression of the receptors on endothelial and vascular SMCs (8,29). These cells make up a relatively large proportion of the normal artery, but less of the atherosclerotic plaque, in which there is influx and proliferation of inflammatory cells, which might dilute OSMR and LIFR expression. The opposite can be reasoned for the increased OSM expression in atherosclerotic arteries, as OSM is mainly produced by activated macrophages and neutrophils (5,6,30). Moreover, OSMR and LIFR expression may be downregulated in endothelial and SMCs in plaques compared to

endothelial and SMCs in normal arteries. Besides, the chronic inflammatory state during atherosclerosis development drives vascular SMC differentiation, which reduces the expression of SMC specific markers (31) and may therefore also reduce expression of LIFR and OSMR. This contention is in line with our observation that OSM is negatively correlated with SMC markers and with Kakutani et al., who showed that OSM induces SMC differentiation (4).

The correlation of OSM with IL-6 and VCAM-1 in the AGES-Reykjavik study is in line with previous findings in vitro (10). However, the inverse association of OSM with E-selectin and ICAM-1 contradicts with previous data showing increased levels induced by OSM in human endothelial cells in vitro (10) and increased serum E-selectin levels in APOE*3-Leiden. CETP mice. The absence of a positive correlation between OSM and ICAM-1, E-selectin and P-selectin may be caused by statin use in the AGES-Reykjavik study (approx. 22%) (21), as statins reduce ICAM-1, E-selectin and P-selectin plasma levels in patients with coronary artery disease (32). Regardless, mice treated with OSM in the present study did show increased serum E-selectin levels which dropped after discontinuation of OSM treatment, indicating a causal relationship between OSM and E-selectin in vivo in mice.

As our present study had a much longer duration than previous intervention studies with OSM in mice (9,10), we first verified if the previously observed short-term inflammatory state (10) is also present after 16 weeks of OSM administration. OSM increased plasma E-selectin levels and monocyte adhesion in the aortic root area, similarly as in our previous study (10), indicating that OSM induces a sustained inflammatory state even after long-term OSM treatment. Although inflammation has been reported to contribute to atherosclerosis development (33), our results show, to our knowledge for the first time, that long-term chronic OSM treatment independently of cholesterol-lowering, results in significantly smaller and less severe atherosclerotic lesions in APOE*3-Leiden.CETP mice, clearly indicating that prolonged exposure to OSM has anti-atherogenic effects. Previously, Zhang et al., using a different approach, showed that OSMR deficient ApoE$^{-/-}$ mice have smaller and more stable plaques than their OSMR expressing littermates (14), suggesting that signaling via the LIFR alone or prevention of IL-31 and OSM signaling through OSMR (34) has a similar beneficial effect.

No difference was observed in the lesion stability index, and although we observed a slight increase in the amount of macrophages as percentage of the total plaque area, the amount of NLRP3 expression was very low and did not differ between any of the groups, indicating that the pro-inflammatory macrophage activity was not affected (26). In line with this, the percentage of pro-inflammatory Ly-6C^{High} monocytes (35) was decreased and the percentage of non-inflammatory Ly-6C$^{Low+Intermediate}$ monocytes, which actively patrol the luminal site of the endothelium where they remove debris and damaged cells and are associated with reparative processes (35), was increased in OSM treated mice. The decrease in Ly-6C^{High} monocytes plausibly contributes to the reduced amount of macrophages and the attenuated atherosclerosis development.

Although our findings are counter-intuitive with several previously described pro-inflammatory characteristics of OSM (9,36), they are in line with studies addressing the anti-inflammatory properties of OSM. It has been shown that OSM administration suppresses TNFα (37) and IL-1β release in vitro (38), whereas TNFα, IL-1β and IFN-γ expression is increased in adipose tissue of OSMR knockout mice (39). Both cytokines are involved in atherosclerosis progression in mice as TNFα promotes atherosclerosis (40) and IL-1β knockout mice have smaller and less severe atherosclerotic lesions (41). In humans, anti-inflammatory treatments targeting TNFα or IL-1β are associated with decreased risk of myocardial infarction and overall cardiovascular events (42,43). Collectively, these and our data indicate that OSM has anti-inflammatory effects as well which may contribute to its anti-atherogenic properties. Moreover, OSM has been reported to induce endothelial proliferation (12,44) and to increase expression of adhesion molecules that bind endothelial progenitor cells (45,46), suggesting that OSM stimulates replacement of leaky, dysfunctional endothelial cells by new and healthy endothelial cells (47) and may therefore attenuate atherogenesis in the initial stages of the disease. This contention is in line with our finding that mice treated with OSM for only 5.5 weeks had a similar lesion size and severity as mice receiving OSM during a 16 week period and suggests that the observed anti-atherogenic effects of OSM have taken place during the initial stages of atherosclerosis development. Furthermore, although the observed increase in SMCs observed in this study was not significant, others have reported that OSM significantly enhances SMC proliferation in vitro (13), which is a contributor to a stable plaque phenotype (48). To conclude, OSM may contribute to attenuation of plaque development and improvement of plaque severity by: (I) its anti-inflammatory properties, (II) regenerating the endothelial barrier, (III) induction of SMC proliferation, and (IV) reducing the pro-inflammatory monocyte phenotype and promoting a more regenerative phenotype (48).

The anti-atherogenic effect of OSM in APOE*3-Leiden.CETP mice is consistent with the increased post incident CHD survival probability in humans with higher OSM levels in the AGES-Reykjavik study. Similarly, OSM treatment increased survival in a mouse injury model of acute myocardial infarction (49), emphasizing the regenerative properties of this cytokine (44,50).

As OSM has been suggested to have a progressive effect in chronic inflammatory diseases such as, rheumatoid arthritis (RA) (51) and inflammatory bowel disease (36,52), it has been proposed as a possible pharmaceutical target to suppress inflammation in these diseases (36,51,52) and the effect of anti-OSM treatment in RA has already been investigated in a phase 2 clinical trial (51). However, considering the anti-atherogenic effects and positive effect of OSM on survival in the present study, we strongly recommend that cardiovascular disease markers and survival are carefully monitored when testing an OSM inhibiting approach. In addition, since this study shows that OSM has beneficial immune modulating effects, the role of OSM in inflammatory diseases possibly needs to be reconsidered.

Taken together, our study provides more insight into the role of OSM in atherosclerosis development. APOE*3-Leiden.CETP mice treated with OSM had smaller and less severe plaques associated with a decrease in pro-inflammatory Ly-6C^{High} monocytes. In line with the favorable effect in mice, we found an increased survival probability in humans that have high OSM levels, suggesting an atheroprotective effect for OSM.

Acknowledgements

The authors thank Anouska Borgman (Quorics), Eveline Gart (TNO), Christa de Ruiter (TNO) and Joline Attema (TNO), for their excellent technical assistance and contribution to the data collection.

Disclosures

Nothing to disclose.

Funding

This work was supported by the European Union Seventh Framework Programme (FP7/2007-2013) [grant number 602936] (CarTarDis project). The funders had no role in study design, data collection and analysis, decision to publish, or preparation of the manuscript. Quorics B.V provided support in the form of salaries for authors DVK and DT, and Molecular Profiling Consulting provided salary for MDSG but did not have any additional role in the study design, data collection and analysis, decision to publish, or preparation of the manuscript.

References

1. Ramji DP, Davies TS. Cytokines in atherosclerosis: Key players in all stages of disease and promising therapeutic targets. Cytokine Growth Factor Rev. 2015 Dec;26(6):673–85.
2. McLaren JE, Michael DR, Ashlin TG, et al. Cytokines, macrophage lipid metabolism and foam cells: implications for cardiovascular disease therapy. Prog Lipid Res. 2011 Oct;50(4):331–47.
3. Schnittker D, Kwofie K, Ashkar A, et al. Oncostatin M and TLR-4 ligand synergize to induce MCP-1, IL-6, and VEGF in human aortic adventitial fibroblasts and smooth muscle cells. Mediators Inflamm. 2013;2013:317503.
4. Kakutani Y, Shioi A, Shoji T, et al. Oncostatin M Promotes Osteoblastic Differentiation of Human Vascular Smooth Muscle Cells Through JAK3-STAT3 Pathway. J Cell Biochem. 2015 Jul;116(7):1325–33.
5. Shioi A, Katagi M, Okuno Y, et al. Induction of bone-type alkaline phosphatase in human vascular smooth muscle cells: roles of tumor necrosis factor-alpha and oncostatin M derived from macrophages. Circ Res. 2002 Jul;91(1):9–16.
6. Hurst SM, McLoughlin RM, Monslow J, et al. Secretion of oncostatin M by infiltrating neutrophils: regulation of IL-6 and chemokine expression in human mesothelial cells. J Immunol. 2002 Nov;169(9):5244–51.
7. Thoma B, Bird TA, Friend DJ, et al. Oncostatin M and leukemia inhibitory factor trigger overlapping and different signals through partially shared receptor complexes. J Biol Chem. 1994 Feb;269(8):6215–22.
8. Brown TJ, Rowe JM, Liu JW, et al. Regulation of IL-6 expression by oncostatin M. J Immunol. 1991 Oct;147(7):2175–80.
9. Modur V, Feldhaus MJ, Weyrich AS, et al. Oncostatin M is a proinflammatory mediator. In vivo effects correlate with endothelial cell expression of inflammatory cytokines and adhesion molecules. J Clin Invest. 1997 Jul;100(1):158–68.
10. van Keulen D, Pouwer MG, Pasterkamp G, et al. Inflammatory cytokine oncostatin M induces endothelial activation in macro- and microvascular endothelial cells and in APOE*3Leiden.CETP mice. PLoS One. 2018;13(10):e0204911.
11. Takata F, Sumi N, Nishioku T, et al. Oncostatin M induces functional and structural impairment of blood-brain barriers comprised of rat brain capillary endothelial cells. Neurosci Lett. 2008 Aug;441(2):163–6.
12. Vasse M, Pourtau J, Trochon V, et al. Oncostatin M induces angiogenesis in vitro and in vivo. Arterioscler Thromb Vasc Biol. 1999 Aug;19(8):1835–42.
13. Albasanz-Puig A, Murray J, Preusch M, et al. Oncostatin M is expressed in atherosclerotic lesions: a role for Oncostatin M in the pathogenesis of atherosclerosis. Atherosclerosis. 2011 Jun;216(2):292–8.
14. Zhang X, Li J, Qin J-J, et al. Oncostatin M receptor beta deficiency attenuates atherogenesis by inhibiting JAK2/STAT3 signaling in macrophages. J Lipid Res. 2017 May;58(5):895–906.
15. Dewey FE, Gusarova V, Dunbar RL, et al. Genetic and Pharmacologic Inactivation of ANGPTL3 and Cardiovascular Disease. N Engl J Med. 2017 Jul;377(3):211–21.
16. Perisic L, Aldi S, Sun Y, et al. Gene expression signatures, pathways and networks in carotid atherosclerosis. J Intern Med. 2016 Mar;279(3):293–308.
17. van Dijk RA, Virmani R, von der Thusen JH, et al. The natural history of aortic atherosclerosis: a systematic histopathological evaluation of the peri-renal region. Atherosclerosis. 2010 May;210(1):100–6.
18. Aldi S, Matic LP, Hamm G, et al. Integrated Human Evaluation of the Lysophosphatidic Acid Pathway as a Novel Therapeutic Target in Atherosclerosis. Mol Ther Methods Clin Dev. 2018 Sep;10:17–28.
19. Anderson CM, Zhang B, Miller M, et al. Fully Automated RNAscope In Situ Hybridization Assays for Formalin-Fixed Paraffin-Embedded Cells and Tissues. J Cell Biochem. 2016 Oct;117(10):2201–8.
20. Harris TB, Launer LJ, Eiriksdottir G, et al. Age, Gene/Environment Susceptibility-Reykjavik Study: multidisciplinary applied phenomics. Am J Epidemiol. 2007 May;165(9):1076–87.
21. Emilsson V, Ilkov M, Lamb JR, et al. Co-regulatory networks of human serum proteins link genetics to disease. Science. 2018 Aug;361(6404):769–73.
22. Kuhnast S, van der Hoorn JWA, Pieterman EJ, et al. Alirocumab inhibits atherosclerosis, improves the plaque morphology, and enhances the effects of a statin. J Lipid Res. 2014 Oct;55(10):2103–12.
23. Kuhnast S, van der Hoorn JWA, van den Hoek AM, et al. Aliskiren inhibits atherosclerosis development and improves plaque stability in APOE*3Leiden.CETP transgenic mice with or without treatment with atorvastatin. J Hypertens. 2012 Jan;30(1):107–16.

24. Stary HC, Chandler AB, Dinsmore RE, et al. A definition of advanced types of atherosclerotic lesions and a histological classification of atherosclerosis. A report from the Committee on Vascular Lesions of the Council on Arteriosclerosis, American Heart Association. Circulation. 1995 Sep;92(5):1355–74.
25. Landlinger C, Pouwer MG, Juno C, et al. The AT04A vaccine against proprotein convertase subtilisin/kexin type 9 reduces total cholesterol, vascular inflammation, and atherosclerosis in APOE*3Leiden.CETP mice. Eur Heart J. 2017 Aug;38(32):2499–507.
26. Awad F, Assrawi E, Jumeau C, et al. Impact of human monocyte and macrophage polarization on NLR expression and NLRP3 inflammasome activation. PLoS One. 2017;12(4):e0175336.
27. Hanna RN, Shaked I, Hubbeling HG, et al. NR4A1 (Nur77) deletion polarizes macrophages toward an inflammatory phenotype and increases atherosclerosis. Circ Res. 2012 Feb;110(3):416–27.
28. Therneau TM, Crowson CS, Atkinson EJ. No Adjusted Survival Curves [Internet]. 2015. Available from: https://cran.r-project.org/web/packages/survival/vignettes/adjcurve.pdf
29. Demyanets S, Kaun C, Rychli K, et al. The inflammatory cytokine oncostatin M induces PAI-1 in human vascular smooth muscle cells in vitro via PI 3-kinase and ERK1/2-dependent pathways. Am J Physiol Heart Circ Physiol. 2007 Sep;293(3):H1962-8.
30. Guihard P, Boutet M-A, Brounais-Le Royer B, et al. Oncostatin m, an inflammatory cytokine produced by macrophages, supports intramembranous bone healing in a mouse model of tibia injury. Am J Pathol. 2015 Mar;185(3):765–75.
31. Chistiakov DA, Orekhov AN, Bobryshev Y V. Vascular smooth muscle cell in atherosclerosis. Acta Physiol (Oxf). 2015 May;214(1):33–50.
32. Seljeflot I, Tonstad S, Hjermann I, et al. Reduced expression of endothelial cell markers after 1 year treatment with simvastatin and atorvastatin in patients with coronary heart disease. Atherosclerosis. 2002 May;162(1):179–85.
33. Libby P. Inflammation in atherosclerosis. Arterioscler Thromb Vasc Biol. 2012 Sep;32(9):2045–51.
34. Zhang Q, Putheti P, Zhou Q, et al. Structures and biological functions of IL-31 and IL-31 receptors. Cytokine Growth Factor Rev. 2008;19(5–6):347–56.
35. Thomas G, Tacke R, Hedrick CC, et al. Nonclassical patrolling monocyte function in the vasculature. Arterioscler Thromb Vasc Biol. 2015 Jun;35(6):1306–16.
36. West NR, Hegazy AN, Owens BMJ, et al. Oncostatin M drives intestinal inflammation and predicts response to tumor necrosis factor-neutralizing therapy in patients with inflammatory bowel disease. Nat Med. 2017 May;23(5):579–89.
37. Wahl AF, Wallace PM. Oncostatin M in the anti-inflammatory response. Ann Rheum Dis. 2001 Nov;60 Suppl 3:iii75-80.
38. Dumas A, Lagarde S, Laflamme C, et al. Oncostatin M decreases interleukin-1 beta secretion by human synovial fibroblasts and attenuates an acute inflammatory reaction in vivo. J Cell Mol Med. 2012 Jun;16(6):1274–85.
39. Komori T, Morikawa Y. Oncostatin M in the development of metabolic syndrome and its potential as a novel therapeutic target. Anat Sci Int. 2018 Mar;93(2):169–76.
40. Boesten LSM, Zadelaar ASM, van Nieuwkoop A, et al. Tumor necrosis factor-alpha promotes atherosclerotic lesion progression in APOE*3-Leiden transgenic mice. Cardiovasc Res. 2005 Apr;66(1):179–85.
41. Kirii H, Niwa T, Yamada Y, et al. Lack of interleukin-1beta decreases the severity of atherosclerosis in ApoE-deficient mice. Arterioscler Thromb Vasc Biol. 2003 Apr;23(4):656–60.
42. Low ASL, Symmons DPM, Lunt M, et al. Relationship between exposure to tumour necrosis factor inhibitor therapy and incidence and severity of myocardial infarction in patients with rheumatoid arthritis. Ann Rheum Dis. 2017 Apr;76(4):654–60.
43. Ridker PM, Everett BM, Thuren T, et al. Antiinflammatory Therapy with Canakinumab for Atherosclerotic Disease. N Engl J Med. 2017 Sep;377(12):1119–31.
44. Zhang X, Zhu D, Wei L, et al. OSM Enhances Angiogenesis and Improves Cardiac Function after Myocardial Infarction. Biomed Res Int. 2015;2015:317905.
45. Zampetaki A, Kirton JP, Xu Q. Vascular repair by endothelial progenitor cells. Cardiovasc Res. 2008 Jun;78(3):413–21.
46. Modur V, Li Y, Zimmerman GA, et al. Retrograde inflammatory signaling from neutrophils to endothelial cells by soluble interleukin-6 receptor alpha. J Clin Invest. 1997 Dec;100(11):2752–6.
47. Du F, Zhou J, Gong R, et al. Endothelial progenitor cells in atherosclerosis. Front Biosci (Landmark Ed. 2012 Jun;17:2327–49.

48. Finn A V, Nakano M, Narula J, et al. Concept of vulnerable/unstable plaque. Arterioscler Thromb Vasc Biol. 2010 Jul;30(7):1282–92.
49. Kubin T, Poling J, Kostin S, et al. Oncostatin M is a major mediator of cardiomyocyte dedifferentiation and remodeling. Cell Stem Cell. 2011 Nov;9(5):420–32.
50. Nakamura K, Nonaka H, Saito H, et al. Hepatocyte proliferation and tissue remodeling is impaired after liver injury in oncostatin M receptor knockout mice. Hepatology. 2004 Mar;39(3):635–44.
51. Choy EH, Bendit M, McAleer D, et al. Safety, tolerability, pharmacokinetics and pharmacodynamics of an anti-oncostatin M monoclonal antibody in rheumatoid arthritis: results from phase II randomized, placebo-controlled trials. Arthritis Res Ther. 2013 Sep;15(5):R132.
52. Kim WM, Kaser A, Blumberg RS. A role for oncostatin M in inflammatory bowel disease. Nat Med. 2017 May;23(5):535–6.

10

General discussion and future perspectives

General discussion and future perspectives

Cardiovascular disease (CVD) is currently globally the major cause of mortality and morbidity, and 85% of all CVD deaths are caused by the formation of atheromatous plaques in the vessels, leading to ischemic heart disease, ischemic stroke and peripheral arterial disease (1). The build-up of an atherosclerotic plaque is a slow process that starts with accumulation of low-density lipoproteins (LDL) into the intima and subsequent the recruitment of inflammatory cells (2). Chronic exposure to cardiovascular risk factors, such as hypertension, smoking, dyslipidemia and diabetes (3), can increase the rate and severity of atherosclerosis. Primary prevention of CVD is achieved through early identification and modification of 'lifestyle risk factors', eventually in combination with interventions to reduce plasma lipids or blood pressure (4). These strategies slow disease progression but do not heal, shifting CVD into a chronic disease. This thesis described a variety of studies that aimed to reduce CVD risk by (I) evaluation of novel lipid-lowering interventions to prevent or regress atherosclerosis development, (II) identification of CV side-effects of registered drugs and an environmental pollutant, (III) development of a novel animal model combining dyslipidemia and diabetes, and (IV) evaluation of the cytokine oncostatin M (OSM) as potential target for CVD.

Mouse models have been extensively used for the study of CVD and permit experimental conditions to be controlled. Moreover, preclinical models enable the investigation of molecular and pathophysiological mechanisms and provide platforms for the development and evaluation of novel pharmaceuticals. Disadvantages are differences in lipoprotein metabolism between commonly used mouse models and man (5), which hamper the translation of preclinical findings to valuable clinical applications. All studies described in this thesis used the APOE*3-Leiden(.CETP) mouse as model for diet-induced hyperlipidemia and experimental atherosclerosis. These mice were initially developed as an animal model for Familial Dysbetalipoproteinemia (FD) or type III hyperlipoproteinemia, and were generated by the introduction of a DNA-construct containing the human *APOE*3LEIDEN* and *APOC1* genes (6,7). Subsequent insertion of the *CETP* gene (8), encoding for cholesteryl ester transfer protein (CETP) that transfers cholesteryl esters from high-density lipoprotein (HDL) to apolipoprotein-B (apoB)-containing lipoproteins in exchange for triglyceride(TG), generated an animal model with a lipoprotein metabolism representative for the human situation with a delayed clearance of apoB-containing particles and CETP expression (8). These mice have been widely used for the evaluation of lipid-lowering interventions and consistently demonstrated their translatable value (9–11).

Proprotein convertase subtilisin kexin 9 (PCSK9) was discovered in 2003 (12) as the major down-regulator of the LDL-receptor and to date, PCSK9 inhibition is among the most powerful strategies to target LDL-C. Two monoclonal antibodies against PCSK9, evolocumab and alirocumab, are currently available in the clinic, and several innovative strategies to modulate PCSK9 levels are under development (12). One approach is

activation of the immune system to eliminate endogenous circulating PCSK9 using PCSK9-peptide-based vaccines. In **Chapter 2** we evaluated such a vaccine and found that immunization induces a strong and long-lasting immune response resulting in reduced plasma levels of PCSK9, total cholesterol (TC) and non-high-density lipoprotein-cholesterol (non-HDL-C), as well as markers of systemic inflammation. Furthermore, atherosclerotic lesion progression and vascular inflammation was reduced. Preliminary data in healthy subjects showed that immunization was safe and well-tolerated. More than 90% of the subjects developed a PCSK9 specific antibody response with a mean LDL-C reduction of 13.3% at week 70 (13). This novel vaccine may have a future role in lowering LDL-C beginning in early adulthood to reduce lifetime risk of CV events, since Mendelian randomization studies have suggested that prolonged exposure to lower LDL-C beginning early in life is associated with a substantially greater reduction in the risk of CVD than the current practice of lipid-lowering beginning later in life (14). The advantage of vaccination over chronic treatment with antibodies to achieve long-term LDL-C reductions is the less frequent application which may enhance tolerability, drug adherence and cost-effectiveness (15). Another advantage is the potential to combine the anti-PCSK9 epitope with epitopes of different potential targets for LDL-C lowering, for instance ANGPTL3, apoC3 or lipoprotein(a). Preventive immunization against viruses/bacteria have been successfully used for decades and is widely accepted, and numerous therapeutic cancer vaccine strategies have been developed or are currently under development (16). Also, two vaccines for hypertension and hyperglycemia are under development (17). These advances demonstrate the possibilities of immunization, which might become an important approach in future preventive medicine. Importantly, regarding the more permanent approach of active immunization, it is crucial to exclude side-effects to ensure a safe application of the vaccine in the future.

Most preclinical studies evaluated novel lipid-lowering interventions in a progression setting, including our study with the PCSK9 vaccine. However, most patients start their treatment when atherosclerosis has already developed and therefore, strategies focusing on regression of pre-existing lesions are warranted. In **Chapter 3** we evaluated whether gradual and aggressive reduction of cholesterol in both LDL and remnant lipoproteins by antibodies against PCSK9 (alirocumab) and/or angiopoietin like 3 protein (ANGPTL3) (evinacumab) on top of atorvastatin could regress experimental atherosclerosis. In this study, alirocumab and evinacumab similarly reduced non-HDL-C levels and fully blocked atherosclerosis progression when administered on top of atorvastatin. In addition, plaque stability was improved, as evidenced by a decrease in macrophages and an increase in collagen content. When administered in triple combination (alirocumab + evinacumab + atorvastatin) non-HDL-C levels were reduced to 1 mmol/L and atherosclerotic lesions regressed beyond the baseline level. This is the first intervention study in a well-established, translational mouse model for hyperlipidaemia and atherosclerosis showing that high-intensive cholesterol-lowering triple treatment with atorvastatin, alirocumab and

evinacumab regresses lesion size, diminishes macrophage accumulation through reduction of proliferation and improves plaque stability.

Recently, Mendelian randomization studies have demonstrated that the CV risk reduction of TG-lowering *LPL* variants (e.g. ANGPTL3) is similar to the CV risk reduction of LDL-C lowering *LDLR* variants (e.g. PCSK9) per unit apoB change (18). These findings correspond with our observation that alirocumab and evinacumab equally block lesion progression. Clinical trials, including the IMPROVE-IT (ezetimibe) (19), ODYSSEY OUTCOMES (alirocumab) (20,21), and FOURIER (evolocumab) (22) trials, demonstrate that the combination of statin therapy with other non-statin agents has a significantly improved clinical benefit over statin treatment alone. Also, these studies demonstrated that long-term (3 years), high-intensive cholesterol lowering with anti-PCSK9 antibodies on top of atorvastatin did not adversely affect new-onset of diabetes, diabetes worsening, hepatic disorders and neurocognitive disorders (23). The present data in APOE*3-Leiden.CETP mice provide evidence that combined lowering of LDL and remnant lipoproteins on top of a statin further reduce CV risk. The efficacy and safety of this combination strategy should be confirmed in clinical trials. Alirocumab is approved by the FDA and EMA for heterozygous Familial Hypercholesterolemia (FH) patients or those with clinical atherosclerotic CVD who require additional lowering of LDL-C as an adjunct to diet and maximally tolerated statin therapy (24). Evinacumab is currently being evaluated in phase II trials for patients with severe hypertriglyceridemia (NCT03452228) and persistent hypercholesterolemia (NCT03175367) and in phase III trials for patients with homozygous FH (NCT03399786 and NCT03409744).

Unexpected cardiovascular toxicities in patients receiving approved anti-cancer treatments are common and have been observed during active treatment as well as in cancer survivors (25). In **Chapter 4**, we explored the etiology of the toxic cardiovascular side-effects of BCR-ABL1 tyrosine kinase inhibitors (TKIs), used for the treatment of chronic myeloid leukemia (CML) patients. While the first line TKI imatinib has proven to be effective and safe, the second and third line nilotinib and ponatinib, respectively, increase the prevalence of myocardial infarction, peripheral arterial occlusive disease and ischemic cerebrovascular events pointing to pro-atherosclerotic, pro-thrombotic or combined effects (26–28). Using APOE*3-Leiden.CETP mice, we found that nilotinib and ponatinib enhance mRNA expression of coagulation factors of both the contact activation (intrinsic) and tissue factor (extrinsic) pathways and increase plasma levels of FVII (ponatinib) and activity of FVIIa (nilotinib), important players in the pathogenesis of atherothrombotic events. Also, we observed a reduction in plasma lipids and atherosclerosis development with imatinib and ponatinib. In **Chapter 5** we investigated the mechanism behind the observed lipid alterations and found that imatinib decreased plasma TC and TG levels by reduction of the very-low-density-lipoprotein (VLDL)-apoB-particle production and cholesterol ester content of the VLDL particles, while ponatinib reduced plasma TC levels by lowering intestinal lipid absorption. Our findings correspond with the lipid-modulating

effects (29–32) and improved cardiovascular outcome (33) of imatinib. In addition, our data provide evidence that nilotinib and ponatinib do not enhance atherosclerosis, but increase coagulability. Patients that suffered from cardiovascular side-effects upon nilotinib and ponatinib treatment commonly presented cardiovascular risk factors (27). Therefore, we propose that the pro-thrombotic effects of nilotinib and ponatinib as found in our study may aggravate a pre-existing atherothrombotic condition. In addition to our findings on coagulation, several reports using *in vivo* or *ex vivo* approaches found pro-thrombotic properties of nilotinib (34,35) and ponatinib (36) via other mechanisms (e.g. platelet aggregation, increased expression of von Willebrandt factor, thrombus growth). Moreover, hematological malignancies increase plasma tissue factor levels (37,38), which further potentiates the pro-thrombotic state. These observations underline the importance to select and monitor CML-patients that have the potential to develop atherothrombotic cardiovascular disease before application of the drugs, to improve therapy decision and patient care.

In addition to unexpected post-market safety events of registered drugs, environmental pollutants like perfluorooctanoic acid (PFOA) may increase CV risk. Before being phased-out, PFOA was widely used as an emulsifier in the manufacture of fluoropolymers, and as it is extremely stable, it persists in the environment (39). Epidemiological studies have reported positive associations between serum PFOA and total and non-HDL-C (40–46). However, the modest association observed in studies of general populations is inconsistent with the weaker associations reported in more highly exposed workers (47–54). In addition, there is no increased risk for coronary artery disease in these populations when compared to internal reference cohorts (55–57). Therefore, in **Chapter 6** we evaluated the effects of three different doses PFOA, representing environmental, occupational and toxicological exposure, on plasma lipid levels and lipoprotein metabolism using APOE*3-Leiden.CETP mice. We found that PFOA did not alter plasma lipid levels or lipoprotein metabolism at environmentally or occupationally relevant exposure levels. However, when mice were exposed to a toxicological PFOA dose, plasma TC, non-HDL-C and TG levels were decreased and HDL-C levels were increased. In the latter mice, PFOA decreased VLDL production and increased VLDL clearance by the liver, leading to a reduction of plasma non-HDL-C levels. Moreover, HDL-C levels increased through reduction of CETP activity and changes in gene expression of proteins involved in HDL metabolism. The majority of these changes were mediated by activation of peroxisome proliferator-activated receptor (PPAR)α. Our data correspond with the reduced plasma TC levels observed in a phase I trial in patients that received high doses of PFOA as an antitumor agent (58). In contrast, our findings do not support the increase in cholesterol as found in some observational epidemiological studies, thereby indicating that the reported associations between plasma cholesterol and PFOA exposure are associative rather than causal.

The number of patients with type 2 diabetes is rising and among these patients, cardiovascular complications are the leading cause of morbidity and mortality. Cardiovascular

safety and efficacy of anti-diabetic drugs received increased attention since the FDA and EMA mandated all new diabetes drugs to demonstrate cardiovascular safety (59,60). Preclinical models are used for the development and evaluation of novel drugs, and translational models combining diabetes and cardiovascular disease are required. In **Chapter 7** we described the characteristics of the APOE*3-Leiden.Glucokinase$^{+/-}$ (E3L.GK$^{+/-}$) mouse model, which was generated by cross-breeding the hyperlipidemic APOE*3-Leiden mouse with the hyperglycemic glucokinase knockout (GK$^{+/-}$) mouse. E3L.GK$^{+/-}$ mice had plasma lipid levels comparable to E3L mice and plasma glucose levels comparable to GK$^{+/-}$ mice, leading to enhanced atherosclerosis progression in E3L.GK$^{+/-}$ mice relative to E3L mice, which was predicted by glucose exposure. Since the E3L mouse model responds similarly as humans do to lipid-lowering agents (61–70) and GK$^{+/-}$ mice to anti-diabetic drugs at doses corresponding to therapeutic drug levels in man (71,72), we propose that the E3L.GK$^{+/-}$ mouse is a promising novel diet-inducible disease model for investigation of the etiology and evaluation of drug treatment on diabetic atherosclerosis. Examples of these applications are the evaluation of novel anti-diabetic and anti-atherosclerotic agents and combinations, investigation of the pathophysiological mechanisms behind the cardiovascular adverse (73–75) and beneficial (76,77) effects of some anti-diabetic agents, and the etiology of statin-induced risk for diabetes (78).

The role of cytokines in the initiation and progression of atherosclerosis is increasingly recognized and consequently, novel therapies targeting cytokines (79), including IL-1β with the anti-IL-1β antibody canakinumab (80), are being developed. In **Chapter 8**, we evaluated the role of the cytokine OSM in the initiation of atherosclerosis and found that OSM induced endothelial activation *in vitro* using human endothelial cells from different vascular beds, and *in vivo* using APOE*3-Leiden.CETP mice. Since endothelial activation is an initial step in atherosclerosis development, we proposed that OSM may play a role in the initiation of atherosclerotic lesion formation. However, remarkably, long-term exposure of APOE*3-Leiden.CETP mice to OSM reduced atherosclerotic lesion size and severity, despite enhanced plasma E-selectin levels and monocyte adhesion to the activated endothelium of the aortic root (**Chapter 9**). These findings correspond to our observation that higher serum OSM levels in humans are associated with post-incident coronary heart disease and overall survival probability in the AGES Reykjavik Study, suggesting a protective cardiovascular effect. Interestingly, knockout of the OSMβ receptor in APOE$^{-/-}$ mice also attenuated atherosclerotic lesion size (81). Similar contradictions have been reported regarding the pro- and anti-inflammatory effects of OSM. OSM is associated with inflammatory diseases including lung inflammation, rheumatoid arthritis and multiple sclerosis. Moreover, intradermal injection of, and intranasal exposure to OSM induces accumulation of inflammatory cells. On the other hand, OSM suppresses inflammation in mouse models of inflammatory bowel disease, arthritis, autoimmune encephalomyelitis and multiple sclerosis (82), and it has been suggested that administration of OSM has favorable effects on the metabolic syndrome (82,83). Given the confusing effects of OSM

and its involvement in many biological processes, including tumorigenesis, hematopoiesis, bone and fat turnover, central nervous system development, liver regeneration and inflammatory responses in several tissues (84), further research is required to ensure safe application of potential OSM-related therapies.

Today, we understand better how to treat CVD, but despite these advances, many patients remain at increased cardiovascular risk. In this thesis, we discussed several strategies that may contribute to further risk reduction in the future. The novel lipid-lowering strategies (e.g. vaccination, combination therapy) that have been evaluated in our studies provide evidence that further LDL-C/non-HDL-C lowering and subsequent cardiovascular risk reduction is achievable, which has to be confirmed in clinical trials. Furthermore, we unraveled (part of) the etiology of the cardiovascular safety issues of the TKIs nilotinib and ponatinib and the mechanistic insights provided by our data may contribute to safer application of the drugs to CML-patients. Serum PFOA in environmental and occupational exposed adults had been found to be associated with increased plasma cholesterol, but our data demonstrate that this association is associative rather than causal . Looking forward, we described a novel mouse model, the E3L.GK$^{+/-}$ mouse, that can be used for the study of diabetic macrovascular complications and the evaluation of anti-diabetic drugs. Shifting towards the role of inflammation in atherosclerosis, we evaluated the potential of the cytokine OSM as new target for CVD. In contrast to our hypothesis and evidence provided by the literature, administration of OSM decreased atherosclerotic lesion size, and this confusing observation has to be elucidated before further development of OSM-related treatment strategies.

References

1. WHO. Hearths: technical package for cardiovascular disease mangement in primary health care [Internet]. 2016. Available from: http://www.who.int/cardiovascular_diseases/publications/en/
2. Libby P. Inflammation in atherosclerosis. Arterioscler Thromb Vasc Biol. 2012 Sep;32(9):2045–51.
3. Yusuf S, Hawken S, Ounpuu S, et al. Effect of potentially modifiable risk factors associated with myocardial infarction in 52 countries (the INTERHEART study): case-control study. Lancet (London, England). 2004 Sep;364(9438):937–52.
4. Catapano AL, Graham I, De Backer G, et al. 2016 ESC/EAS Guidelines for the Management of Dyslipidaemias. Eur Heart J. 2016 Oct;37(39):2999–3058.
5. Zadelaar S, Kleemann R, Verschuren L, et al. Mouse models for atherosclerosis and pharmaceutical modifiers. Arterioscler Thromb Vasc Biol. 2007 Aug;27(8):1706–21.
6. van den Maagdenberg AM, Hofker MH, Krimpenfort PJ, et al. Transgenic mice carrying the apolipoprotein E3-Leiden gene exhibit hyperlipoproteinemia. J Biol Chem. 1993 May;268(14):10540–5.
7. de Knijff P, van den Maagdenberg AM, Stalenhoef AF, et al. Familial dysbetalipoproteinemia associated with apolipoprotein E3-Leiden in an extended multigeneration pedigree. J Clin Invest. 1991 Aug;88(2):643–55.
8. Westerterp M, van der Hoogt CC, de Haan W, et al. Cholesteryl ester transfer protein decreases high-density lipoprotein and severely aggravates atherosclerosis in APOE*3-Leiden mice. Arterioscler Thromb Vasc Biol. 2006 Nov;26(11):2552–9.
9. Kuhnast S, Fiocco M, van der Hoorn JWA, et al. Innovative pharmaceutical interventions in cardiovascular disease: Focusing on the contribution of non-HDL-C/LDL-C-lowering versus HDL-C-raising: A systematic review and meta-analysis of relevant preclinical studies and clinical trials. Eur J Pharmacol. 2015 Sep;763(Pt A):48–63.
10. Dewey FE, Gusarova V, Dunbar RL, et al. Genetic and Pharmacologic Inactivation of ANGPTL3 and Cardiovascular Disease. N Engl J Med. 2017 Jul;377(3):211–21.
11. Princen HMG, Pouwer MG, Pieterman EJ. Comment on "Hypercholesterolemia with consumption of PFOA-laced Western diets is dependent on strain and sex of mice" by Rebholz S.L. et al. Toxicol. Rep. 2016 (3) 46-54. Toxicol reports. 2016;3:306–9.
12. Seidah NG, Prat A, Pirillo A, et al. Novel strategies to target proprotein convertase subtilisin kexin 9: beyond monoclonal antibodies. Cardiovasc Res. 2019 Mar;115(3):510–8.
13. Bauer M, Matzneller P, Wulkersdorfer B, et al. Specific Active immunotherapy (SAIT) against PCSK9 is safe and lowers circulating LDL-C in humans. In: Abstract ESC Congress [Internet]. 2018. Available from: https://esc365.escardio.org/Congress/ESC-Congress-2018/Late-Breaking-Pharmacological-Science/181488-sait-specific-active-immunotherapy-sait-against-pcsk9-is-safe-and-lowers-circulating-ldl-c-in-humans#esctv
14. Ference BA, Yoo W, Alesh I, et al. Effect of long-term exposure to lower low-density lipoprotein cholesterol beginning early in life on the risk of coronary heart disease: a Mendelian randomization analysis. J Am Coll Cardiol. 2012 Dec;60(25):2631–9.
15. Kazi DS, Penko J, Coxson PG, et al. Updated Cost-effectiveness Analysis of PCSK9 Inhibitors Based on the Results of the FOURIER Trial. JAMA. 2017 Aug;318(8):748–50.
16. Lopes A, Vandermeulen G, Preat V. Cancer DNA vaccines: current preclinical and clinical developments and future perspectives. J Exp Clin Cancer Res. 2019 Apr;38(1):146.
17. Nakagami H. Design of therapeutic vaccines as a novel antibody therapy for cardiovascular diseases. J Cardiol. 2017 Sep;70(3):201–5.
18. Ference BA, Kastelein JJP, Ray KK, et al. Association of Triglyceride-Lowering LPL Variants and LDL-C-Lowering LDLR Variants With Risk of Coronary Heart Disease. JAMA. 2019 Jan;321(4):364–73.
19. Cannon CP, Blazing MA, Giugliano RP, et al. Ezetimibe Added to Statin Therapy after Acute Coronary Syndromes. N Engl J Med. 2015 Jun;372(25):2387–97.
20. Schwartz GG, Steg PG, Szarek M, et al. Alirocumab and Cardiovascular Outcomes after Acute Coronary Syndrome. N Engl J Med. 2018 Nov;379(22):2097–107.
21. Szarek M, White HD, Schwartz GG, et al. Alirocumab Reduces Total Nonfatal Cardiovascular and Fatal Events: The ODYSSEY OUTCOMES Trial. J Am Coll Cardiol. 2019 Feb;73(4):387–96.
22. Sabatine MS, Giugliano RP, Keech AC, et al. Evolocumab and Clinical Outcomes in Patients with Cardiovascular Disease. N Engl J Med. 2017 May;376(18):1713–22.

23. Jukema JW, Szarek M, Zijlstra LE, et al. Patients with Recent Acute Coronary Syndrome and Polyvascular Disease Derive Large Absolute Benefit from Alirocumab: ODYSSEY OUTCOMES Trial. J Am Coll Cardiol. 2019 Mar;
24. US Food and Drug Administration. FDA approves Praluent to treat certain patients with high cholesterol: first in a new class of injectable cholesterol-lowering drugs. [Internet]. 2015. Available from: www.fda.gov/NewsEvents/Newsroom/PressAnnouncements/ucm455883.htm
25. Turner JR. Integrated cardiovascular safety: multifaceted considerations in drug development and therapeutic use. Expert Opin Drug Saf. 2017 Apr;16(4):481–92.
26. Castagnetti F, Breccia M, Gugliotta G, et al. Nilotinib 300 mg twice daily: an academic single-arm study of newly diagnosed chronic phase chronic myeloid leukemia patients. Haematologica. 2016 Oct;101(10):1200–7.
27. Moslehi JJ, Deininger M. Tyrosine Kinase Inhibitor-Associated Cardiovascular Toxicity in Chronic Myeloid Leukemia. J Clin Oncol. 2015 Dec;33(35):4210–8.
28. Valent P, Hadzijusufovic E, Schernthaner G-H, et al. Vascular safety issues in CML patients treated with BCR/ABL1 kinase inhibitors. Blood. 2015 Feb;125(6):901–6.
29. Gottardi M, Manzato E, Gherlinzoni F. Imatinib and hyperlipidemia. Vol. 353, The New England journal of medicine. United States; 2005. p. 2722–3.
30. Franceschino A, Tornaghi L, Benemacher V, et al. Alterations in creatine kinase, phosphate and lipid values in patients with chronic myeloid leukemia during treatment with imatinib. Vol. 93, Haematologica. Italy; 2008. p. 317–8.
31. Gologan R, Constantinescu G, Georgescu D, et al. Hypolipemiant besides antileukemic effect of imatinib mesylate. Leuk Res. 2009 Sep;33(9):1285–7.
32. Rea D, Mirault T, Cluzeau T, et al. Early onset hypercholesterolemia induced by the 2nd-generation tyrosine kinase inhibitor nilotinib in patients with chronic phase-chronic myeloid leukemia. Haematologica. 2014 Jul;99(7):1197–203.
33. Giles FJ, Mauro MJ, Hong F, et al. Rates of peripheral arterial occlusive disease in patients with chronic myeloid leukemia in the chronic phase treated with imatinib, nilotinib, or non-tyrosine kinase therapy: a retrospective cohort analysis. Leukemia. 2013 Jun;27(6):1310–5.
34. Alhawiti N, Burbury KL, Kwa FA, et al. The tyrosine kinase inhibitor, nilotinib potentiates a prothrombotic state. Thromb Res. 2016 Sep;145:54–64.
35. Hadzijusufovic E, Albrecht-Schgoer K, Huber K, et al. Nilotinib-induced vasculopathy: identification of vascular endothelial cells as a primary target site. Leukemia. 2017 Nov;31(11):2388–97.
36. Latifi Y, Moccetti F, Wu M, et al. Thrombotic microangiopathy as a cause of cardiovascular toxicity from the BCR-ABL1 tyrosine kinase inhibitor ponatinib. Blood. 2019 Jan;
37. Elice F, Rodeghiero F. Hematologic malignancies and thrombosis. Thromb Res. 2012 Mar;129(3):360–6.
38. Simkovic M, Vodarek P, Motyckova M, et al. Venous thromboembolism in patients with chronic lymphocytic leukemia. Thromb Res. 2015 Dec;136(6):1082–6.
39. Lau C, Anitole K, Hodes C, et al. Perfluoroalkyl acids: a review of monitoring and toxicological findings. Toxicol Sci. 2007 Oct;99(2):366–94.
40. Eriksen KT, Raaschou-Nielsen O, McLaughlin JK, et al. Association between plasma PFOA and PFOS levels and total cholesterol in a middle-aged Danish population. PLoS One. 2013;8(2):e56969.
41. Frisbee SJ, Shankar A, Knox SS, et al. Perfluorooctanoic acid, perfluorooctanesulfonate, and serum lipids in children and adolescents: results from the C8 Health Project. Arch Pediatr Adolesc Med. 2010 Sep;164(9):860–9.
42. Geiger SD, Xiao J, Ducatman A, et al. The association between PFOA, PFOS and serum lipid levels in adolescents. Chemosphere. 2014 Mar;98:78–83.
43. Jain RB, Ducatman A. Associations between lipid/lipoprotein levels and perfluoroalkyl substances among US children aged 6-11 years. Environ Pollut. 2018 Dec;243(Pt A):1–8.
44. Liu H-S, Wen L-L, Chu P-L, et al. Association among total serum isomers of perfluorinated chemicals, glucose homeostasis, lipid profiles, serum protein and metabolic syndrome in adults: NHANES, 2013-2014. Environ Pollut. 2018 Jan;232:73–9.
45. Nelson JW, Hatch EE, Webster TF. Exposure to polyfluoroalkyl chemicals and cholesterol, body weight, and insulin resistance in the general U.S. population. Environ Health Perspect. 2010 Feb;118(2):197–202.
46. Steenland K, Tinker S, Frisbee S, et al. Association of perfluorooctanoic acid and perfluorooctane sulfonate with serum lipids among adults living near a chemical plant. Am J Epidemiol. 2009 Nov;170(10):1268–78.

47. Costa G, Sartori S, Consonni D. Thirty years of medical surveillance in perfluorooctanoic acid production workers. J Occup Environ Med. 2009 Mar;51(3):364–72.
48. Olsen GW, Zobel LR. Assessment of lipid, hepatic, and thyroid parameters with serum perfluorooctanoate (PFOA) concentrations in fluorochemical production workers. Int Arch Occup Environ Health. 2007 Nov;81(2):231–46.
49. Olsen GW, Burris JM, Burlew MM, et al. Plasma cholecystokinin and hepatic enzymes, cholesterol and lipoproteins in ammonium perfluorooctanoate production workers. Drug Chem Toxicol. 2000 Nov;23(4):603–20.
50. Olsen GW, Burris JM, Burlew MM,et al. Epidemiologic assessment of worker serum perfluorooctanesulfonate (PFOS) and perfluorooctanoate (PFOA) concentrations and medical surveillance examinations. J Occup Environ Med. 2003 Mar;45(3):260–70.
51. Olsen GW, Ehresman DJ, Buehrer BD, Gibson BA, Butenhoff JL, Zobel LR. Longitudinal assessment of lipid and hepatic clinical parameters in workers involved with the demolition of perfluoroalkyl manufacturing facilities. J Occup Environ Med. 2012 Aug;54(8):974–83.
52. Sakr CJ, Kreckmann KH, Green JW, et al. Cross-sectional study of lipids and liver enzymes related to a serum biomarker of exposure (ammonium perfluorooctanoate or APFO) as part of a general health survey in a cohort of occupationally exposed workers. J Occup Environ Med. 2007 Oct;49(10):1086–96.
53. Sakr CJ, Leonard RC, Kreckmann KH,et al. Longitudinal study of serum lipids and liver enzymes in workers with occupational exposure to ammonium perfluorooctanoate. J Occup Environ Med. 2007 Aug;49(8):872–9.
54. Steenland K, Fletcher T, Savitz DA. Epidemiologic evidence on the health effects of perfluorooctanoic acid (PFOA). Environ Health Perspect. 2010 Aug;118(8):1100–8.
55. Steenland K, Zhao L, Winquist A. A cohort incidence study of workers exposed to perfluorooctanoic acid (PFOA). Occup Environ Med. 2015 May;72(5):373–80.
56. Raleigh KK, Alexander BH, Olsen GW, et al. Mortality and cancer incidence in ammonium perfluorooctanoate production workers. Occup Environ Med. 2014 Jul;71(7):500–6.
57. Steenland K, Woskie S. Cohort mortality study of workers exposed to perfluorooctanoic acid. Am J Epidemiol. 2012 Nov;176(10):909–17.
58. Convertino M, Church TR, Olsen GW, et al. Stochastic Pharmacokinetic-Pharmacodynamic Modeling for Assessing the Systemic Health Risk of Perfluorooctanoate (PFOA). Toxicol Sci. 2018 May;163(1):293–306.
59. FDA. Guidance for industry: diabetes mellitus - evaluating cardiovascular risk in new antidiabetic therapies to treat type 2 diabetes Title [Internet]. 2008. Available from: http://www.fda.gov/downloads/drugs/guidance-complianceregulatory-information/guidances/ucm071627.pdf
60. EMA. European Medicines Agency guideline on clinical investigation of medicinal products in the treatment or prevention of diabetes mellitus. London: Committee for Medicinal Products for Human Useitle [Internet]. 2012. Available from: https://www.ema.europa.eu/en/documents/scientific-guideline/guideline-clinical-investigation-medicinal-products-treatment-prevention-diabetes-mellitus-revision_en.pdf
61. Ason B, van der Hoorn JWA, Chan J, Lee E, et al. PCSK9 inhibition fails to alter hepatic LDLR, circulating cholesterol, and atherosclerosis in the absence of ApoE. J Lipid Res. 2014 Nov;55(11):2370–9.
62. van de Steeg E, Kleemann R, Jansen HT, et al. Combined analysis of pharmacokinetic and efficacy data of preclinical studies with statins markedly improves translation of drug efficacy to human trials. J Pharmacol Exp Ther. 2013 Dec;347(3):635–44.
63. Delsing DJM, Jukema JW, van de Wiel MA, et al. Differential effects of amlodipine and atorvastatin treatment and their combination on atherosclerosis in ApoE*3-Leiden transgenic mice. J Cardiovasc Pharmacol. 2003 Jul;42(1):63–70.
64. Verschuren L, Kleemann R, Offerman EH, et al. Effect of low dose atorvastatin versus diet-induced cholesterol lowering on atherosclerotic lesion progression and inflammation in apolipoprotein E*3-Leiden transgenic mice. Arterioscler Thromb Vasc Biol. 2005 Jan;25(1):161–7.
65. van der Hoorn JWA, Kleemann R, Havekes LM, et al. Olmesartan and pravastatin additively reduce development of atherosclerosis in APOE*3Leiden transgenic mice. J Hypertens. 2007 Dec;25(12):2454–62.
66. van Vlijmen BJ, Pearce NJ, Bergo M, et al. Apolipoprotein E*3-Leiden transgenic mice as a test model for hypolipidaemic drugs. Arzneimittelforschung. 1998 Apr;48(4):396–402.
67. Delsing DJM, Post SM, Groenendijk M, et al. Rosuvastatin reduces plasma lipids by inhibiting VLDL production and enhancing hepatobiliary lipid excretion in ApoE*3-leiden mice. J Cardiovasc Pharmacol. 2005 Jan;45(1):53–60.

68. Kleemann R, Princen HMG, Emeis JJ, et al. Rosuvastatin reduces atherosclerosis development beyond and independent of its plasma cholesterol-lowering effect in APOE*3-Leiden transgenic mice: evidence for antiinflammatory effects of rosuvastatin. Circulation. 2003 Sep;108(11):1368–74.
69. Kooistra T, Verschuren L, de Vries-van der Weij J, et al. Fenofibrate reduces atherogenesis in ApoE*3Leiden mice: evidence for multiple antiatherogenic effects besides lowering plasma cholesterol. Arterioscler Thromb Vasc Biol. 2006 Oct;26(10):2322–30.
70. van der Hoorn JWA, de Haan W, Berbee JFP, et al. Niacin increases HDL by reducing hepatic expression and plasma levels of cholesteryl ester transfer protein in APOE*3Leiden.CETP mice. Arterioscler Thromb Vasc Biol. 2008 Nov;28(11):2016–22.
71. Baker DJ, Atkinson AM, Wilkinson GP, et al. Characterization of the heterozygous glucokinase knockout mouse as a translational disease model for glucose control in type 2 diabetes. Br J Pharmacol. 2014 Apr;171(7):1629–41.
72. Baker DJ, Wilkinson GP, Atkinson AM, et al. Chronic glucokinase activator treatment at clinically translatable exposures gives durable glucose lowering in two animal models of type 2 diabetes. Br J Pharmacol. 2014 Apr;171(7):1642–54.
73. Lago RM, Singh PP, Nesto RW. Congestive heart failure and cardiovascular death in patients with prediabetes and type 2 diabetes given thiazolidinediones: a meta-analysis of randomised clinical trials. Lancet (London, England). 2007 Sep;370(9593):1129–36.
74. Home PD, Pocock SJ, Beck-Nielsen H, et al. Rosiglitazone evaluated for cardiovascular outcomes--an interim analysis. N Engl J Med. 2007 Jul;357(1):28–38.
75. Nissen SE, Wolski K. Effect of rosiglitazone on the risk of myocardial infarction and death from cardiovascular causes. N Engl J Med. 2007 Jun;356(24):2457–71.
76. Marso SP, Daniels GH, Brown-Frandsen K, et al. Liraglutide and Cardiovascular Outcomes in Type 2 Diabetes. N Engl J Med. 2016 Jul;375(4):311–22.
77. Zinman B, Wanner C, Lachin JM, et al. Empagliflozin, Cardiovascular Outcomes, and Mortality in Type 2 Diabetes. N Engl J Med. 2015 Nov;373(22):2117–28.
78. Sattar N, Preiss D, Murray HM, et al. Statins and risk of incident diabetes: a collaborative meta-analysis of randomised statin trials. Lancet (London, England). 2010 Feb;375(9716):735–42.
79. Tousoulis D, Oikonomou E, Economou EK, et al. Inflammatory cytokines in atherosclerosis: current therapeutic approaches. Eur Heart J. 2016 Jun;37(22):1723–32.
80. Ridker PM, Everett BM, Thuren T, et al. Antiinflammatory Therapy with Canakinumab for Atherosclerotic Disease. N Engl J Med. 2017 Sep;377(12):1119–31.
81. Zhang X, Li J, Qin J-J, Cheng W-L, et al. Oncostatin M receptor beta deficiency attenuates atherogenesis by inhibiting JAK2/STAT3 signaling in macrophages. J Lipid Res. 2017 May;58(5):895–906.
82. Wallace PM, MacMaster JF, Rouleau KA, et al. Regulation of inflammatory responses by oncostatin M. J Immunol. 1999 May;162(9):5547–55.
83. Komori T, Morikawa Y. Oncostatin M in the development of metabolic syndrome and its potential as a novel therapeutic target. Anat Sci Int. 2018 Mar;93(2):169–76.
84. Richards CD. The enigmatic cytokine oncostatin m and roles in disease. ISRN Inflamm. 2013 Dec;2013:512103.

Summary
Samenvatting
Author affiliations
List of publications
Curriculum vitae
Dankwoord

Summary

Cardiovascular disease (CVD) is currently globally the major cause of mortality and morbidity, and 85% of all CVD deaths are related to the formation of atheromatous plaques in the vessels. Chronic exposure to cardiovascular risk factors, such as dyslipidemia, hypertension and diabetes, increases the rate and severity of atherosclerosis. Despite advances in treatment strategies, many patients remain at increased cardiovascular risk. This thesis described a variety of studies that aimed to reduce CVD risk by (I) evaluation of novel lipid-lowering interventions, (II) identification of cardiovascular side-effects of registered drugs and an environmental pollutant, (III) development of a novel animal model combining dyslipidemia and diabetes, and (IV) evaluation of the cytokine oncostatin M (OSM) as potential target for CVD. In all studies, the APOE*3-Leiden(.CETP) mouse model was used as translational model for human lipoprotein metabolism and atherosclerosis development.

In **Chapter 2** we evaluated the effects of a vaccine against proprotein convertase subtilisin/kexin type 9 (PCSK9), which induced an effective immune response against PCSK9 thereby decreasing plasma cholesterol levels, markers of systemic inflammation and atherosclerosis progression. However, as most patients at CVD risk are treated after development of atherosclerosis, therapies that regress pre-existent lesions are required. Therefore, **Chapter 3** evaluated whether pre-existent atherosclerotic lesions could regress by aggressive lipid lowering using a combination of antibodies against PCSK9 (alirocumab) and angiopoietin-like 3 protein (ANGPTL3) (evinacumab) on top of atorvastatin. This strategy decreased plasma non-HDL-C levels to 1 mmol/L and subsequently regressed atherosclerotic lesion size, improved lesion stability and diminished macrophage accumulation.

In **Chapter 4** we explored the etiology of reported toxic cardiovascular off-target effects of three generations tyrosine kinase inhibitors (TKIs), imatinib, nilotinib and ponatinib, respectively, that are used for the treatment of patients with chronic myeloid leukaemia (CML). The first generation TKI imatinib reduced atherosclerosis development, whereas the second and third generation TKIs, nilotinib and ponatinib, respectively, increased cardiovascular risk through induction of a prothrombotic state. In addition, imatinib and ponatinib decreased plasma cholesterol levels, by a mechanism that was investigated in **Chapter 5**. Imatinib was found to decrease plasma TC and TG levels by reduction of the very-low-density-lipoprotein (VLDL) particle production and cholesterol ester content of the VLDL particles, while ponatinib reduced plasma total cholesterol levels by lowering intestinal lipid absorption.

The dose effects of perfluorooctanoic acid (PFOA) on lipoprotein metabolism are presented in **Chapter 6**. Before being phased-out, PFOA has been widely used as an emulsifier in the manufacture of fluoropolymers, is extremely stable and therefore persists in the environment. Positive associations between serum PFOA levels and plasma cholesterol have been reported in environmentally and occupationally exposed adults,

though the observations are inconsistent. Using APOE*3-Leiden.CETP mice, we demonstrated that PFOA did not alter plasma lipid levels or lipoprotein metabolism at environmentally or occupationally relevant exposure levels. However, when mice were exposed to toxicologically relevant PFOA doses, non-HDL-C levels were decreased and HDL-C levels were increased. In the latter mice, PFOA decreased VLDL particle production and increased VLDL clearance. Moreover, HDL-C levels were increased through reduction of CETP activity and changes in gene expression of proteins involved in HDL metabolism. These data indicate that the reported associations observed in epidemiological studies are associative rather than causal.

Diabetes is an important risk factor for CVD and currently, novel anti-diabetic drugs have to demonstrate their cardiovascular safety before approval. Consequently, translational models are warranted for the evaluation of these drugs. In **Chapter 7** we described the characteristics of the APOE*3-Leiden.Glucokinase$^{+/-}$ (E3L.GK$^{+/-}$) mouse model, which was generated by cross-breeding the hyperlipidemic APOE*3-Leiden mouse with the hyperglycemic glucokinase knockout (GK$^{+/-}$) mouse. E3L.GK$^{+/-}$ mice had elevated plasma lipid levels as in E3L mice, and elevated plasma glucose levels as in GK$^{+/-}$ mice, leading to enhanced atherosclerosis progression which was predicted by glucose exposure. We propose that the E3L.GK$^{+/-}$ mouse is a promising novel diet-inducible disease model for investigation of the etiology and evaluation of drug treatment on diabetic atherosclerosis.

The role of cytokines in the initiation and progression of atherosclerosis is increasingly recognized and consequently, novel therapies targeting cytokines are being developed. In **Chapter 8** we evaluated the role of the cytokine OSM in the initiation of atherosclerosis and found that OSM induced endothelial activation *in vitro* using human endothelial cells from different vascular beds, and *in vivo* using APOE*3-Leiden.CETP mice. In **Chapter 9** we exposed APOE*3-Leiden.CETP mice for 16 weeks to OSM which increased plasma E-selectin levels and endothelial activation in the aortic root. However remarkably, we found a reduction in atherosclerotic lesion size, corresponding to our observation that higher serum OSM levels in humans are associated with post coronary heart disease and overall survival probability in the AGES Reykjavik Study, suggesting a protective cardiovascular effect. However, the confusing effects of the increased endothelial activation on the one hand, and reduced atherosclerosis on the other hand, need to be further elucidated.

In conclusion, we discussed several strategies that may contribute to further CVD risk reduction in the future. We described two novel lipid-lowering strategies, we unraveled (part of) the etiology of the cardiovascular safety issues of TKIs that are used for the treatment of CML, and we investigated the dose effects of PFOA on lipoprotein metabolism. Looking forward, we developed a novel mouse model that can be used for the study of diabetic macrovascular complications, and we evaluated the potential of OSM as novel target in CVD.

Samenvatting

Hart- en vaatziekten zijn wereldwijd doodsoorzaak nummer één. 85% van deze gevallen zijn toe te schrijven aan de ontwikkeling van aderverkalking in de slagaders (ook wel 'arteriosclerose of atherosclerose' genoemd). Aderverkalking ontstaat als er witte bloedcellen en cholesterol in de vaatwand ophopen waarbij een verdikking van de vaatwand optreedt, ook wel plaques genoemd. Wanneer een (instabiele) plaque openscheurt, komt de inhoud van de plaque in contact met het bloed waarbij stolsels kunnen ontstaan die bloedvaten in het hart (hartinfarct) of hersenen (herseninfarct) afsluiten. Langdurige blootstelling aan risicofactoren voor hart- en vaatziekten, zoals roken, een verhoogd cholesterol in het bloed en diabetes, vergroot het aantal gevallen en de ernst van aderverkalking. Ondanks verbeterde therapieën is het risico op hart- en vaatziekten nauwelijks afgenomen. In dit proefschrift zijn verschillende onderzoeken beschreven waarvan de opgedane kennis kan bijdragen aan de vermindering van het risico op hart- en vaatziekten. In alle studies zijn genetisch gemodificeerde muizen, APOE*3-Leiden(.CETP) transgene muizen, gebruikt als proefdiermodel voor vetstofwisseling en aderverkalking bij mensen. De APOE*3-Leiden(.CETP) muizen bevatten 3 genen van de mens die een belangrijke rol spelen in de cholesterol- en vetstofwisseling.

In **Hoofdstuk 2** is de werking van een nieuw vaccin tegen het lichaamseigen eiwit, proprotein convertase subtilisin/kexin type 9 (PCSK9), in het muismodel onderzocht. Mensen en muizen met meer van dit eiwit in hun bloed hebben een hoger cholesterol en krijgen eerder aderverkalking. Na toediening van dit vaccin maakte de muis antilichamen aan tegen PCSK9, met als resultaat een verlaging van het plasma cholesterol en ontstekingswaardes, verminderde ontsteking van de vaatwand en minder aderverkalking. Echter, omdat de meeste mensen met hart- en vaatziekten pas worden behandeld als de aderverkalking zich al ontwikkeld heeft, is het noodzakelijk dat er behandelingen komen die de al aanwezige aderverkalking kunnen verminderen. Daarom is in **Hoofdstuk 3** onderzocht of er een mogelijkheid bestaat tot verminderen van de al aanwezige aderverkalking. Met een combinatietherapie van antilichamen tegen PCSK9 (alirocumab) en angiopoietin-like 3 protein (ANGPTL3) (evinacumab) bovenop de standaardtherapie met een statine, in dit geval atorvastatine, lukte het om de plasma non-HDL cholesterolwaardes (ook wel 'slechte' cholesterol genoemd) sterk te verlagen. Dit had als gevolg dat de al gevormde plaques kleiner werden. Daarnaast werden de overgebleven plaques stabieler en verdwenen de ontstekingscellen uit de plaques.

In **Hoofdstuk 4** is onderzocht hoe geneesmiddelen voor patiënten met bloedkanker, hetgeen leidt tot een overmatige productie van witte bloedcellen (chronische myeloïde leukemie (CML)), de kans/het risico op hart- en vaatziekten verkleinen of juist vergroten. Het eerste keuze geneesmiddel imatinib verkleint het risico op hart- en vaatziekten en wij hebben ontdekt dat dit komt doordat imatinib het plasma cholesterol verlaagt en de plaque ontwikkeling vermindert. De tweede en derde keuze geneesmiddelen, respectievelijk

nilotinib en ponatinib, die gegeven worden als imatinib niet meer werkt, verhogen juist het risico op hart- en vaatziekten doordat ze een stollingsverhogende werking hebben die de kans op vorming van bloedstolsels verhoogt als een instabiele plaque openscheurt. Daarnaast vonden wij dat zowel imatinib als ponatinib het plasma cholesterol verlaagden. In **Hoofdstuk 5** hebben we de plasma cholesterolverlagende werking van deze geneesmiddelen verder onderzocht. Imatinib verlaagde de plasma cholesterol- en vetwaardes door het verminderen van de productie van vetdeeltjes door de lever, waarbij zowel het aantal deeltjes als de cholesterolinhoud van de deeltjes afnam. Ponatinib verlaagde het plasma cholesterol door de opname van cholesterol in de darm te verlagen.

In **Hoofdstuk 6** werden de effecten onderzocht van verschillende doseringen perfluorooctanoic acid (PFOA) op de cholesterol- en vetstofwisseling. PFOA is een door de mens geproduceerde chemische stof die werd gebruikt voor de productie van fluoropolymeren. Fluoropolymeren werden bijvoorbeeld toegepast bij het produceren van de antiaanbaklaag in pannen, of als brandvertrager in tapijt of om kleding en schoenen water- en vetafstotend te maken. PFOA is niet afbreekbaar en blijft daarom achter in het milieu. Populatiestudies hebben een verband gevonden tussen serum PFOA-waardes en een verhoogd plasma cholesterol in mensen die via hun leefomgeving of door hun werk blootgesteld werden aan PFOA. Echter, de gevonden effecten op plasma cholesterol zijn tegenstrijdig en daarom hebben wij in muizen onderzocht wat de wezenlijke effecten van PFOA op de cholesterol- en vetstofwisseling zijn. In deze studie had PFOA geen effect op de cholesterol- en vetstofwisseling wanneer muizen werden blootgesteld aan doseringen die vergelijkbaar zijn met die voor blootstelling vanuit de omgeving of door werk. Echter, een hogere dosering PFOA verlaagde plasma cholesterol als gevolg van een afgenomen productie van vet- deeltjes in de lever en toegenomen opname van vetdeeltjes door de verschillende organen. Daarnaast was het HDL-cholesterol (ook wel 'goede' cholesterol genoemd) verhoogd. Onze bevindingen suggereren dat het verband tussen PFOA blootstelling en plasma cholesterol zoals gevonden in populatiestudies geen oorzakelijk (causaal) verband is.

Diabetes (ook wel 'suikerziekte' genoemd) is een belangrijke risicofactor voor hart- en vaatziekten. In het verleden lieten sommige diabetesmedicijnen de kans op hart- en vaatziekten toenemen. Daarom moeten op dit moment alle nieuwe diabetesmedicijnen laten zien dat ze veilig zijn voordat ze worden toegelaten op de Amerikaanse en Europese markt. Om deze medicijnen te ontwikkelen en te testen is het belangrijk dat er een muismodel is dat, net zoals mensen, diabetes en hart- en vaatziekten heeft en dat goed reageert op cholesterolverlagende en diabetesmedicijnen. In **Hoofdstuk 7** werden de kenmerken van de APOE*3-Leiden.Glucokinase$^{+/-}$ (E3L.GK$^{+/-}$) muis beschreven. Deze muis was ontwikkeld door twee verschillende genetisch gemodificeerde muizen, de APOE*3-Leiden muis, die goed reageert op cholesterolverlagende medicijnen, en de 'diabetische' GK$^{+/-}$ muis, waarin het bloedsuiker (glucose) verlaagd wordt door medicijnen net zoals bij de mens, met elkaar te kruisen. Dit nieuwe model had verhoogde cholesterol- en vetwaardes

zoals de APOE*3-Leiden muis, en verhoogde glucosewaardes zoals de GK$^{+/-}$ muis, met als gevolg méér aderverkalking. Nadat is onderzocht hoe dit nieuwe muismodel reageert op al bestaande medicijnen voor de behandeling van een verhoogd cholesterol of diabetes, kan het model ingezet worden voor de ontwikkeling van nieuwe medicijnen voor deze ziektes.

De invloed van cytokines (ook wel 'ontstekingsmediatoren') op het ontstaan en verergeren van aderverkalking wordt steeds meer erkend en op dit moment worden verschillende nieuwe therapieën voor hart- en vaatziekten ontwikkeld die zich richten op cytokines. Een nog niet zo'n bekend cytokine is OSM. In **Hoofdstuk 8** werd bekeken wat de rol van OSM was in het ontstaan van aderverkalking. Met behulp van een proef met menselijke vaatwandcellen vonden we dat OSM een ontsteking veroorzaakte in de cellen die de binnenbekleding van de bloedvaten vormen. Dezelfde tekenen van vaatwandontsteking zagen we ook nadat we muizen kortstondig (3 weken) hadden blootgesteld aan OSM. Omdat toegenomen vaatwandontsteking de vorming van aderverkalking kan verergeren, hebben we in **Hoofdstuk 9** onderzocht of langdurige (16 weken) blootstelling van muizen aan OSM inderdaad meer aderverkalking veroorzaakte. Ook in deze studie zagen we tekenen van toegenomen ontsteking in zowel het plasma als in de vaatwand, maar vonden we een opmerkelijke vermindering van de hoeveelheid aderverkalking. Deze laatste bevinding kwam overeen met de resultaten uit de AGES Reykjavik Studie, waarbij mensen met een verhoogd OSM in het bloed een verbeterde overlevingskans hadden na een hartinfarct of hartkramp (ook wel 'coronair lijden'). De tegenstrijdige resultaten, met aan de ene kant de verhoogde vaatwandontsteking en aan de andere kant minder aderverkalking, moeten verder onderzocht worden voordat OSM als target voor hart- en vaatziekten kan worden gebruikt.

Samenvattend, in dit proefschrift zijn verschillende strategieën besproken die kunnen bijdragen aan het verminderen van het risico op hart- en vaatziekten. Er zijn twee vernieuwende cholesterolverlagende behandelstrategieën geëvalueerd, het achterliggende mechanisme van de afgenomen of juist toegenomen kans op hart- en vaatziekten bij patiënten die behandeld worden voor CML is bestudeerd, en de effecten van verschillende doseringen PFOA op de cholesterol- en vetstofwisseling zijn onderzocht. Daarnaast zijn de karakteristieken van een nieuw muismodel besproken dat in de toekomst gebruikt kan worden voor het onderzoek naar hart- en vaatziekten in diabetespatiënten, en is onderzocht of het cytokine OSM een interessant target is voor de behandeling van hart- en vaatziekten.

Author affiliations

Jurjan Aman	Departments of Physiology and Pulmonary Diseases, VU University Medical Center, Amsterdam, The Netherlands
Anne-Christine Andreásson	Cardiovascular, Renal and Metabolism, IMED Biotech Unit, AstraZeneca, Gothenburg, Sweden
Margareta Behrendt	Cardiovascular, Renal and Metabolism, IMED Biotech Unit, AstraZeneca, Gothenburg, Sweden
Ivana Bobeldijk-Pastorova	The Netherlands Organization of Applied Scientific Research (TNO), Metabolic Health Research, Leiden, The Netherlands
Martien P. M. Caspers	The Netherlands Organization of Applied Scientific Research (TNO), Microbiology and Systems Biology, Zeist, The Netherlands
Shu-Ching Chang	Medical Department, 3M Company, St Paul, Minnesota, USA
Valur Emilsson	Icelandic Heart Association, Lopavogur, Iceland | Faculty of Pharmaceutical Sciences, University of Iceland, Reykjavik, Iceland
Gergana Galabova	AFFiRis AG, Vienna, Austria
Ricardo A. Garcia	Cardiovascular Drug Discovery, Bristol-Meyers Squibb, New York, USA
Eveline Gart	The Netherlands Organization of Applied Scientific Research (TNO), Metabolic Health Research, Leiden, The Netherlands
Martin Giera	Center for Proteomics and Metabolomics, Leiden University Medical Center, Leiden, The Netherlands
Alain J. van Gool	The Netherlands Organization of Applied Scientific Research (TNO), Microbiology and Systems Biology, Zeist, The Netherlands
Jesper Gromada	Regeneron Pharmaceuticals, Tarrytown, NY
Vilmundur Gudnason	Icelandic Heart Association, Kopavogur, Iceland | Faculty of Medicine, University of Iceland, Reykjavik, Iceland
Viktoria Gusarova	Regeneron Pharmaceuticals, Tarrytown, NY
Ulf Hedin	Department of Molecular Medicine and Surgery, Karolinska Instituted, Solna, Sweden
Suvi E. Heinonen	Cardiovascular, Renal and Metabolism, IMED Biotech Unit, AstraZeneca, Gothenburg, Sweden
Anita M. van den Hoek	The Netherlands Organization of Applied Scientific Research (TNO), Metabolic Health Research, Leiden, The Netherlands
Kim Holmstrøm	Bioneer A/S Horshølm, Denmark
José W. A. van der Hoorn	The Netherlands Organization of Applied Scientific Research (TNO), Metabolic Health Research, Leiden, The Netherlands
Ann-Cathrine Jönsson-Rylander	Cardiovascular, Renal and Metabolism, IMED Biotech Unit, AstraZeneca, Gothenburg, Sweden
Lori L. Jennings	Novartis Institutes for Biomedical Research, Cambridge, Massachusetts, USA
Claudia Juno	AFFiRis AG, Vienna, Austria
J. Wouter Jukema	Cardiology, Leiden University Medical Center, Leiden, the Netherlands | Einthoven Laboratory for Experimental Vascular Medicine, Leiden University Medical Center, Leiden, the Netherlands
Nanda Keijzer	The Netherlands Organization of Applied Scientific Research (TNO), Metabolic Health Research, Leiden, The Netherlands
Danielle van Keulen	Laboratory of Experimental Cardiology, University Medical Centre Utrecht, Utrecht, The Netherlands | Laboratory of Clinical Chemistry and Haematology, University Medical Centre Utrecht, Utrecht, The Netherlands | Quorics B.V., Rotterdam, The Netherlands | The Netherlands Organization of Applied Scientific Research (TNO), Metabolic Health Research, Leiden, The Netherlands
Cornelis Kluft	Good Biomarker Sciences, Leiden, The Netherlands

Arianne van Koppen	The Netherlands Organization of Applied Scientific Research (TNO), Metabolic Health Research, Leiden, The Netherlands
Christine Landlinger	AFFiRis AG, Vienna, Austria
Brendan Leighton	The Research Network, Sandwich, Kent, UK
Jan H. N. Lindeman	Department of Vascular Surgery, Leiden University Medical Center, The Netherlands
Ljubica P. Matic	Department of Molecular Medicine and Surgery, Karolinska Instituted, Solna, Sweden
Aswin Menke	TNO-Triskelion, Zeist, The Netherlands
Boye S. Nielson	Bioneer A/S Horshølm, Denmark
Geary Olsen	Medical Department, 3M Company, St Paul, Minnesota, USA
Gerard Pasterkamp	Laboratory of Experimental Cardiology, University Medical Centre Utrecht, Utrecht, The Netherlands | Laboratory of Clinical Chemistry and Haematology, University Medical Centre Utrecht, Utrecht, The Netherlands
Elsbet J. Pieterman	The Netherlands Organization of Applied Scientific Research (TNO), Metabolic Health Research, Leiden, The Netherlands
Hans M. G. Princen	The Netherlands Organization of Applied Scientific Research (TNO), Metabolic Health Research, Leiden, The Netherlands
Maarten D. Sollewijn Gelpke	Molecular Profiling Consulting, London, England
Guenther Staffler	AFFiRis AG, Vienna, Austria
Dennie Tempel	Laboratory of Experimental Cardiology, University Medical Centre Utrecht, Utrecht, The Netherlands | Laboratory of Clinical Chemistry and Haematology, University Medical Centre Utrecht, Utrecht, The Netherlands | Quorics B.V., Rotterdam, The Netherlands | SkylineDx B.V., Rotterdam, The Netherlands.
Lars Verschuren	The Netherlands Organization of Applied Scientific Research (TNO), Microbiology and Systems Biology, Zeist, The Netherlands
Nicole Worms	The Netherlands Organization of Applied Scientific Research (TNO), Metabolic Health Research, Leiden, The Netherlands

List of publications

Expression and clinical relevance of paired box protein 7 and sex determining region Y-box 2 in canine corticotroph pituitary adenomas
Sarah J. van Rijn, Marianne G. Pouwer, Marianna A. Tryfonidou, Guy C. M. Grinwis, Joanne E. E. van der Bend, Pauline E. P. F. Beukers, Nadie Vastenhout, Jacques Drouin, Louis C. Penning, Björn P. Meij
Vet J. 2015 Jun;204(3):315-21

Comment on "Hypercholesterolemia with consumption of PFOA-laced Western diets is dependent on strain and sex of mice" by Rebholz S.L. et al. Toxicol. Rep. 2016 (3) 46-54
Hans M. G. Princen, Marianne G. Pouwer, Elsbet J. Pieterman
Toxicol Rep. 2016 Feb 11;3:306-309

The AT04A vaccine against proprotein convertase subtilisin/kexin type 9 reduces total cholesterol, vascular inflammation, and atherosclerosis in APOE*3Leiden. CETP mice
Christine Landlinger*, Marianne G. Pouwer*, Claudia Juno, José W. A. van der Hoorn, Elsbet J. Pieterman, J. Wouter Jukema, Guenther Staffler, Hans M. G. Princen, and Gergana Galabova
Eur Heart J. 2017 Aug 21;38(32):2499-2507

The BCR-ABL1 inhibitors imatinib and ponatinib decrease plasma cholesterol and atherosclerosis, and nilotinib and ponatinib activate coagulation in a translational mouse model
Marianne G. Pouwer, Elsbet J. Pieterman, Lars Verschuren, Martien P. M. Caspers, Cornelis Kluft, Ricardo A. Garcia, Jurjan Aman, J. Wouter Jukema and Hans M. G. Princen
Front Cardiovasc Med. 2018 Jun 12;5:55

Inflammatory cytokine oncostatin M induces endothelial activation in macro- and microvascular endothelial cells and in APOE*3Leiden.CETP mice
Danielle van Keulen, Marianne G. Pouwer, Gerard Pasterkamp, Alain J. van Gool, Maarten D. Sollewijn Gelpke, Hans M. G. Princen and Dennie Tempel
PLoS One. 2018 Oct 1;13(10):e0204911

* both authors contributed equally to this work

The APOE*3-Leiden heterozygous glucokinase knockout mouse as novel translational disease model for type 2 diabetes, dyslipidemia, and diabetic atherosclerosis
Marianne G. Pouwer*, Suvi E. Heinonen*, Margareta Behrendt, Anne-Christine Andréasson, Arianne van Koppen, Aswin L. Menke, Elsbet J. Pieterman, Anita M. van den Hoek, J. Wouter Jukema, Brendan Leighton, Ann-Cathrine Jönsson-Rylander, and Hans M. G. Princen
J Diabetes Res. 2019 Feb 21;2019:9727952

Dose effects of ammonium perfluorooctanoate on lipoprotein metabolism in APOE*3-Leiden.CETP mice
Marianne G. Pouwer, Elsbet J. Pieterman, Shu-Ching Chang, Geary W. Olsen, Martien P.M. Caspers, Lars Verschuren, J. Wouter Jukema and Hans M. G. Princen
Toxicol Sci. 2019 Apr 1;168(2):519-534

Oncostatin M reduces atherosclerosis development in APOE*3-Leiden.CETP mice and is associated with increased survival probability in humans
Danielle van Keulen, Marianne G. Pouwer, Valur Emilsson, Ljubica Perisic Matic, Elsbet J. Pieterman, Ulf Hedin, Vilmundur Gudnason, Lori L. Jennings, Kim Holmstrøm, Boye Schnack Nielsen, Gerard Pasterkamp, Jan H.N. Lindeman, Alain J. van Gool, Maarten D. Sollewijn Gelpke, Hans M.G. Princen*, Dennie Tempel*
PLoS One. 2019 Aug 28;14(8):e0221477

The second generation tyrosine kinase inhibitor nilotinib inhibits discoid domain receptor 2 in human aortic valves, increases aortic valve thickness and induces valvular interstitial cell calcification
Miguel Carracedo, Gonzalo Artiach, Marianne G. Pouwer, Elsbet J. Pieterman, Oscar Persson, Peter Saliba Gustafsson, Ewa Ehrenborg, Per Eriksson, Hans M. G. Princen, Anders Franco-Cereceda, Magnus Bäck
Submitted

Triple treatment with alirocumab and evinacumab on top of atorvastatin regresses lesion size and improves plaque phenotype in APOE*3-Leiden.CETP mice
Marianne G. Pouwer, Elsbet J. Pieterman, Nicole Worms, Nanda Keijzer, J. Wouter Jukema, Jesper Gromada, Viktoria Gusarova, Hans M. G. Princen
Submitted

* both authors contributed equally to this work

The BCR-ABL1 inhibitors imatinib and ponatinib decrease plasma cholesterol through different effects on lipoprotein metabolism
Marianne G. Pouwer, Eveline Gart, Elsbet J. Pieterman, Martin Giera, J. Wouter Jukema, Hans M. G. Princen
Submitted

Novel high intensive cholesterol-lowering therapies do not ameliorate knee OA development in humanized dyslipidemic mice
Yvonne van Gemert, Anne E. Kozijn, Marianne G. Pouwer, Nik N. L. Kruisbergen, Martijn H. van den Bosch, Arjen B. Blom, Elsbet J. Pieterman, Harry Weinans, Reinout Stoop, Hans M. G. Princen, Peter L. E. M. van Lent.
In preparation

Curriculum vitae

Marianne Pouwer was born on 7 January 1989 in Veghel, the Netherlands and grew up in Kesteren, the Netherlands. In 2007, she graduated from the Christelijk Lyceum Veenendaal. The same year, she moved to Utrecht and enrolled for a bachelor Veterinary Medicine at the faculty of Veterinary Medicine at Utrecht University (UU), in Utrecht, the Netherlands. In 2010, she started a minor Biomedical Sciences at the faculty of Life Sciences at UU, followed by a master Veterinary Medicine at UU from which she graduated in 2014. During her master, Marianne developed and coordinated a summer school for elementary school kids, Summerschool Junior, for which she received the 'student of the year' award from the UU in 2014. In 2015, Marianne started her PhD at the Leiden University Medical Center (LUMC), department of Cardiology, and at the Netherlands Organization for Applied Research (TNO), department Metabolic Health Research, under supervision of Prof. Dr. J. Wouter Jukema and Dr. Hans M. G. Princen. Her PhD research, of which the results are described in this thesis, included a variety of preclinical studies that aimed to reduce cardiovascular disease risk. During her PhD studies she received a young investigator travel grants for the EAS congress in 2016 in Innsbrück, for the EAS congress in 2017 in Prague, and for the ISA congress in 2018 in Toronto. After completion of her thesis in 2019, Marianne will pursue a career in life sciences.

Dankwoord

De afgelopen 4 jaar zijn razendsnel gegaan en dat was niet gelukt zonder de hulp en steun van vele collega's, vrienden en familie die ik graag wil bedanken. Veel eer komt toe aan mijn copromotor Hans Princen en promotor Wouter Jukema. Hans, ik heb ontzettend veel van je geleerd en elke keer weer verbaasde je me met het opnoemen van publicaties met de bijbehorende jaartallen en auteurs. We hebben samen heel wat congressen bezocht waarbij je nooit te beroerd was om een stuk met me mee te wandelen door de desbetreffende stad. Wouter, bedankt voor de goede discussies en frisse (klinische) blik op mijn onderzoeksresultaten. Na onze besprekingen ging ik altijd weer met veel positieve energie verder met mijn onderzoek.

Leden van de promotiecommissie, Prof. Dr. Arnoud van der Laarse, Prof. Dr. Bert Groen, Dr. Ilze bot en Prof. Dr. Patrick Rensen, bedankt voor het kritisch lezen en beoordelen van mijn proefschrift.

Alle leden van het CarTarDis consortium, in het bijzonder Ivana van Bobeldijk, Danielle van Keulen en Dennie Tempel. Ivana, door jouw organisatie en inzet is het CarTarDis consortium een succes geworden. Danielle en Dennie, bedankt voor de prettige samenwerking en discussies, met twee prachtige papers als resultaat.

Lieve TNO-collega's, door jullie gezelligheid ging ik elke dag weer met plezier naar mijn werk. Zonder jullie hulp was dit proefschrift nooit tot stand gekomen. Anita, bedankt voor je wetenschappelijke bijdrage en gezelligheid tijdens de koffiepauzes. Elsbet, dank voor de leuke etentjes en je geduld en medeleven als er weer eens een apparaat kapot ging tijdens de uitvoer van mijn experimenten. Linda en Frits, de crème de la crème van het TNO fietsteam: dank voor al die prachtige fietstochten door Nederland, waarvan er zekerweten nog heel veel meer gaan komen. Dr. Offie, bedankt voor je altijd enthousiaste instelling als er weer hartjes gesneden moesten worden. Nikki en Eveline, jullie hebben als studenten ontzettend veel data voor mij verzameld en ik vind het zo leuk dat jullie daarna allebei TNO-collega's zijn geworden. Collega promovendi Petra, Martine, Anne en Eveline, dank voor jullie steun en gezelligheid. Mijn liefste kamergenoten Eveline, Nanda, Anne en Nicole, we hadden de gezelligste kamer ooit en niemand kan dat evenaren want we krijgen straks flexplekken. Daarnaast wil ik mijn welgemeende excuses aanbieden voor het steeds weer leegeten van de snoep pot. Eveline, na je onderzoeksstage ben jij mijn mede-promovenda en kamergenoot geworden en ik ben supertrots dat je naast me staat als paranimf.

Vrienden wil ik graag bedanken voor alle steun en nodige afleiding de afgelopen 4 jaar. Tim, liefste spook van de wereld. Bedankt voor die heerlijke tijd samen en je support tijdens het afronden van mijn promotie. Lieve diergeneeskunde vrienden, Bob, Elles, Gineke, Herrik, Jennifer, Kees, Lisanne, Mathieu, Nirita, Nina, Peter, René, Reinier, Robert, Roel en Stein. Bedankt voor de geweldige studententijd waar we samen maximaal van genoten hebben. Bedankt ook voor alle mooie feestjes en vakanties die daarop volgden.

Mijn dierbare vrienden van heel vroeg, Geeke, Henk, Jantine, Jorieke, Marianne, Michelle, Mischa en Nienke. We zijn samen volwassen geworden met nu elk ons eigen leven. Ik zal nooit vergeten wat we allemaal met elkaar hebben gedeeld en hoop dat er nog vele nieuwe herinneringen volgen. Marianne, bedankt voor al je steun de laatste jaren en de vele mooie fietstochtjes en weekendjes weg. Gaby, je bent de beste huisgenoot die er bestaat, meer woorden heb ik niet nodig.

Joost, Mathieu, Leonie, Ruud, Gineke en Suzanne, dank jullie wel voor al die fijne, gezellige etentjes. Ons wekelijks samenkomen is ontzettend waardevol. Niet alleen om de beste Aziatische maaltijden te eten, maar zeker ook om al mijn privé- en werk gerelateerde missers en succesjes te bespreken, inclusief de 'champagne problems'. Joost en Leonie, jullie liefde voor de wetenschap is ongelofelijk en ik kan niet wachten tot ik jullie proefschriften kan lezen. Joost, ik ben zo blij met je als vriend en vereerd dat jij mijn paranimf wil zijn.

Niemand kent mij beter als mijn familie. Mathijs, Heleen en Anne-Floor, broer en zussen, samen opgroeien is iets bijzonders en schept een band als geen ander. We hebben al zoveel avonturen met z'n allen beleefd en er gaan er nog zoveel meer komen. Papa, Mama, dit proefschrift is voor jullie. Er zijn geen woorden genoeg om jullie te bedanken voor jullie steun en vertrouwen in mijn keuzes.